JAERI-M
85-006

ANNUAL REPORT OF THE FUSION RESEARCH CENTER FOR THE PERIOD OF APRIL 1, 1983 TO MARCH 31, 1984

March 1985

Fusion Research Center

日本原子力研究所
Japan Atomic Energy Research Institute

JAERI-Mレポートは，日本原子力研究所が不定期に公刊している研究報告書です。
入手の問合わせは，日本原子力研究所技術情報部情報資料課（〒319-11茨城県那珂郡東海村）あて，お申しこしください。なお，このほかに財団法人原子力弘済会資料センター（〒319-11茨城県那珂郡東海村日本原子力研究所内）で複写による実費頒布をおこなっております。

JAERI-M reports are issued irregularly.
Inquiries about availability of the reports should be addressed to Information Division Department of Technical Information, Japan Atomic Energy Research Institute, Tokai-mura, Naka-gun, Ibaraki-ken 319-11, Japan.

編集兼発行　日本原子力研究所
印　　刷　いばらき印刷㈱

JAERI-M 85-006

Annual Report of the Fusion Research Center for the period of April 1, 1983 to March 31, 1984

Fusion Research Center
Tokai Research Establishment, JAERI

(Received January 11, 1985)

Research and development activities of the Fusion Research Center (Department of Thermonuclear Fusion Research and Department of Large Tokamak Development) from April 1983 to March 1984 are described.

Installation and commissioning of the new tokamak JFT-2M had been completed. The 2nd ICRF heating experiment and LH current drive experiment were started. In the field of plasma theory, the scaling law of the critical beta in a tokamak was obtained and the ICRF heating was analyzed in detail. The first phase of the cooperation of Doublet III will be finished in Sept. 1984.

The JT-60 program progressed as scheduled. Installation of the tokamak machine, initiated in Feb. 1983, will be finished in Sept. 1984. The tests of power supply and control system on site and the fabrication of the neutral beam injectors in factory proceeded successfully.

Performance tests of prototype injector unit for JT-60 NBI progressed as scheduled. A new advanced source plasma generator was developed to provide a high proton ratio exceeding 90%. Klystrons for JT-60 LH heating achieved the output power of 1 MW for 10 sec. Performance tests of titanium evaporators for JT-60 were completed.

The Japanese coil for IEA Large Coil Task was installed in a test facility at ORNL and the partial cool-down was carried out. Construction of the Tritium Process Laboratory was completed.

Design studies of the Fusion Experimental Reactor (FER) and INTOR proceeded.

Keywords: Annual Report, Plasma Confinement, JFT-2M, Doublet III, JT-60, NBI heating, RF heating, Surface Study, Superconducting Magnet, Tritium Technology, FER, INTOR

JAERI－M 85－006

核融合研究センター年報（昭和58年度）

日本原子力研究所東海研究所
核融合研究センター

（1985年1月11日受理）

核融合研究センターにおける昭和58年度の研究開発の現状と成果をまとめた。

新装置JFT－2Mの試験運転を完了し，第2高調波ICRF加熱実験・LH電流駆動実験を行った。理論では，ベータ限界値の比例則を明らかにすると共に，ICRF加熱の詳細な解析を行った。Doublet Ⅲによる第1期の共同実験は59年9月には終了の予定である。

JT－60の建設は順調に進み，58年2月に開始した本体の据付は59年9月完了の予定である。電源および制御系の試験，および中性粒子入射加熱装置の工場製作も進められている。

JT－60中性粒子入射加熱装置原型ユニットの性能試験を順調に進めると共に，新イオン源の開発を行い，90％以上の高水素比を達成した。JT－60高周波加熱用大電力クライストロンの開発も1MW 10秒の出力を達成し，順調に進んでいる。又，JT－60用チタン蒸着装置の性能試験を完了した。

超電導磁石開発では，国際エネルギー機関による大型コイル事業の為の日本のコイルの，米国オークリッジ研究所の試験装置への据付けを完了し，実験が開始された。トリチウムプロセス研究棟が完成した。

実験炉（FER）およびINTORの設計検討も進められている。

CONTENTS

目　　次

I. PLASMA THEORY AND COMPUTATION

1. Introduction

The objectives of the theoretical plasma physics program at JAERI are to develop methods including development of computer codes for comprehensive analyses of a tokamak plasma under realistic conditions, and to analyze the plasma to attain the basic understanding of the tokamak. Through the program the theoretical effort contribute to the experimental programs of the JT-60 and JFT-2M tokamaks, and the design studies of future fusion devices, such as the FER and INTOR. These objectives are pursured by developing the computer code system TRITON and analyzing various physics problems concerning the plasma confinement, heating, and transport on the basis of the combined use of the fluid, kinetic, and particle models.

Notable progresses of the studies attained in this fiscal year are: (1) as for the MHD beta limit extensive parameter survey has been performed and the optimized beta scaling law has been obtained, (2) the various problems concerning the ICRF heating have been studied by the use of the previously developed two-dimensional (2D) kinetic code and three-dimensional (3D) MHD code, and (3) efforts have been successful concerning the nonlinear MHD analyses, such as the analysis of kinetic effect on the resistive internal mode and development of a new numerical method of nonlinear kink mode. The construction of the TRITON-I code system has been also continued.

2. Transport and Heating Studies

2.1 Introduction

Effects of poloidal electric field, generated by high-energy ion beam due to ICRF or NBI heating processes, on transport in a tokamak plasma was studied in the MHD regime and formation of sheath and presheath in the divertor plasma were studied by particle simulation.

Up to the present, the mechanism of the transport in a tokamak plasma is not clarified and it is important to study the role of microinstabilities on the transport process. Diffusion flux of electron was estimated when there exists a high-n ballooning mode fluctuation and saturation mechanism of electrostatic ballooning instability is studied by 2D nonlinear model equation.

Beam-driven ICRF (Ion Cyclotron Range of Frequency) instability

was studied and nonclassical transport due to this instability was estimated. Damping mechanism of ICRF wave in an inhomogenious magnetic field was studied by kinetic model and study of 3D wave structure of ICRF wave was performed by cold plasma model.

2.2 Transport

2.2.1 Effects of poloidal electric field on transport

High-energy beam, generated by ICRF heating or NBI heating processes and trapped in outer region of torus, can produce a poloidally varying electrostatic potential $\tilde{\varphi}(\theta)$.

Plasma equilibria and transport are influenced by such a poloidal asymmetry. Effects of the poloidal electric field on transport phenomena was examined in MHD regime. When number density of trapped ion is $\tilde{n}_b(\theta)$, the electrostatic potential, $e\tilde{\varphi}(\theta)(1/T_e + 1/T_i)\sim\tilde{n}_b/n_0$ is created. If $\tilde{n}_b(\theta)\propto\cos\theta$ is assumed particle and ion heat flux is given as

$$\Gamma = 0.26 \frac{T_i}{T_e+T_i} \frac{m_i T_e}{\tau_i e^2 B^2 \theta^2} \frac{\tilde{n}_b}{A n_0} \frac{dn_0}{dr} \quad ,$$

and

$$Q_i = \frac{5}{2} n T_i \Gamma$$

respectively, where $\theta=B_\theta B_t$, A is the aspect ratio, m_i is the ion mass, and τ_i is collision time. The value of these fluxes is small in the practical system and effect of poloidal electric field on background-plasma transport is negligible.

2.2.2 Particle simulation of divertor plasma

A poloidal divertor is considered to be the most reliable concept for a tokamak reactor from the view points of impurity and neutral particle control and heat flux density reduction. Characteristics of the scrape-off layer plasma in a divertor tokamak have been studied experimentally and theoretically. The fluid model has been usually applied for analyses of divertor plasmas. It is not clear, however, whether the usual fluid equations can describe the scrape-off layer plasma.

In a scrape-off layer plasma bounded by divertor plates, the self-consistent electrostatic field, i.e., sheath and pre-sheath field, plays the most important role. Velocity distribution functions of

electrons and ions are much distorted from the Maxwellian. Therefore, the electrostatic particle model is suitable to study divertor plasmas. Coulomb collisions play a very important role to supply electrons with large velocity parallel to the magnetic field, which can pass through the sheath potential barrier near the divertor plate.

We aim to study the importance of collisions in a divertor plasma, and we have developed a one-dimensional electrostatic particle simulation code with a binary collision model. The pre-sheath with the scale length of the system size is formed by the collisional relaxation of the velocity distribution as well as by the particle source. The flow speed is increased by this potential and exceeds the sound speed.

2.2.3 Electron diffusion in a tokamak due to high-n ballooning mode[1)]

The radial diffusion of electrons due to high-n ballooning modes (n is the toroidal mode number) in a sheared magnetic field of a tokamak is investigated. The $E\times B$ drift motion of an electron in a fluctuating electric field with many poloidal mode numbers is described by a radial kink. By a Taylor expansion of the safety factor $q(r)=q(r_s)+q'(r_s)(r-r_s)$ at a rational surface r_s, where $q(r_s)=m/n$, we reduce the equation of motion to a standard map. The diffusion coefficient D is estimated to be inversely proportional to the parallel velocity of an electron $v_{\parallel}$;

$$D=\frac{q(r_s)R}{8\pi v_{\parallel}}\left(\frac{m\varphi_m}{r_s B_t}\right)^2 \quad ,$$

where R is the major radius, B_t the toroidal magnetic field, and φ_m the fluctuation potential of the poloidal mode number m.

When the radial magnetic field fluctuation B_r exists, the diffusion coefficient is estimated to be proportional to $v_{\parallel}$ as

$$D=\frac{q(r_s)Rv_{\parallel}}{8\pi}\left(\frac{B_r}{B_t}\right)^2 \quad .$$

2.2.4 Simulation of electrostatic ballooning mode[2)]

As the first step to estimate the transport coefficient due to ballooning instability, we study the saturation mechanism of electrostatic ballooning mode by a two-dimensional model. We use two-fluids equation system with resistivity in Cartesian coordinates. The strong magnetic field is in the z-direction. The plasma density n_0 and magnetic field strength B vary in the x-direction. In the case of ballooning modes with long wave length ($k_{\perp}^2\rho_s^2\ll 1$), the dominant nonlinear

effect is the convective term, and the typical localization length along the field line is given as qR for $\omega \sim \omega_* > Cs/qR$ (q: safety factor, C_s: sound velocity, ω_*: drift frequency, and ρ_s: ion gyroradius at electron temperature). Using these assumptions, we derive a two-dimensional model equation for electrostatic ballooning mode as,

$$\frac{\partial N}{\partial t}+\upsilon_*\frac{\partial N}{\partial y}+\frac{\upsilon_*\upsilon_d}{\omega_s}\frac{\partial^2 N}{\partial y^2}+\nu\Delta_\perp{}^2 N=\frac{\upsilon_d}{\omega_s}\frac{T_e}{eB}\left\{\frac{\partial N}{\partial x}\frac{\partial^2 N}{\partial y^2}-\frac{\partial N}{\partial y}\frac{\partial^2 N}{\partial x\partial y}\right\},$$

where $N=\tilde{n}/n_0$, $\upsilon_*=T_e/eBL_n$, $\upsilon_d=(T_e+T_i)/eBR$, $\omega_s=\tau_e T_e/0.51 m_s q^2 R^2$, $1/L_n=-\nabla n_0/n_0$, τ_e is the electron collision time and ν is the ion perpendicular viscosity. This model equation is solved numerically with the boundary condition that $N=0$ at $x=0$ and $x=L_x$. Single mode saturation is realized for wide range of plasma parameters. Laminar convective flow appears rather than turbulence. The mode with maximum linear growth rate remains in the final state and saturated amplitude is order of $N=L_x/L_n$. Nonlinear saturation originates from convective term; background modification is produced by mode-mode coupling.

2.2.5 Integral of wave kinetic equation of drift waves[3)]

Integral of wave kinetic equation of electostatic drift waves is obtained on the basis of the weak turbulence approach for arbitrary number of modes, N. If the stationary spectrum of N modes exists, the wave amplitude is bounded for any initial conditions. The stationary spectrum, which appears only if the initial spectrum coincides with it, is estimated to be the most probable one, if the amplitude of the stationary spectrum is large.

2.2.6 Beam-driven ICRF instability and associated nonclassical transport in tokamak[4)]

Nonlocal eigenmode of ICRF instability in the presence of parallel high energy beam component is obtained in a toroidal plasma in an inhomogeneous magnetic field. The mode is the combination of the fast wave and Bernstein wave and is excited via kinetic interactions with beam particles. When the driving source of high energy particles overcomes the total dampings due to the bulk plasma and the resistive loss on the wall, the instability can occur. Nonclassical energy/momentum transfer rates due to this mode between different plasma species are obtained. Nonlocal energy/momentum transport is simultaneously induced. The rate of nonclassical energy transfer reaches the classical level at

the low level of wave amplitude.

2.3 Heating

2.3.1 Numerical calculation of ICRF waves

ICRF wave in a two ion component plasma in a tokamak is studied by solving the wave propagation equation based on a cold plasma model. The numerical solution for the three dimensional structure is obtained by use of the finite difference method.

2.3.2 Three dimensional structures of ICRF waves in tokamak plasmas[5)]

The 3D structure of the ICRF waves in a tokamak plasma is investigated. In two-ion species plasma (majority deuterium and minority hydrogen) with radial density inhomogeneity, the wave equation is numerically solved by employing a cold plasma approximation. The plasma is immersed in toroidal magnetic field with the gradient and is surrounded by the vacuum region and the conducting wall. Waves are launched by a Faraday-shielded poloidal-current antenna which has the finite extents in toroidal and poloidal directions. The wave field and the energy deposition profile are obtained by an introduction of a simple model collision. The wave accessibility condition is examined for plasma parameters and density profiles. In a cold fluid approximation, two mechanism of power absorption, i.e., two-ion hybrid resonance and the cavity resonance, are found and the differences are studied. The loading impedance of the antenna is also calculated for each case. High- and low-field-side excitation are compared. Non-plasma losses on the wall are considered to obtain the coupling efficiency. Good coupling condition and desirable antenna design are also discussed. It is found that the efficient coupling is expected in a wide range of plasma parameters.

2.3.3 Study of ICRF waves in second cyclotron resonance and two-ion hybrid resonance heating[6)]

Propagation and absorption structures of ICRF wave excited by antenna current are analyzed. The kinetic wave equation is solved for a high-temperature plasma which has a pressure profile and is in an inhomogeneous magnetic field. The two-dimensional power deposition profile for each plasma species and the coupling to a finite-size antenna are simultaneously obtained for the second harmonic resonance case and for the two-ion hybrid resonance case. The accessibility

condition of the fast wave, the minority and/or majority ion heating condition as well as the electron heating condition are numerically obtained in bulk-plasma parameter spaces. The theoretical analysis is done for the results, and scaling laws of the heating conditions are obtained. The total impedance of the antenna is also calculated and the coupling efficiency is studied with inclusion of a resistive wall loss. The guiding principle for antenna design is also discussed.

2.3.4 Simultaneous heating by ICRF wave and neutral beam injection[7)]

A theoretical analysis of ICRF wave heating in a plasma with neutral-beam injection (NBI) is performed. Wave propagation and absorption are examined kinetically in the presence of high-energy ion beam component. The following findings are reported: 1) the wave coupling efficiency does not deteriorate by the beam,; 2) co-operative heating is to be expected, and 3) selective heating of high-energy ions is possible.

2.3.5 Fusion engine cycle in reactor system by adiabatic compression[8)]

Cycle operation in magnetic confinement reactors is proposed in order to convert fusion energy directly to electro-magnetic energy. By the adiabatic compression, the fuel plasma is heated to exceed the ignition criterion. Thermal energy due to reactions is converted to the electromagnetic energy through decompression. Decrease of the temperature closes the cycle. The energy conversion efficiency is studied. Considerable fraction of fusion energy can be directly converted.

References

1) Shigeta M., Fukuyama A., Takizuka T., J. Phys. Soc. Japan 53 (1984) 1958.
2) Tuda T. et al., Proc. 1984 ICPP, Vol.1, p.202.
3) Itoh K., Itoh S-I., "Integral of wave kinetic equation of drift waves", HIFT-88 (1984).
4) Itoh S-I., Itoh K., Fukuyama A., "Beam-driven ICRF instability and associated nonclassical transport in tokamak", HIFT-89 (1984).
5) Itoh K., Itoh S-I., Fukuyama A., Nucl. Fusion 24 (1984) 13.
6) Fukuyama A., Itoh S-I., Itoh K., "Study of ICRF waves in second cyclotron resonance and two-ion hybrid resonance heating", HIFT-88 (1983).

7) Itoh S-I., Fukuyama A., Itoh K., Nucl. Fusion 24 (1984) 224.
8) Itoh S-I., Itoh K., "Fusion engine cycle in reactor system by adiabatic compression", HIFT-77 (1983).

3. Equilibrium and Stability

3.1 Introduction

The two main objectives of the computational analyses in the project TRITON are, presently, the clarification of the MHD stability limit scaling and the mechanism of disruptive instabilities. As for the former, efforts are made to carry out stability analyses with very high accuracy. For this purpose development of MHD equilibrium codes with high performance is continued and a MHD equilibrium database for the stability analyses is being developed. An algorithm to calculate an optimized beta state efficiently is developed and used to find a scaling law of a limiting beta value. As for the latter the kinetic effect on the resistive internal kink mode and the nonlinear evolution of external kink mode are studied. The resistive internal kink mode is assumed to play a role in suppression of the internal disruption and the external kink mode is, sometimes, considered to be responsible to the major disruption.

3.2 Equilibrium analyses

3.2.1 Equilibrium database CLIO-V1

The equilibrium database CLIO-V1 was developed to avoid repeating equilibrium computations with the same input data and to enable to analyze systematically the MHD stability of the family of equilibria. The CLIO-V1 system has two main parts: one is a group of data files (mass data, index and MT-control files) generated by the GAEA-MT system and accessed under the system, the other is a group of source programs. The group of programs is composed of the standardized equilibrium codes SELENE40, two programs to refer the variables characterizing the equilibria and to retrieve a family of equilibria from magnetic tapes, a graphic program supported by the ARGUS system and the ballooning stability analysis code BOREASGM which works under the CLIO system. The equilibrium codes SELENE40 solve the Grad-Shafranov equation by the nonlinear eigenvalue problem algorithm (SELENE40N) or FCT (Flux Conserving Tokamak) algorithm (SELENE40F). The codes SELENE40 are supported by the EOS preprocessor system and the users can easily

change the profiles of the pressure and the poloidal current function.

3.2.2 SELENE10 and SELENE-ERATO interface module

The code SELENE10 solves the Grad-Shafranov equation in the flux coodinates. Several improvements were made on the SELENE10 code in order to be fit for accurate stability analyses. The SOR iterative scheme is adopted in solving the large simultaneous linear equation to compute equilibria with a large mesh number. The code constructs the flux surfaces in the vacuum region near the plasma surface so that the metric quantities near the plasma surface can be computed accurately. The SELENE10-ERATO interface module was reformed according to the above improvements of the SELENE10. Consequently, the metric quantities near the magnetic axis and the plasma surface have high accuracy and also uniform accuracy in the poloidal direction.

3.2.3 Equilibria of anisotropic pressure tokamaks with high-energy alpha particles[1)]

In an experimental tokamak fusion reactor, the anisotropy in the plasma pressure is produced by the beam component during the neutral beam injection heating phase. The anisotropy is also produced by high-energy alpha particles with finite shift of drift orbits from a magnetic surface, though alpha particles are generated with the isotropic pitch-angle distribution by DT fusion reactions. When the characteristic length of the pressure pradient is comparable with the banana size of a trapped alpha particles with energy of 3.5MeV, trapped alpha particles born in the high-pressure region are drifted out to the low-pressure region, and they produce the flow along magnetic field lines and the anisotropy in the plasma pressure.

Equilibrium equations are derived by considering the anisotropy. The anisotropy is obtained by orbit integration during the classical slowing-down process.

3.2.4 MHD equilibria in a straight system with a non-planar magnetic axis[2)]

Numerical investigations of equilibria with free boundary are made in the straight system with a three dimensional magnetic axis. Grad-Shafranov equation is solved by both iterative SOR method and direct method on the basis of LU matrix decomposition. From the standpoint of CPU time, SOR method is better than the direct method, when number

of outer iterations is executed. A part of the "self-stabilization effect" due to the increase of the plasma pressure is successfully simulated. On the parameter space where the relation between the rotational transform due to the torsion of helical magnetic axis is subtractive, the convergence region is very small.

3.3 Linear MHD instabilities

3.3.1 Scaling of beta limit for infinite-n ballooning mode[3)]

The critical beta of a tokamak against infinite-n ballooning mode is studied in the wide range of ellipticity, triangularity, and safety factor profile. The triangularity and large ellipticity cooperatively play a role to increase the critical beta value of a tokamak with low safety factor at the plasma surface (Fig.I.3-1(a)). The critical beta can be further increased by increasing the safety factor at the magnetic axis from unity (Fig.I.3-1(b)), unless the plasma suffers from degradation of confinement by other instabilities.

3.3.2 Model equation analysis of internal kink mode

The ideal MHD stability of a tokamak plasma can be analyzed by using the ERATO code, which solves the generalized eigenvalue problem on large matrices. However, when we make good use of the character of tokamak plasmas, that is, $q \sim O(1)$, $B_p/B_t \sim O(\varepsilon)$ and $\beta_p \sim 1$ or $\varepsilon\beta_p \sim 1$ (ε: inverse aspect ratio), the eigenvalue problem can be reduced to the problem on a single variable. In addition, the resultant matrices are small when the variable is Fourier-decomposed and only a few components are kept. A model equation of the m=1 internal kink mode was developed by using this approximation[4)]. The stability of the mode with m=1/n=2 was studied. The eigenfunction obtained from this model equation represents well the character of the m=1 internal kink mode and the stability limit of the lower β_p region computed by the model equation is in good agreement with that by the ERATO calculation.

3.3.3 Stability of anisotropic pressure plasma

The code TERA has been developed for the linear stability analysis of anisotropic pressure tokamak plasmas. The Lagrangian of the guiding center model (C.G.L. model)[5)] was discretized by using the finite hybrid element method used in the ERATO code. The n=10 ballooning mode and the internal kink mode were analyzed by using the model equilibrium

heated by the perpendicular neutral beam injection. The n=10 ballooning mode is stabilized by the inward shift of the pressure surface from the flux surface. The stabilizing effect is remarkable in low β_p plasmas (the case of low shear) as shown in Fig.I.3-2. The internal kink mode is stabilized in higher β_p region (Fig.I.3-3).

3.3.4 Eigenvalue solver MAIA for a linear resistive MHD system

A code MAIA for solving growth rates of a plasma represented by a reduced set of linear resistive MHD equations has been developed. By numerical formulation the equations are reduced to an eigenvalue problem of a block tridiagonal matrix. Both determinant and inverse iteration methods are employed as solution methods of the eigenvalue problem.

3.4 Nonlinear MHD instabilities

3.4.1 Development of a nonlinear resistive MHD code AEOLUS-RT

Development of a nonlinear resistive MHD code AEOLUS-RT, which solves a reduced set of resistive MHD equations, has been continued. Several improvements and restructuring of the code were made to attain high performance in calculation and to make the code intelligible.

3.4.2 Simulation of nonlinear kink mode[6)]

The recent tokamak experiments indicate that the major disruption can be suppressed by the control of plasma current profile when the safety factor at the plasma surface, q_a, is greater than 2. In this case, the cause of major disruption is considered to be the nonlinear coupling between the tearing modes with different helicities. On the other hand, when $q_a \sim 2$, the major disruption occurs in the case without the conducting wall close to the plasma surface. This fact indicates that the m=2/n=1 free boundary mode plays an important role in the major disruption. Thus, to investigate the role of the free boundary modes in the major disruption process, we developed the nonlinear free boundary code using an usual reduced set of resistive MHD equations. To avoid the complexity of tracing the plasma surface in the nonlinear calculation, we assume that the plasma is surrounded by a high resistive region instead of a real vacuum. To determine the plasma boundary, we add a convective equation of resistivity to a reduced set of MHD equations. As the first step of the nonlinear calculations, we calculate

the saturation of the m=2/n=1 free boundary mode in cylindrical plasma. Figure I.3-4 shows the time evolutional helical flux contours. The plasma surface (bold line) is gradually distorted in elliptic form, and the last figure (Fig.I.3-4(c)) shows the saturated state. The profile of equilibrium plasma current is taken parabolic, and the ratio of the position of the conducting wall to the initial position of the plasma surface is 1.5.

3.4.3 Kinetic effect on resistive internal mode[6)]

The kinetic effect on m=1/n=1 resistive mode was studied in a cylindrical model. The reduced set of equations with the density perturbation was used. The linear analysis shows that the growth rate decreases as the increase of ω_*/γ_T, where ω_* and γ_T are the diamagnetic drift frequency and the growth rate of a tearing mode. The result by using only m=0/n=0 and m=1/n=1 modes agrees with that shown by Biskamp[7)]. However, the saturation level of the m=0 component of the magnetic energy increases as M^2 (Fig.I.3-5) where M is the number of modes. This result indicates the importance of the coupling with higher modes and also suggests the internal disruption even for $\omega_*/\gamma_T>1$.

References

1) Takizuka T. et al., "Equilibrium of anisotropic pressure tokamaks with high energy alpha particles", Proc. 1984 ICPP, Vol.1, p.111.

2) Harafuji K. et al., "MHD equilibria in a straight system with a non-planar magnetic axis", JAERI-M 84-035 (March, 1984)

3) Azumi M. et al., "Scaling of beta limit in a tokamak for infinite-n ballooning modes", Proc. 1984 ICPP, Vol.1. p.200.

4) Tokuda S., "Stability analyses of tokamak plasmas by computer simulation", JAERI-M 84-040 (March, 1984).

5) Kruskal M.D., Oberman C.R., Phys. Fluids 1 (1958) 275.

6) Tsunematsu T. et al., "Nonlinear evolution of external kink mode in tokamak and comment on resistive internal kink mode", Proc. US-Japan Workshop on 3D MHD Studies, CONF-840370 (March, 1984) p.158.

7) Biskamp D., Phys. Rev. Lett. 46 (1981) 1522.

4. TRITON System

4.1 TRITON system

In the project TRITON various kinds of numerical codes are being developed. These codes are classified into several code groups, i.e., the physics code group ASTRAEA, the numerical analysis code group PARIS, the graphic I/O code group ARGUS, and the supervisor and other supporting code group PEGASUS.

As for development of the physics codes in the TRITON-I system the emphasis was put on the equilibrium codes, beta optimization codes against the infinite-n ballooning mode, linear MHD stability code for any mode number, nonlinear MHD codes, and various supporting codes for code development and maintenance. In order to facilitate maintenance and use of the codes the TRITON-I code system is now being constructed by registering these codes to the index file supervised by the HARMONIA code.

4.2 Supporting codes

Efforts have been continued to develop supporting codes which facilitate development and use of the TRITON system. In the following some of these codes are described briefly.

<ARGUS>[1)]

The ARGUS-V4 subsystem is completed after several improvements are made on the previously developed version. The basic idea of the ARGUS code-group is that any single graphic procedure is composed of three elementary processes, i.e., registration of a graphic data set, processing of the data to match with the required graphic format, and plotting of the graph. The package based upon the concept contains various subroutines clearly classified according to the above elementary processes. By using the package graphic procedures in scientific or engineering programs are coded very easily and the programs become intelligible. As the package ARGUS-V4 is written in the standard FORTRAN77 language and uses only basic plotting subroutines in the CALCOMP library, it can be installed with a few alterations in various computer systems.

By following the basic idea of the ARGUS code-group, we start designing the advanced graphic subsystem ARGUS-V5 which deals with more complicated objects on a 3D color graphic terminal.

<HARMONIA-IPF>

The TRITON system is supervised by the use of the HARMONIA code which is almost completed in the previous fiscal year. In this fiscal

year the IPF (Interactive Programing Facility) is made most of and the procedures of indexing TRITON codes and storing the codes become extremely efficient.

<GAEA and GAEA-MT>

We have continued development of supervisors of a data base on numerical results GAEA and GAEA-MT: the former deals with comparatively small amount of data to be stored in magnetic disks and the latter deals with a large amount of data to be stored in magnetic tapes. The subsystems supervise data by the three key parameters, i.e., run group name, run name, and automatically generated run number. The subsystems have three modules : data files, preprocessor and editor. The subsystems store data of numerical results and key data. By using the key data, the subsystems can refer, sort and retrieve the numerical results. Users can write the data on data files of the subsystems through the preprocessor. By the editor a user can submit a job, refer data of numerical results and display tables and the graphs of them on a terminal.

<PLUTO>

The interactive version of PLUTO was developed, to make document and user's mannual of a program written in FORTRAN77. The result of the analysis of a source program is stored in disk files. Comments for variables, COMMON blocks and subroutines can be added interactively on the screen of a terminal with the help of IPF. The processed data is stored in a disk file.

<ISP and APPLE>

For realization of efficient man-machine interfaces in the computational studies within the framework of the project TRITON, we are developing basic output softwares which make output data interchangeable among various output devices, such as CD (Character Display terminal), GD (Graphic Display terminal), and NLP (Nihongo Line Printer usable as plotter).

In this fiscal year two such basic software, ISP (IPF Screen Plotter) and APPLE (dot pattern editor of NLP-formatted data) are developed. The former makes it possible to extract data from the CD screen buffer of the IPF module and plot them by an NLP. By this procedure "ruled lines" and "inverted characters" displayed on the CD screen are also plotted faithfully on the NLP output. The latter extracts dot patterns from a SYSOUT file of an NLP and rearrange them to

be acceptable by a GD. By this program overlay, insertion, rotation, shift, and zooming of a figure are made possible and it becomes very easy to combine figures, tables, and texts on a single screen.

References

1) Takeda T., Tsunematsu T., Tokuda S., to be published in Comput. Phys. Commun..

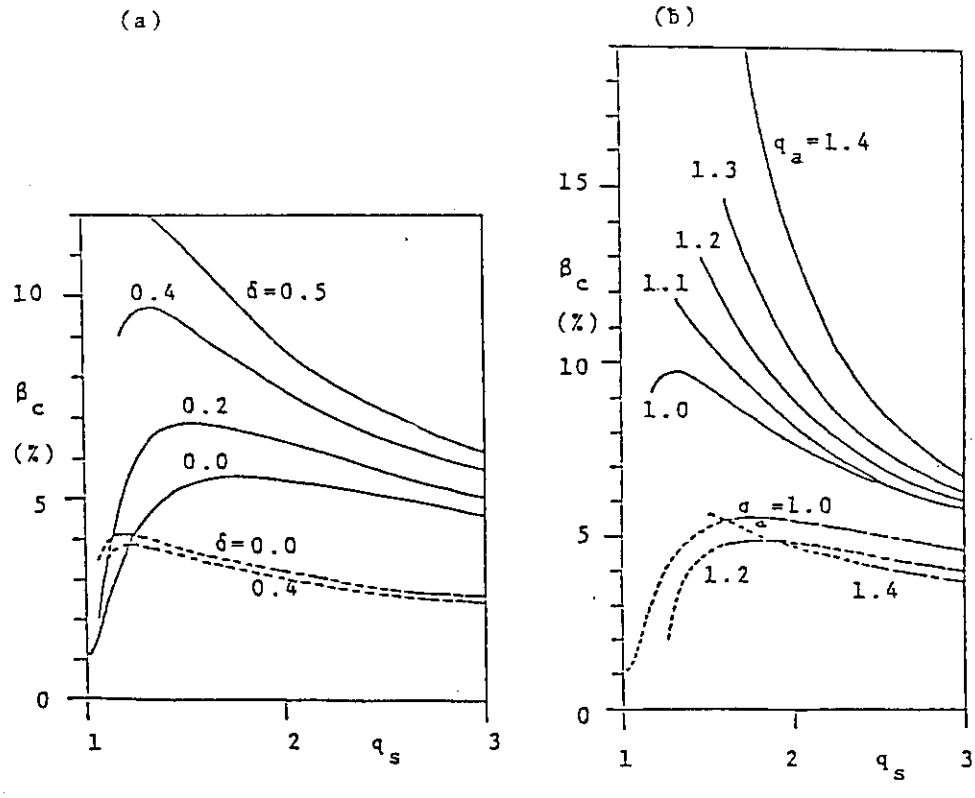

Fig. I.3-1
(a) Dependence of critical beta, β_c, on q_s for different values of δ. Elongation κ=1.6 (solid line) and κ=1.0 (dashed line). The safety factor at axis, q_a is 1.0.
(b) Dependence of β_c on q_s for different values of q_a. Triangularity δ=0.4 (solid line) and δ=0.0 (dashed line). For both the subfigures the aspect ratio A is chosen to be 3.375.

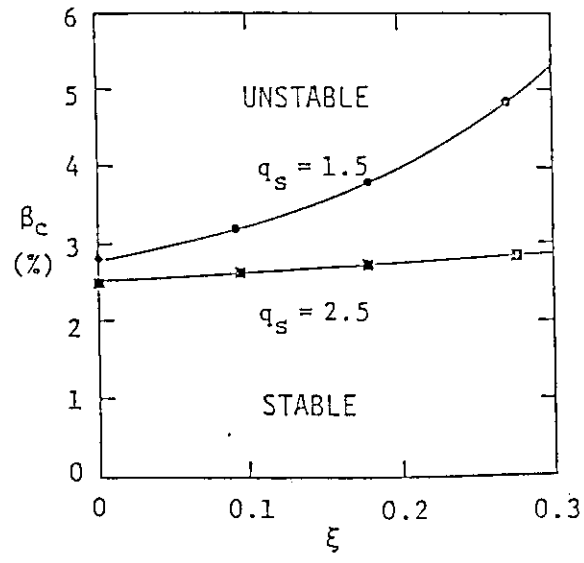

Fig. I.3-2
Critical beta value vs. anisotropy defined by $\xi=(P_\perp-P_\parallel)/P_0$. The upper line and the lower line correspond to the case q_s=1.5 and q_s=2.5 (q_s: safety factor at the plasma surface), respectively.

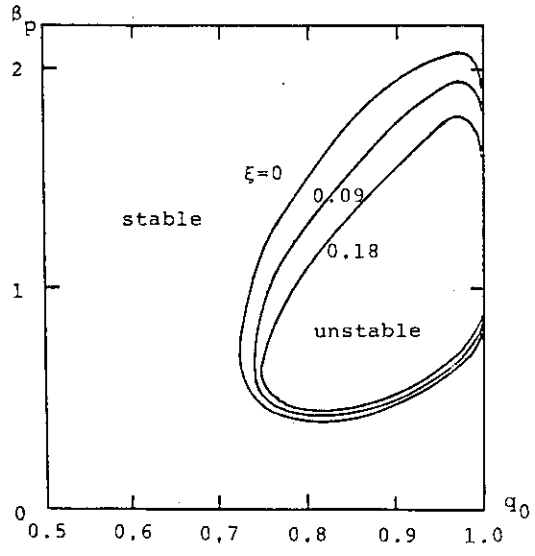

Fig. I.3-3
Stability diagram of the internal kink mode in q_0-β_p plane. In the enclosed region the mode is unstable.

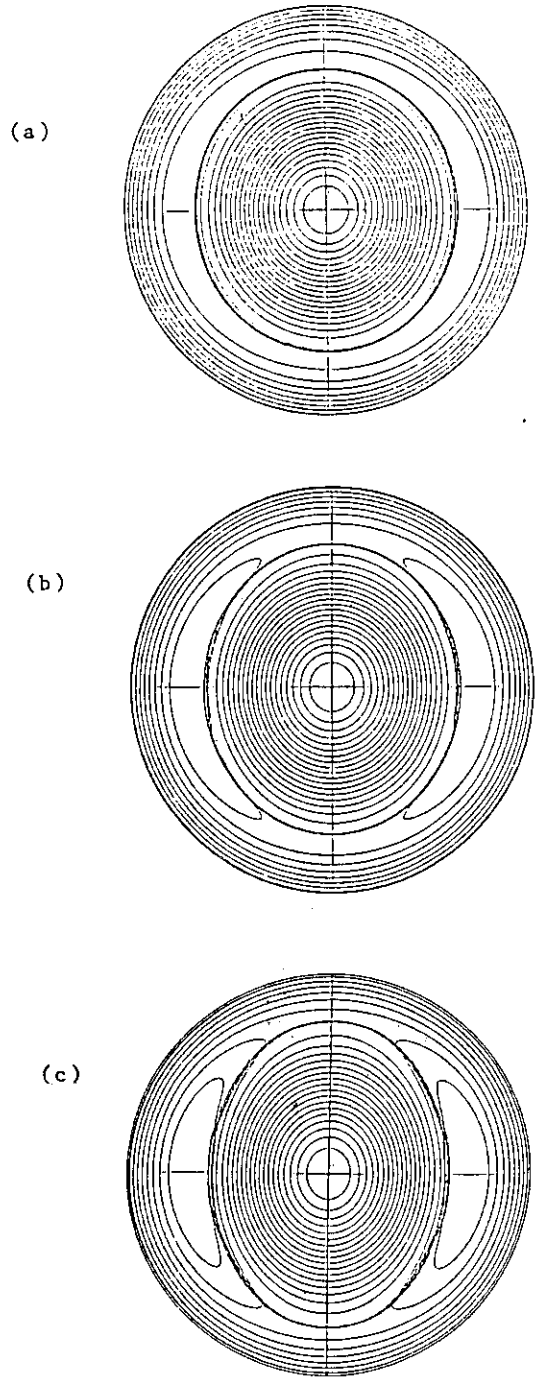

Fig. I.3-4
Nonlinear evolution of the helical flux contours of a free boundary kink mode. The bold lines denote plasma surfaces, and the subfigure (c) shows the saturated state.

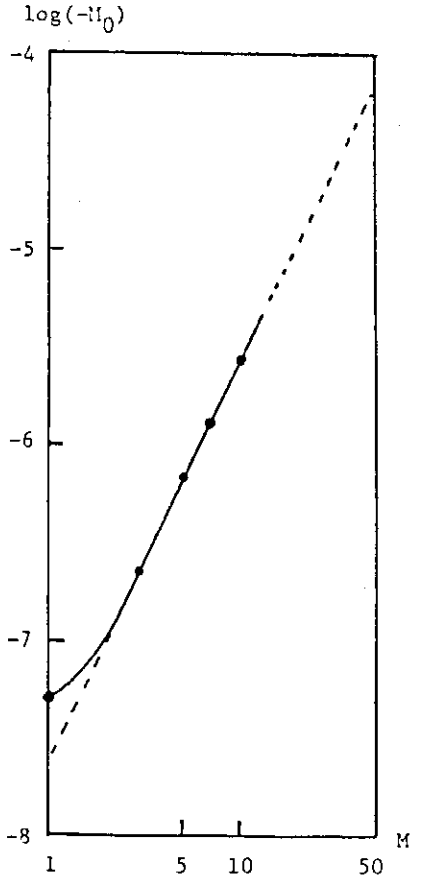

Fig. I.3-5
Maximum value of $-\delta M_0$ vs. M for $\omega_*/\gamma_T=3$. This value scales as M^2.

II. TOROIDAL CONFINEMENT EXPERIMENT

1. Introduction

After 11 years operation, the JFT-2 tokamak had been shut down on June 1982. On the other hand, installation and commissioning of the new tokamak named JFT-2M had been completed on April, 1983. Successively, the plasma experiment was commenced. The standard Joule heated plasma was achieved in June, 1983, even though the plasma parameters were not the full rating of the JFT-2M tokamak for the sake of limitation in poloidal power supplies. These results are described in Subsection 2.

From July, the 2nd ICRF heating combined with the NBI heating was carried out. The key results of this experiment were intence electron heating by the 2nd ICRF and some sort of recover on the gross energy confinement time from a NBI heated plasma, nevertheless, such an intence electron heating could not be explained by a simple theory. In addition, we recognized that even in an electron heating mode of ICRF, there was a severe impurity problem. This suggests that a near field of antennae should be carefully re-examined to overcome an impurity problem in the ICRF heating scheme. Along this line, some refinements of loop antennae are continued. These results are described in Subsection 3.

From September to October, the lower hybrid current drive experiment had done using the old RF generator and the new tokamak. Improvement of a current drive efficiency and current ramp-up by LHCD were demonstrated. These results are described in Subsection 4.

From November, 1983 to February, 1984, an extended experiment on the 2nd ICRF and the NBI heating were continued. The NBI heating result was basically the same as that of the JFT-2 tokamak, that is, a soft saturation of the poloidal beta in any sense was observed with increasing the heating power up to 2 MW. The data on the 2nd ICRF heating were also obtained in this period. These results provided our previous preliminary result of the 2nd ICRF in more detail.

In order to give reasonable estimation on physics study of the tokamak plasma, continuous improvement of diagnostic quality is quite crucial. One of those developments in the JFT-2M program is a high counting pulse height analyzer, which is described in Subsection 5.

On March, 1984, installation of a high power RF generator of ICRF was initiated. A graphite toroidal limiter and a single pellet injector

were also installed for the poloidal magnetic limiter experiment.

An ECRH generator of 60 GHz, 200 kW will be installed in September, 1984. Manufacturing of the poloidal field power supply is now ongoing to get full rating of the JFT-2M tokamak, such as, 500 kA plasma current and variety of noncircular plasma shaping. Installation of this power supply is to be in February, 1985.

2. Joule Heated Plasma of the JFT-2M Tokamak

2.1 Introduction

The JFT-2M Tokamak was brought into operation for joule heating experiments in the end of April. After the conventional cleaning procedures such as the baking and TDC, extensive studies of plasma start-up, feedback control of plasma position, plasma shaping and gas puffing allowed for JFT-2M to produce plasma with reasonably low q without titanium gettering in a relatively short time of operation. After the power up of poloidal field power supplies a non-circular diverted plasma with the higher plasma current will be studied.

2.2 JFT-2M[1] and diagnostics

The D-shaped vacuum vessel ($415mm^{W}\times595mm^{H}$) was made of SUS-304L stainless steel of 25mm thickness with two Teflon breaks which were shunted by SiC nonlinear resistors. The skin time of the vessel is nearly 7ms and baking temperature is 120°C. Plasma radius is limited by back-up limiter ($350mm^{W}\times530mm^{H}$) and/or by three movable limiters (outer, upper and lower sides). The maximum toroidal field is 14.5kG with 16 toroidal coils. The poloidal coil system is composed of 4 coils inside the toroidal coils and 4 coils outside the toroidal coils as shown in Fig.II.2-1, and each coil has several taps so as to optimize the plasma position and shape. Power supplies for poloidal coils are 2 capacitor banks for plasma start-up and 5 thyristor power supplies for plasma current and position controls. A feedback control system is composed of an analog computer, magnetic probes, and a mini-computer for producing reference commands. Main diagnostics in operation are conventional magnetic measurements, 4mm (vertical path) and 2 mm (horizontal path) microwave interferometers for $\bar{n}_e$, Laser scattering, $2\omega_{ce}$ and soft/hart X-ray for $T_e(r)$, C.X. and neutron detectors for T_i, visible and vacuum ultraviolet spectrometers for impurity analysis and bolometers for radiation monitor, in start-up of JFT-2M.

2.3 Plasma position control[2)]

As a horizontal position control, three methods such as $<B_\theta>$ method, $<B_\theta>+<B_\rho>$ method and iso-flux method[3)] were examined subsequently. From viewpoints of simplicity and flexibility for non-circular plasma, the iso-flux method might be useful. Horizontal field coils for vertical position control are usually independent of the vertical field coil, but in JFT-2M, the hybrid control of vertical and horizontal position was examined with upper and lower vertical field coils. The horizontal position is controlled by the vertical field of these coils and the necessary horizontal field is generated by unbalance of coil currents between the upper and lower vertical field coils. By this method, it is possible to decrease number of poloidal coils, and it is not required for a thyristor power supply to generate both positive and negative currents. In order to obtain non-circular plasma, a feedback control of vertical position is necessary to suppress a positional instability. The instability of plasma with non-circularity of 1.37 was suppressed by this operation. The observed growth rate without the feedback control was $70s^{-1}$ and this value is consistent with a calculated one, taking account of passive feedback effects of the vacuum vessel and poloidal coils.

2.4 Joule heated plasma results[2)]

For the initial experiment, JFT-2M was operated as a circular and weakly non-circular tokamak with the following parameters, $B_T \leq 14.2$kG, $\kappa=1$-1.37, $R_0=1.21$-1.31m, $a=0.25$-0.35m, $I_p=130$-300kA, $q_a=2$-5, $\bar{n}_e=1$-$3.5\times 10^{13}cm^{-3}$, $\bar{Z}=2.5$-6, and pulse length$\sim$0.5s. Typical time evolutions of plasma parameters for a weakly non-circular hydrogen discharge of 200kA are shown in Fig.II.2-2. The ellipticity of this plasma was determined as 1.16 from the numerical calculation of equilibrium configuration including effects of iron core as shown in Fig.II.2-1. The electron temperature was measured by $2\omega_{ce}$ emission of 70.6 and 78.4 GHz and its absolute value was calibrated by Thomson scattering measurements; $T_e=1200\pm200$eV at 250ms. The ion temperature was measured at z=0 and z=−10 cm from perpendicular direction and its maximum value is 670 ± 70eV, which is in good agreement with the Artsimovitch scaling. The maximum electron density determined by microwave interferometer is $3.5\times10^{13}cm^{-3}$ which corresponds to the Murakami coefficient of 3.5. Radiation loss power monitored by bolometric detectors was fairly constant during

discharge period. Impurities observed by VUV spectrometer are C, O and FeIX-FeXX and their time behaviors of CVI, OVI and FeXIX are shown in Fig.II.2-3. The absolute values of the impurity concentration are now under calibration.

The electron temperature profile of $2\omega_{ce}$ at t=300ms measured by scanning the toroidal field strength is shown in Fig.II.2-4 with ion temperatures at z=0 and z=-10cm. Using these profiles and electron density profile assumed as parabolic distribution, the gross energy confinement time and effective ion charge, $\bar{Z}$ could be obtained as shown in Fig.II.2-2, and these values at 300ms are τ_E=23±5ms and $\bar{Z}$=4.5±1. This confinement time is almost the same as that expected by ALCATOR type scaling ($\tau_E=10^{-18}\bar{n}a^2$). The position of q=1 surface calculated from the electron temperature profile is in good agreement with that from q=1 surface determined from the sawtooth oscillation.

An attempt to obtain low q discharge was carried out with careful control of plasma current built up, position control and gas puffing. Thus we could obtain a discharge of q_a=2. In this case, the current rise time and plasma position was adjusted so as to pass through the unstable region of q_a=3 at the speed of $\dot{q}$=1.2/50ms. Typical parameters of this discharge were I_p=300kA, V_L=1.8V, $\bar{n}_e=3.5\times10^{13}cm^{-3}$, $T_e(0)$=1keV, and τ_E=15-20ms. Its electron temperature profile is fairly broader than that of q_a=3 discharge as shown in Fig.II.2-4 (dotted line).

In the initial operation, intense hard X-ray emission was detected. In order to decrease runaway electrons, we attempted to pre-ionize the plasma with a small capacitor bank (50μF) at 5ms before main capacitor bank discharge. With this pre-ionization, a breakdown voltage decrease from 15V to 10V (Fig.II.2-5) and hard X-ray intensity was reduced to less than one hundredth. $2\omega_{ce}$ intensity without pre-ionization is larger than that of with pre-ionization. This may suggest that the production of high energy electrons is suppressed by sufficient pre-ionization.

References

1) Shoji, T., et al., "An outline of the JFT-2M device", JAERI-M 83-194 (December 1983).

2) Shoji, T., et al., "Results from the JFT-2M experiments", Proc. of the 11th Europ. Conf. on Controlled Fusion and Plasma Physics (Aachen) 1, (1983) 55.

3) Schneider, F.: Operation of the ASDEX Feedback Control System, 11th Symp. on Fusion Techn. Oxford (1980).

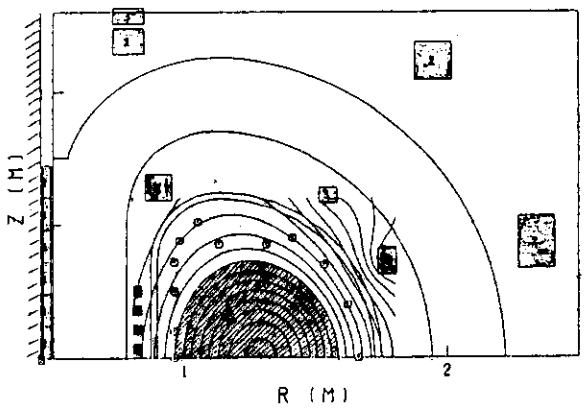

Fig. II.2-1
Calculated magnetic configuration for typical 200 kA plasma with ellipticity of 1.16. Plasma region is shaded and the poloidal coil system is also shown.

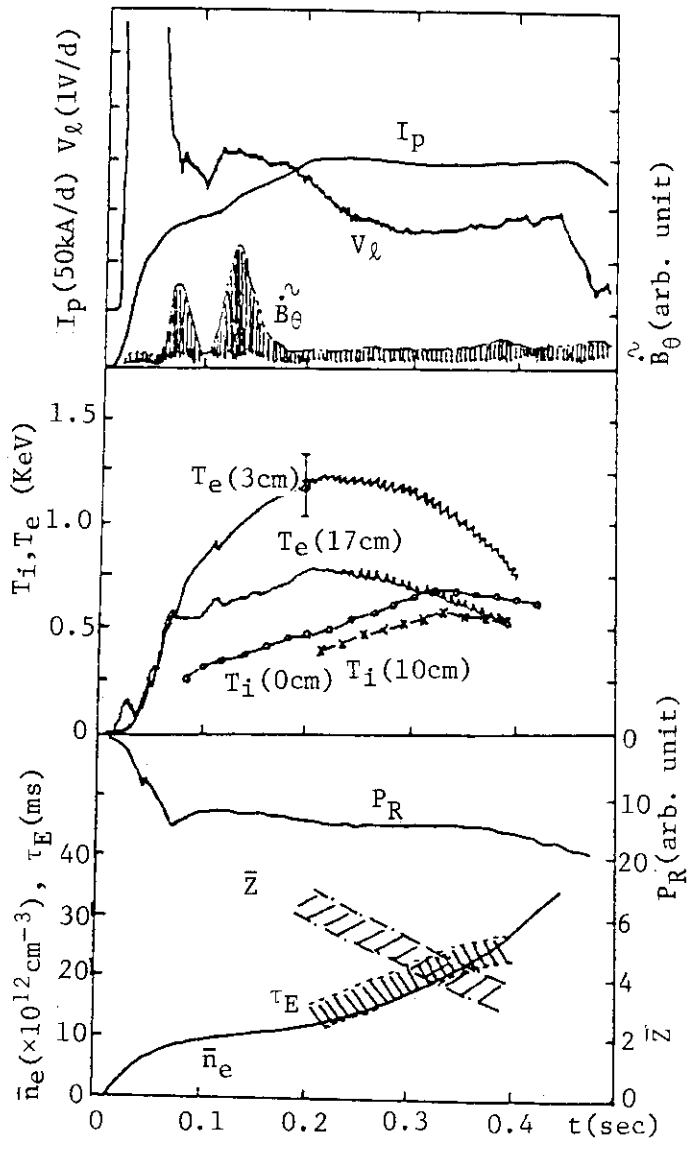

Fig. II.2-2 Plasma parameters for 200 kA discharge

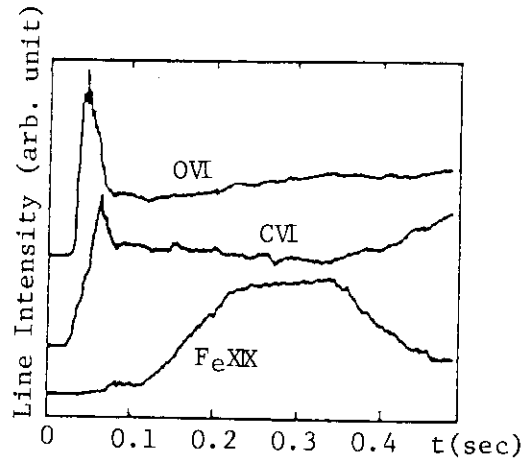

Fig. II.2-3
Typical impurity line intensities for 200 kA plasma

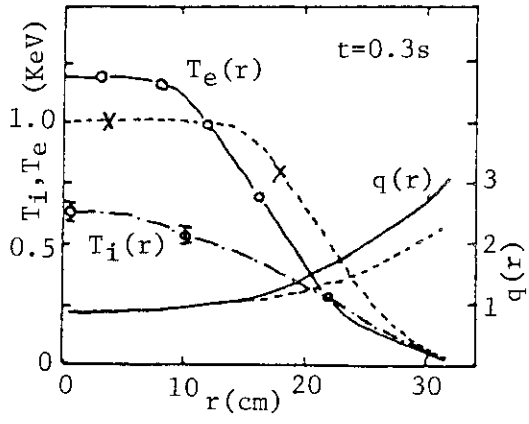

Fig. II.2-4
T_e, T_i and estimated q profiles. Solid line for 200 kA, dotted for 300 kA.

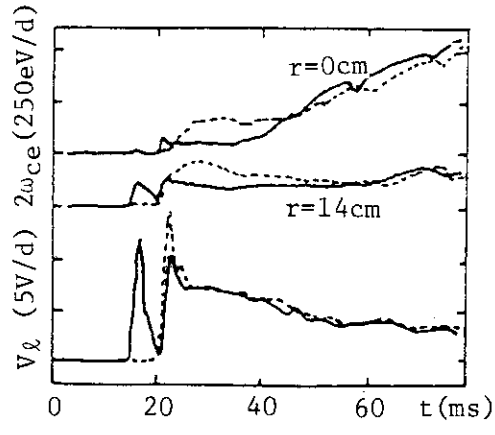

Fig. II.2-5
Effect of pre-ionization by a small capacitor bank So. Solid line with So bank, dotted line without So bank.

3. Ion Cyclotron Range of Frequency (ICRF) Heating

3.1 Introduction

The second harmonic ICRF heating is successfully demonstrated in a NBI heated plasma. Both electron and ion temperature increases by applying rf power, and the increase is consistent with a magnetic measurement. Enhanced impurity contaminations were observed during the rf heating and the contamination may be due to sputtering of materials of wall near the antenna and the Faraday shield by ions accelerated by the rf electric field near the antenna.

In the following, these results are briefly described.

3.2 RF system and antennae

The rf generator is operated at 38 MHz which is the second harmonic cyclotron frequency of protons with the toroidal magnetic field B_T=12.5kG. The output power of generator which has single TH116 power triode is about 0.8MW at the 50Ω dummy load, and the maximum pulse duration is 50ms. There are two types of loop antenna, those are, low field side (LFS) and high field side (HFS) antennae. They are shown in Fig.II.3-1(a)-(b). The LFS antenna is bent to the toroidal direction so as to avoid an interference with a horizontal port section. The radiative part of these antennae is 50 cm long, and the width of center conductors is 7 cm. The design of the Faraday shield which is made of titanium is optimized so as to minimize an ohmic loss at the shield screen.

The coupling resistance is critically dependent on the horizontal position, and is about 1 Ω for LFS antenna and 2 Ω for HFS antenna in an ordinary operation, where plasma is shifted about 4-5 cm inward during the heating phase. The circuit loss in the antenna is about 0.3Ω, which is mainly attributed to an ohmic dissipation in the feeder between the vacuum feedthrough and the radiative part.

3.3 Heating experiment[1,2)]

In a tokamak plasma, it is known that the minority hydrogen in a deuterium plasma produces two-ion hybrid resonance layer at the higher magnetic field side of the fundamental cyclotron resonance layer of minority protons. The impressed ICRF field generates a fast magnetosonic wave beyond the evanescent region in the peripheral plasma. This wave propagates to the hybrid resonance layer and is converted to an ion Bernstein wave near the layer. The energy of the wave which is

converted to the ion Bernstein wave is efficiently transferred to the three species of particles, deuterons, protons, and electrons.

In second harmonic heating case, in which minority component is absent, a mode coupling layer also exists at the high field side of the second harmonic cyclotron resonance layer as in the two-ion hybrid scheme. The thickness of this layer is proportional to $\beta_i R_0$, where β_i is the local ion toroidal beta value and R_0 is the major radius. In this layer, mode coupling to ion Bernstein waves and enhanced harmonic cyclotron damping can occur[3]. We can thus expect a plasma heating in the second harmonic regime.

Typical experimental conditions are as follows; the plasma current I_p=150-170kA, the toroidal magnetic field B_T=12.5kG, in which a second ion cyclotron layer is at the center of plasma, and the line average electron density $\bar{n}_e$=2-3 $\times$ $10^{13}cm^{-3}$. Target plasma for ICRF heating is heated up by 500kW neutral beam co-injection.

In the case of the second harmonic heating, the following merits are expected in the NBI heated plasma; (i) a higher temperature and β_i plasma absorbs the rf power more effectively, (ii) a high energy ion component produced by NBI enhances the absorption of rf power, (iii) power deposition from the neutral beam stabilizes the disruption by compensating the radiation loss. Thus, 600kW of rf power has been coupled to the plasma by the assist of NBI. In the following experiments, the rf power is applied to the 30ms after the NBI on, when the increase of ion and electron temperature are almost saturated. The NBI heating power is 500-550kW.

Figure II.3-2 shows increment of electron and ion temperatures as a function of the rf input power, and $\Delta(\Lambda + 1/2)$. The increment of electron and ion temperatures increases almost linearly as the rf power increases. The increment of the plasma pressure measured with magnetic probes also increases linearly up to the maximum power. Appreciable difference between the case of high field side and low field side excitation was not found.

Clear dependence of the heating characteristic on the hydrogen beta value can be obtained in a hydrogen plasma with deuterium impurity. Because the second harmonic ion cyclotron frequency for hydrogen is the fourth harmonics for deuterium. The mixture of deuterium slightly changes the propagation characteristics of the fast wave, but it mainly changes the absorption characteristics through the hydrogen beta value

which control the mode coupling between the fast wave and ion Bernstein wave. Figure II.3-3 shows the increment of the electron and ion temperatures and $(\Lambda+1/2)$ as a function of hydrogen concentration ratio of hydrogen-deuterium two ion plasma with the injection of a hydrogen neutral beam. $\Delta\Lambda$ increases with the increase of a hydrogen component. This means that the absorption of the rf power is determined by a hydrogen component which has the second harmonic resonance at the center. The electron temperature also increases with the increase of the hydrogen concentration. On the contrary, the increment of the hydrogen temperature decreases as a hydrogen concentration. This observation indicates that the rf power is absorbed by electrons with the increase of hydrogen pressure.

Time evolution of plasma parameters before and during the NBI and ICRF heating are shown in Fig.II.3-4. The rf power is applied 30ms after the initiation of the NB co-injection. With 540kW of the NBI, the plasma is heated up to T_i=0.8keV and T_e=0.65keV.

Then 550kW of the ICRF power heats the plasma up to T_i=1.05keV and T_e=1.0keV. The increment of plasma pressure $\Delta\beta_p$ from the joule phase to the NBI heated phase is 0.2 and from the NBI heated phase to the ICRF heated phase is 0.4. The electron density increases by about 20% during the ICRF phase, compared to the NBI heated phase. The loop voltage V_L increases about 0.5V compared to the case without the NBI but immediately decreases. The increment of a radiation loss is less than 70% of the rf input power, but still too large compared to the NBI heated phase. Figure II.3-4(c) shows the electron temperature profile before and during the rf heating. Large sawtooth activities can be observed in the figure, and those are also observed in $(\Lambda+1/2)$ signal. The sawtooth oscillation suggests that the electron absorbs the rf power in a relatively narrow region.

The dotted line in Fig.II.3-4(a) shows the case that the NBI is stopped at 405ms. The $(\Lambda+1/2)$ signal decreases only 0.1 compared to the case where the NBI is fully combinated, and significant difference is not observed in the loop voltage. Applying 500 kW of the rf power to the joule plasma, the plasma is disrupted within 5ms. On the other hand, if the plasma is sufficiently heated up, the plasma is not disrupted by the rf power even without the NBI and the plasma pressure continues to increase. This indicates that the pressure of the target plasma is a very important parameter for the second harmonic heating.

3.4 Summary of second harmonic heating

The second harmonic ICRF heating was successfully demonstrated in the JFT-2M tokamak. The heating results are summarized as follows.

1. Both electron and ion temperatures increase by applying rf power. The increase of the plasma energy is confirmed in the magnetic measurement of the poloidal beta.
2. There is a tendency that the more hydrogen pressure increases, the more percentage of rf power is absorbed by electrons.
3. If the plasma is sufficiently heated up, the plasma pressure continues to increase after the turn off of NBI heating. This suggests that very gradual increase of the rf power can lead to the high power second harmonic ICRF heating.
4. Significant differences are not observed between LFS and HFS excitation. An appreciable part of the rf power is absorbed by electrons. This results is inconsistent with the theoretical works using 1-D kinetic full wave equation in a bounded plasma[3]. The electron heating may be due to Landau damping via mode converted ion Bernstein wave. The above results suggest that the mode conversion might be stronger than the present theoretical predictions.

3.5 Impurities during the ICRF heating[4]

The line-integrated emissions from low ionization state impurity ions, which are, OIV (wave length λ=238.4Å, ionization potential IP= 77.4 eV), CIV (λ=312.4 Å, IP=64.5 eV), FeX (λ=174.5 Å, IP=271.7 eV) and TiXI (λ=386.1 Å, IP=279.9 eV), were radiated at the peripheral region of the plasma. For example, a radiation profile of FeX shows that this state exists in a shell about 5 cm width at the radial location r=25 cm.

Figure II.3-5 shows a typical time evolution of the line-integrated intensities of FeX, TiXI, OIV and CIV lines measured along the central chords. The intensities of the line emission are the function of the electron density and temperature, and the impurity ion density. In this experiment, the change of the electron density and temperature, in the region where the emission from those metal ion concentrates is small compared with that of the intensities of these impurity spectral lines. Thus it was considered that the change of the intensities are due to the density change of the impurity ion (Fe^{9+}, Ti^{10+}). In the first approximation, the change of impurity ion density is due to the

influx of the impurity ions.

Figure II.3-6 shows an increment of those line emissions during ICRF heating phase, as a function of the rf power. Increases of these line emissions are saturated within 10 ms after the start of the rf pulse, so the increment of the line emissions are plotted at that time.

Increases of impurity emissions during the additional heating were compared between the ICRF and NBI with almost the same heating power. From these figures we can see that the increment of light impurity emission during the ICRF heating is about two times as large as that of NBI heating phase. On the other hand, an increment of metal impurity emissions is five times for LFS and seven times for HFS as large as that of the NBI.

The simultaneously measured boundary electron temperature (T_{eb}) and density (n_{eb}) are also shown in Fig.II.3-7 as a function of the rf power. T_{eb} is 7-9 eV at OH phase and 13-14 eV at 540 kW NBI phase. In ICRF heating phase, T_{eb} increases with the increase of the rf power increases, and the increment of T_{eb} by the rf is 1.5 times (for HFS) and 3 times (for LFS) as large as that of the NBI with the same power. n_{eb} decreases to about 70% of the NBI heating phase.

We can consider a sputtering by ions accelerated by a sheath potential as a cause of impurity release from the wall. Thus it is significant to know the relation between the intensities of line emission from impurity ions and the boundary electron temperature, because the sheath potential is determined by the boundary electron temperature and given by 4 T_{eb}. Figure II.3-8 shows intensities of the impurity line emissions as a function of T_{eb}. This indicates that in an OH and NBI heating phase, all of those impurity emissions are closely correlated to the boundary electron temperature. In the ICRF heating phase, carbon impurity emissions are also proportional to T_{eb}. On the other hand, metal impurity emissions such as TiXI, FeX are enhanced compared with the OH and NBI heating phase.

From these results, we can conclude that the carbon impurity, which is limiter material, is released from the limiter mainly by the sputtering induced by the ions accelerated by the sheath potential in the OH and NBI heating phase. In the ICRF heating phase, a carbon impurity is also released by the same mechanism. On the other hand, another mechanism must be considered as a cause of the metal impurity release during the ICRF heating phase.

The difference between LFS and HFS excitation may be caused by the difference of the electron density, because the averaged line density in the case of the HFS experiments is a factor of 1.5 as large as that in the case of LFS experiment.

A source of titanium impurities is mainly the Faraday shield of the ICRF antenna because titanium is not used in the other part of the vacuum vessel. On the other hand, the source of iron impurities is not directly identified from the instrumental materials, because the iron is used everywhere in the vacuum vessel. But we can infer the source of iron as follows; the emission of the iron impurity has the same dependence on the T_{eb} as that of the titanium impurities. If the source of the iron is not localized near the antenna, the emission from carbon impurity should increase in the same way as the iron impurity, since carbon is a limiter material. However, the increase of the emission from a carbon impurity has the different dependence on the T_{eb} as that from an iron impurity. Thus, we can infer that the source of the iron impurities is the antenna and/or the neighbourhood of the antenna.

3.6 Summary and discussion of impurity problem during the ICRF heating

Impurity behaviour during ICRF heating is observed in JFT-2M. The experimental results are summarized as follows:

1) In the ICRF heating phase, the increment of light impurity emissions such as OIV and CIV are a factor of 2 as large as that of the same power NBI heating. On the other hand, that of metal impurity emissions by the RF such as FeX and TiXI are a factor of 5-7 as large as that of the NBI.
2) In the ICRF heating phase, a carbon impurity line emission intensity is roughly proportional to T_{eb}, but metal impurity intensities are enhanced compared with the OH and NBI heating phase.
3) The difference in impurity release between LFS and HFS exitation experiment is not recognized.

From these results, we conclude as follows:

1) A carbon impurity (limiter material) was released by sputtering by the ions accelerated by the sheath potential, and may not correlate to the additional mechanism induced by the rf power.
2) Metal impurities such as titanium and iron are released by some additional mechanism by applying the RF from the antenna or near the antenna during the ICRF heating phase.

Sputtering induced by ions accelerated by the electric field near the antenna is one of the possible mechanism for the metal impurity release. Three dimensional ICRF full wave code shows that such an electric field is formed in the vicinity of the antenna edge by a reactive part of an antenna loading impedance[5]. In that calculation, an ion energy inducing sputtering is proportional to the rf input power.

References

1) K. Odajima et al., JAERI-M 83-190.

2) K. Odajima et al., 4th Joint Varenna-Grenoble Symp. on Heating in Toroidal Plasma (Rome), CI2 (1984).

3) A. Fukuyama, et al., "Study of ICRF Waves in Second Cyclotron and Two-ion-hybrid Resonance Heating" Research Report HIFT-86 (Hiroshima Univ., 1983).

4) H. Ogawa et al., International Conference on Plasma Surface Interaction (Nagoya, 1984), to be published in Jr. of Nuclear Materials.

5) S-I. Itoh, et al., 4th Joint Varenna Grenoble Symposium On Heating in Toroidal Plasma (Rome), C23 (1984).

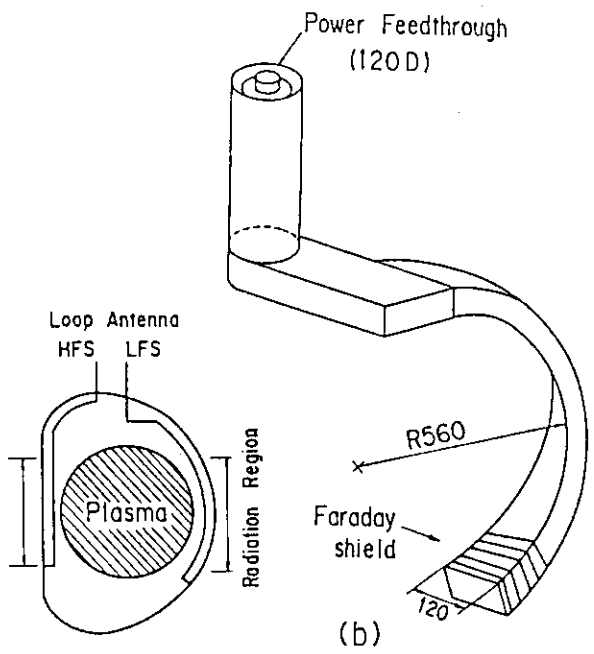

Fig. II.3-1 Low field side (LFS) and high field side (HFS) antennae.

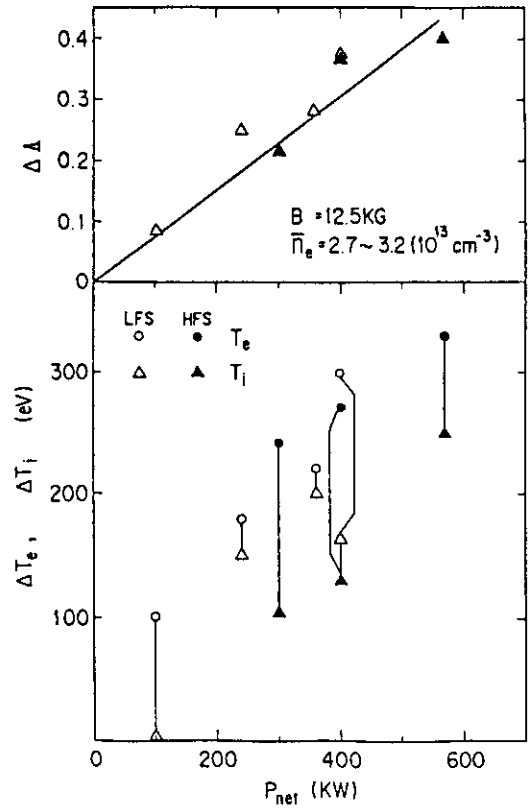

Fig. II.3-2 Power dependence of ICRF heating

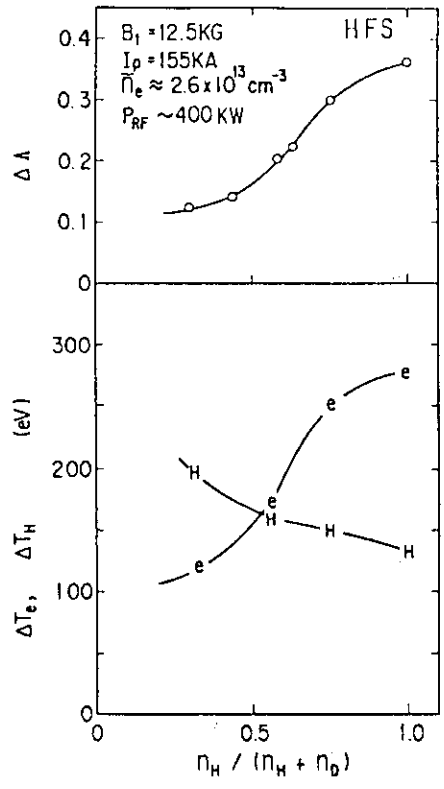

Fig. II.3-3 Increment of electron and ion temperature, and Δ (Λ+1/2) vs. hydrogen concentration.

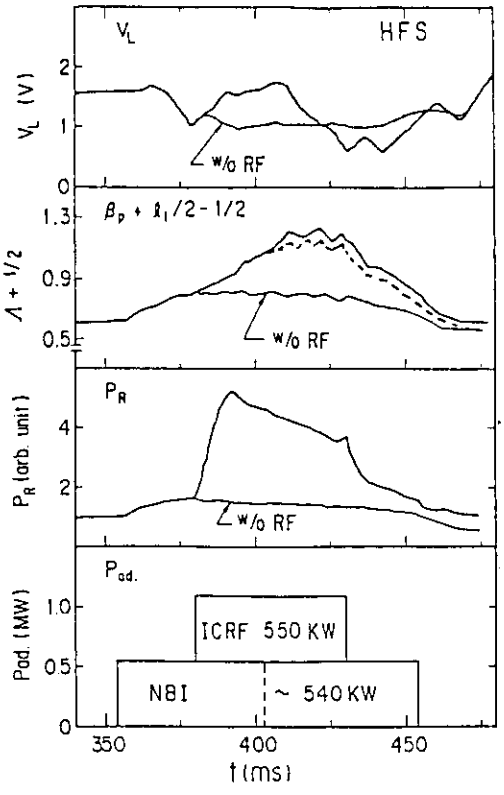

Fig. II.3-4(a)

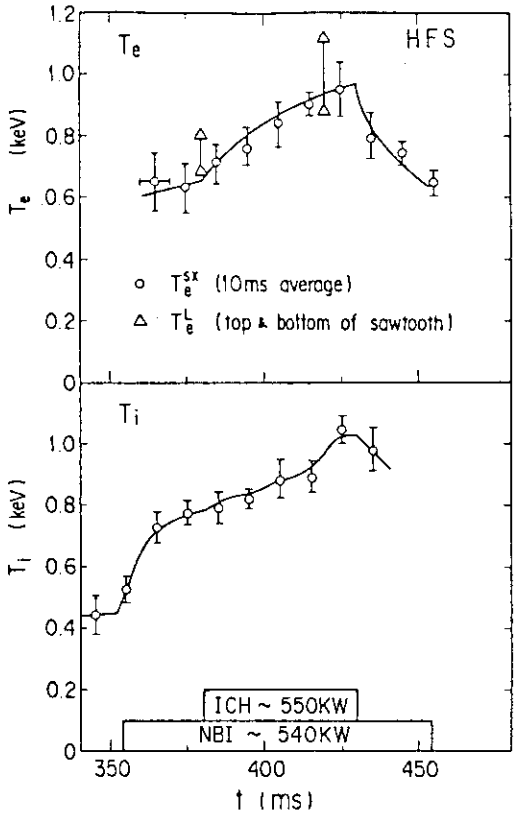

Fig. II.3-4(b)

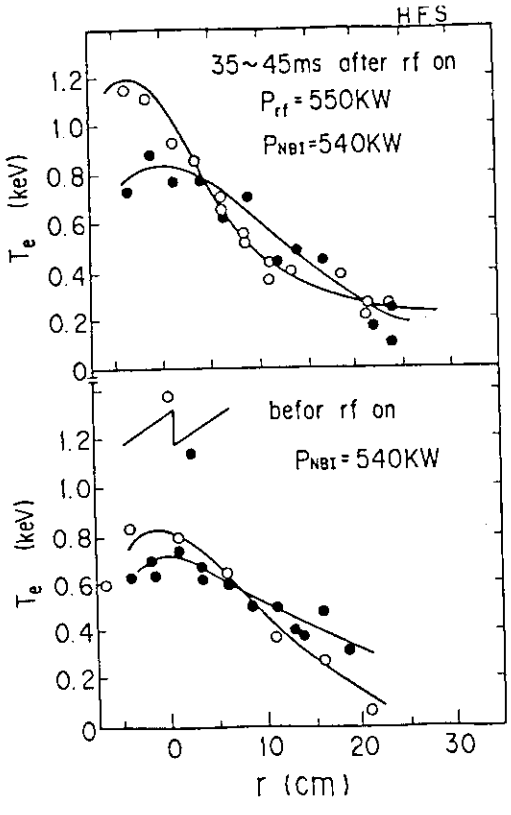

Fig. II.3-4(c)

Fig. II.3-4 Time evolution of plasma parameters before and during ICRF heating, and profile of electron temperature (c).

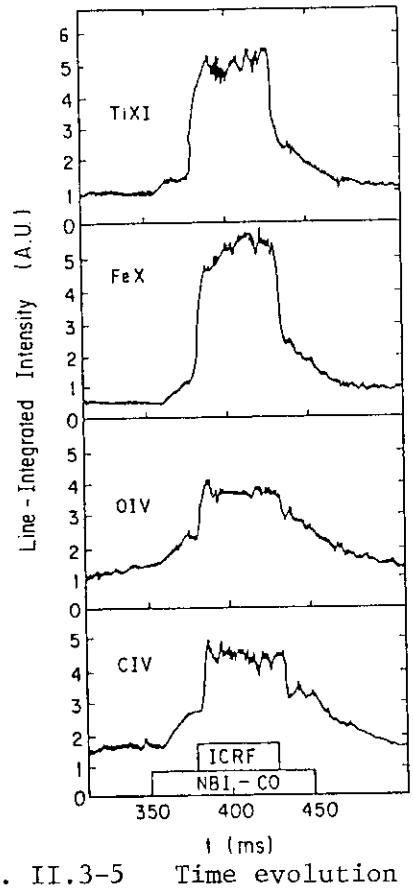

Fig. II.3-5 Time evolution of emissions from CIV, OIV, FeX and TiXI lines.

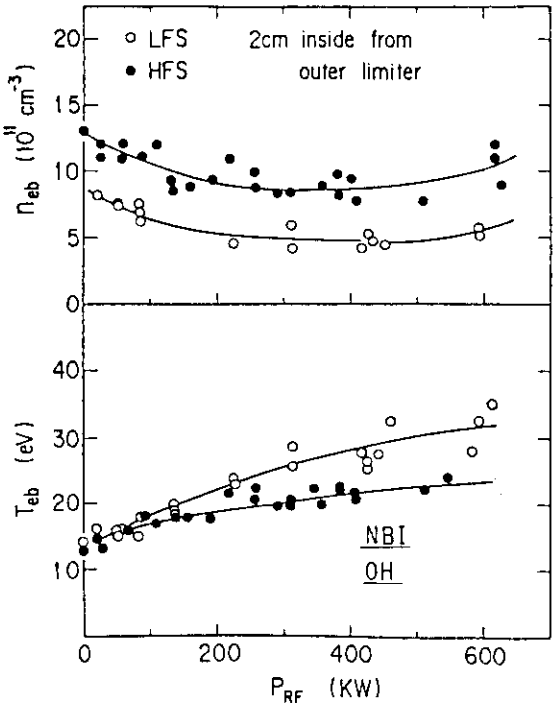

Fig. II.3-6 Electron temperature and density in the scrape-off layer.

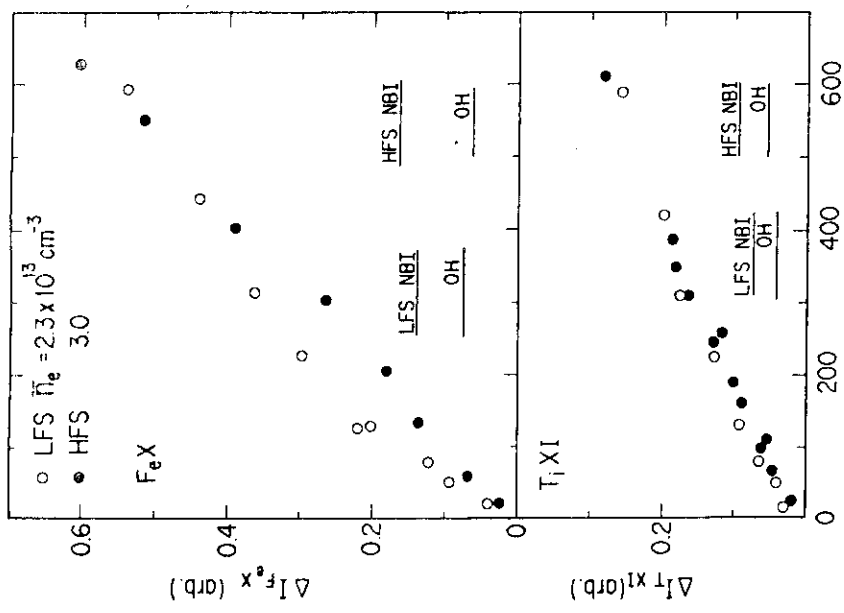

Fig. II.3-7(b)

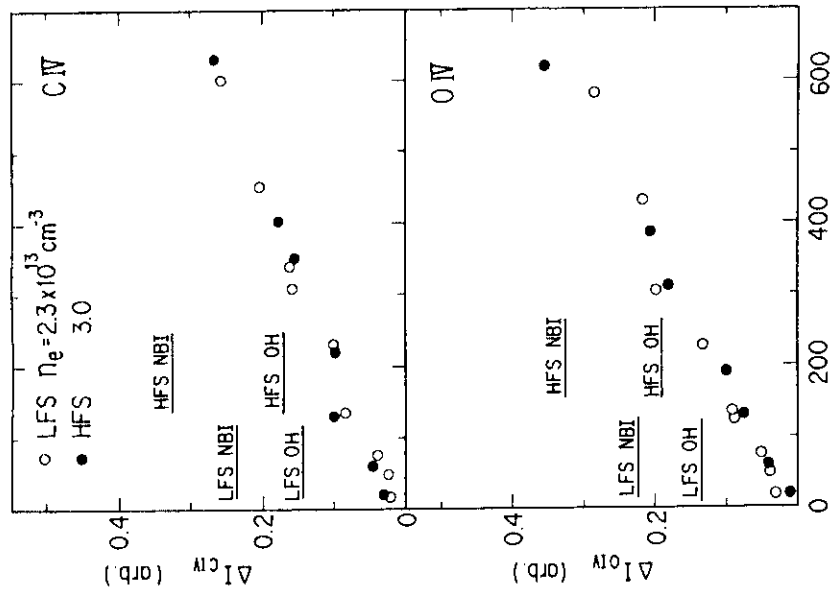

Fig. II.3-7(a)

Fig. II.3-7 Increment of impurity line emissions, level of the emission in OH and NBI heating phase are indicated by OH and NBI.

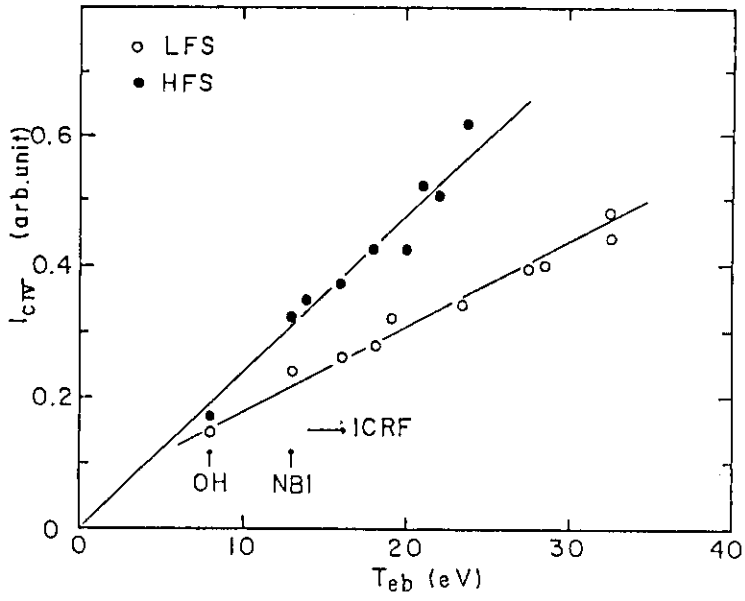

Fig. II.3-8(a)

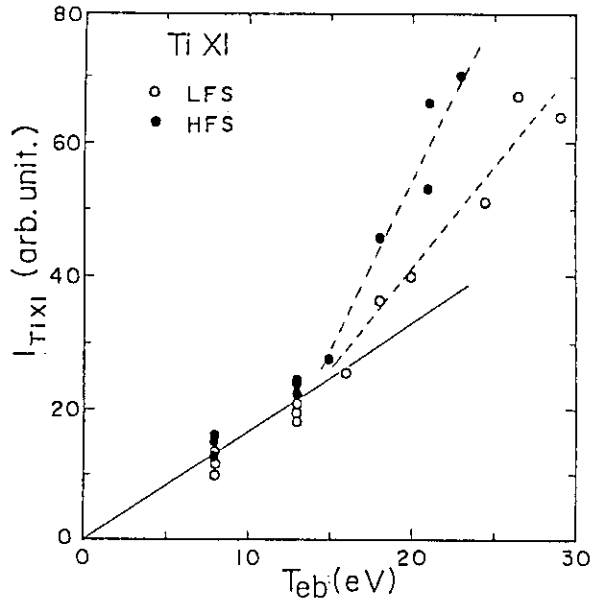

Fig. II.3-8(b)

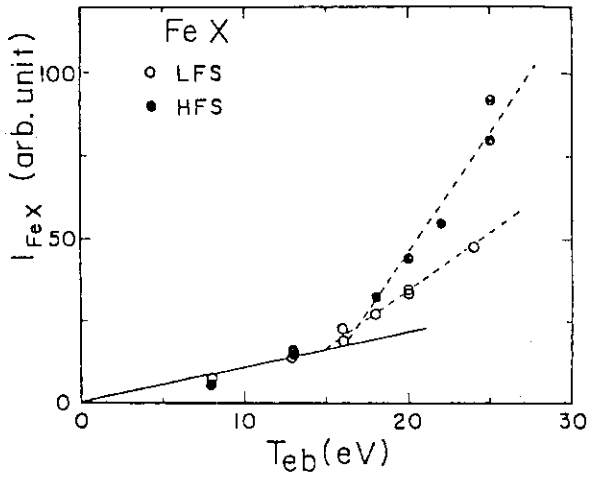

Fig. II.3-8(c)

Fig. II.3-8 Intensities from impurity ions vs. the boundary electron temperature (T_{ed}).

4. Lower Hybrid Current Drive in the JFT-2M Tokamak

4.1 Introduction

The current drive experiments by lower hybrid waves with V_{ph}/V_{te}= 4-5 were carried out in the JFT-2M tokamak. Two different tokamak operations, ACR and AVR modes were employed to investigate the plasma control during the lower hybrid current drive. In the ACR mode, the current of the poloidal field coils which produce the main magnetic flux is controlled by the thyristor power supplies, while the voltage of them does in the AVR mode. The ACR mode is the ordinary tokamak operation in the JFT-2M.

A high current drive efficiency was obtained and the efficiency increases in proportion to $I_p^{1.5-2}$ up to I_p=150 kA. The interaction of the excited lower hybrid waves with electrons was investigated by the pulse height analysis of the soft X-ray signals. It is shown that the soft X-ray energy spectrum is consistent with that expected from the theoretical spectrum of the launcher.

4.2 Tokamak operation for lower hybrid current drive

The RF system employed in the lower hybrid current drive experiments is the same as that of JFT-2[1]. The RF power source generates a maximum power of 600 kW at a frequency of 750 MHz. The power spectrum of the waves excited by a four waveguides launcher has a peak near n_z=5 and a full half width of Δn_z=7 when the phase difference between the neighboring waveguides is 90 degrees. The ratio of the parallel phase velocity of the excited waves to the electron thermal velocity at a temperature of 1 keV is about 5. The lower hybrid waves with the phase velocity of $V_{ph}=5V_{te}$ are expected to interact with the bulk thermal electrons[2].

The control of the poloidal magnetic field plays an important role in the RF current drive experiments. The RF power interacts with the power supplies of the poloidal field coils through the plasma. When the RF power is applied, the loading resistance of the plasma against the primary power supplies decreases because of the unidirectional acceleration of the electrons by the lower hybrid waves. Consequently, the voltage or current of the primary power supplies change responding to the RF pulse. The poloidal field power supplies of the JFT-2M can be operated in both automatic current regulation (ACR) and automatic voltage regulation (AVR) modes.

The time evolution of the plasma parameters, and the voltage and current of the poloidal field power supplies in the case of the ACR mode is shown in Fig.II.4-1. The solid line shows the results in the presence of the RF and the dotted line indicates those in the absence of the RF. When the RF is applied, although the plasma current shows a small increase, the loop voltage of the plasma as well as the voltage of the poloidal field coils drops nearly to zero responding to the RF pulse. The current of them stays constant. In the ACR mode, the current drive is shown mainly by the loop voltage drop. The cyclotron emission from r=-12 cm and r=-24 cm shows rapid increase as the RF is applied. This means the presence of the high energy electrons accelerated by the lower hybrid waves. The larger increase of the cyclotron emission from r=-12 cm indicates that the strong interaction between the lower hybrid waves and the electrons occurs at the center part of the plasma rather than the peripheral region. The effective driven current deduced from the loop voltage drop is about 100 kA. The electron temperature measured from the energy spectrum of the soft X-ray signals shows an abrupt decrease. A decrease of the electron temperature is caused by a lack of the RF power compensating a reduction of the joule input power. The loop voltage drop is inversely proportional to the electron density up to $\bar{n}_e=6\times10^{12}cm^{-3}$. Above $\bar{n}_e=1\times10^{13}cm^{-3}$ no loop voltage drop is observed.

In the AVR mode, the current drive is shown by the change of the plasma current. The time evolution of the plasma parameters, and the voltage and current of the poloidal field coils is shown in Fig.II.4-2. The plasma current rises slightly in contrast to the case of no RF. The loop voltage reduces to be nearly zero and the voltage of the poloidal field stays constant. The current of the plasma equilibrium field coil shows a large increase responding to the change of the plasma current. From the analysis of the tokamak circuit in current drive, it is indicated that the decay time of the joule current is about 50 ms, and after that decay time the plasma current is sustained only by the RF power. Therefore, if we have a CW power source the plasma current will be sustained up to the limitation of the power supplies of the tokamak machine.

The efficiency of the current drive defined by $\eta=I_{rf}/P_{rf}\cdot\bar{n}_e$ (A/W $10^{13}cm^{-3}$) is shown in Fig.II.4-3. The efficiency increases with the plasma current both in the ACR and AVR modes. The same relation is

obtained in the cyclotron emission and the soft X-ray signals. From the experimental observations that the current drive efficiency does not depend on whether the high energy electrons exists just before the RF is applied or not, the plasma current dependence of the efficiency means that the higher plasma current leads the stronger interaction of the waves with the electrons because of the higher bulk electron temperature. And also the confinement of the fast electrons produced by the waves is considered to be dependent on the plasma current.

4.3 Investigation of fast electrons by soft X-ray measurements

The high energy electrons produced by the lower hybrid waves can be investigated by energy spectrum of the soft X-ray signals. We used a fast pulse height analyzer for energy spectrum analysis of the soft X-ray signals. The energy range of fast electrons is determined by the power spectrum of the excited lower hybrid waves. Typical energy spectra of the soft X-ray signals as a parameter of the phasing of the launcher are shown in Fig.II.4-4. The observed energy spectra agree qualitatively with those expected from the Brambilla theory. This agreement shows that the fast electrons are produced by the resonant absorption of the RF energy. The rise time of the high energy electron tail in the electron distribution function deduced from the time behavior of the energy spectra coincided with the decay time of the loop voltage drop in the ACR mode. This characteristic time increases with increasing the electron density and decreases with increasing the plasma current. The electron density dependence of the characteristic time is $\tau \propto \bar{n}_e$. While a theory[3] gives that the characteristic time of the modification of the electron distribution function is inversely proportional to the electron collision frequency. This discrepancy indicates that the another mechanism has to do with the lower hybrid current drive.

4.4 Conclusion

In conclusion, we have obtained following results.

1) Interaction of the electrons with the lower hybrid waves is consistent with the Brambilla theory. The fast electrons are produced by the resonant absorption of the waves.
2) Efficiency of the current drive about η=1 is attained and it is improved with increasing the plasma current.
3) Tokamak operation in the lower hybrid current drive is investigated

and it is shown that the control of the poloidal field is important in RF current drive.

References

1) N. J. Fisch, Phys. Rev. Lett. 41, (1978) 873.

2) T. Yamamoto and JFT-2 Group, in Proceeding of the IAEA Technical Committee Meeting, Culham Laboratory, 1983, Vol. I, p.224.

3) C. F. F. Karney and N. J. Fisch, Phys. Fluids, 22, (1979) 23.

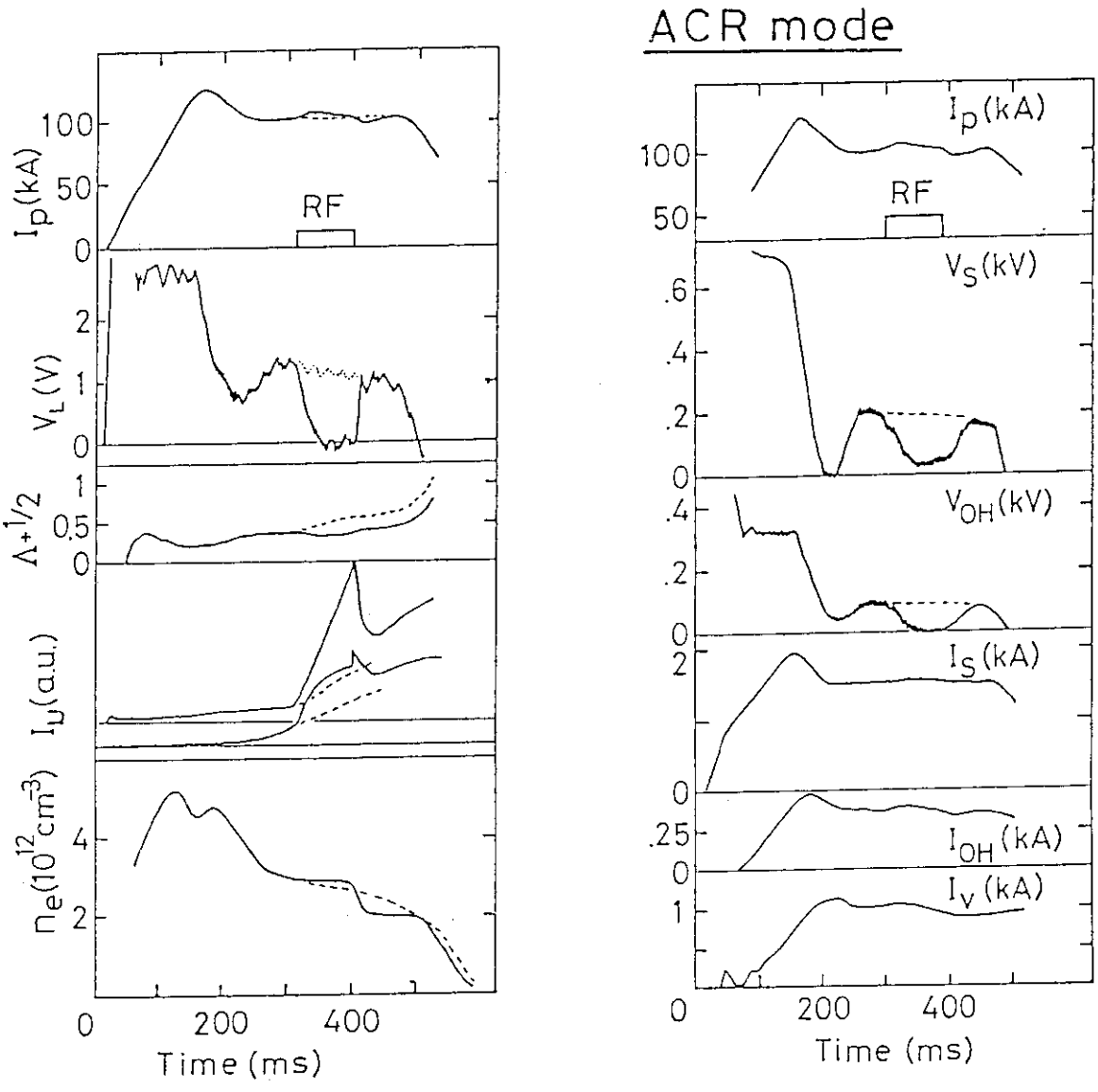

Fig. II.4-1 Time evolution of the plasma parameters, and the voltage and current of the poloidal field power supplies in the ACR mode. The subscripts S, OH and V indicate the poloidal field coils of S-coil, OH-coil and the vertical field coil, respectively. The solid lines indicate the time behaviors with RF and the dotted lines show those without RF. The phase difference is $\Delta\phi$=75 degrees and the RF power is 65 kW. The toroidal field is 11 kG. The cyclotron emission (I_μ) from r=-12 cm is shown by upper curve and that from r=-24 cm is shown by lower one.

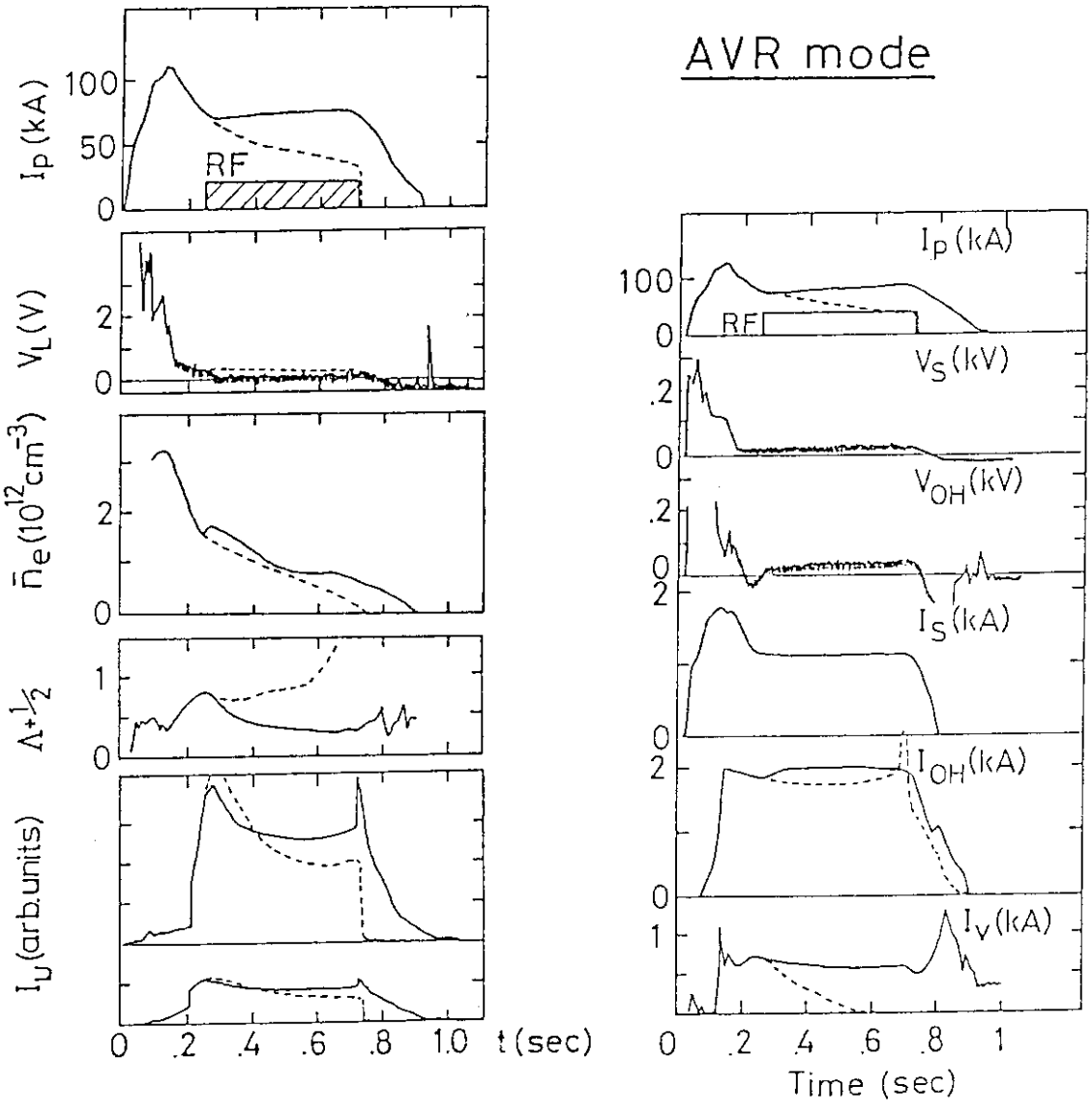

Fig. II.4-2 Time evolution of the plasma parameters, and the voltage and current of the poloidal field power supplies in the AVR mode. The RF power is 40 kW. The used symbols are the same as Fig. II.4-1.

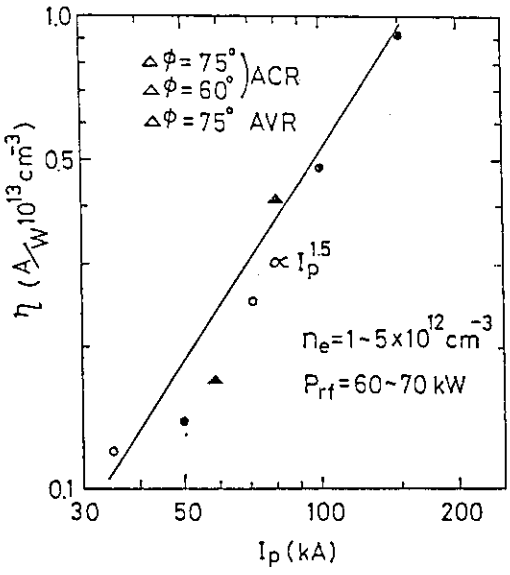

Fig. II.4-3 Plasma current dependence of the current drive efficiency. The efficiency is derived from the loop voltage drop in the ACR mode and the stationary current sustained by RF in the AVR mode.

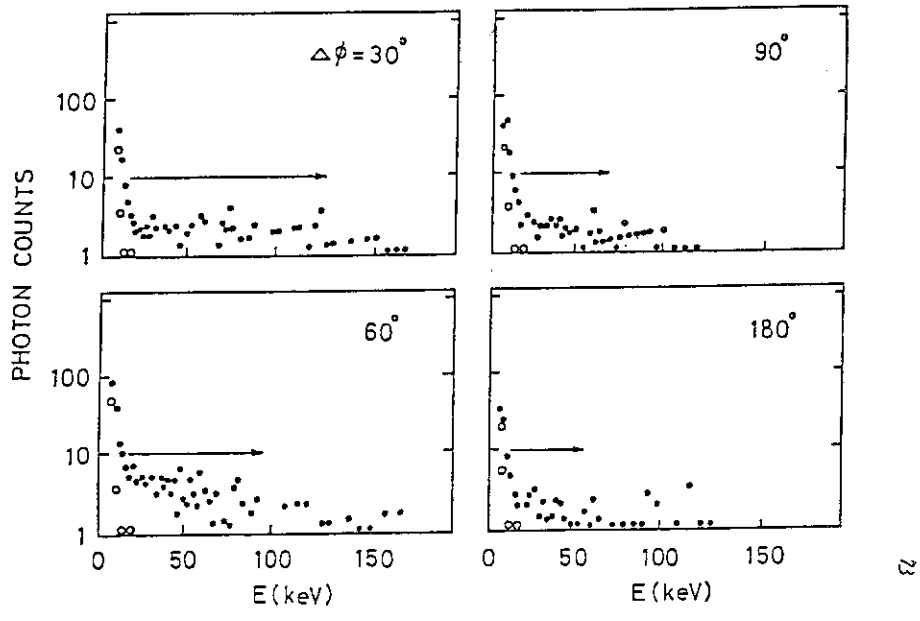

Fig. II.4-4 Energy spectra of the soft X-ray signals, taking the phase difference of the launcher as a parameter. The open and closed circles indicate the photon counts without and with RF, respectively. When RF is not applied, no high energy electrons is observed. The arrows in the figure indicate the energy region where the high energy electrons are producted by RF. The sampling time is 20 msec after RF was turned on. The sampling inetrval is 20 msec.

5. Development of a High Counting Rate Pulse Height Analyzer[1)]

New type pulse height analyzer (PHA) was developed and tested for tokamak plasma diagnosis. Main developing targets are as follows.

(1) Time resolving spectrum of X-ray or others can be measured at single discharge of tokamak plasma.

(2) In the near future, this type PHA will have capability of real time mode operation.

The trial PHA is the high counting rate 4 channel PHA by CAMAC standard interface, and the schematic diagram is shown in Fig.II.5-1. Each channel consists of lower level and upper level fast discriminators and main specifications are summarized in Table II.5-1. This PHA has ability to measure pulse signals at the maximum counting rate of 20 MHz. Analyzing levels of input pulses can be preset with digital values from CAMAC bus. Integral nonlinearities are less than 1.5% for all channels.

This PHA satisfied specifications in the measurement of the soft X-ray spectrum for the JFT-2M tokamak plasma. A typical time behavior of soft X-ray radiation is shown in Fig.II.5-2. The ordinate gives the counting rate of the analyzed soft X-ray signals. The detector was a lithium drifted silicon detector and four spectral windows (indicated as (1E) to (4E)) were preset in the range of 1.5 keV to 11 keV. The data labelled as (5E) are total counting rates of the detector signals. The spectral data can be measured at the total counting rate of more than 100 kcps. These results give good technical base for a practical fast PHA system.

Reference

1) MATOBA T., OGAWA T., KAWASHIMA H. and KIMURA T. : "Development of a High Counting Rate Pulse Height Analyzing System for Plasma Diagnosis", JAERI-M 83-162 (Sep. 1983).

Table II.5-1 Specifications of the trial fast 4 channel PHA.

Input signal	level -30 mV∿-1 V pulse width more than 15 nsec impedance 50 Ω
Window level	programable in 8 bits digital value
Output signal	level -0.7 V pulse width 5 nsec
Double pulse resolution (Dead time)	50 nsec
Integral nonlinearity	less than 1.5 %
Packaging	CAMAC #1 module

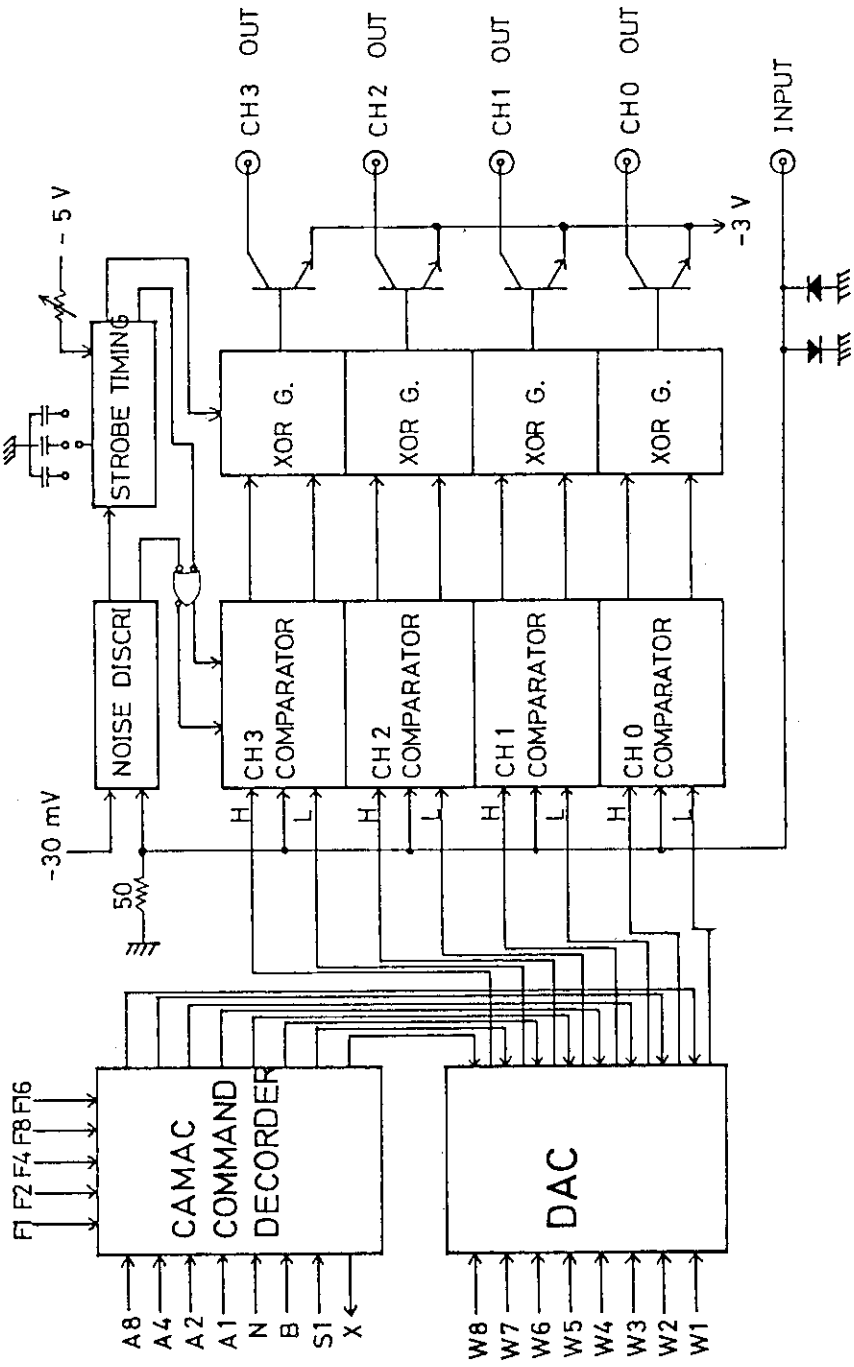

Fig. II.5-1 Schematicn diagram of the trial fast 4 channel PHA.

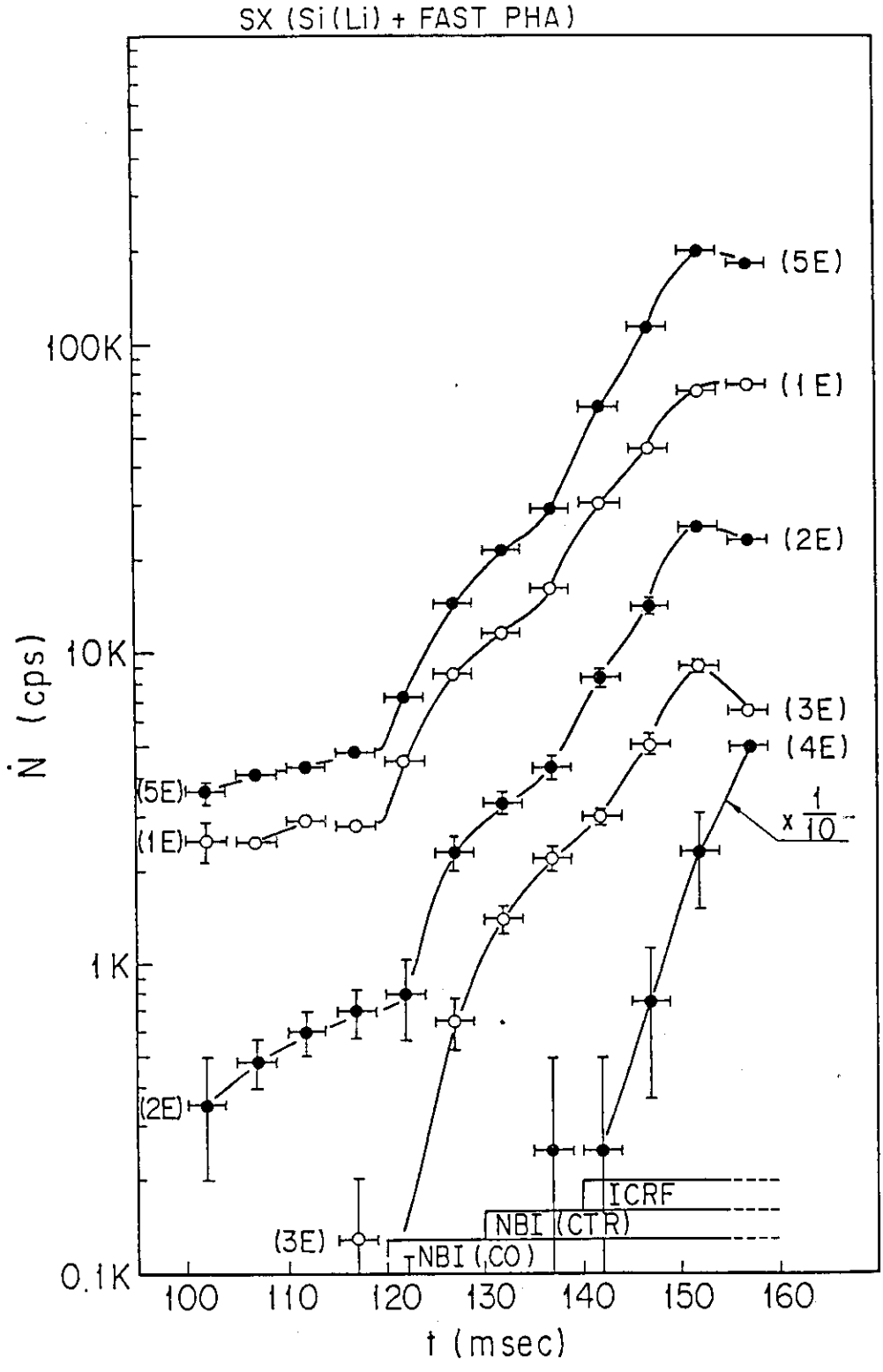

Fig. II.5-2 Time variations of the soft X-ray spectra in JFT-2.
NBI : neutral beam injection heating
ICRF : ion cyclotron range of frequency heating
(1E)-(4E) : counting rates for four window outputs of the fast PHA
(5E) : total counting rate

Ⅲ. OPERATION AND MAINTENANCE

1. Introduction

Facility Operation and Engineering Division has been engaged in operation and maintenance of JFT-2M tokamak. Neutral Beam Injection (NBI) system, Lower Hybrid Heating (LHH) device and flywheel motor-generator (MG), and development of auxiliary equipments and instruments. On April 27th, 1983 the first discharge on JFT-2M tokamak was ignited, and then it has been operated smoothly with NBI system, LHH device and MG on schedule without major troubles.

2. Operation and Maintenance

In this fiscal year, JFT-2M tokamak was begun to operate on April, and has been operated from April to June for Joule-heated plasma experiments. At the end of June the vacuum chamber was vented and antennae of ICRF were installed. From July to September the additional heating experiments (NBI, ICRF, LHH) were performed. In October the primary cooling water system was remodelled for the reinforcement and purifying the water. After that the machine has been operated smoothly in spite of a few troubles on turbomolecular pumps and on primary cooling system.

Complying with the operation schedule, NBI system has been operated smoothly during the experiments. For obtaining long pulse duration up to 200 ms beam dump, beam lines and drift tubes have been reinforced in heat resistance and control system has been remodelled. The waveform of 200 ms beam injection is shown in Fig.III.2-1. As the result of the remodelling, multiple-short-pulse injection experiments were accomplished.

LHH device has been also operated smoothly mainly for current drive experiments.

The operation schedule of JFT-2M, NBI, LHH and MG is shown in Table III.2-1.

3. Development of Equipments and Instruments

3.1 Pellet injection system

Present tokamak experiments rely on gas puffing to maintain the plasma density. Injection of solid hydrogen pellets at high speed has been proposed as a method of fueling more deeply into the hot core of the plasma. A single pellet injection system has been developed in

JAERI. The schematic diagram of the system is illustrated in Fig. III.3-1. Hydrogen gas is inlet to a disk-shaped stainless-steel pellet carrier with a thickness of 1 mm. The pellet carrier is covered by a double heat-shield plate at liquid-nitrogen temperature outside and liquid-helium temperature inside to avoid the heat transfer. There are two holes of 1 mm in diameter on the pellet carrier. In the lower hole the hydrogen is frozen, then the disk is rotated by 180° to change the hole position in line with gun barrel. The pellet is propelled forward to the chamber by pressurized helium gas, maximum pressure of which is 30 kg/cm^2, admitted by a fast magnetic valve. The propellant gas is evacuated from the chamber by a 500 m^3/h mechanical booster pump and a 100 ℓ/s turbomolecular pump.

The operation and experiment have been done and the preliminary results were as follows. The cooling time for producing the pellet environment was about 2.5 hours and cycle time of producing and injecting the pellet was 8 minutes. The probability of normal injection was over 80% and angular dispersion in pellet trajectory was within 5.3×10^{-5} sr. Velocity measured by time-of-flight method using two photodiodes was 800 m/s at the maximum velocity.

3.2 In-situ titanium coating device

It has been recognized to use an in-situ titanium gettering method for reducing the light impurities in tokamak experiments. A RF-sputtering titanium coating device (Fig.III.3-2) has been developed and settled in JFT-2M. A titanium target is inserted in the vacuum chamber by motor drive and the chamber is filled with about 7×10^{-4} Torr argon as a working gas. A 13.56 MHz RF power is supplied to the target through a matching box. The argon plasma produced by RF power is confined near the target by the magnetic field generated by a coil current installed inside the target. After setting the device on JFT-2M, we measured the titanium evaporation rate, which was 11.36 Å/min. at a point of 30 cm away from the target.

Table III.2-1 Operation of JET-2M NBI, LHH and MG

(Month)	1983 4	5	6	7	8	9	10	11	12	1984 1	2	3
JFT-2M	Con-struc-tion	Operation and maintenance										
NBI	Operation and maintenance					remodelling		Operation and maintenance				
M-G	Operation and maintenance											
LHH	Operation and maintenance											

Detail of the operation (JFT-2M, NBI, M-G and LHH).

	(Fiscal year)	1982	1983 APR-JUN	JUL-SEP	OCT-DEC	1984 JAN-MAR	TOTAL
JFT-2M	Total days of operation (days)	39	31	45	23	29	128
	Times of discharge (shots)	4611	1845	2696	1092	2024	7657
	Baking (times)	3	2	2	2	0	6
	Discharge cleaning (hours)	47.1	30.6	83.1	51.2	54.4	219.3
	Vent. of vacuum chamber (times)	3	2	0	2	1	5
NBI	Total days of operation (days)	14	19	27	22	17	85
	Flashing and injection (shots)	A: 1498 B: 1137	A: 0 B: 0	2779 5448	257 2081	578 5640	A: 3614 B:13169
	Conditioning (shots)	A: 2194 B: 1309	A: 7900 B: 9663	5396 6179	2873 4658	346 1482	A:16515 B:21982
	Vent. of vacuum tank (times)	2	0	0	1	1	2
	Change of filament (times)	A: 0 B: 0	A: 0 B: 0	1 0	1 1	0 0	A: 2 B: 1
M-G	M-G (#1) (hours)	115	289	399	188	239	1115
	M-G (#2) (hours)	115	287	394	186	237	1104
LHH	Total days of operation (days)	22	0	16	4	0	20
	Times of power injection (times)	5780	0	720	734	0	1454

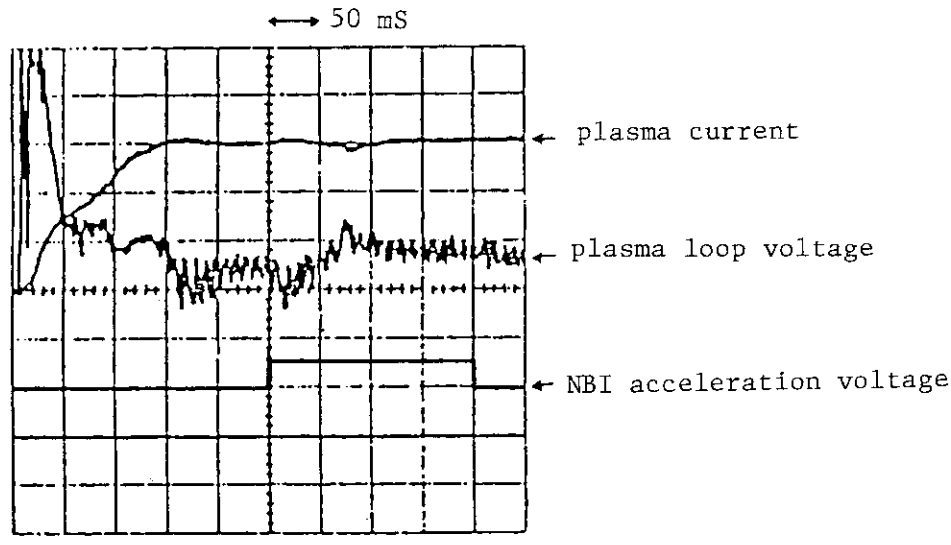

Fig. III.2-1 The waveforms of 200 ms neutral beam injection.

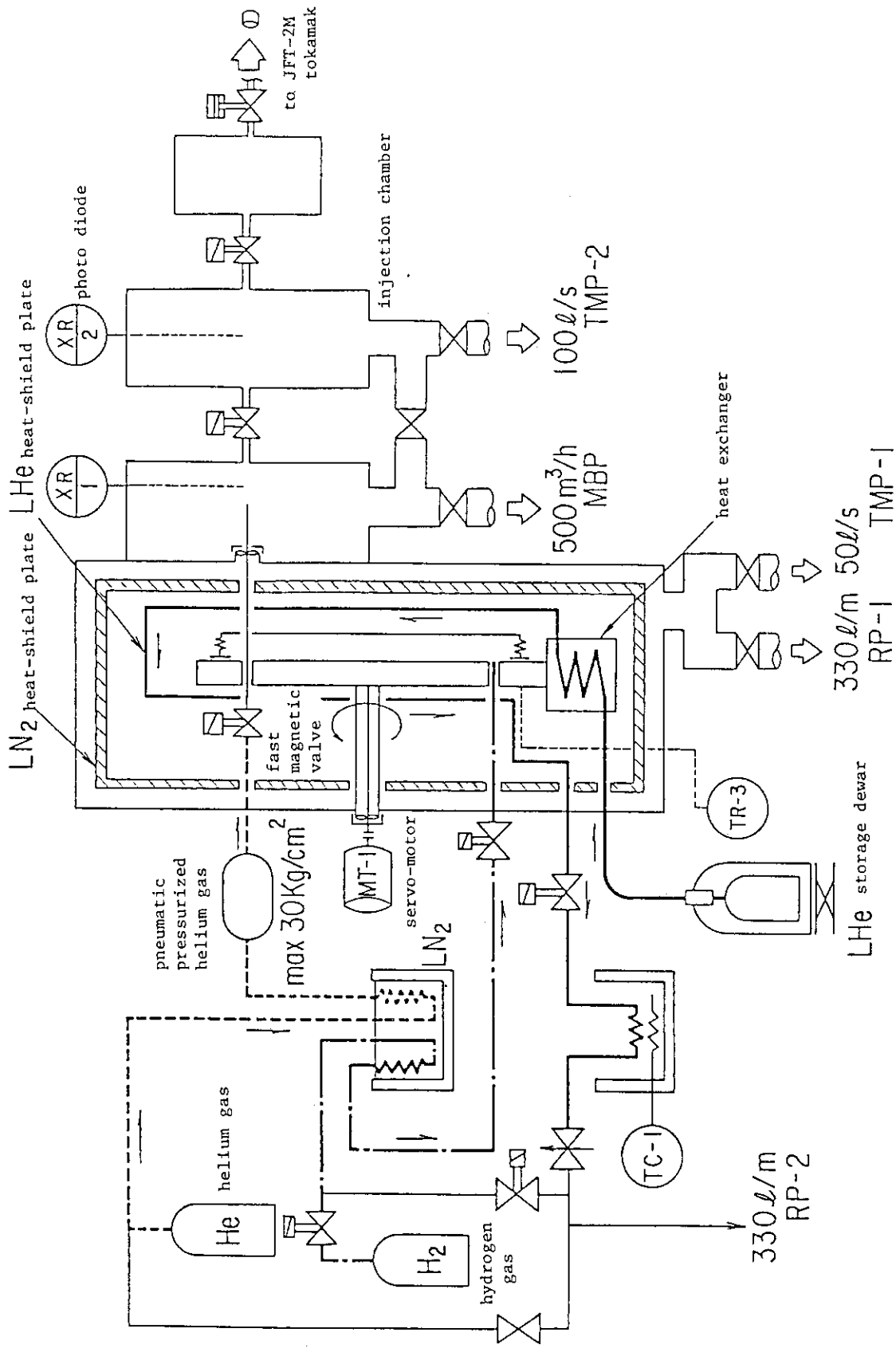

Fig. III.3-1 A schematic diagram of pellet injection system.

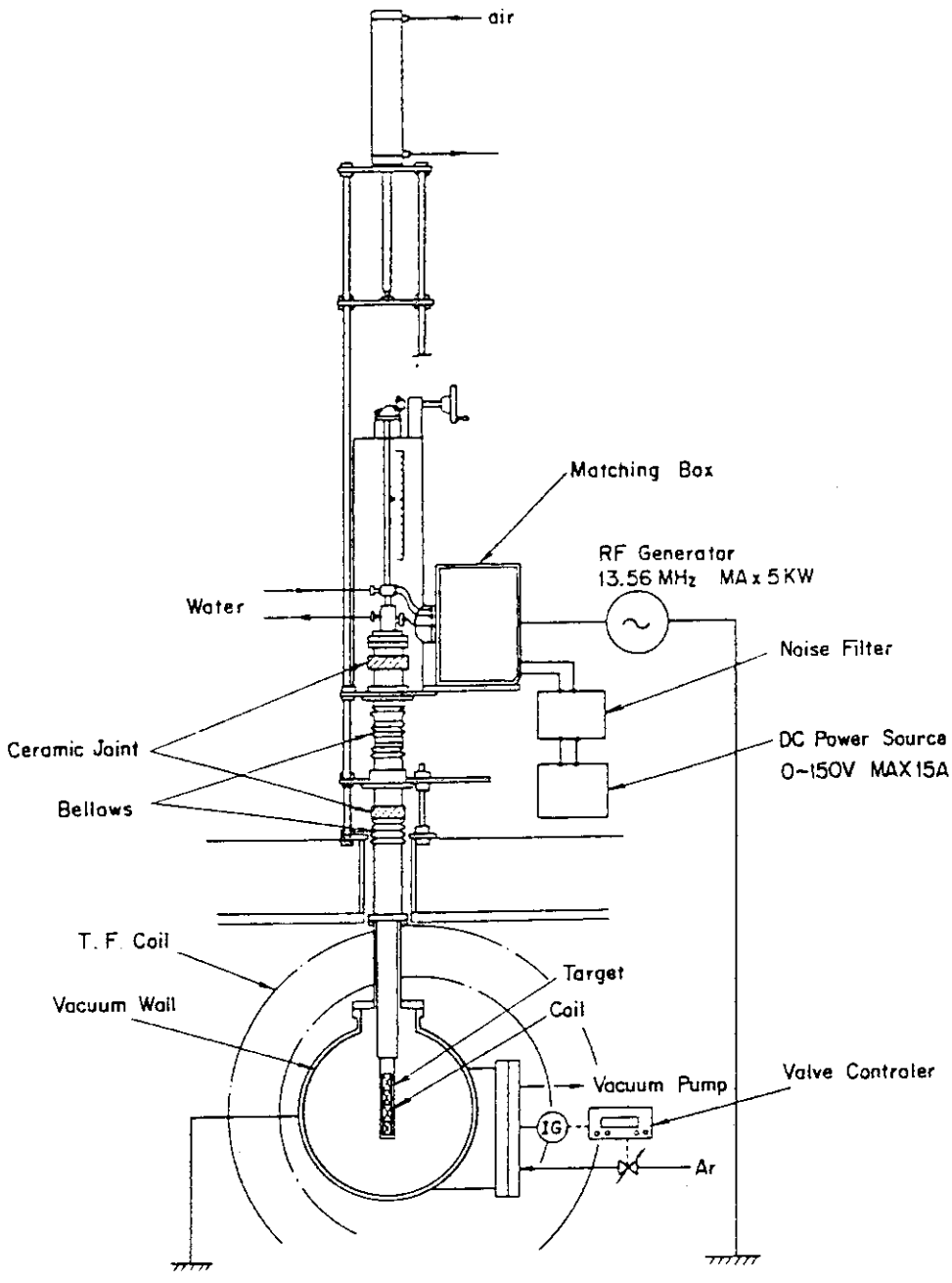

Fig. III.3-2 A schematic diagram of RF sputtering titanium coating device.

IV. JAPAN - US RESEARCH COOPERATION IN DOUBLET III

1. Japan - U.S. Joint Program

A cooperative program on thermonuclear fusion research between the United States and Japan was started in August 1979 using the Doublet III facility at GA Technologies, Inc. (GA), California. A group of Japanese experimental scientists called the "JAERI team" has been staying at General Atomic and carrying out research as an independent group under their own leadership. They are sharing the Doublet III machine time with the American experimental team, the GA physics group. The first phase of the cooperation will be finished in Sept. 1984.

The focus of activities on the part of the Japanese experimental team is to carry out experimental research on higher beta tokamak plasmas with dee-shaped cross sections.

Until March '81, Doublet III was operated for Joule-heating experiments. It was then shut down for six months in order to install two tanks of neutral beam injection (NBI) heating with rating values of 80keV, 7.2MW and 0.5 sec pulse length. The NBI device started operation in Sept. '81 and gradually increased the power. 2MW was obtained in Dec. '81 and 5MW in July '82. The NBI heating experiment with two NBI tanks was continued until mid-February 1983, and Doublet III was then shut down for five months to install NBI tank No.3. Fourteen months of experiments with three NBI (7-10MW) has been carried out through the end of August 1984, the end of the original 5-year cooperation in Doublet III. The cooperative program in Doublet III was extended four more years until Aug. 1988 to include the Big Dee Experiments. The vacuum vessel and a part of the poloidal field coils will be replaced with a new Big Dee device which will start operations in late 1985.

Several noteworthy results had already been obtained in the Joule-heated Dee-shape plasma experiments. A volume-averaged beta value of 4.6% was obtained in Aug. '82 and reported at the 9th IAEA Conference on Plasma Physics and Controlled Nuclear Nuclear Fusion Reseach at Baltimore where our results

were one of the highlights. Since then the JAERI team has concentrated on getting n·T as high as possible, and $T_i(0)$ and $T_e(0)$ higher than 5keV at $\bar{n}_e > 7\times10^{13}$ cm^{-3} was recently achieved with ~8MW NBI heating. The JAERI team owes much of these successes to the outstanding cooperation and friendship of their GA colleagues.

2. Experimental Results

2.1 High Pressure Dee-Shaped Plasma Experiments

During the ohmic heating experiment phase, plasma properties were improved by Ti-gettering and TiC-coated carbon primary limiters; and high density, low-q discharges were stably obtained with dee shaped cross sections and a low toroidal magnetic field [1]. After the installation of the neutral beam injection system and during its power-up phase neutral beam heating experiments were carried out to investigate the dependence of β and τ_E on the discharge parameters as n_e, I_p, and elongation of plasma cross section K. The unique feature of Doublet III in this study was a very high plasma current of up to 1MA and a dee-shaped plasma cross section. A scaling of $\langle\beta_T\rangle$ is

$$\langle\beta_T\rangle[\%] = 3.3B_T[T]^{-2}\ I_p[MA]\ (0.5+0.4P_{abs}[MW])K_a^{-0.5}$$

which is shown in Fig. IV.2-1. This was obtained with up to 2.4 MW neutral beam injection. It was predicted from this scaling that $\langle\beta_T\rangle$ of 5% would be obtained when the machine status allowed plasma discharge with B_T = 0.6T, I_p = 350kA, K = 1.4 (q^*=1.5), P_{abs} = 3.4MW. As the beam power was increased, a record beta value of $\langle\beta_T\rangle$ = 4.6% was obtained with P_{inj} = 3.5 MW, B_T = 0.62T, I_p = 340kA, K = 1.4 as was predicted, with one difference: a = 0.39m. Typical data is shown in Fig. IV.2-2 where $q^{\psi} \sim 1.7$, $T_e(0) \simeq 550$eV, and $\tau_E \sim$ 20ms [2].

In the experiments between late 1982 and early 1983, a new discharge mode was found with an elongated single-null divertor configuration where the energy confinement time during neutral beam heating is proportional to $\bar{n}_e$ (on the INTOR scaling) and shows no deterioration with increasing injection power. The result of analysis shows that a low particle recycling at the edge is the

key to a good discharge. Figure IV.2-3 shows the central ion temperature $T_i(0)$ measured by the neutron counter and Doppler (OVIII) method as a function of absorbed power P_{abs} for $\bar{n}_e \sim 4.5\text{-}7.2\times10^{13}$ cm^{-3} and B_T = 23-24kG. The highest stored energy of ≳500kJ was also obtained with I_p~900kA, $P_{abs} \sim$ 7MW and $\tau_E \sim$ 70ms.

2.2 Pellet Injection Experiment

Continuous pellet fueling experiments were performed in D-III using the ORNL centrifuge injector which can inject 1.3mm diameter D_2 pellets up to 32 pellets per second at a speed of 800m/s. For example, seven pellets were injected into an estblished diverted plasma which had an $\bar{n}_e$ of 2.5×10^{13} cm^{-3} increasing the density to 1×10^{14} cm^{-3}. The energy confinement time also increased up to ~120ms at $\bar{n}_e = 1.1 \times 10^{14}$ cm^{-3}. Even in a limitered discharge with NB heating of ~2.4MW, good confinement was observed at high density (P-mode: $\tau_E \sim 1.6\ \tau_E^{gas}$, $\bar{n}_e$ 1×10^{14} cm^{-3}). Figure IV 2.-4 shows a comparison of the waveforms of pellet- and gas-fueled limitered discharges. The plasma density shown in the second box increases step-wise with injection of each pellet. The neutron production rate during NB heating with pellet fueling is aproximately an order higher than that of the gas-fueled discharge, which shows better heating efficiency.

2.3 Remote radiative cooling with neutral beam heating in diverted plasma

Impurity suppression and helium ash exhaust were demonstrated in the single null poloidal divertor experiments in Doublet III [4]. With the increase of the main plasma electron density, radiative cooling at the divertor region was also observed to increase which resulted in a reduction of the heat load to the divertor plate. All of these results, the impurity reduction with open divertor geometry, the helium ash exhaust, and the remote radiative cooling give a bright forecast to the solution of the crucial points of a future reactor design.

The power balance of the beam-heated divertor discharge is shown in Fig. IV.2-4. The radiative power in the divertor increased with the increase of the main plasma density, while the radiative pwoer of the main plasma stayed almost constant over the whole electron density range. As a result, the heat load of the divertor plate was observed to decrease by a factor of two in the high density conditon. The heat load of the divertor plate is measured by the 28 thermocouple array embedded in the divertor plate. The reduction of the heat load of the divertor plate was also observed with an infra-red camera and the widening of the divertor channel in high density condition was also observed. With the increasing plasma density of the main plasma, the electron dnesity of the divertor is observed to increse non-linearly to 2.8×10^{14} cm^{-3} ($n_e = 3.4 \times 10^{13}$ cm^{-3}). Simultaneously, the electron tmperature at the divertor plate is reduced to 3.5eV as the electron density of the main plasma increases. This dense and cold divertor is obtained with B_T = 20kG, I_p = 290 kA. Out of the 1.5MW absorbed power, 0.5 MW is radiated in the main plasma and another 0.5 MW is radiated in the divertor in high density condition.

In a high density and high temperature diverted discharge with 4-5MW NBI heating, the radiative cooling power was 25-40% (~30-50% of the radiative power comes from the divertor) of the heating power and was almost constant over the electron density range investigated. The divertor plate receives 40-60% of the heating power (thermocouple meausrement). The enhancement of the radiative cooling power in the divertor and the resultant reduction of the heat load have not been observed up to $n_e = 7 \times 10^{13}$ cm^{-3}. This is probably because of the suppressed particle recycling and the high injection power. However, even with 4-5MW beam injection, the Langmuir probe measurement showed that the plasma near the divertor plate is still dense and cold ($n_e \sim 1 \times 10^{14}$ cm^{-3} and $T_e < 20$eV).

This work was performed under a cooperative agreement between the Japan Atomic Energy Research Institute and the United States Department of Energy under DOE Contract No. DE-AT03-80SF11512.

References

[1] M. Nagami, et al., Nuclear Fusion 22 (1982) 409.
H. Yokomizo, et al., Nuclear Fusion 22 (1982) 797.

[2] M. Nagami, et al., and D. Overskei, et al., paper IAEA-CN-41/A2 at the Ninth International Conference on Plasma Physics and Controlled Nuclear Fusion Research, Baltimore, Sept. 1982.
K. Burrell, et al., Nuclear Fusion 23 (1983) 536.

[3] M. Nagami, et al., "Energy Confinement of Beam Heated Divertor and Limiter Discharges in Doublet III". Nuclear Fusion 24 (1984) 183.

[4] M. Shimada, et al., Nuclear Fusion 22 (1982) 643.
M. Shimada, et al., Phys. Rev. Letters 47 (1981) 796.

[5] S. Sengoku, et al., "Observations of Very Dense and Cold Plasma in Beam Heated Doublet III Tokamak with Single-Null Poloidal Divertor". Nuclear Fusion 24 (1984) 415.

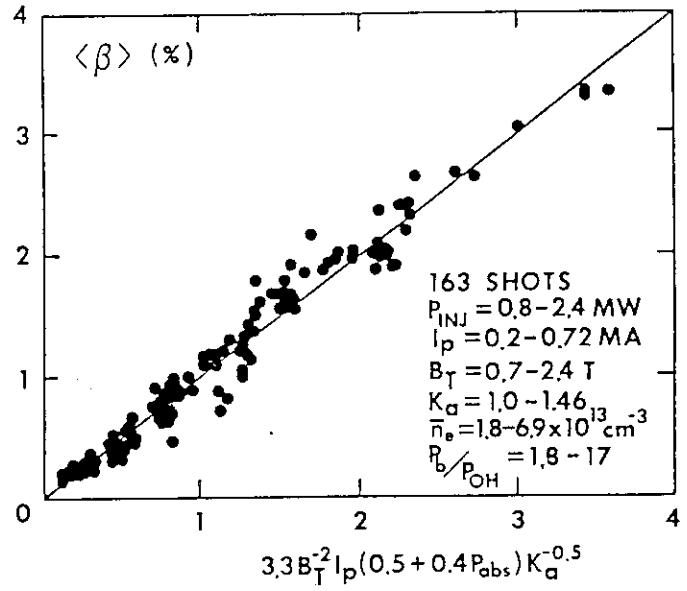

Fig. IV.2-1
β scaling of neutral beam heated discharges. This scaling predicts <β> ∿5% can be obtained with B_T= 0.6T, I_p=350kA, K=1.4, P_{abs}=3.4MW.

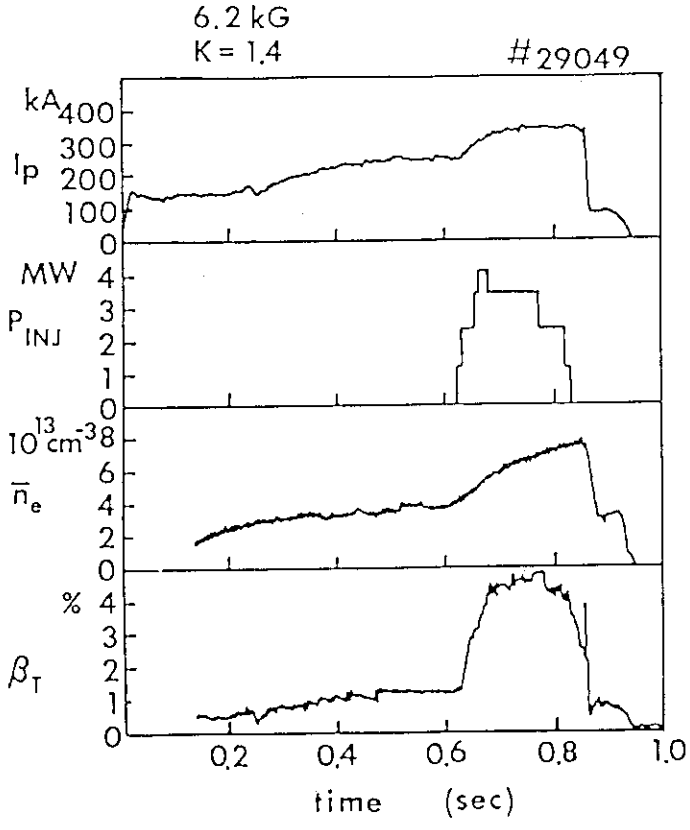

Fig. IV.2-2
Volume average beta <β> ∿4.6% was sustained for more than 0.1 sec with B_T=0.62T, K=1.4, P_{abs}=3.5MW. q^{ψ} ∿1.7, τ_E ∿20ms and $T_e(0)$=550eV.

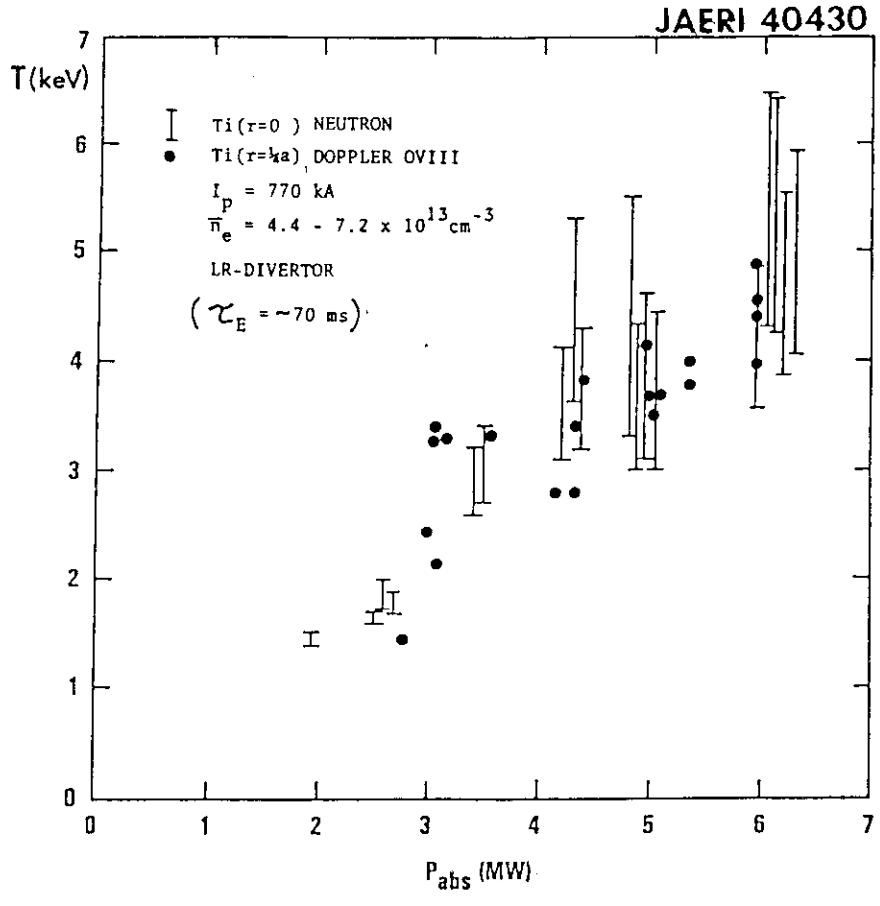

Fig. IV.2-3
$T_i(o)$ measured with neutron counter and Doppler spectroscopy vs. abosrbed power P_{abs} for low-recycling divertor discharges with $\bar{n}_e \sim 5 \times 10^{13}$ cm^{-3} and B_T=23-24kG. Circle, triangle, square are I_p=480kA, 600kA, 750kA, respectively.

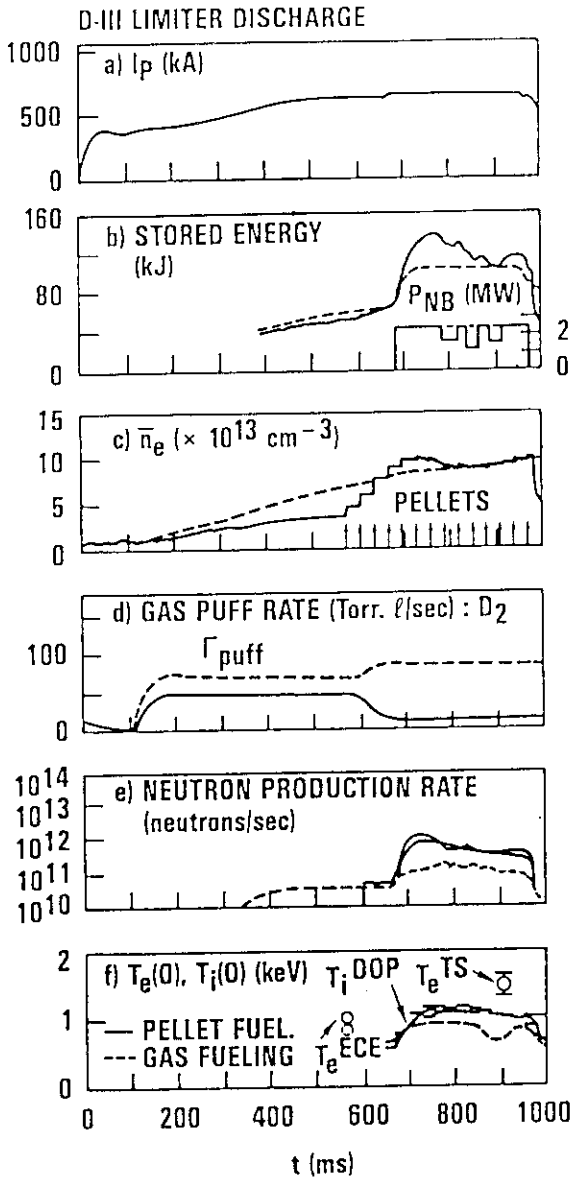

Fig. IV.2-4
Pellet Injection Experiment. Pellets were injexcted at each arrow in the 3rd box. The broken line shows a case with gas puffing only. Note the difference of the neutron yield rate shown in the 5th box.

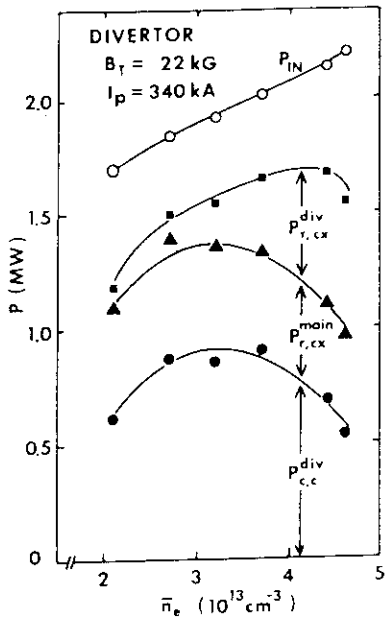

Fig. IV.2-5
The power balance of the beam-heated divertor discharge. P_{IN}: the total absorbed power, $P_{r,cx}^{main}$ and $P_{r,cx}^{div}$: the radiation power in the main plasma and in the divertor, $P_{c,c}^{div}$: the power to the divertor plate (sum of conduction and convection).

V. DEVELOPMENT OF PLASMA HEATING SYSTEM

1. Neutral Beam Injection System

1.1 Ion source development

1.1.1 Improvements of the ion source for JT-60

The ion source for JT-60 NBI is designed to produce ion beams of 40 A at 100 keV for 10 sec. The maximum rated ion beam was obtained in March 1983. Based on the test performed so far, we tried further improvements in the characteristics and the reliability of the ion source. Among the improvements, a development of long life filament cathode is described.

The most significant cause of consumption of directly heated tungsten filament is arc spotting on the filament. Damages due to the occurrence of the arc spotting on the filament can be minimized if the overcurrent is detected and cut off as fast as possible. For this purpose, an electric circuit as shown in Fig. V.1-1 was devised[1]. The arcing detector is set on the current limiting resistance (R_L) in the arc current circuit. If there arises unbalance among the discharge current flowing into the respective filaments, the maximum unbalance is measured as the difference between the maximum and the minimum voltages on the positive terminals of these resistors. When the difference exceeds a preset value, the discharge current is immediately cut off. The delay time necessary to cut off the current is less than 1 ms. Before employing this circuit, it took about 20 ms for cut off. Figure V.1-2 shows the damages left on the used filaments before and after employing this circuit, respectively. It is apparent that a formation of craters on the filament is almost completely prevented by this circuit.

1.1.2 Development of ion source for 200 keV, 3.5 A helium beam injector[2]

A 200 keV, 3.5 A helium beam injector will form part of a diagnostic system to measure the central ion temperature for JT-60. The required performance characteristics of the ion source for this injector are tabulated in Table V.1-1. The energy level of this system is of interest since it enables us to foresee the high-voltage problems associated with future plasma heating injectors. The injector beam line was installed in a test bay to facilitate ion source development prior to installation on JT-60. A schematic figure of the ion source for the injector is shown in Fig. V.1-3. In the source of system

debugging, the source was gradually conditioned to produce a 195 keV, 3.5 A, 0.1 sec helium beam so far. The improvements of the ion source are now being continued to raise the characteristics and the reliability of the ion source untill installation on JT-60.

1.1.3 Development of negative ion source[3)]

In order to achieve an acceptable power efficiency at energies in excess of 200 keV, injectors based on negative ions will be required for future devices. Out of many methods to produce negative ion beams, volume production method is the most attractive one, because this method needs no cesium handling and the structure of the ion source is simple enough to scale up.

As a first step of the development of negative ion source, the yield of volume produced H^- ions was investigated in several configurations of multiple line cusp plasma sources as a function of plasma density, gas pressure, electron temperatures and other operating parameters. At optimum conditions, H^- ion beam with a current density of 12 mA/cm^2 was extracted at beam energy of 10 keV for 0.2 s. Since the gas pressure in the plasma source was as low as 0.5 Pa, high gas efficiency is expected. The low-z impurity content in the beam was less than 1-2%. Scale up of the extractor is now under planning.

1.2 Performance tests of the prototype injector unit for JT-60[4,5,6)]

The prototype injector unit was constructed to test and demonstrate single beam line unit for JT-60. Operation of the system was started in December 1981, and ion beams of 75 keV, 70 A, which is the standard design conditions for JT-60, were extracted for 10 sec in February, 1982. This beam produced a total neutral beam power of 1.43 MW. Reionization loss was 4% of the total neutral beam power and no beam chocking effects were observed even when the stray magnetic field was applied to the neutral beam drift region. An attempt to increase beam energy up to 100 keV, resulted in successful operation at 100 keV, 70 A, 10 sec in March 1983. Through these tests, design performance of the ion sources, beam line components, and cryopumping system was confirmed. The typical performance characteristics obtained so far are summarized in Table V.1-2.

In parallel with these tests, a new advanced source plasma generator was developed to provide a high proton ratio exceeding 90%[7)].

Performance tests on this new source were initiated at the prototype injector unit in August 1983. Ion beams of 100 keV, 40 A were extracted for multi-seconds using one advanced source. The neutral beam power of 0.73 MW, which corresponds to 20 MW neutral beam injection from 14 injector units, was produced with a beam energy of 70 - 100 keV and a reionization loss of 4-5%. The advanced source has been adopted as the production ion source for the JT-60 neutral beam injection system.

1.3 Improvement of accel power supply[8)]

The switching/regulating tube used in the accel power supply causes an unnegligible amount of power loss and it often causes problems such as oscillation, internal spark, water leak, etc. Thus the tube introduces unreliability and complexity in the control and protection system. To avoid the power loss and to simplify the system, a gate turn off thyristor (GTO) valve instead of the tube was proposed. However, GTO valve is lacking in voltage regulation. In particular, the no-load voltage just after the breakdown becomes higher than the rated voltage, which in turn produces overshoot in the beam recovery phase and induces unneccessary breakdown. To solve this problem we devised a voltage regulated GTO valve as shown in Fig. V.1-4. A 100 series thyristor stack (GTAS) is dedicated to switch on and off the DC current only, while a 20 series stack, each provided with a parallel non-linear resistor (GTAR), serves a role of holding overcharged voltage and becomes conducting one by one as the load current starts to rise again.

This system was applied in the accel power supply of the prototype injector unit for JT-60 with particular intension to check its applicability to the JT-60 NBI power supplies. High reliability and applicability were confirmed by performance tests. Based upon test results, we decided to use GTO valve in accel power supplies for JT-60 NBI.

References

1) S. Tanaka, et al., 8th Symp. on Ion Sources and Ion-Assisted Technology Tokyo, 1984.
2) T. Itoh et al., 4th Int. Symp. on HEATING IN TOROIDAL PLASMAS, Rome, Italy, 1984.
3) Y. Okumura, et al., JAERI-M 84-098 (1984).
4) M. Akiba, et al., Rev. Sci. Instrum., 53 (12), 1982, 1984.
5) H. Horiike, et al., ibid., 55 (3), 332, 1984.

6) S. Tanaka, et al., IEEE Int. Conf. on Plasma Science, St. Louis, 1984.

7) Y. Okumura, et al., Rev. Sci. Instrum., 55 (1), 1, 1984.

8) M. Matsuoka, et al., JAERI-M 84-112 (1984).

Table V.1-1 Specification of ion source for 200 keV He beam injector.

BEAM	He
BEAM ENERGY	40 ～ 200 keV
BEAM CURRENT	3.5A
BEAM DIVERGENCE	0.4° (1/e)
PULSE LENGTH	0.1 sec
DUTY	1/200

Table V.1-2 Typical performance characteristics of JT-60 protorype NBI.

	DESIGN VALUE	ACHIEVED VALUE				
BEAM ENERGY (keV)	75 (50～100)	75		75	100	100
BEAM CURRENT (A)	70 (80) TWO SOURCES	70 TWO SOURCES		71 TWO SOURCES	70 TWO SOURCES	41 ONE SOURCE
PULSE LENGTH (Sec)	10	10		10	10	10
GAS SUPPLY INTO ION SOURCES(IS) AND NEUTRALIZER(N) ($Pa \cdot m^3/S$)	≤2.67×2 INTO IS ≤2.67×2 INTO N	1.30×2 INTO IS		0.93×2 INTO IS 0.53×2 INTO N	0.88x2 TO IS 1.1 x2 TO N	0.9 INTO IS 1.0 INTO N
BEAM DIVERGENCE 1/e (Deg)	1.0 (0.9～1.2)	1.05 [1]		1.1 [1]	~0.8 [2]	~0.8 [2]
ION CURRENT DENSITY (A/cm^2)	0.27	0.27		0.28	0.27	0.32
ATOMIC FRACTION- $H_1^+ : H_2^+ : H_3^+$ (%)	75:20:5	——		82:13:5 [3] 77:12:11 [4]	——	——
IMPURITY IN NEUTRAL BEAMS	Low Z ≲ 1 % High Z ≲ 0.1 %	——		Low Z ≲ 0.3 % [3] ≲ 0.5 % [4] High Z ≲ 0.1 % [3]	——	——
SIMULATING STRAY FIELD	ON	OFF	ON	OFF	OFF	OFF
RE-IONIZATION LOSS (%)	5	——	4	——	——	——
COLD GAS FLOW THROUGH THE INJECTION PORT ($Pa \cdot m^3/S$)	0.05	——		0.07～0.08	——	——
CRYO PANEL PUMPING SPEED (m^3/S)	1.37×10^3	1.43×10^3				
REFRIGERATION CAPACITY (W)	300 at 3.7°K	280～300 at 3.6°K				
NEUTRAL BEAM POWER THROUGH THE INJECTION PORT (MW)	1.43	1.31	1.26	1.44	1.43	0.740

1) Beam divergence of 0.1 Sec neutral beam measured at the focal point 8 m apart from the ion source.
2) Extrapolation by the data of 75 kV beam divergence.
3) Measured by the magnetic mass analyzer.
4) Measured by the doppler shift spectrometer at the beam current of 60 A.

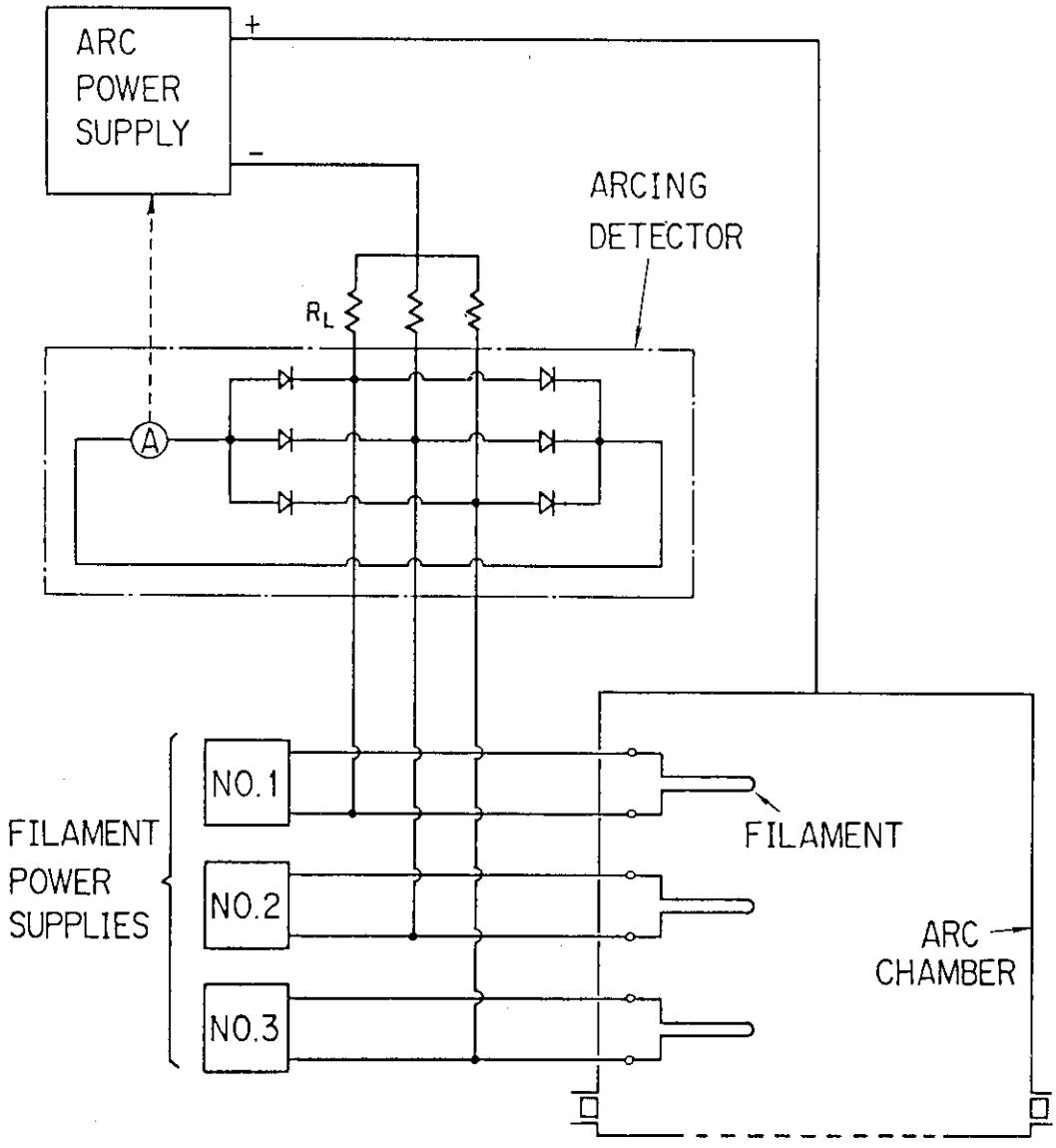

Fig. V.1-1 Schematic diagram showing the arcing detector as well as the discharge circuit and power supplies.

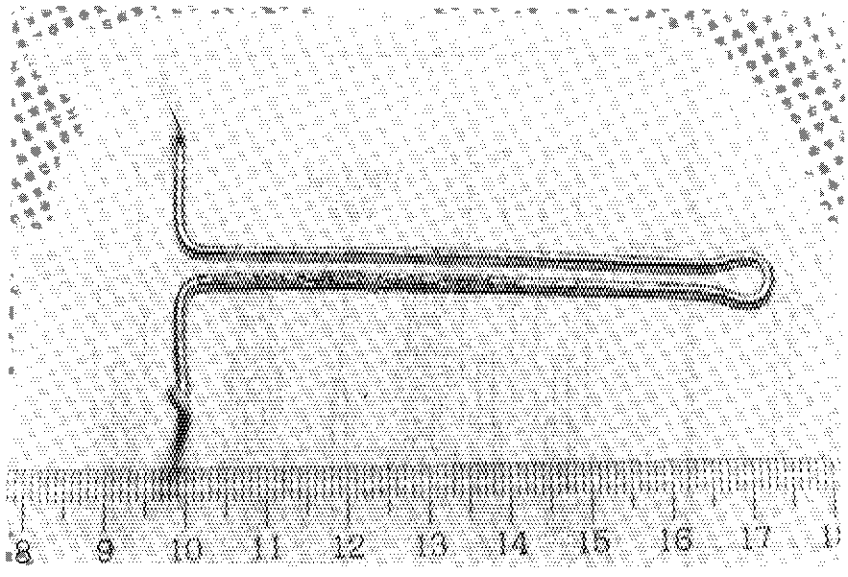

(a)

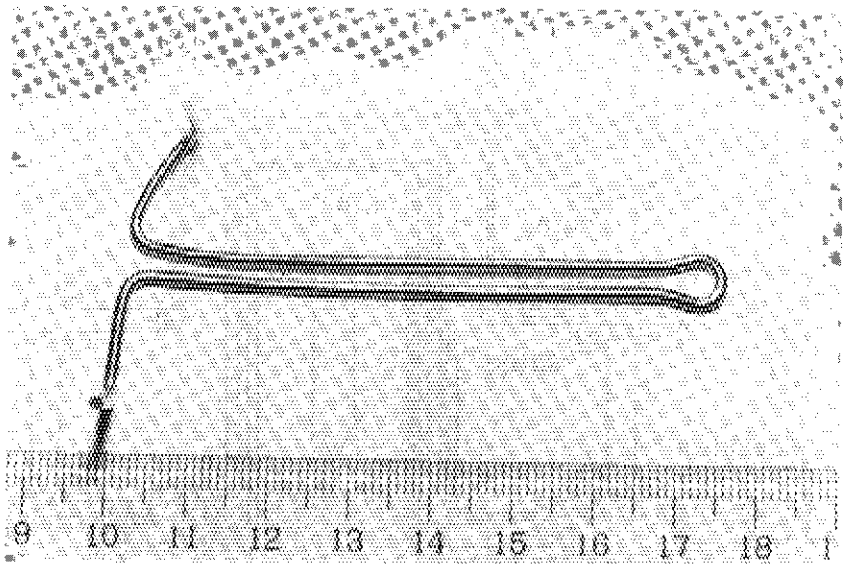

(b)

Fig. V.1-2 Damages left on the used filaments before (a) and after (b) employing the circuit for fast detection and cut off of the arcing.

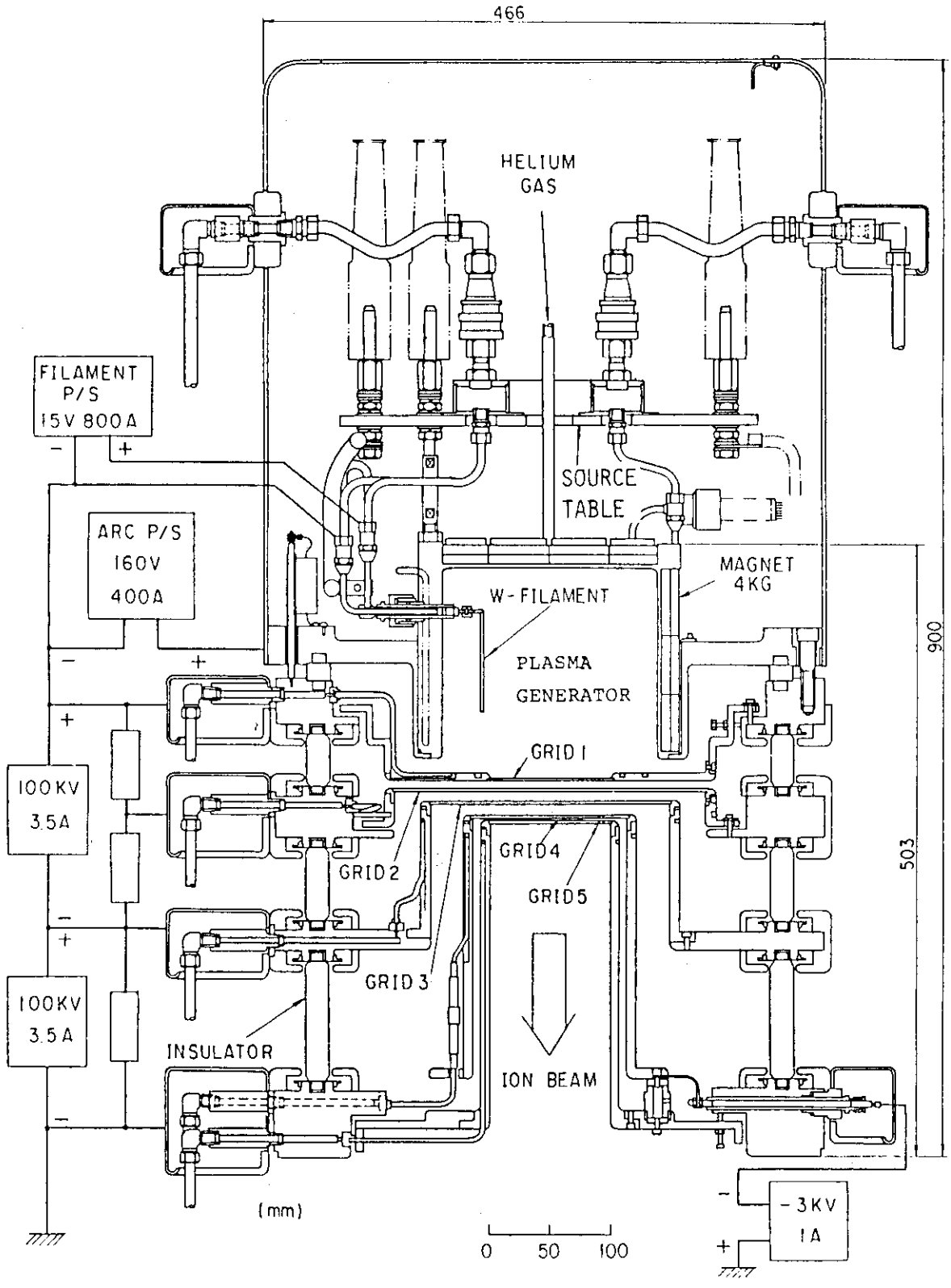

Fig. V.1-3 Schematic of the ion source for 200 keV He beam injector.

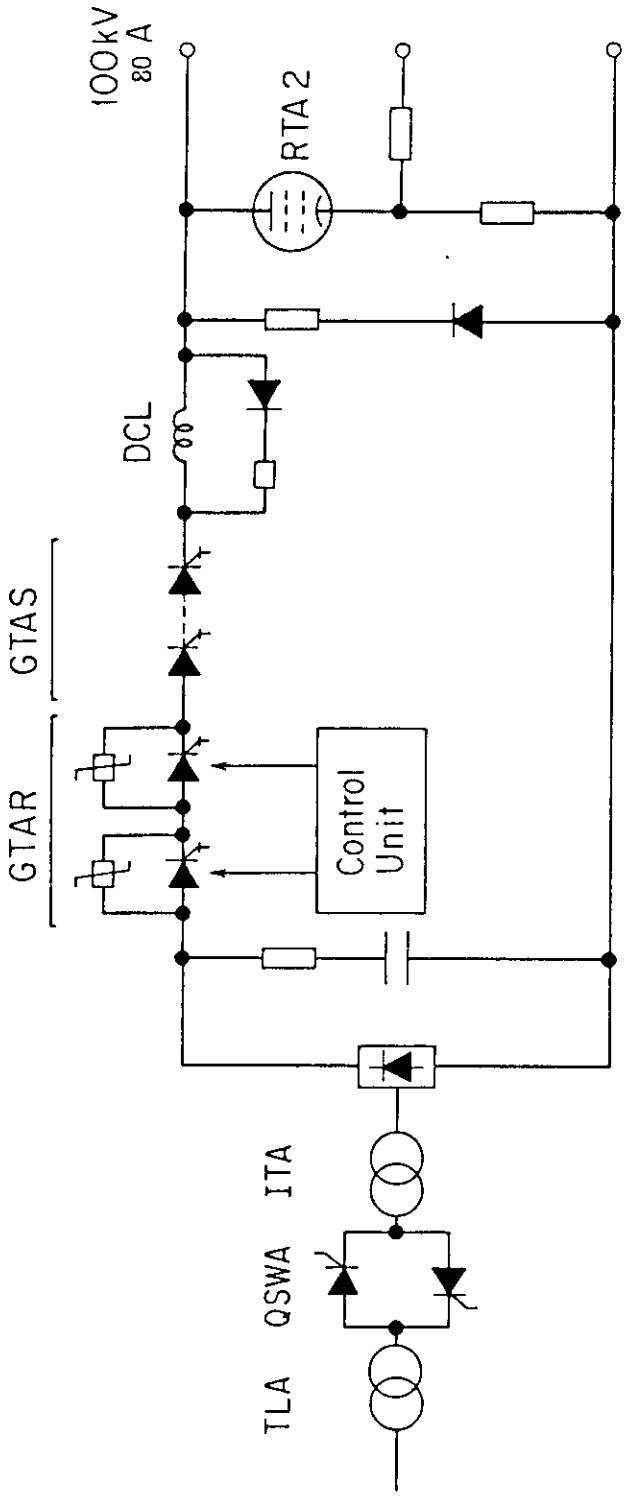

Fig. V.1-4 Schematic diagram of the accel power supply using the gate turn off thyristor.

2. Radio Frequency (RF) Heating System

2.1 Introduction

From the recent experimental results on RF heating, it is very promising to realize the reactor level high temperature and high density plasmas in large tokamaks. However, in order to construct the RF heating system in such a tokamak, we must make further research and development on many RF components because of high power operation in long pulse or steady state. Among them, the development of the high power RF source and the launcher is the most important.

In JT-60, we plan to inject the 10 MW RF power into a plasma core for 10 sec. The JT-60 RF heating system consists of three heating units of lower hybrid range of frequencies (LHRF) at ∿2 GHz and one heating unit of ion cyclotron range of frequencies (ICRF) at ∿120 MHz. As for an LHRF launcher, we have been developing a phased array of waveguides in the RF test stand II because of successful heating results in JFT-2 and other tokamaks with the same type of launcher. As for an ICRF launcher, we have studied a phased array of loop antennas as well as a T-ridged waveguide. Moreover, R&D works of 1 MW class klystron as a high power RF source for an LHRF heating unit has been completed in JAERI under contract with Toshiba Corporation (TOSHIBA) and Nippon Electric Company (NEC), individually.

2.2 R&D works of launcher

2.2.1 Introduction

A launcher faces directly to a plasma to radiate RF power into it. Plasma heating efficiency depends on the design of launcher which is restricted by heat input due to plasma influx and joule loss of RF power, electromagnetic force associated with plasma disruption, transmission power density, port sizes and so on. To increase the transmission power density of the launcher also simplifies RF heating system. Therefore, R&D works of launcher aiming at the increase of power density under such restrictions are the most important among those of the RF components.

2.2.2 LHRF launcher

As for an LHRF launcher, a phased array of waveguides has been studied[1]. RF test stand II (RFTS II) was constructed to develop

transmitting of high power density and aging techniques in the launcher. Overview of the RFTS II is shown in Fig. V.2-1. In the RFTS II, the launcher is bakable up to 500 °C by means of gas loop to reduce the outgassing of the launcher. The gas loop is also used for cooling the launcher in the high power long pulse test. Power density of $\sim$4.5 kW/cm^2 for 10 sec is required in order to inject the 10 MW -10 sec power through four RF ports in JT-60. In the RFTS II, RF power of 1 MW at 2 GHz can be obtained by using the developed 1 MW klystron as an RF power source. Plasma load which simulates the scrape-off layer plasma in JT-60 will be prepared in the middle of 1984.

Two types of launcher were fabricated. One of them is a four waveguide launcher which consists of the similar cross section of waveguide to that of the JT-60 launcher. The other is a two waveguide launcher. The four waveguide launcher has been tested in the RFTS II. Low outgassing rate of $\sim 2 \times 10^{-11}$torr 1/s cm^2 was obtained after the 400 °C baking for 3 days[2]. Transmission power density of 5 kW/cm^2 for 10 sec in the dummy load termination was achieved in February, 1984.

The two waveguide launcher is as long as the JT-60 launcher and is also a separable type as shown in Fig. V.2-2 line the JT-60 one. The launcher was baked at 250 °C for 2 days. We have no trouble in mechanical distortion. Pressure in the launcher reduced to $\sim 4 \times 10^{-8}$ torr. The test of high power transmission will be conducted in the early summer of 1984.

2.2.3 ICRF launcher

As for an ICRF launcher, we have studied a phased array of loop antennas as well as a T-ridged waveguide. Loop antennas have been widely used in the ICRF heating in the present tokamaks and efficient plasma heating was observed. However, the high power long pulse operation like the one in JT-60 has not yet been performed. Length of the present loop antenna is comparable to a minor radius of tokamak, which results in unreliability against the electromagnetic force associated with major plasma disruption, difficulty in maintenance of installation and removal and so on. The phased array of loop antennas designed for JT-60 consists of 4 short length loop antennas, 2 rows × 2 columns, and has the casing as shown in Fig. V.2-3. Therefore, it is relatively strong against the electromagnetic force and is easily installed and removable in radial direction like the LHRF waveguide

launcher. Its coupling properties including phase control between the antennas is calculated with three dimensional model of loop antenna[3,4]. From the calculation results, the sufficient coupling and efficient plasma heating by phase control can be expected.

The characteristics of a T-ridged waveguide also has been investigated in cooperation with Prof. N. Goto of Tokyo Institute of Technology. A simple T-ridged waveguide for testing RF characteristics was made. The experimental results on RF propagation in the ridged waveguide well agreed with those of calculation, which indicates that the ridged waveguide designed for JT-60 has the possibility of the power transmission of about 5 MW. However, according to the numerical results by the method of parallel plate approximation, the coupling efficiency of the ridged waveguide for JT-60 with the simple open mouth is not enough in the present JT-60 condition[5]. In order to improve the coupling efficiency, we are now investigating the shaping of the mouth of the ridged waveguide.

2.3 R&D works of 1 MW class klystron

R&D works of the high power klystron has been intensively performed under contract with TOSHIBA and NEC[6]. Key features of the klystron for JT-60 are (1) high power output (1MW), (2) long pulse (10 sec), (3) wide mechanical tuning range (1.7-2.3 GHz), (4) strong endurance against the reflected power (VSWR of 2), which are required for the fusion application not for the broadcasting and the accelerator.

The JT-60 Klystron Test Facility was constructed in order to age the klystron and make the output power test. In the Test Facility, the programmed operation can be made by the control system with a micro computer so as to test the klystron sufficiently and efficiently.

Both klystrons manufactured by TOSHIBA and NEC have achieved the output power of 1 MW for 10 sec. The typical performances and waveforms are shown in Table V.2-1 and Fig. V.2-4, respectively. Through the R&D works of the klystron for 3 years, it is found that main cause which limits the output power is the discharges on the ceramic window.

References

1) Annual Report of April 1, 1982 to March 31, 1983, JAERI-M 83-182 (1983).

2) T. Fujii, et al., in the proceeding of 10th Symposium on Fusion

Engineering, Philadelphia, U.S.A., Dec. 5-9, 1983.

3) H. Kimura, et al., in the proceeding of the 4th International Symposium on Heating in Toroidal Plasma, Rome, Italy, March, 1984.

4) Y. Ikeda, et al., to be published in JAERI-M.

5) M. Saigusa, et al., to be published in JAERI-M.

6) T. Nagashima, et al., in the proceeding of 10th Symposium on Fusion Engineering, Philadelphia, U.S.A., Dec. 5-9, 1983.

Table V.2-1 Typical performances of 1 MW class klystrons.

	TOSHIBA	NEC
Frequency	2.01 GHz	2.09 GHz
Output Power	1 MW	1 MW
Pulse Width	10 sec	10 sec
Beam Voltage	83.0 kV	84.7 kV
Beam Current	26.5 A	25.2 A
Power Gain	53 dB	48 dB

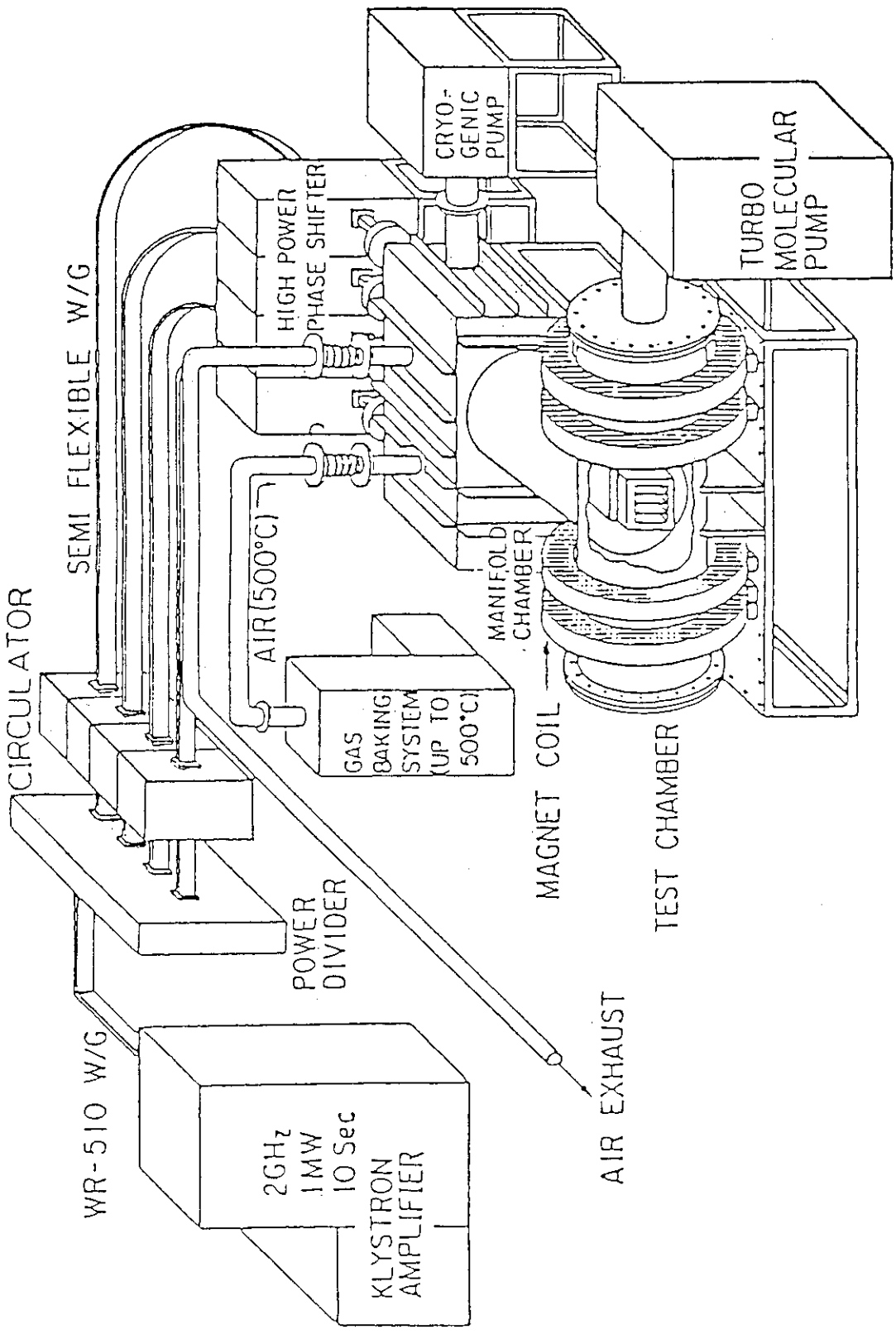

Fig. V.2-1 Overview of RF Test Stand II.

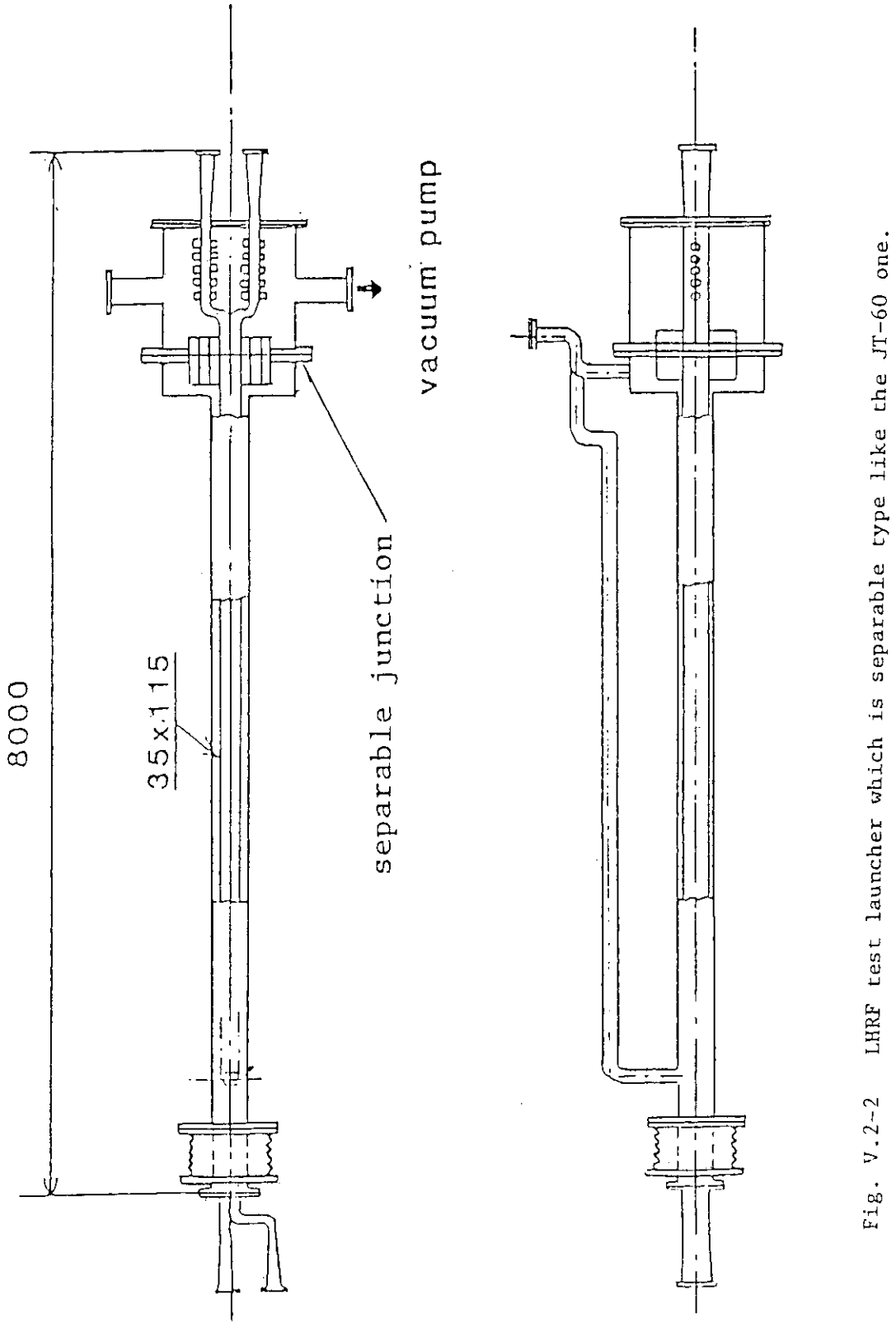

Fig. V.2-2 LHRF test launcher which is separable type like the JT-60 one.

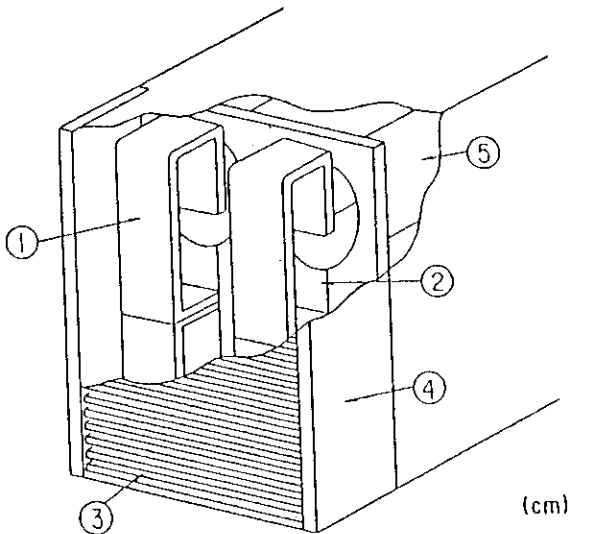

① Central Conductor
② Return Conductor
③ Gas/Water Cooled Faraday Shield
④ Guard Limiter
⑤ Coaxial Line

Fig. V.2-3 JT-60 ICRF launcher, phased array of 2 x 2 loop antennas.

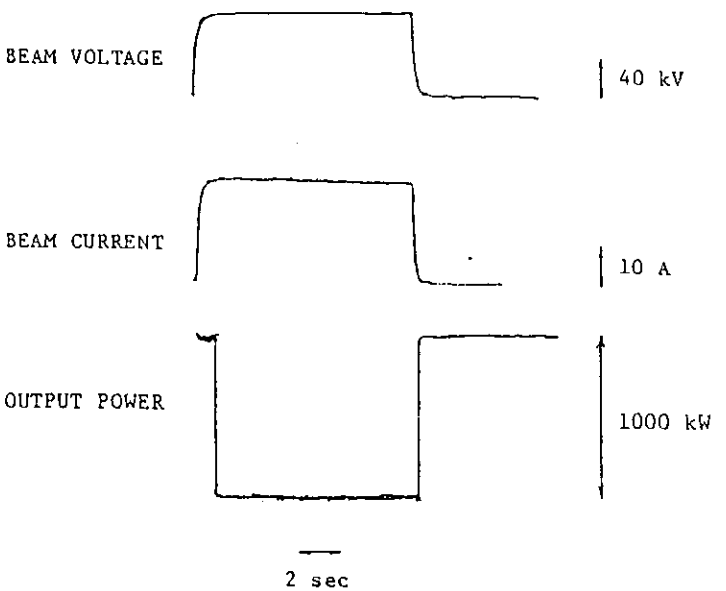

Fig. V.2-4 Typical waveforms observed in the output power test of the klystron

VI. SURFACE PHYSICS AND VACUUM TECHNOLOGY

1. Surface Physics

1.1 Introduction

Surface physics studies which are related to plasma surface interactions have been continued in close connection with the JT-60 project, the design study of the next step tokamaks and the tokamak experiments in JFT-2M. Especially in this fiscal year, international cooperation was made in the TEXTOR (KFA Jülich, F. R. of Germany) programme. The primary objective of these studies is to investigate the interaction of the plasma with wall and limiter materials using ion accelerators and tokamak machines to find conditions which minimize impurity production and control hydrogen recycling rate.

In this fiscal year, progress was made with measurement of the effect of oxygen on sputter erosion of refractory metals, measurement of sputtered neutral Ti atoms from TiC and Ti targets by laser induced fluorescence, in-situ measurement of the hydrogen recycling constant of the TEXTOR liner, improvement of the modelling of hydrogen recycling at TiC wall surface, and the boundary plasma diagnostics in JFT-2M.

1.2 Effect of exygen on sputter-erosion of refractory metals[1)]

The sputtering yield of molybdenum and tungsten due to the bombardment with 7 keV Ar^+, Ne^+ and CO^+ ions has been measured between room temperature and 1500 °C by means of the weight loss measurement. For Ar^+ and CO^+ ion bombardment of tungsten and Ar^+ ion bombardment of molybdenum the erosion yield shows a weak temperature dependence, whereas for CO^+ ion bombardment of molybdenum the erosion yield increases up to a factor of three in a complicated manner as the temperature rises. These results are shown in Fig. VI.1-1.

Auger electron spectroscopy was applied to measure the content of carbon and oxygen as a function of depth in the CO^+ ion bombarded molybdenum and the results are shown in Fig. VI.1-2. It is clearly seen that carbon and oxygen remains in the targets after bombardment at 25 °C and 500 °C, whereas they completely come out after bombardment at 1000 °C. These results strongly suggest that the increase of the erosion yield of molybdenum bombarded with CO^+ ion at temperature above 500 °C is due to the chemical reaction between molybdenum and the implanted oxygen, since molybdenum oxide becomes volatile above 500 °C.

In order to get a further insight of the effect of oxygen on the sputtering properties, Ar^+ sputtering of molybdenum under the oxygen exposure was carried out at various temperatures. Figure VI.1-3 shows the sputtering yield as a function of the ratio of the impinging oxygen to Ar^+ ion flux. It is clearly seen that the sputtering yield is strongly dependent on oxygen pressure as well as temperature. It should be pointed out that the sputtering yield is almost constant above 1000 °C, but total erosion rate increases above 1000 °C because of the additional contribution of the oxide vaporization which is not the beam induced component.

Present results indicate that tungsten is superior to molybdenum in the sputtering properties under the oxygen atmosphere because of lower volatility of oxides.

1.3 Plasma-wall interaction study in cooperation with IPP of KFA

There were cooperative works with Institute of Plasma Physics of KFA (Kernforschungsanlage) under the international cooperative programme of TEXTOR (Torus Experiment for Technology Oriented Research). The first six months were used for the in-situ measurement of the hydrogen recycling constant of the TEXTOR liner[2]. Another six months were devoted to the measurements of neutral Ti atoms from TiC and Ti targets sputtered by low energy H^+ and Ar^+ ion using laser induced fluorescence[3].

The recycling constant $R_c = D/2\sigma k_r$ of the TEXTOR liner has been determined by in-situ observation of the wall pump and release effect, where D is the diffusion constant, σ is the surface roughness factor and k_r is the recombination constant. The results indicate that R_c is about 2×10^{15} cm^{-2} for the well conditioned clean surface of the liner. A thin carbidic layer on the liner surface was obtained by radiofrequency assisted glow discharge in H_2-CH_4(0.9 at%) mixture. The value of R_c on that surface is 3×10^{14} cm^{-2}. The above results shown in Fig. VI.1-4 suggest that R_c, which can be determined by the in-situ measurement of the pressure of H_2 gas in a tokamak device, is a good measure to estimate the surface condition.

The sputtering of Ti from TiC and also from pure Ti targets for 500 eV H^+ and Ar^+ ion irradiation at normal incidence has been investigated by means of laser induced fluorescence. The sputtered neutral Ti atoms in the ground state were observed as a function of fluence and target temperature. This technique is shown to be applicable for in-situ

sputtering investigations of TiC. The obtained results are as follows.

1) There are strong fluence dependences of the fluorescence intensity for Ti targets bombarded with Ar^+ ions, which are considered to depend on the surface conditions related on the chemisorption of impurities (i.e. oxygen). On the other hand, the rather small fluence dependences for TiC targets indicate that the TiC surface is less active for the chemisorption than the Ti surface (see Figs. VI.1-5,6).
2) In the case of TiC target bombarded with H^+ ions, the fluence dependence of the fluorescence intensity shows that the depleted layer of carbon atoms due to the chemical sputtering influences the transient period of the sputtering of Ti component of TiC.
3) After the steady fluorescence signals were obtained during 500 eV Ar^+ ion bombardment, the ratio of fluorescence intensities between TiC and Ti targets is about 0.6 ± 0.1, which suggests the physical sputtering yield of the Ti component of TiC is about half of the yield of Ti targets if the mean velocities of Ti atoms sputtered from TiC and Ti targets are assumed to be the same.
4) No significant temperature dependence of the Ti-sputtering yield of TiC for Ar^+- and H^+-ion bombardment was found after the steady fluorescence signals were obtained as shown in Figs. VI.1-7,8.

1.4 Modelling of hydrogen recycling at TiC wall surface

The effect of hydrogen trapping action of the TiC wall on hydrogen recycling area in a limiter configuration of the JT-60 tokamak was previously discussed for the case of 20 MW neutral beam injection used[4]. All wall and limiter surfaces of JT-60 will be coated with TiC of 20 μm in thickness. Surface compositional changes of the TiC wall are expected to occur by the bombardment with energetic charge exchange neutrals. One of them is carbon atom depletion from the TiC wall surface, which is mainly due to chemical sputtering to form CH_4 and preferential sputtering of C atoms. It finally makes the TiC wall surface a Ti-rich one at a high fluence of hydrogen, $\sim 1 \times 10^{19}$ H/cm^2 [5]. The Ti-rich surface reacts with the residual oxygen impurity. Thus the effect of the chemical sputtering and titanium oxide formation on hydrogen recycling was estimated by model calculations[6].

Figure VI.1-9 shows the calculated recycling rates as a function of discharge time, when the energy distribution and the flux of charge exchange neutrals are assumed to be 400 eV Maxwellian and 1×10^{16} H/cm^{2}s,

respectively. The corresponding recycling coefficient R_s in the steady state is approximately 0.75, above which we need to pump an excess amount of hydrogen gas. It is found in Fig. VI.1-9 that the recycling coefficient in Ti is less than the R_s value at any temperature. The most practical case is the one for TiO_2 after a number of discharge shots. The suitable wall temperature regions at which the recycling coefficient is less than 0.75 are, for 10 s discharge, 150 °C ≤ T ≤ 220 °C (TiC) and 60 °C ≤ T ≤ 80°C (TiO_2), and, for 5 s discharge, T ≤ 370°C (TiC) and T ≤ 100 °C (TiO_2).

From a viewpoint of machine operation, it is not practical to thermally desorb hydrogen atoms trapped at relatively low temperature (∿100 °C) by baking the wall at ∿500 °C every time after a discharge shot. In the case of TiC, however, it is possible to desorb 60-70 % of trapped hydrogen atoms during 10 min interruption by keeping the wall temperature of 300-370 °C[7], and this percentage will become higher for longer interruption. Therefore, it is possible to keep the recycling coefficient less than 0.75 by using such a hot TiC wall for 5 s discharge. But it will be impossible for 10 s discharge, because a relatively low percentage (20-40 %) of hydrogen atoms trapped in TiC wall can be desorbed during 10 min interruption at wall temperature of 150-220 °C[7]. On the contrary, such a hot wall discharge to keep a low recycling coefficient will be of no significance in TiO_2 wall. However, it should be noted in TiO_2 wall that thermal desorption of hydrogen atoms trapped during a discharge will become an essential procedure after every discharge. Thus the oxidation of Ti-rich wall surface will eventually add the wall baking procedure to the machine operation.

1.5 Plasma-wall interaction study on JFT-2M

A possibility of an intrinsic impurity control by using characteristics of drift motions of impurities in a tokamak was studied in JFT-2M. The basic idea has already been proposed by Alcator group[8] but the verification has not yet been made experimentally.

The plasma was forced to contact with limiters asymmetrically with respect to the median plane: namely, the dominant contact was made on top or bottom limiters. The released amount of limiter material which was estimated by VUV spectrometer was compared between the two cases. When the direction of the toroidal drift of the impurity ion was upward, the impurity level of the top-side contact was found to be 20-30 % lower

than that of the bottom-side one. These results agree with the effect expected and we concluded that the method is promising for impurity control in toroidal devices.

References

1) M. Saidoh, Presented at the 6th Int. Conf. on Plasma Surface Interactions in Controlled Fusion Devices, Nagoya, May 14-18, 1984 (to be published in J. Nucl. Mater.).
2) P. Wienhold, F. Waelbroeck, J. Winter, E. Rota, T. Banno and R. Yamada, Presented at the 3rd Topical Meeting on Fusion Reactor Materials, Albuquerque, Sept. 19-22, 1983 (to be published in J. Nucl. Mater.).
3) R. Yamada, H. L. Bay and B. Schweer, Presented at the 6th Int. Conf. on Plasma Surface Interctions in Controlled Fusion Devices, Nagoya, May 14-18, 1984 (to be published in J. Nucl. Mater.).
4) K. Sone and Y. Murakami, J. Nucl. Mater., 121 (1984) 254.
5) H. Tanaka, K. Saiki, S. Otani, A. Koma and S. Tanaka, J. Nucl. Mater., 118 (1983) 317.
6) K. Sone, Presented at the 6th Int. Conf. on Plasma Surface Interactions in Controlled Fusion Devices, May 14-18, 1984 (to be published in J. Nucl. Mater.).
7) S. T. Picraux and W. R. Wampler, J. Nucl. Mater., 93&94 (1980) 853.
8) J. L. Terry et al., Phys. Rev. Lett., 39 (1977) 1615.

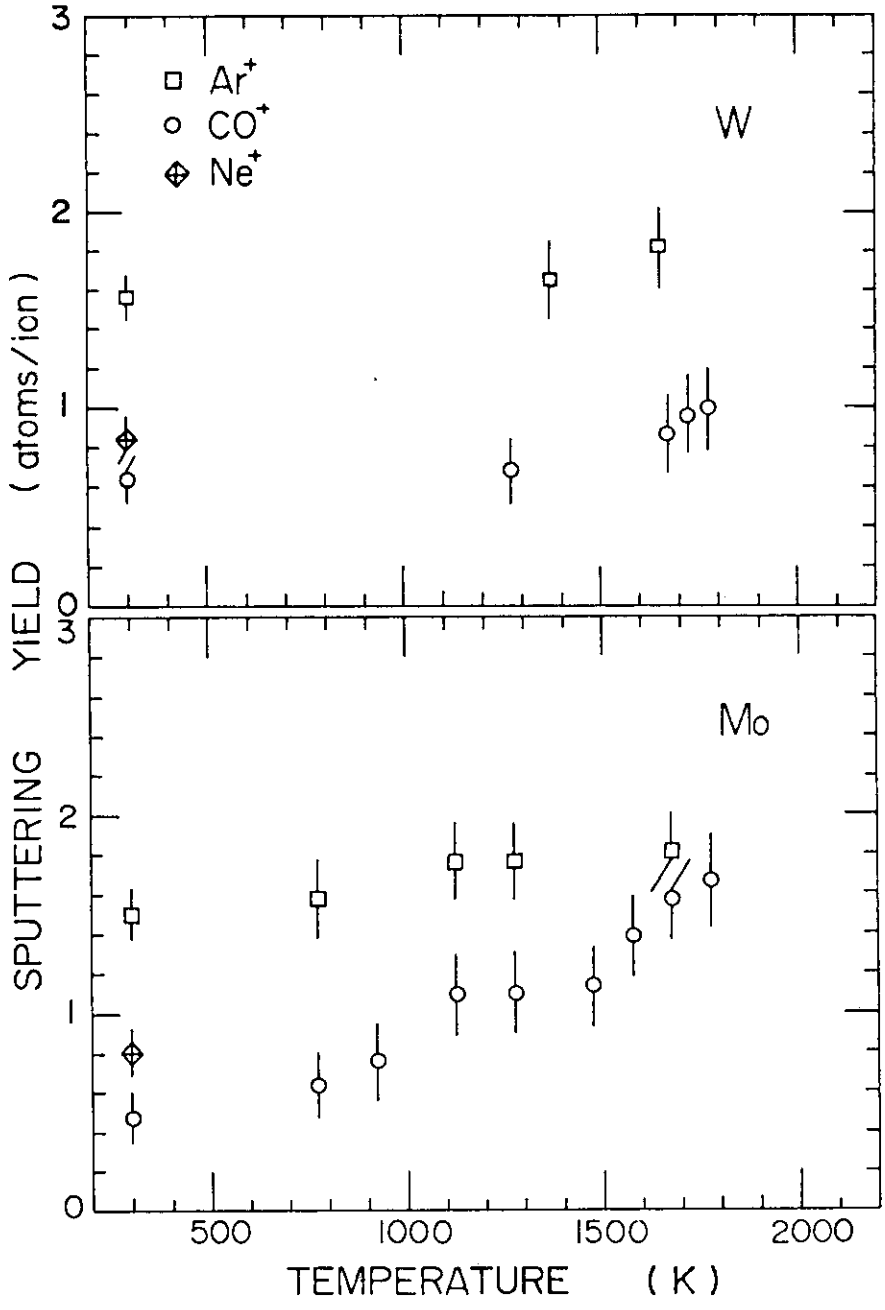

Fig. VI.1-1 Sputtering yield as a function of temperature in molybdenum and tungsten for 7 keV Ar^+, Ne^+ and CO^+.

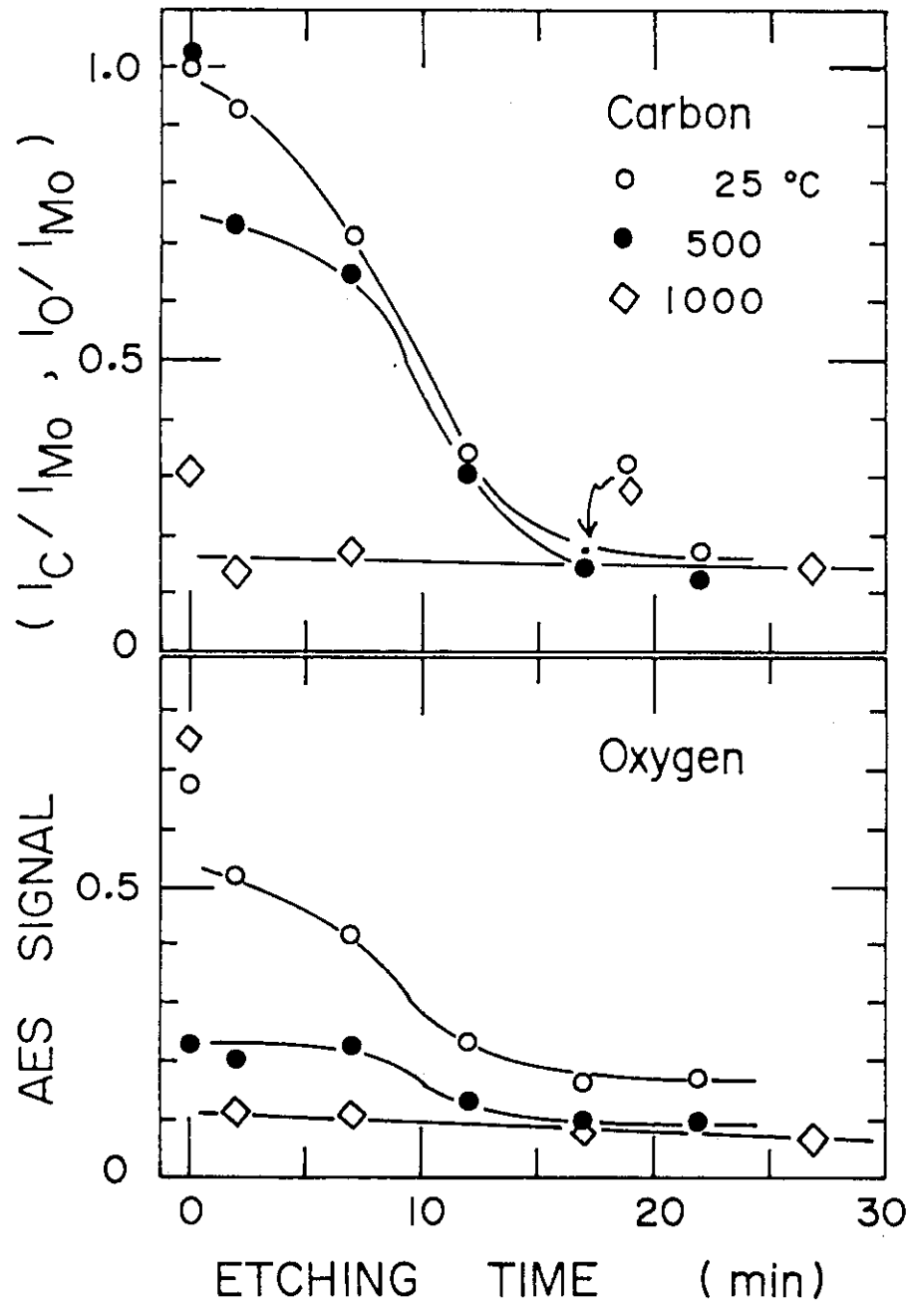

Fig. VI.1-2 AES signal intensity ratios, I_C/I_{Mo} and I_O/I_{Mo}, as a function of Ar^+ ion sputter-etching time for molybdenum targets bombarded with CO^+ to a dose of 1.6×10^{18} CO^+/cm^2 at various temperatures.

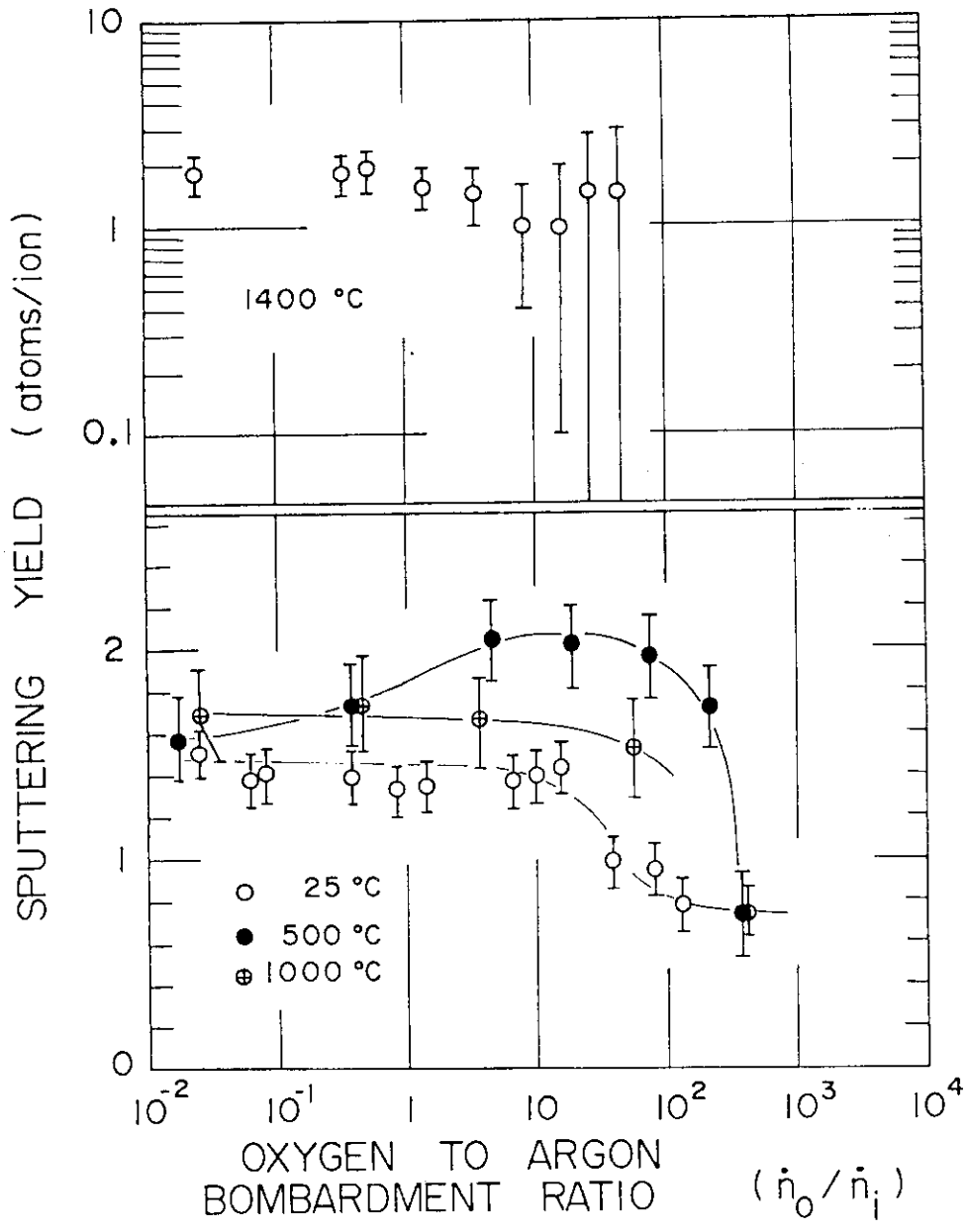

Fig. VI.1-3 Sputtering yield for Ar^+ bombardment under oxygen exposure as a function of oxygen to Ar^+ ion flux ratio at various temperatures.

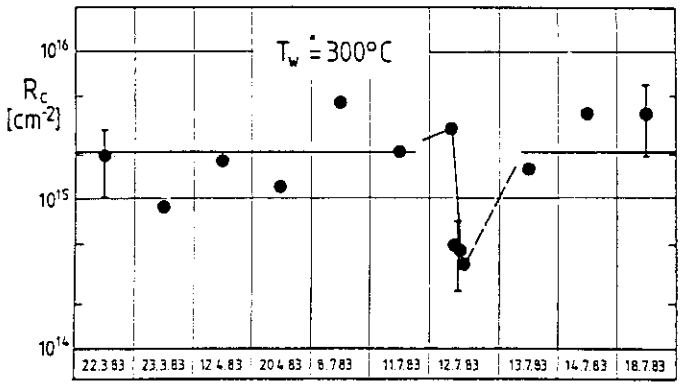

Fig. VI.1-4 The recycling constant $R_C=D/2\sigma k_r$ in TEXTOR at 300°C of Inconel 625 liner. R_C was determined from the wall pump and release effect after switching on or off of the radiofrequency assisited glow discharge.

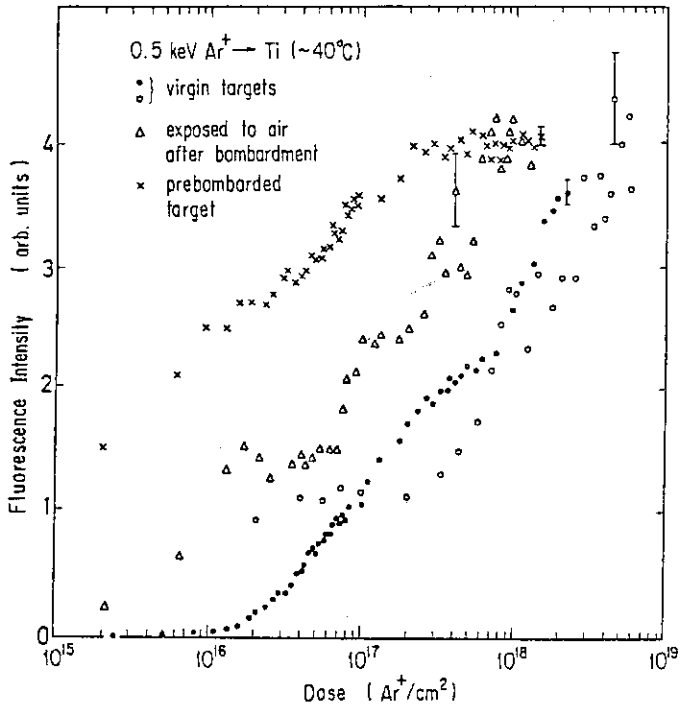

Fig. VI.1-5 Fluorescence intensities of neutral Ti atoms in the ground state sputtered from Ti targets as a function of 0.5 keV Ar^+ ion dose. Target temperature was ∿40°C, and both the excimer-pumped (●, ○, ×) and the flashlamp-pumped (○) dye laser were used. Target conditions prior to bombardments were as follows: virgin sample (●,○); prebombarded samples with 0.5 keV Ar^+ ions until the steady states of fluorescence intensities were obtained and then exposed to the air (△) or held in vacuum for one hour (×).

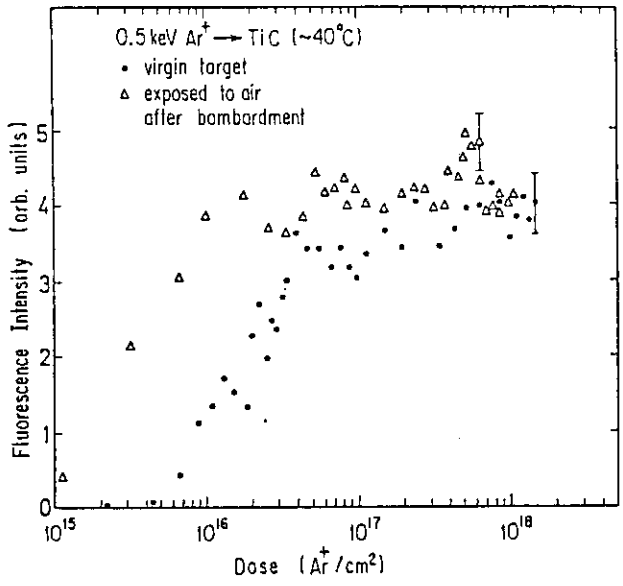

Fig. VI.1-6 Fluorescence intensities of neutral Ti atoms in the ground state sputtered from TiC targets as a function of 0.5 keV Ar^+ ion dose. Target temperature was ∿40°C and the excimer-pumped dye layser was used. Target conditions prior to bombardments were as follows: virgin sample (●); prebombarded sample which was exposed to the air after the steady state of fluorescence intensity was obtained by 0.5 keV Ar^+ ion bombardment (△).

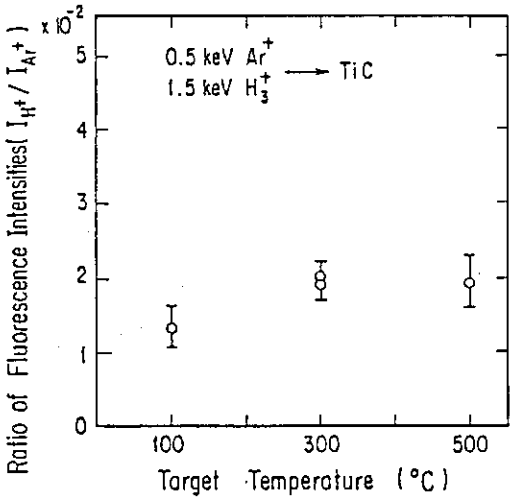

Fig. VI.1-7 Ratio of the fluorescence intensity of neutral Ti atoms in the ground state from TiC to that from Ti by 0.5 keV Ar^+ bombardment as a function of target temperature.

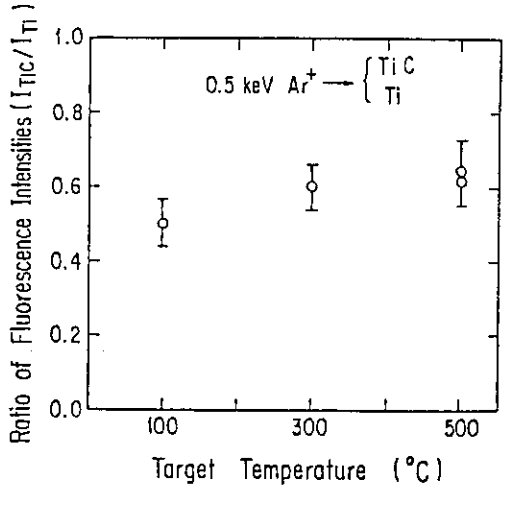

Fig. VI.1-8 Ratio of the fluorescence intensity of neutral of Ti atoms in the ground state from TiC by 1.5 keV H_3^+ bombardment to that by 0.5 keV Ar^+ bombardment as a function of target temperature.

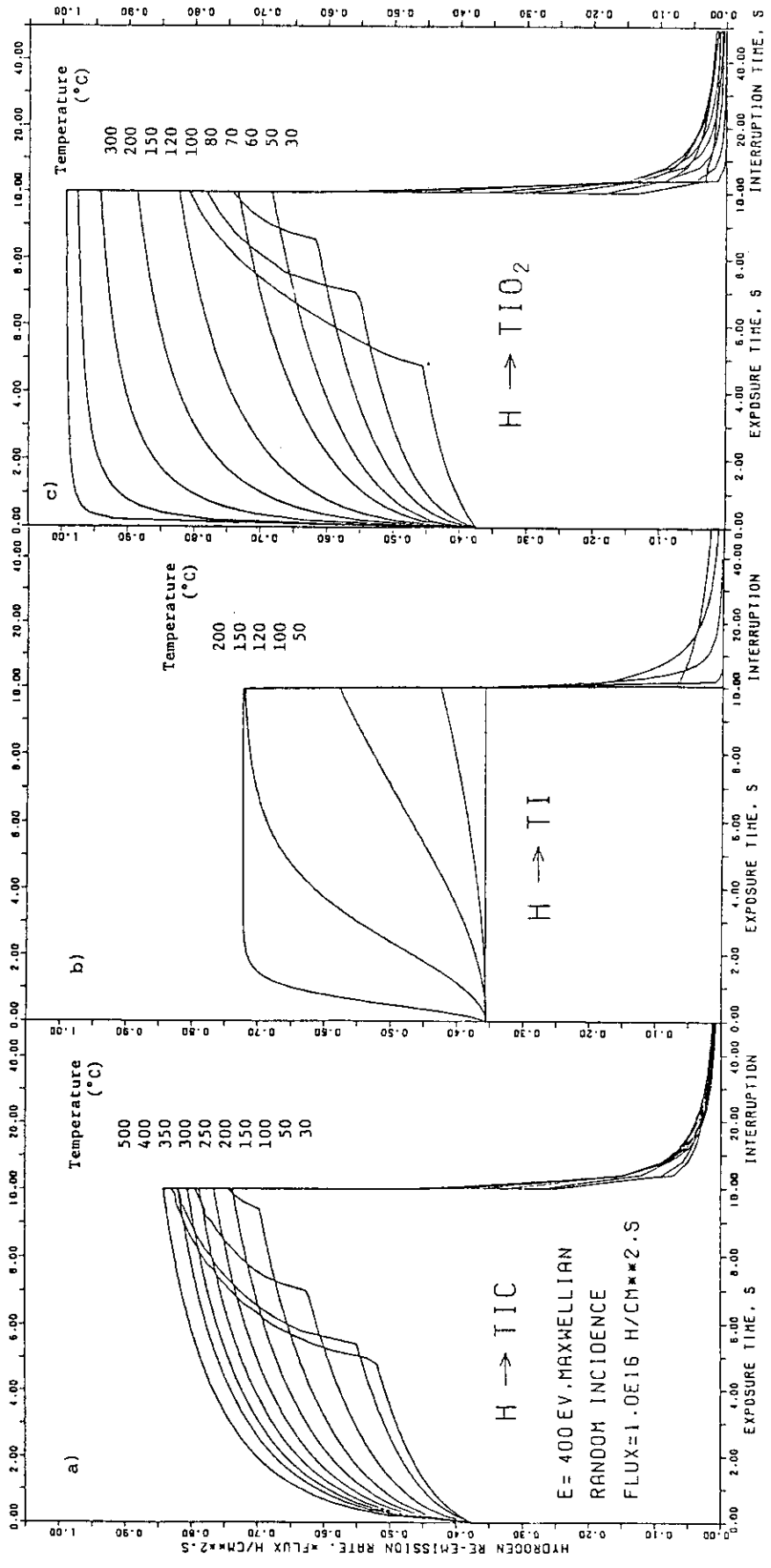

Fig. VI.1-9 Calculated recycling coeffecients as a function of time and wall temperature for a Maxwellian energy distribution of 400 eV. a) TiC, b) Ti, c) TiO_2.

2. Vacuum Technology

2.1 Introduction

The JT-60 device creates a necessity for solving new problems in the vacuum and surface technological area. They include elaborate wall preparation processes such as coating of low-Z materials and discharge cleaning, development of leak locating techniques applicable to large vacuum vessels, and improvements of vacuum components[1]. In this fiscal year, significant progress was made on the preparation and characterization of TiC-coated first walls to be installed in the JT-60 vacuum vessel, and the development of an in-situ coating device and leak locating devices.

2.2 Preparation and characterization of TiC-coated first walls for JT-60

The small sample test for selecting coating materials and methods in FY 1981 and the improvement in coating technique for making large-sized first walls in FY 1982 were followed by the construction of large coaters at industries to mass-produce nearly 10,000 first walls and the characterization of the coated walls in FY 1983. The material and thickness of the coatings are titanium carbide (TiC) and 20 μm, respectively. A plasma-assisted CVD method named TP-CVD[2] was used for the walls of molybdenum substrate, and an activated reactive evaporation method named HCD-ARE[3] was used for the walls of Inconel substrate. The respective temperatures of TiC deposition were 900°C for molybdenum substrate and 500°C for Inconel substrate. Figure VI. 2-1 shows the TP-CVD coaters, and Fig. VI. 2-2 shows the HCD-ARE coater.

Material characterization of the walls was done by X-ray diffraction analysis, electron probe micro analysis, X-ray photoelectron spectroscopy (ESCA), Auger electron spectroscopy and metallurgical micrography[2,3]. Some characteristics of the coatings determined by these analytical methods are summarized in Table VI. 2-1. The XPS analysis showed that the chemical shifts for C1s and $Ti2p_{3/2}$ are nearly equal to those in TiC single crystals.

2.3 Development of an in-situ coating device for JT-60

An in-situ coating device for TiC deposition is also being developed for the repair of TiC-coated walls. In FY 1981 the coating method was

decided to be reactive evaporation, i.e., evaporating titanium in a low pressure acetylene atmosphere. In the JT-60 device, four vertical ports 20 cm in diameter are provided to mount titanium evaporation sources.

In FY 1983, the performance test was made of different types of ohmic-heating titanium evaporators[4]. The evaporator which exhibited the best performance consists of three tungsten wires twisted as the core of the composite, three titanium wires and one molybdenum wire densely wound around the core, and a thin tungsten wire coarsely wound at the outermost side of the composite. A typical size of the evaporator is 4 mm in diameter and 14 cm in length. In this case, 2 - 2.5 g of titanium, which corresponds to 70 - 80 % of charged amount, can be evaporated at a rate of about 0.14 g/min. Figure VI. 2-3 shows the novel evaporators prior to and after titanium evaporation.

The design of a prototype coating device was also developed in cooperation with industries.

2.4 New leak locating techniques for large vacuum systems

New techniques for leak checking large vacuum vessels are being extensively developed since FY 1981. For the in-vessel leak sensor method, fabrication and testing of a prototype manipulator with built-in motors and a small ionization gauge are steadily advanced.

A new helium sniffing method was also developed[5]. The low sensitivity problem of the conventional helium sniffing method has been overcome by increasing the gas draw rate from around leaks into the detector up to about 0.1 $Pa \cdot m^3/s$. The devised system consists of a flexible stainless steel capillary tube 0.6 mm in inner diameter and 10 m long, a sorption pump using molecular sieve and a helium leak detector in series, as shown in Fig. VI. 2-4. This method is particularly useful for locating very fine leaks down to 10^{-11} $Pa \cdot m^3/s$, and has been successfully applied for leak checking the magnetic limiter coil cans of JT-60.

References

1) Murakami Y., Proc. 9th Intern. Vacuum Congr. & 5th Intern. Conf. on Solid Surfaces (Madrid, 1983) p.532.

2) Fujimori N., Yashiki T., Doi A., Abe T., Murakami Y., Mizoguchi T., and Itou Y., to be published in Proc. 11th Intern. Conf. on Metallurgical Coatings (San Diego, 1984).

3) Inagawa K., Watanabe K., Tanaka I., Itoh A., Abe T., Murakami Y., and Mizoguchi T., to be published in Proc. 6th Intern. Conf. on Plasma Surface Interactions in Controlled Fusion Devices (Nagoya, 1984).

4) Inagawa K., Abe T., Hiroki S., Obara K., and Murakami Y., JAERI-M 84-105 (1984) (in Japanese).

5) Murakami Y., Shimomura Y., Abe T., and Obara K., submitted to J. Vac. Sci. Technol.

Table VI. 2-1 Some characteristics of the TiC coatings determined by X-ray diffraction analysis, EPMA, AES and metallurgical micrography.

Coating method	Substrate material	Thickness (μm)	Composition C/Ti	Cristal orientation (Relative intensity) 111	200	220	311	222	Lattice constant* (Å)
TP-CVD	molybdenum	20 ± 5	0.97	79	100	79	44	28	4.328
HCD-ARE	Inconel 625	20 ± 5	0.97	17	58	100	6	2	4.33

* The value appeared in ASTM is 4.3285 Å.

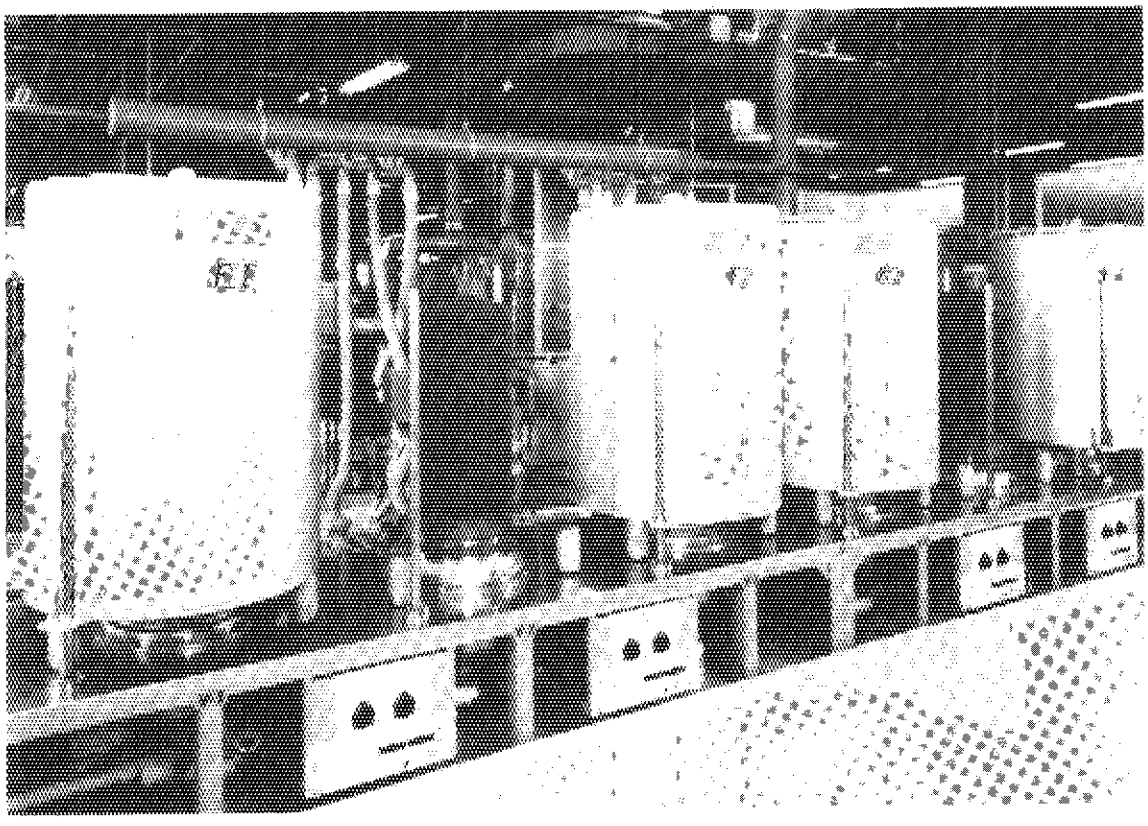

Fig. VI. 2-1 TP-CVD coaters for depositing TiC on molybdenum substrates (Courtesy of Sumitomo Electric Industries).

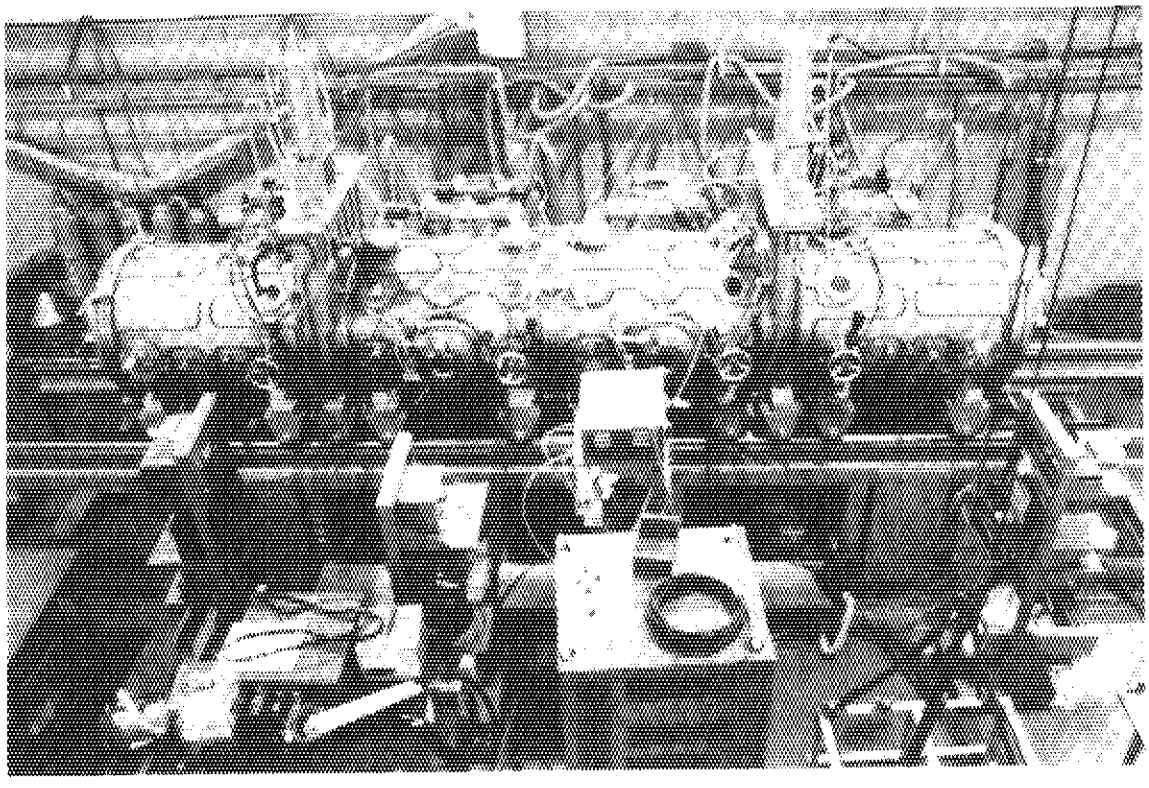

Fig. VI.2-2 HCD-ARE coater for depositing TiC on Inconel substrates (Courtesy of ULVAC Corporation).

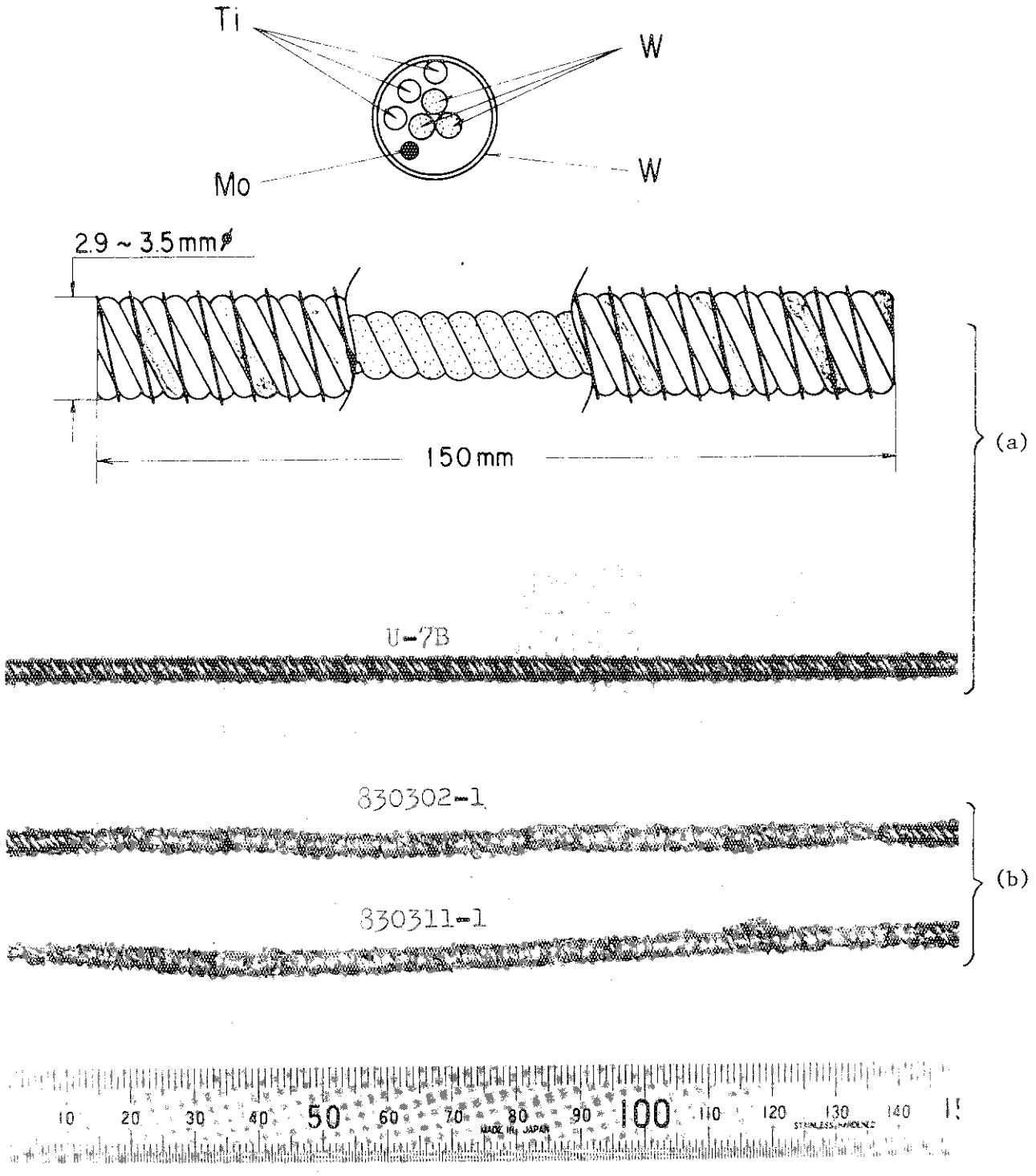

Fig. VI. 2-3 A new type of ohmic-heating titanium evaporators. (a) prior to titanium evaporation, (b) after titanium evaporation.

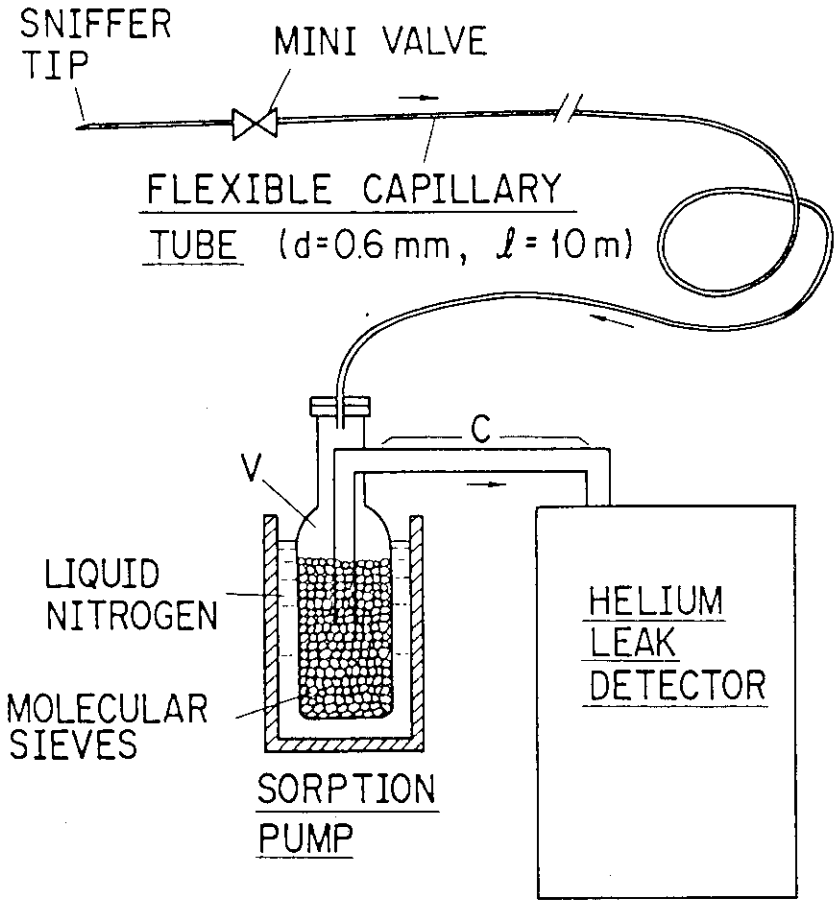

Fig. VI. 2-4 Schematic diagram of a new helium sniffing device for locating very fine leaks of large vacuum vessels.

VII. SUPERCONDUCTING MAGNET DEVELOPMENT

1. Introduction

The objective of superconducting magnet development in JAERI is to establish the design, fabrication and operation technique for Tokamak Fusion Experimental Reactor. As toroidal coil development, two projects are being carried out. One is Cluster Test Program for high field generation and another is Large Coil Task, an international collaboration, for scaling-up. As poloidal coil development, high current pulsed conductor has been developed. Cryogenic technology, structural material, measurement and control technique are intensively being developed. Main achievements in FY 1983 in JAERI Supercondcting Magnet Laboratory are as follows.

1) The Japanese LCT coil was installed in ORNL's LCTF and partial cool-down was carried out.

2) Extended test of Nb_3Sn Test Module Coil was successfully performed.

3) Three different type poloidal conductors of 15 - 30 kA were fabricated and tested.

4) 4K fatigue test machine of structural material was installed and automatic J_{ic} measurement system was attached.

5) New stainless steel and manganise steel, which have yield strength over 1500 MPa and K_{ic} over 200 MPa$\sqrt{m}$, have been developed.

2. Cluster Test Program

2.1 The second test on the TMC-I[1)]

The Cluster Test Program (CTP) was started at 1977 as the development of high field toroidal coil in tokamak device. The first Test Module Coil (TMC-I) was completed in July of 1982 and was set in the Cluster Test Facility (CTF). This CTF is composed of a helium liquefier/refrigeration, a power supply with protection, a vacuum vessel, a computer, and a pair of the Cluster Test Coil (CTC) which produces toroidal magnetic field on the TMC-I. The first test of the TMC-I was carried out in October of 1982 and a magnetic field of 10.2 T was successfully generated. Table VII.2-1 shows the parameters of the TMC-I and Fig. VII.2-1 shows the TMC-I being installed in the CTC.

In April of 1983, the second test of the TMC-I as the extention of the stability, the manual dump and the out-of-plane force mode tests, was carried out. Under this severe test, the TMC-I was operated without

any damage. Thus, we have demonstrated that a Nb_3Sn conductor has the feasibility to apply large and high field superconducting coils for fusion. The following is the main results.

(1) Current charge and mechanical behavior

After the TMC-I was reconfirmed to be in a magnetic field of 10 T at 6 kA with a back-up field of 3.3 T from the CTC, the observation of the mechanical behavior of the coil was performed with a number of strain gauges attached on the conductor and on the coil case. Figure VII.2-2 shows the measured strain curve on the conductor during the TMC-I charge with a background field of 3.3 T from the CTC. The maximum strain due to electromagnetic force at 10 T on the Nb_3Sn conductor in the innermost turn is 0.13 %. The total strain of Nb_3Sn is 0.67 % including a bending strain of 0.54 % during winding. These values are in good agreement with the calculated ones.

In the out-of-plane force mode operation using one of the CTC, 323 MPa which is 80 % of yield strength of S.S. 316 L at 4 K appears in the outer ring of the helium vessel. In the practical experiment, the TMC-I was stably operated under high stress condition.

(2) Stability test

The extended stability test was carried out using 192 cm length heater which was located in the innermost one turn. Figure VII.2-3 shows the tap voltage and the temperature profiles of the conductor at 10 T and 6 kA. After the innermost turn became normal and the temperature reached more than 20 K by heating, the normalcy recovered spontaneously to the superconducting state in 5.7 second. This result shows that the cold end recovery to superconductivity was practically demonstrated in 10 T on the Nb_3Sn coil. The measured generation heat flux level is 1.08 W/cm^2.

(3) Manual dump test

A manual dumping test of the TMC-I was carried out to check possible damage due to high voltage, and to measure the dump losses, the temperature rise of the conductor and the pressure rise of helium in the coil due to the losses generated by the charging field. Figure VII.2-4 shows the temperature rise and the pressure rise during the manual dumping from 5.4 kA with a time constant of 4.0 second. The measured maximum temperature is 8.5 K, which is below the critical temperature of Nb_3Sn, and no significant normalcy appeared. In this case, the dump

loss is around 150 kJ.

Figure VII.2-5 shows dump loss vs. dump decay time constant. The dump losses are proportional to an inverse of the dump time constant. These measured dump losses agree well with the analyzed values and the advantage of Nb barrier for ac loss has been verified.

2.2 Research and development for the TMC-II[2)]

For the TMC-II which is the second test coil in the Cluster Test Program, a 12 T-10 kA Nb_3Sn forced flow cooled conductor was designed in the last period, as shown in Fig. VII.2-6 (a). To develop this conductor, two verification test programs were started in this period. One is the Segment TEst Program (STEP) whose purpose is to measure precisely Nb_3Sn critical current characteristic with conductor strain, and to study a stability of the conductor and a behavior of coolant in a large size conductor (10 kA, 12 T). In this program, two test coils (STEP-I,II) were fabricated in the end of 1983. The experimental arrangement of these coils is shown in Fig. VII.2-/. The STEP-I conductor has been designed to simulate the form of the TMC-II conductor, as shown in Fig. VII.2-6 (b). This test coil was charged up to 10 kA at 8 T without quench, and the coolant behavior in this conductor was measured. The stability test by the heater technique will be carried out in the next period. The key characteristic of STEP-II (Fig. VII.2-6 (c)) is that its conductor is stabilized by high purity aluminum. The measured critical current density of this conductor is 400 A/mm^2 at 12 T, and nearly equal to that of the usual conductor. The STEP-II will be tested in the next period. Another is FC-100M program whose purpose is to study a behavior of coolant in a long length conductor, as shown in Fig. VII.2-6 (d). The test coil of this program was completed, and will be tested in the next period.

3. Large Coil Task of IEA

3.1 Status of the Japanese test coil in ORNL

In this year, the installation work and preliminary cool-down test were performed in Oak Ridge National Laboratory (ORNL). The installation work of the Japanese test coil in the Large Coil Test Facility (LCTF) at ORNL was performed under the supervision of JAERI's staffs. During the work, the US-GD coil was delivered to ORNL in June, 1983, and the installation work was started in parallel. The two-coil instal-

lation was completed in December, 1983. Figure VII.3-1 shows the coils in the LCTF vacuum tank. Preliminary two-coil cool-down was started on January 10, 1984. Figure VII.3-2 shows the cool-down characteristic of the Japanese coil. In the test, the minimum temperature of the coil reached around 120 K. The Japanese coil showed the same performance during the cool-down as that in the domestic test[3]. On the other hand, the leakage of helium gas was found in the GD coil. Therefore, GD coil was removed from the vacuum tank and was repaired. In the meantime, the Swiss coil was delivered to ORNL in February. Considering these conditions, the Project Officers agreed to the installation of the Swiss coil in the vacuum tank and to the three-coil test in which only the Japanese and GD coils are charged. The preparation for the three-coil test is under way.

3.2 Test plan of LCT coils in ORNL

Major objectives of the preliminary two-coil cool-down test were, (1) to obtain cool-down characteristics on the pool-cooling coils (Japanese and GD coils) and large amount of structures (bucking post, upper and lower colors, torque rings, etc.), and (2) to do the shake-down of the cryogenic system and data acquisition system in the LCTF. In the test, some important results were obtained on both items above. And it was demonstrated that two pool-cooling coils had almost the same characteristic of the cool-down in spite of different configurations of the windings. As the next step to the six-coil test, three-coil test is scheduled as shown in Table VII.3-1. In this test, the Swiss coil, which is forced-cooling type, is cooled down with Japanese and GD coils. Further informations on the refrigeration technique are expected.

4. Pulsed Poloidal Coil Development[4,5,6]

4.1 Highlights

New technology for superconducting poloidal coils has been under development for the Fusion Experimental Reactor (FER). In 1983, large sized samples for testing of three high-current poloidal conductors, JA-50, JB-50, and JF-30, were fabricated and tested. These conductors have already been developed by 1982. By testing of these samples, characteristics of these conductors were measured and in addition, operating experiences of high-current pulsed coils up to 30 kA and a forced-flow supercritical helium up to 60 g/s were obtained.

4.2 Verification tests for pool-cooled conductors (JA-50, JB-50)

As the maximum capacity of the DC power supply in the Superconducting Engineering Test Facility (SETF) is 30 kA, 3/5-sized pulsed conductors of 50-kA, JA-50 and JB-50 were fabricated and wound in 30-kA, 12-turn windings. The inner diameter of this winding is 500 mm, and the outer diameter is 820 mm. These windings were attached to a pulsed coil, Pulser-C, one by one. Figure VII.4-1 shows the combination of Pulser-C and the winding of JA conductor. The maximum field at the windings was about 2 T under this arrangement, and both windings of JA and JB conductors were successfully charged up to 30 kA in 18 sec. Fast discharge experiments were carried out from 30 kA by the discharge time constant of 60 msec, which is to be compared to 10 - 100 sec for DC coils. Loss energy generated by such a fast discharge is expressed by the following equation:

$$\text{(Pulsed loss energy)} : Q_p = \frac{\tau_c}{\tau_p + \tau_c} \text{(Magnetic Energy within the Coil)}$$

Here, τ_p is the discharge time constant and τ_c is the loss time constant of the winding. Loss time constant corresponds to a decay time of induced current in the superconductors, and this value for pulsed coils has been decreased down to 1/100 of DC pulsed coils. Therefore, any problem was not found during 60-msec discharge.

4.3 Verification tests for a forced-cooled conductor (JF-30)

A 4-turn, 15-kA loop with the diameter of 2.3 m was fabricated, using a 1/2-sized pulsed conductor of 30-kA JF-30. This loop was installed in the 5-m-dia., 8-m-high vacuum tank of the SETF and the cryogenic characteristics of JF conductors were measured. Figure VII.4-2 shows external view of the forced-cooled loop. A normal zone was artificially generated by a heater attached to this loop and its propagation characteristics were measured. Figure VII.4-3 shows a result of this experiment. It was confirmed that no destructive expansion of normal zone does occur and its propagation is under control of helium flow.

5. Cryogenic System Development

5.1 Introduction

Refrigeration of superconducting magnet for fusion machine requires helium liquefier/refrigerator which has bigger capacity and higher reliability. In JAERI, such a big refrigerator has been investigating. According to the plan of development of refrigerator, in this period, technique of forced-cooled was accomplished through the construction and the experiment of the forced-cooled test facility and, in regard to the development of cryogenic devices, cryogenic helium pump and new type of current lead were fabricated and tested.

5.2 Experiment of forced-cooled superconducting test loop

Forced-cooled superconducting test facility was designed and constructed in order to advance the forced-cooled technique in JAERI. After construction, the experiment was performed and then it succeeded in generating supercritical helium of 60 g/s, 10 atm, and 4.5 K. By using this facility, 15 kA superconducting test loop which aims to develop the forced-cooled type of pulsed poloidal coil was experimented and it gave us a lot of data which are, for example, stability of conductor under forced-cooled helium and flow characteristics of supercritical helium. As an example of these data, pressure drop characteristics of supercritical helium is shown in Fig. VII.5-1.

5.3 Development of cryogenic helium pump

It is necessary for forced-cooled technique that the coolant of helium should be compulsorily circulated by a certain circulator. Cryogenic helium pump which might have a higher thermodynamic efficiency is needed to develop in this point. In JAERI, cryogenic helium pump was designed and fabricated as the flow capacity of about 100 g/s and adopting the bellows type. Figure VII.5-2 shows the appearance of this pump.

5.4 Development of new type of current lead[7)]

Fusion Experimental Reactor requires the current lead whose capacities are more than 30 kA of charging current and more than 20 kV of insulation voltage. Heat load of current lead is big problem for cryogenic system because it is connected from about 4 K to room temperature. As a new type of current lead, the type of cable-in-conduit

is employed to extend the surface of copper conductor to get a good heat transfer to coolant of helium. The new current lead, which was designed as 3 kA of charging current, was fabricated and tested. According to the results, it required only 0.05 g/s of helium coolant for every 1 kA of charging current. JAERI intends to perform the verification test of new current lead at 6 kA, 15 kA, and finally 30 kA of charging current in future.

6. Development of the New Cryogenic Structural Material

We have been developing the new cryogenic structural materials, which have yield strength of more than 1,200 MPa and fracture toughness of more than 200 MPa$\sqrt{m}$, for Fusion Experimental Reactor (FER)[8].

The kinds of steels were selected from the results of tensile and Charpy impact tests at 4K[9]. Fracture toughness test and fatigue test on these materials are necessary to develop the new cryogenic structural materials in future. Therefore, cryogenic fatigue test machine which has the capacity of ± 5 ton in condition of dynamic loading and ± 10 ton in condition of static loading was installed. Then Jic measurement system was prepared in order to measure fracture toughness Kic (J) efficiently at 4 K. This system consists of the cryogenic fatigue test machine, mini computer PDP/11-70 and interface between them.

Up to now, fracture toughness Kic (J) using computerized unloading compliance method of three kinds of high manganese austenitic stainless steels and two kinds of austenitic stainless steels were measured. Figure VII.6-1 shows the relation between fracture toughness and yield strength at 4K. One austenitic stainless steel satisfies very high requirements, which are yield strength over 1,200 MPa and fracture toughness over 200 MPa$\sqrt{m}$. Other steels also have high fracture toughness compared with existing stainless steels which have the same yield strength.

7. Design Study for a Medium Sized Superconducting Tokamak[10]

7.1 Necessity of a medium sized superconducting tokamak

Along the progress in the scientific research of plasma initiation and control, the verification of a long pulse tokamak has become a significant and realistic target in the fusion research. For the realization of a long pulse tokamak, steady state magnetic field generation by superconducting coils is indispensable. For this purpose the Fusion

council in Japan proposed a development plan for superconducting coils and the construction of a medium sized tokamak, called Superconducting Tokamak Test Assembly (STTA). Along this plan, JAERI has made development step by step towards the realization of superconducting toroidal field (TF) coils.

7.2 Management of the design study

JAERI started the design work of the STTA based on the technical experience obtained through the development of Cluster Test Coils (7T), IEA LCT coil (8T), and the Test Module Coil (11T). Four companies were involved in this work and design meetings were held monthly at JAERI. JAERI's role in this meeting was not only to indicate the design requirements but also to make design proposals to the meeting as well as the industries. Five design proposals from JAERI and industries were compared through discussion in the design meeting, and the unified design was selected at each intermediate step.

7.3 Major results of the design

In 1983, design work was carried out on the following items;

*1 Basic design of coil systems
*2 Structural design and analysis
*3 Thermal system design and analysis
*4 Power supply circuit and coil protection
*5 Arrangement of material data at 4 K

Table VII.7-1 shows the tentative parameters for the present design of the STTA, and Fig. VII.7-1 shows a bird's-eye view of the coil system.

Evaluation of electromagnetic forces indicated that the centering force is 9554 ton/(one TF coil) and turning force is 1035 ton/(upper half of one TF coil) at the moment of the plasma flat top. Stress analysis of the torus composed of 12 TF coils was carried out based on 5 different mechanical model which covers wide variety of mechanical interactions between structural elements. As a whole result of the analysis, the inner bore width of TF coils at the mid plane is estimated to increase by 3.5 mm (1.5 % of original width), the maximum stress on the stainless steel conductor conduit is 410 MPa, and the maximum stress on the structure is 750 MPa. Yield strength of new structural material being developed at JAERI is more than 1200 MPa with high fracture toughness of more than 200 MPa m. Therefore, these materials can be applied

to the STTA with sufficient margin and thus, also from the structural view point, it was indicated that the STTA has become a feasible target for the construction at JAERI.

References

1) Ando T., et al., 8th International Conference on Magnet Technology, (Grenoble, Sept. 1983).
2) Ando T., et al., The 10th Symposium on Engineering Problems of Fusion Research, (Philadelphia, Dec. 1983).
3) Shimamoto S., et al., ANS 5th Topical Meeting on Technology of Fusion Energy, (Knoxville, April 1983).
4) Shimamoto S., et al., ibid.
5) Tsuji H., et al., Cryogenic Engineering Conference, (Colorado, August 1983).
6) Shimamoto S., et al., The 10th Symposium on Engineering Problems of Fusion Research, (Philadelphia, Dec. 1983).
7) Tada E., et al., Cryogenic Engineering 18 (1984) 324.
8) Yoshida K., et al., Austenitic Steels at Low Temperature, 1983.
9) Nakajima H., et al., Advances in Cryogenic Engineering (Materials), Vol.30, 1983.
10) Shimamoto S., et al., The 10th Symposium on Engineering Problems of Fusion Research, (Philadelphia, Dec. 1983).

Table VII.2-1 Main parameters of the TMC-I.

COIL SIZE	
WINDING INNER DIA.	600 mm
WINDING OUTER DIA.	1854 mm
WINDING WIDTH	300 mm
WINDING CONCEPT	10 DOUBLE PANCAKES
COOLING CONCEPT	POOL COOLING at 4.2 K
GRADING CONCEPT	TWO GRADES (10T/6.2T)
MAX. MAGNETIC FIELD	10 T
OPERATING CURRENT	6 kA
AVE. CURRENT DENSITY	30 A/mm^2 (in WINDING)
SELF INDUCTANCE	0.46 H
SUPERCONDUCTOR	
MATERIAL	Nb_3Sn / Nb_3Ti
SIZE	12.6 mm x 13.0 mm
CRITICAL CURRENT	10 kA at 10T / 6.2T
Cu/NON-Cu	5.36 / 10.1
STRUCTURAL MATERIAL	304L, 316L
FINAL ASSEMBLY	ELECTRON BEAM WELDING
LIQ. HELIUM INVENTORY	191 liter
COIL WEIGHT	7.71 ton

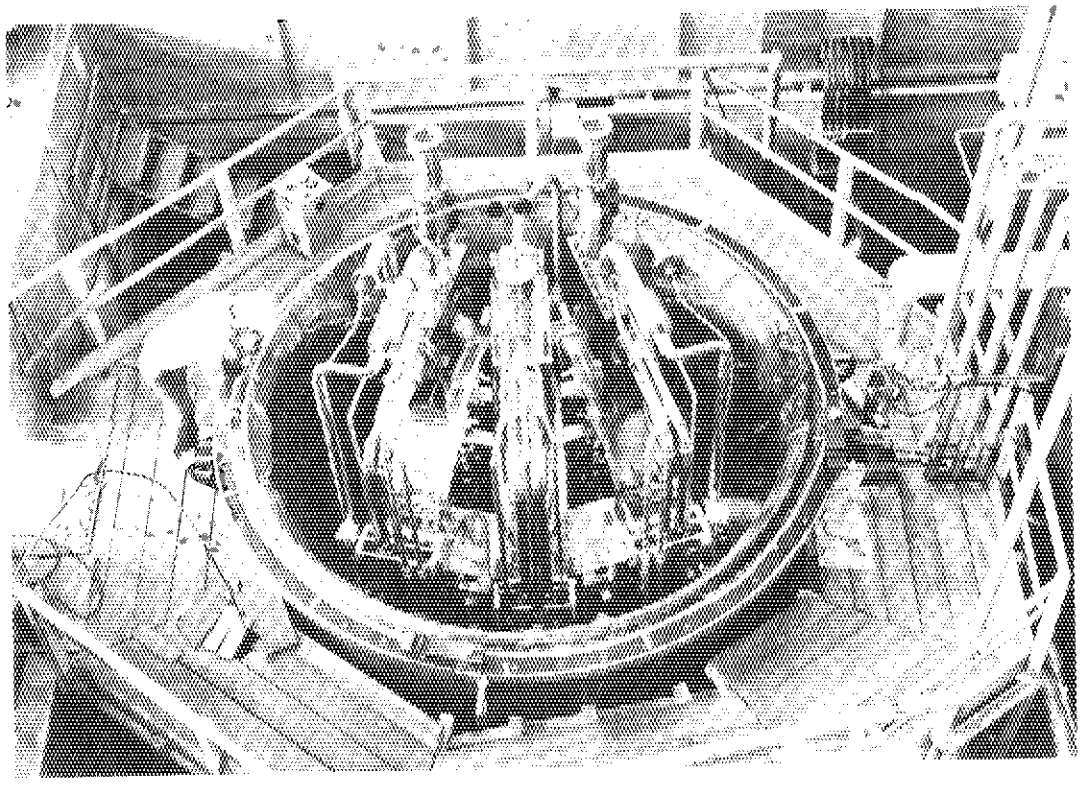

Fig. VII.2-1 Installation of the TMC-I in the Cluster Test Facility.

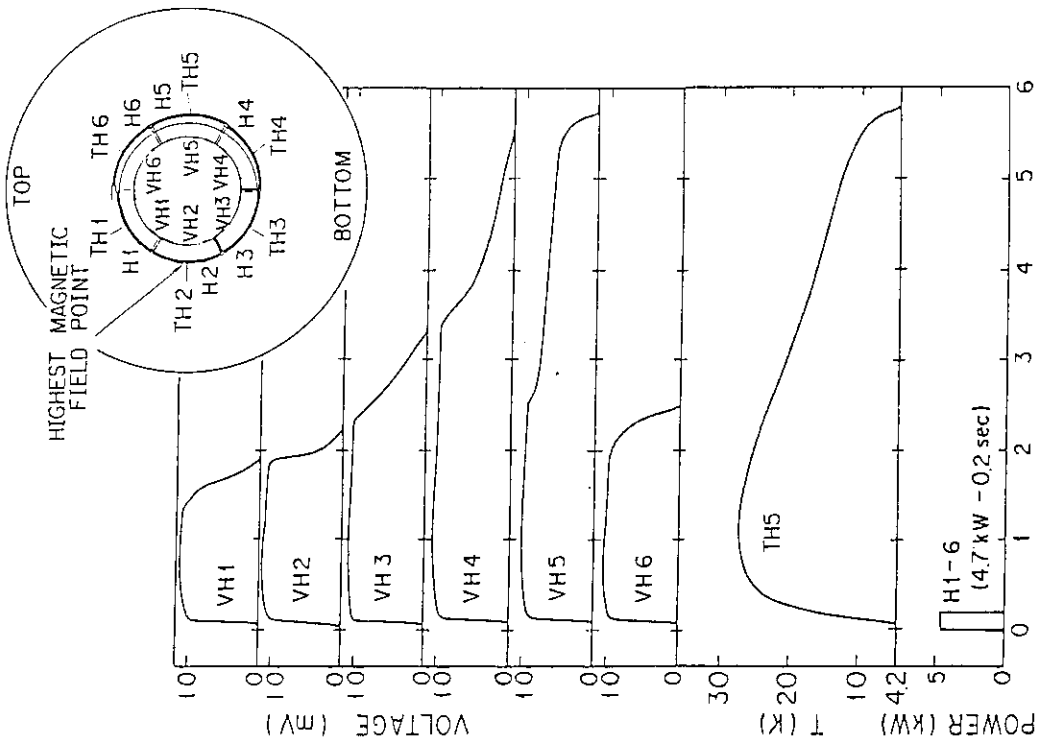

Fig. VII.2-3 Voltage and temperature profiles on the innermost one turn in the middle pancake at 6 kA after heater input.

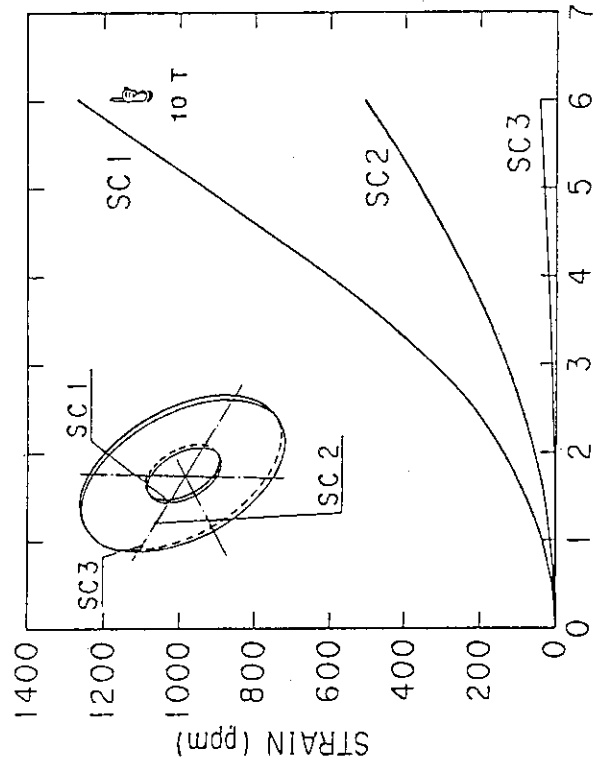

Fig. VII.2-2 Strain values of the conductor in the winding.

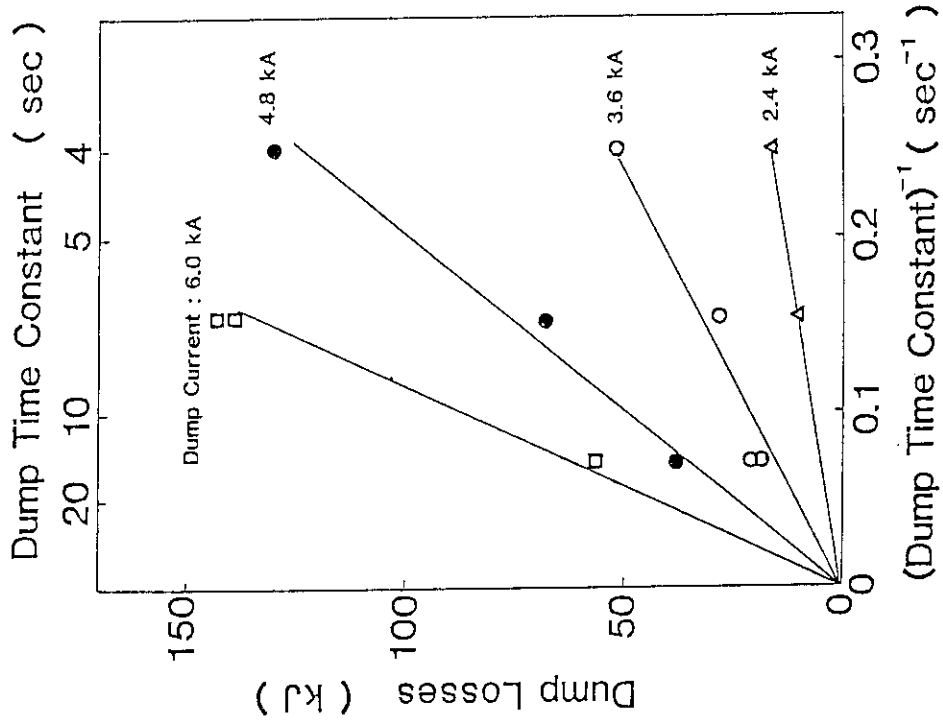

Fig. VII.2-5 Dump losses vs. dump decay time constant for several transport currents.

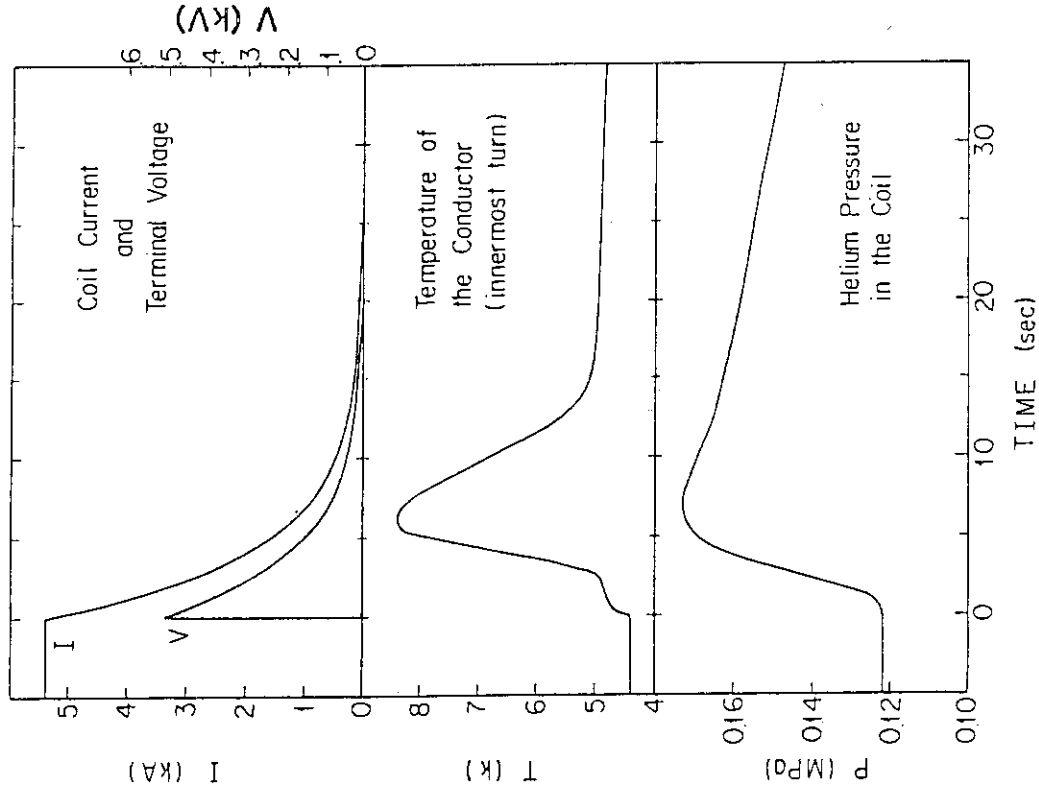

Fig. VII.2-4 Temperature and pressure rise due to manual dumping from 5.4 kA with a time constant of 4.0 second.

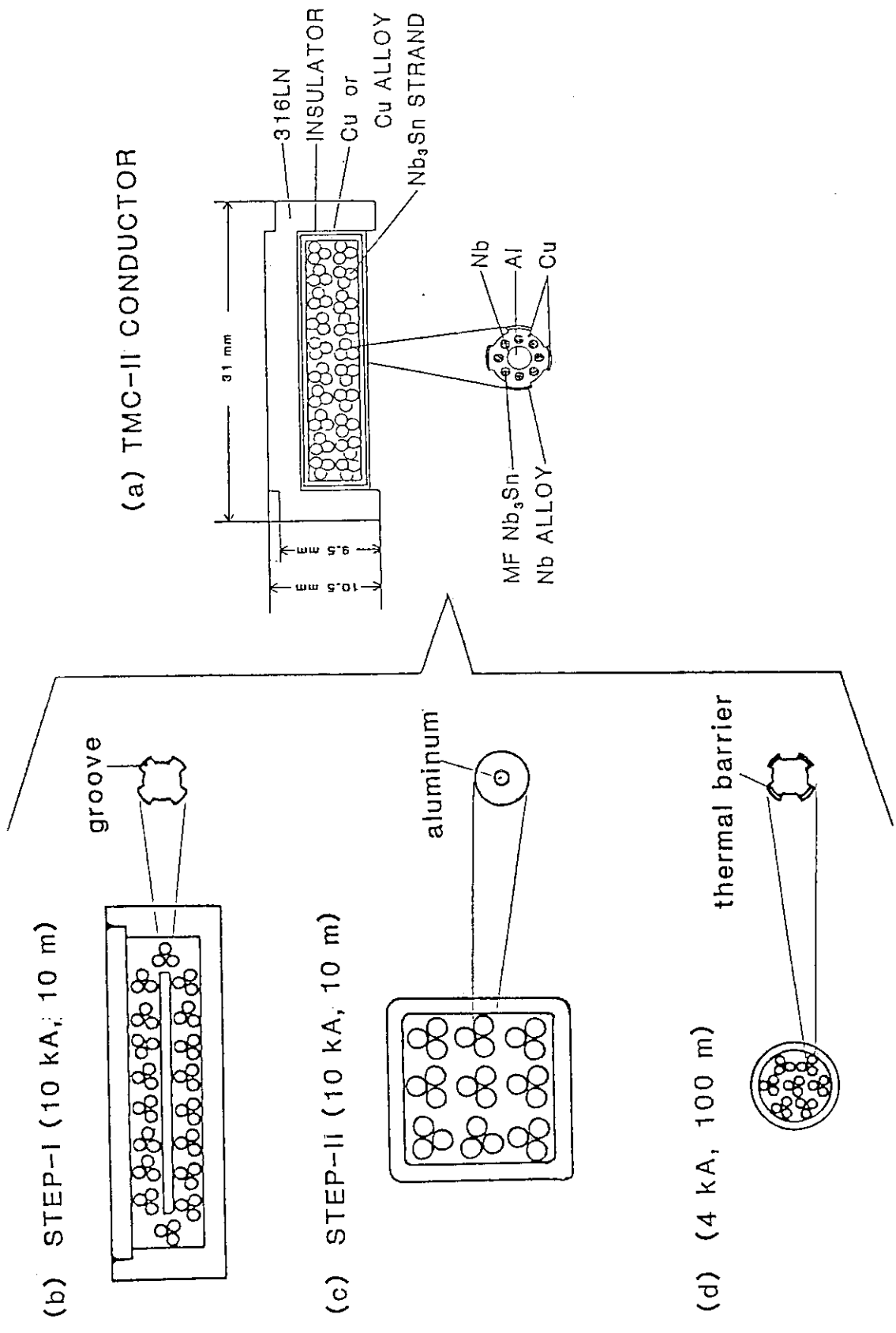

Fig. VII.2-6 R & D conductors for the TMC-II conductor.

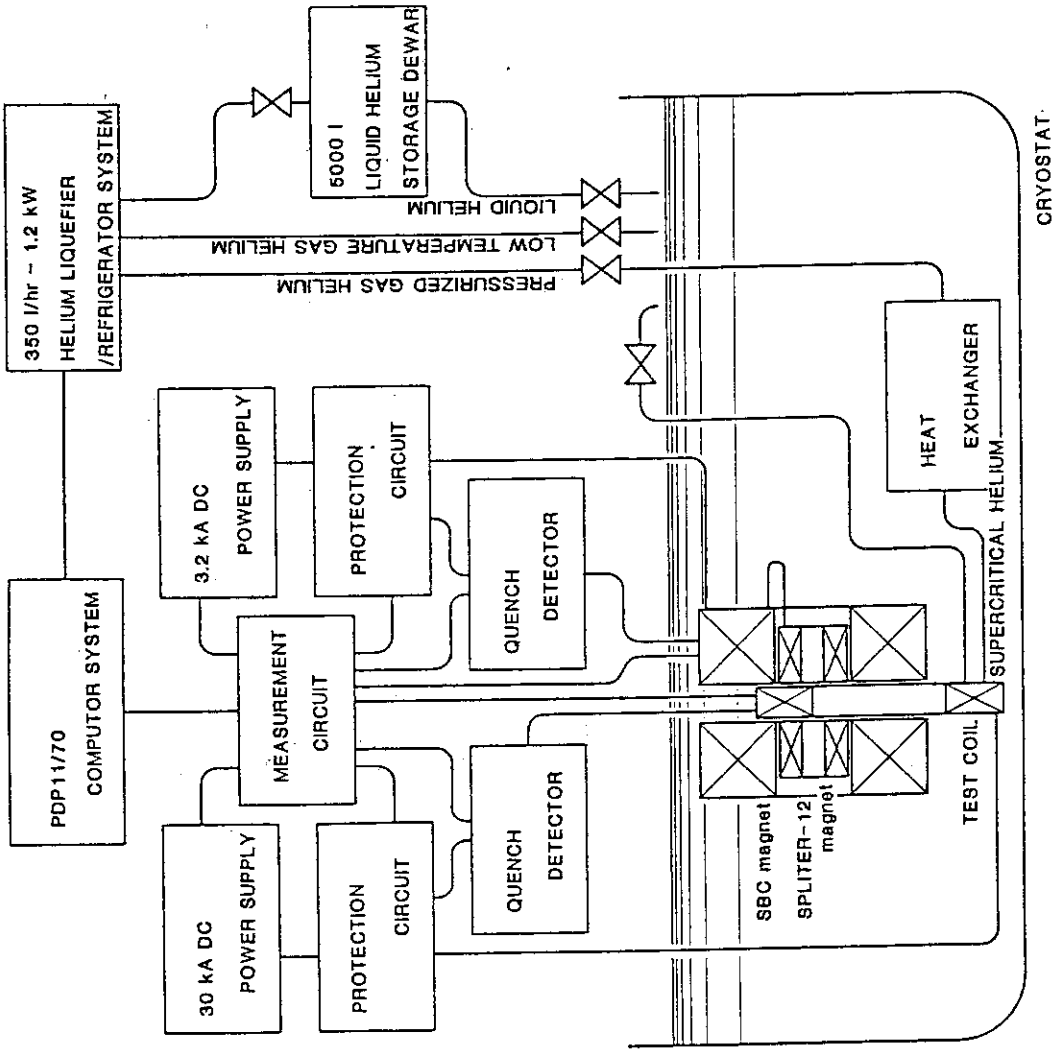

Fig. VII.2-7 Diagram of the Segment Test Facility for R & D of the TMC-II.

Table VII.3-1 Progress and schedule of the Large Coil Task.

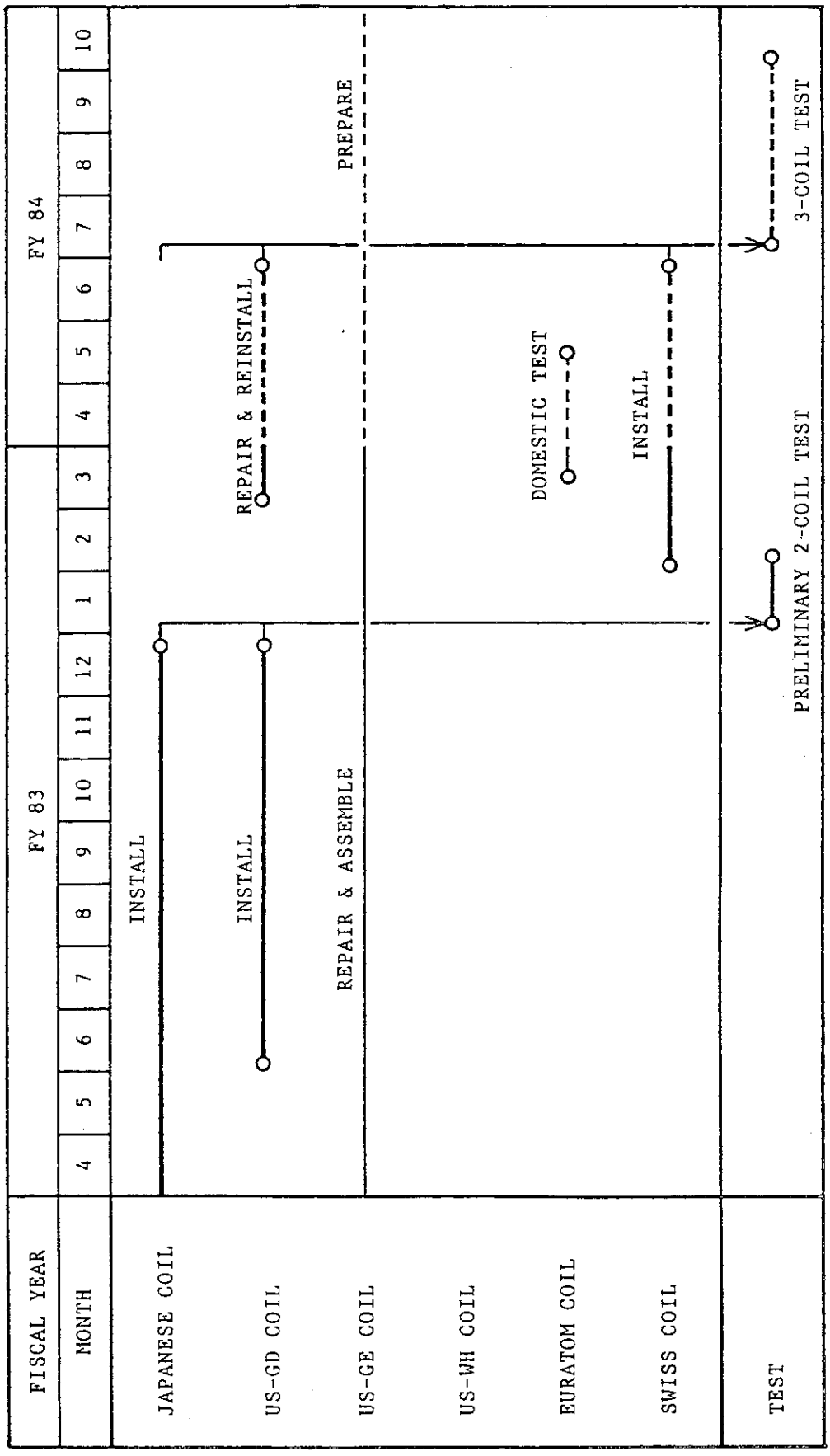

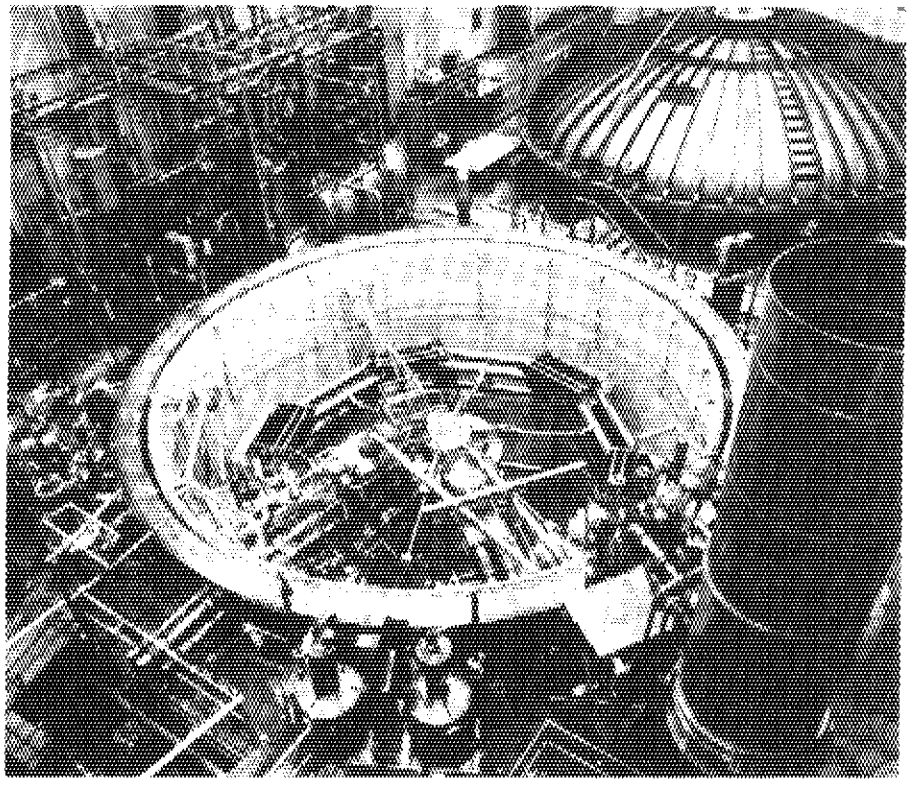

Fig. VII.3-1 The Japanese coil (left) and US-GD coil (right) were installed in the LCTF vacuum tank in ORNL.

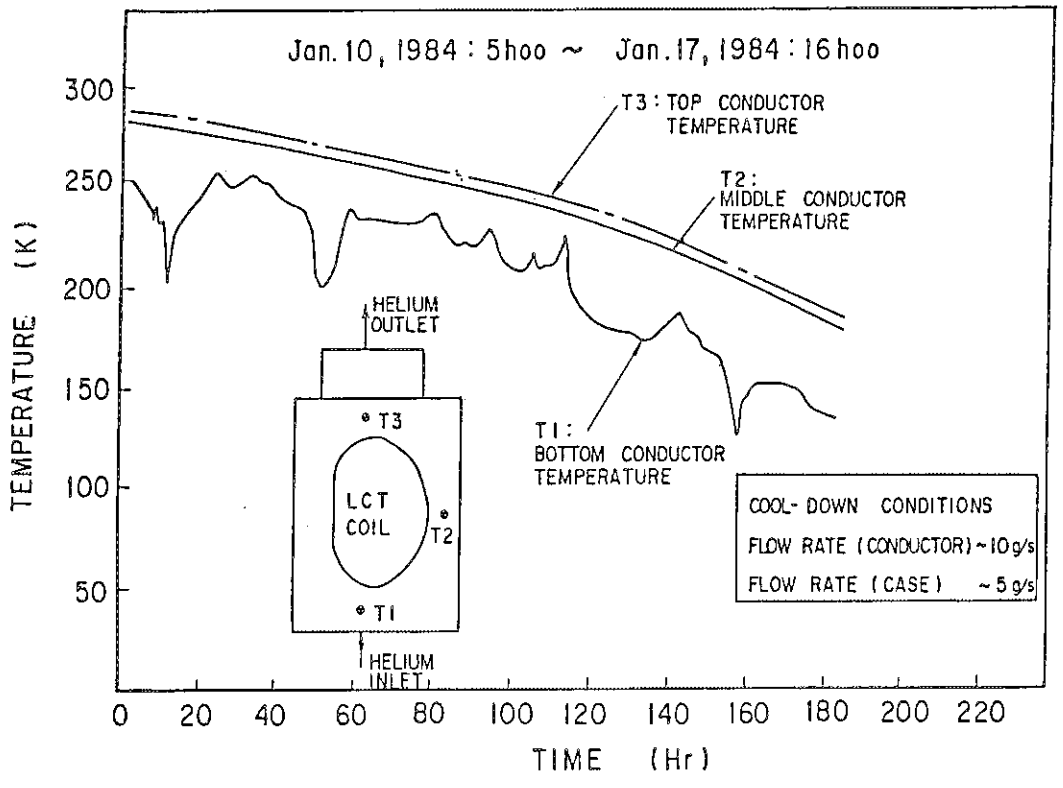

Fig. VII.3-2 Characteristic of the preliminary cool-down of the Japanese LCT coil in ORNL.

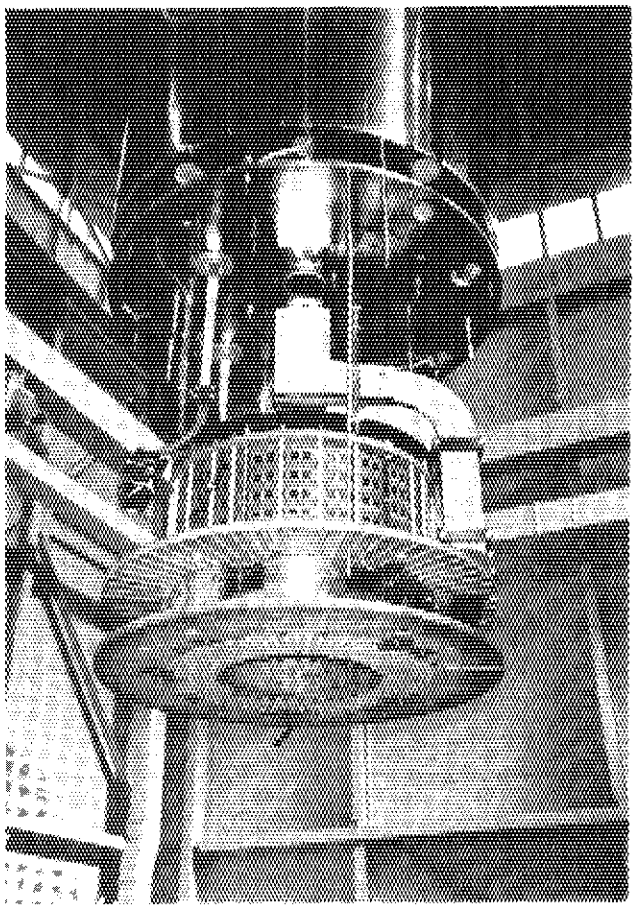

Fig. VII.4-1 External view of a 30-kA winding of JA conductor with Pulser-C.

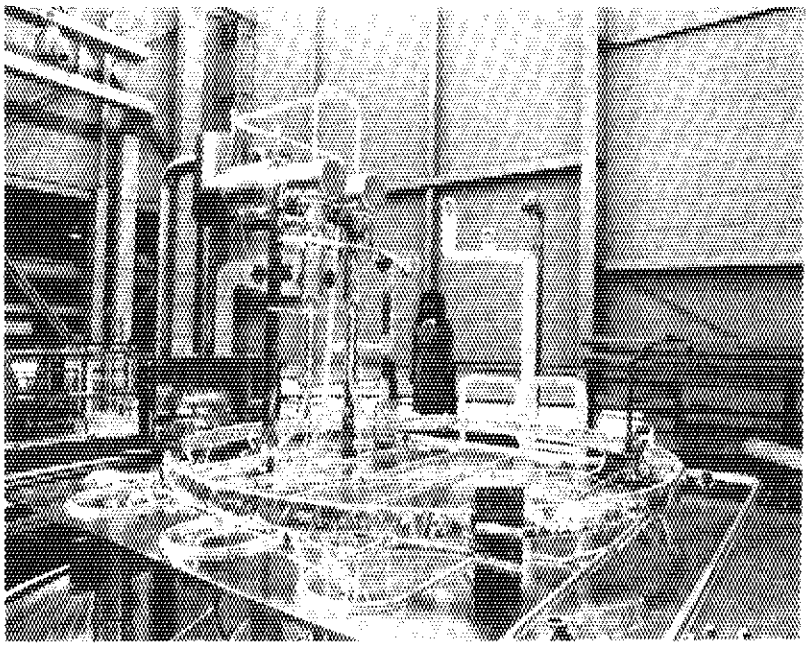

Fig. VII.4-2 External view of a 15-kA forced-flow loop.

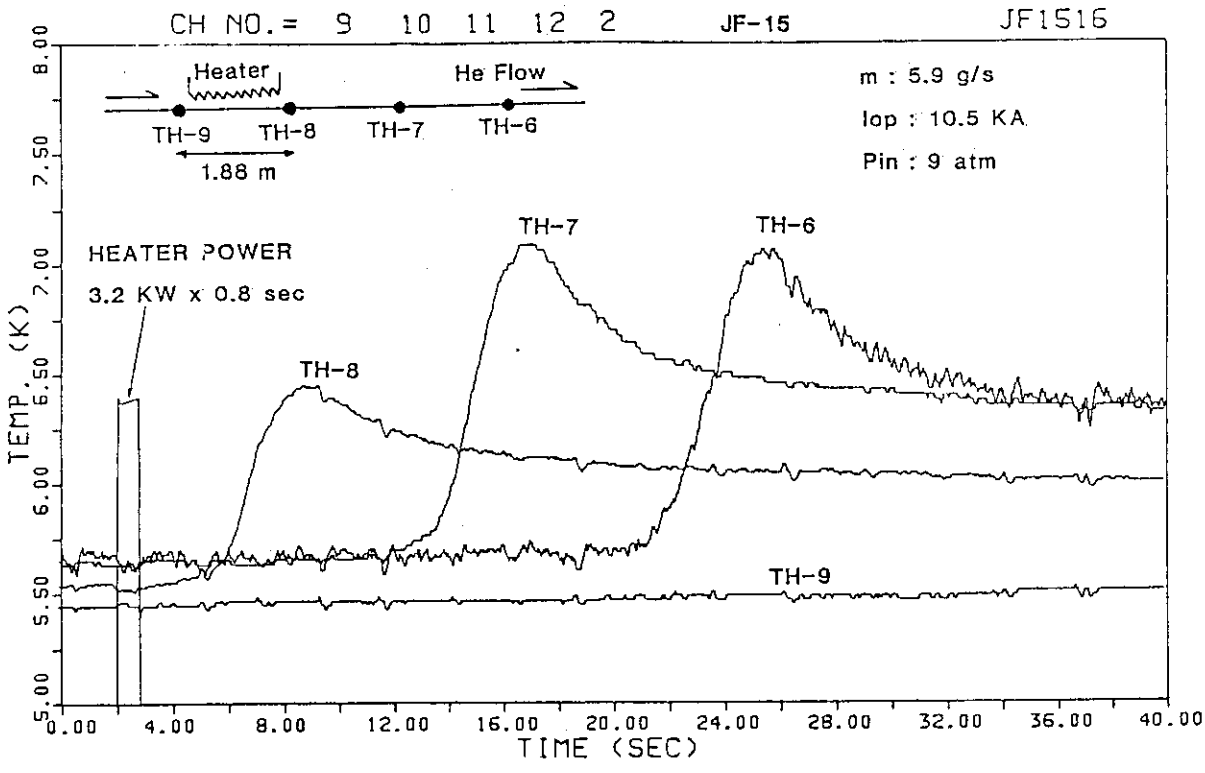

Fig. VII.4-3 Propagation of hot zone generated artificially in a forced-flow loop of JF conductor.

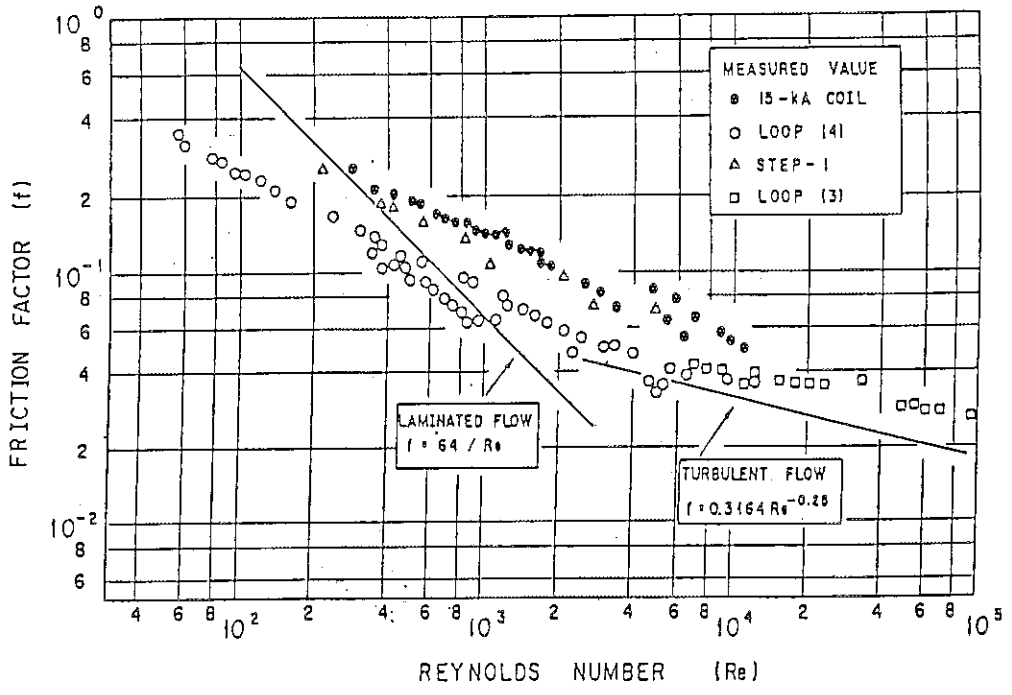

Fig. VII.5-1 Pressure drop characteristics of supercritical helium shown by using the relation between friction factor and Reynolds number.

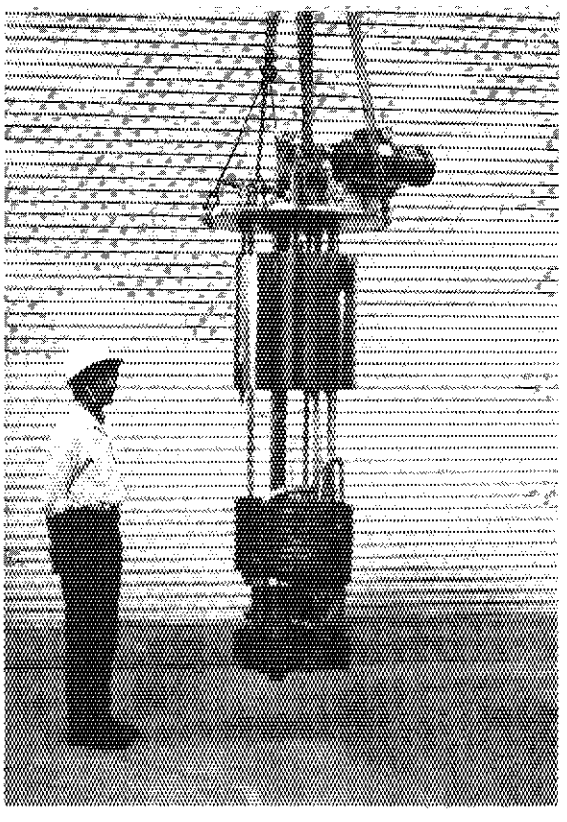

Fig. VII.5-2 Over view of cryogenic helium pump.

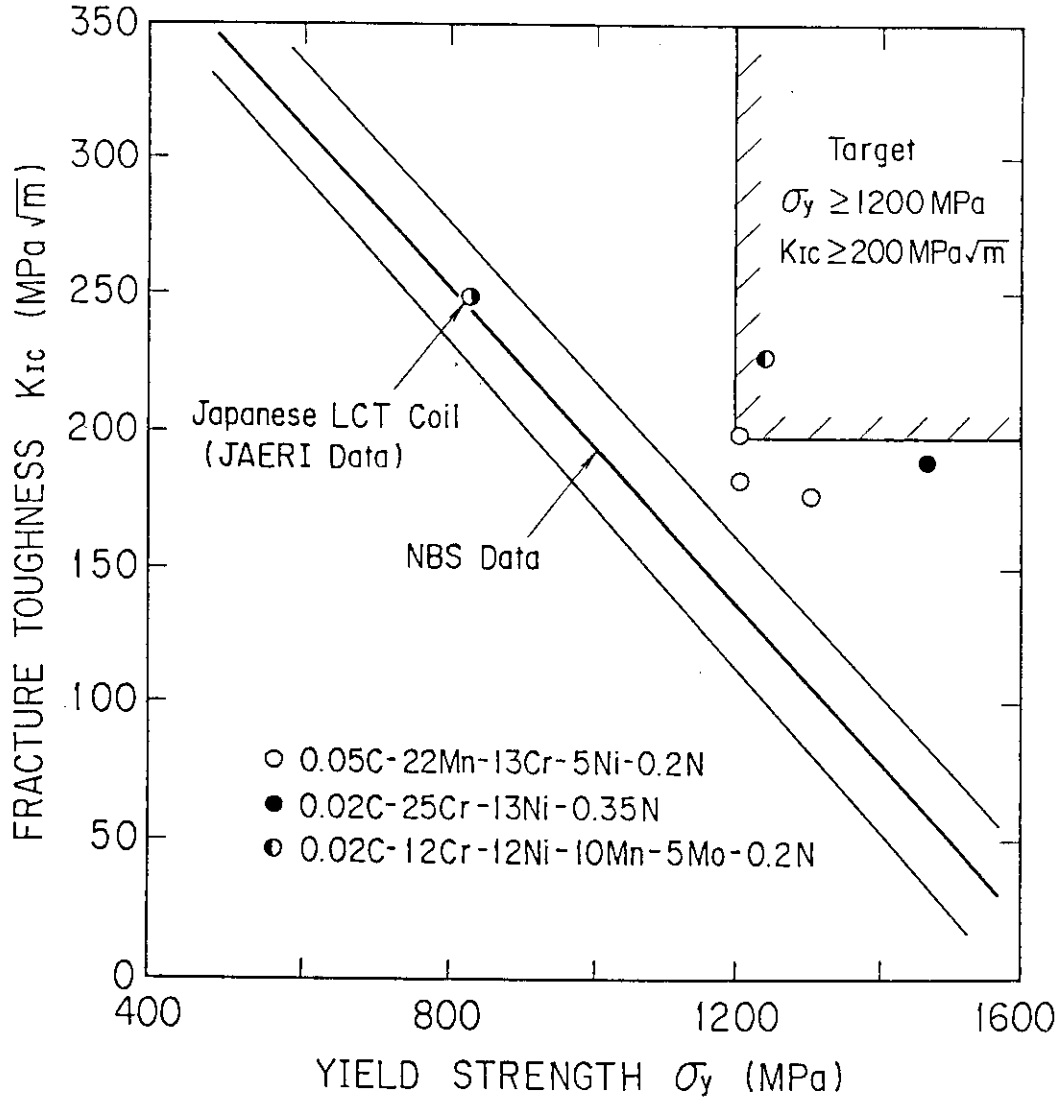

Fig. VII.6-1 Relation between Fracture Toughness and Yield Strength.

Table VII.7-1 Tentative Parameters of STTA Coil System.

Major Radius	Ro	2.70 m
Minor Radius	a	0.70 m
	b	1.05 m
	k(ref)	1.5
Toroidal Field	Bo	7.1 T
Plasma Current	Ip	3.6 MA
Safety Factor	q_a	2.7
Cycle Duration	CT	100 sec
Number of Operation	NOP	2×10^5
Maximum Field	Bmax	12 T
Number of TF Coils		12
Number of PF Coils		12
Maximum Current Density		
TF Coil	J_{TF}	30.0 A/mm^2
PF Coil	J_{PF}	20.0 A/mm^2

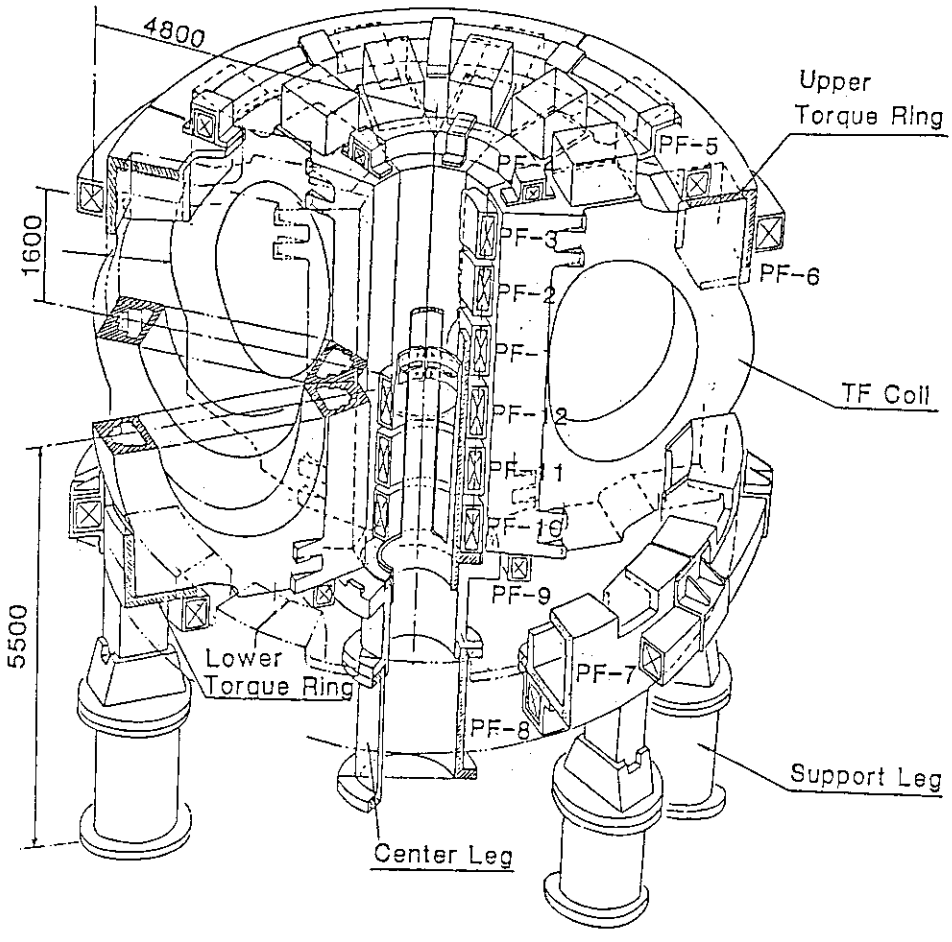

Fig. VII.7-1 Bird's-eye View of STTA Coil System.

VIII. TRITIUM TECHNOLOGY

1. Development of Tritium Processing Technology

1.1 Fuel purification

1.1.1 JAERI-LANL (DOE) fusion technology cooperation

"Testing of Small Scale Tritium Handling Components" program (LQ3) has been carried out under the JAPAN-DOE Fusion Technology Cooperation in Development of Improved Components for the Fuel Cleanup Systems.

A palladium alloy membrane diffuser and a ceramic electrolysis cell are the key components for an alternative fuel cleanup system proposed at JAERI. The former component can separate hydrogen isotope from all other impurities assumed to be included in a plasma exhaust gas, the latter will decompose tritiated water vapor for recovery of fuel.

Various efforts such as design, fabrication, delivery tests, preliminary performance tests without tritium, and shipping have been performed for both components by JAERI. Assembling of each components and installation to Tritium Systems Test Assembly (TSTA) have also started at Los Alamos National Laboratory.

1.1.2 Demonstration test of a small detritiation system

A performance test of a small detritiation system composed of a catalytic oxidation bed with domestic Pd-Al_2O_3 catalyst and molecular sieve bed with MS-5A has been carried out during the In-pile Tritium Recovery Experiment (See 1.3.2). Decontamination factor 10^4 of tritium was obtained at 200 °C of the catalyst bed temperature. The experimental conditions are as follows: catalyst; 5wt%Pd-Al_2O_3 (4.0g), flow rate; 360-436 cm^3 (STP/min), space velocity; 2400-2900 hr^{-1}, tritium concentration; 0.1-125Ci/m^3, gas composition; He 48.6-40.1 %, air 51.4-59.8 %, H_2 140-115 ppm, CO 700-570 ppm.

1.2 Hydrogen isotope separation

As part of a research program to explore the characteristics of a hydrogen isotope distillation column, the authors have performed a preliminary experimental study using a cryogenic distillation column separating N_2 and Ar. The experimental column simulates adequately some significant features of the hydrogen isotope distillation column : the inner diameter and the sizes of the packings are both very small ;

and the column is operated at cryogenic temperature. A significant result obtained was that the dynamic column behavior predicted by computer-aided simulation was in close agreement with the experimental observation. The HETP value was measured for Dixon Ring under a variety of vapor flow rates within the column. The measured value was approximately 5.5 cm, and it remained constant in the range from 20 mol/h to 70 mol/h. Thus, the effect of the vapor flow rate on column behavior was studied by using Dixon Ring.

Another important subject which should be studied is the effect of the packing species on column characteristics. For this purpose, four different packing species were tested in terms of the pressure drop and separating performance under the same operational conditions.

Figure VIII.1-1 illustrates a schematic diagram of the distillation column. The inner diameter and the packed height of the column are 1.94 cm and 50 cm, respectively. The packing species tested in the present study were Dixon Ring, Helix, Coil Pack and Heli-Pak. The specifications of the packings are summarized in Table VIII.1-1. The sizes of the packings are about ~1/6 of the inner diameter.

Figure VIII.1-2 shows the relation between the pressure drop across the column and the vapor flow rate. Dixon Ring presents the smallest pressure drop. Additionally, the inflexion point indicating the flooding is not observed for Dixon Ring and Helix.

Figure VIII.1-3 shows the HETP values for the four packings measured for a variety of vapor flow rates. The value for Dixon Ring and Coil Pack is approximately 5.5 cm and that for Helix and Heli-Pak is about 6 cm. Dixon Ring and Coil Pack present slightly higher separating performance. As another result observed from Fig. VIII.1-3, the HETP values for all the packings are not affected by the vapor flow rate.

The packing species to be used are required to satisfy the following conditions : the HETP value is smaller ; and the flooding velocity is larger. Accordingly, Dixon Ring is the excellent among the four packing species.

1.3 Blanket technology

1.3.1 Tritium recovery from lithium-based materials

In aspects of tritium recovery from a fusion reactor blanket, the thermal release behavior of tritium produced by the $^{6}Li(n,\alpha)T$ reaction in solid materials such as Li_2O, Li_3N, Li_2C_2, LiAl and Li_7Pb_2 has been

investigated. The results of kinetic studies in the tritium release process have suggested that the HT release from Li_2C_2, LiAl and Li_7Pb_2 is controlled by the diffusion of tritide anion (T^-) in the solid. On the other hand, the rate-determining step of the HTO(g) release from Li_2O crystals was suggested to be the diffusion of cationic tritium (T^+), although HTO molecules would eventually be evolved resulting from the thermal decomposition of LiOT at the solid surface.

For further understanding of the tritium release mechanism, it is required to elucidate the chemical state of tritium in solids. Chemical states of tritium existing in neutron-irradiated solid lithium compounds were analyzed by using a radiometric method. Table VIII.1-2 lists the results obtained for several lithium compounds. Nearly 100 % of tritium was found in the T^+ state in LiOH, Li_2O_2 and Li_3N, while the T^- state predominated in LiH, Li_7Pb_2 and Li_2C_2. Tritium incorporated in Li_2O, Li_2S, LiF, LiCl, LiBr and LiI was distributed over the T^+, T^- and T^0 states. In Li_2O crystals, the distribution of tritium in the T^+ state increased from 58 % to 81 % with neutron fluence from 2.5×10^{16} cm^{-2} to 6.3×10^{17} cm^{-2}.

1.3.2 In-situ tritium recovery experiment from Li_2O

In-pile experiment for tritium recovery from sintered lithium oxide pellets was performed under high neutron fluence as a feasibility study of Li_2O for the tritium breeding material. The experiment, which was conducted by Fuel Property Lab., was carried out with JRR-2 (irradiation hole; VT-10, thermal neutron flux; 1×10^{14} $n/cm^2 \cdot sec$). The effective irradiation time and total tritium production were 990 hr and 31 Ci, respectively. The average tritium concentration in helium sweep gas from in-pile capsule was about 5×10^{-6} Ci/cm^3. In this work, two types of ionization chambers were employed to measure comparatively high concentration tritium gas stream. Figure VIII.1-4 shows a monitoring result of tritium concentration under various operating conditions of JRR-2.

In order to reduce tritium release to the environment and to keep safety in tritium handling, the experimental apparatus was equipped with a detritiation system composed of a catalytic oxydizer and two molecular sieve dryers in a hood. Figure VIII.1-5 shows a typical monitoring result of the hood ventilation air and the inner surface of the hood.

Table VIII.1-1 Specifications of packing materials.

name	mat'l	dimen.	void fraction	descript.
Dixon Ring	Sus-316	φ3 × 3 mm	92%	wire net coils #42 100 mesh
Coil Pack	Sus-316	3 mmφ × 3 mmH	83%	wire coils 0.3 mmφ
Helix	Sus-316	3.0 mmφ	82%	metal rings #30(0.315 mm)
Heli-Pak	Sus-316	1.25 × 2.5 × 2.5 mm	80%	flattened helices #36(0.2 mm)

Table VIII.1-2 Chemical states of tritium in solids irradiated with neutrons at ambient temperature.

Material	Neutron fluence cm^{-2}	Distribution, %				
		T^+	T^-	T^O		
				HT	T_2	Hydrocarbons
LiOH	2.5×10^{16}	∿100	0.01	0.02	n.d.	n.d.
Li_2O_2	2.5×10^{16}	∿100	0.01	n.d.	n.d.	n.d.
Li_3N	2.5×10^{16}	98.2	1.4	0.3	n.d.	0.1
LiH	2.5×10^{16}	1.3	97.8	0.9	n.d.	n.d.
Li_7Pb_2	2.5×10^{16}	1.5	97.3	1.0	n.d.	0.2
Li_2C_2	2.5×10^{16}	14.9	80.2	2.1	n.d.	2.8
Li_2O	2.5×10^{16}	58.3	34.3	5.7	0.9	0.8
	6.3×10^{17}	81.1	18.4	0.3	0.2	0.1
Li_2S	5.0×10^{15}	78.5	17.6	1.2	1.7	0.9
LiF	5.0×10^{15}	58.7	39.2	0.5	0.1	1.5
LiCl	5.0×10^{15}	74.5	11.1	12.6	0.1	1.7
LiBr	5.0×10^{15}	30.8	46.8	18.1	0.7	3.6
LiI	5.0×10^{15}	39.2	22.0	32.3	0.3	6.4

n.d.; not detected.

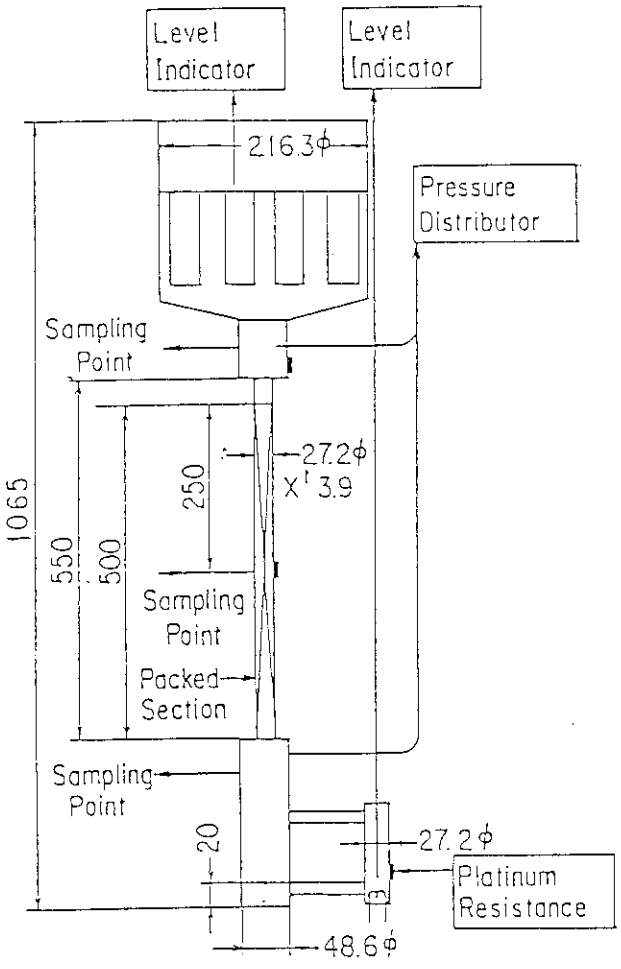

Fig. VIII.1-1 Schematic diagram of distillation column used for experiment.

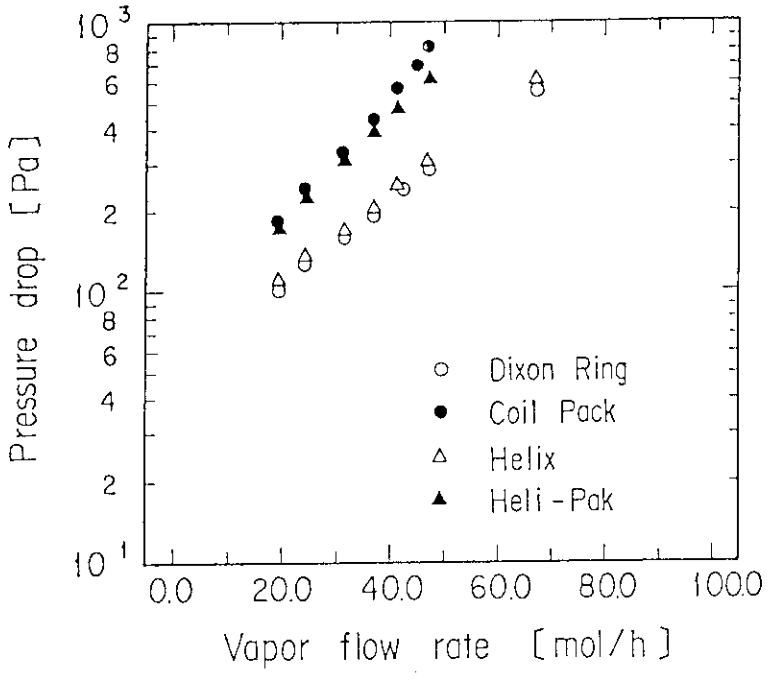

Fig. VIII.1-2 Relationship between pressure drop across column and vapor flow rate.

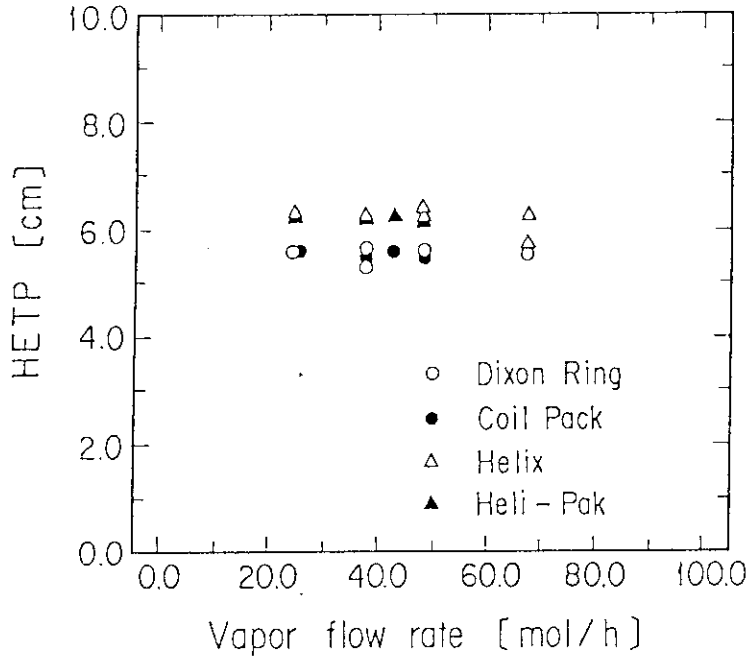

Fig. VIII.1-3 Effect of packing species on HETP.

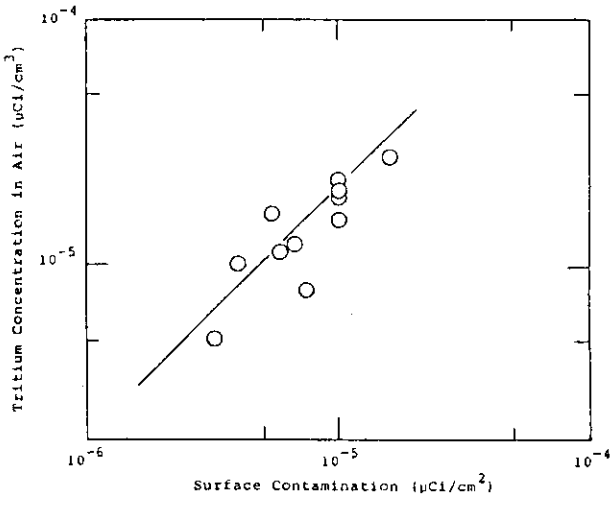

Fig. VIII.1-5 Relationship between Tritium Concentration in the Ventilation Air and Surface Contamination in the vicinity of the Exhaust Hole of Hood (4th Cycle).

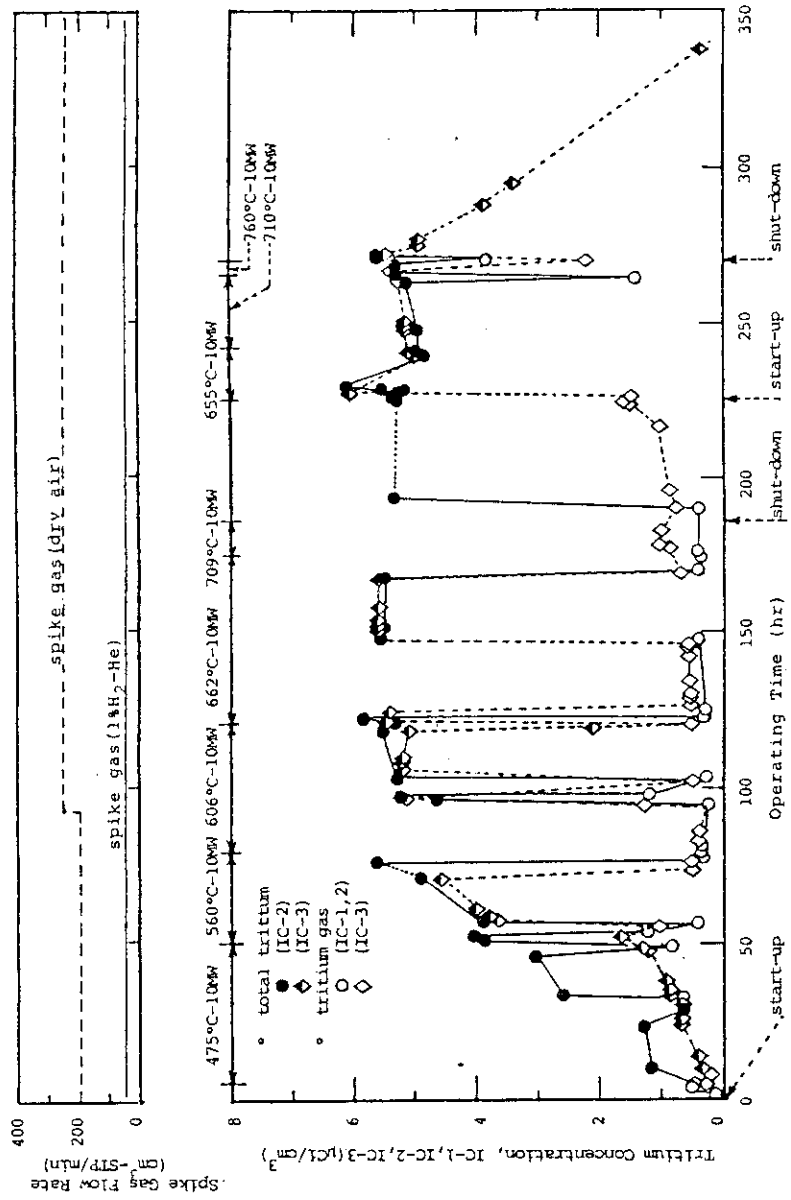

Fig. VIII.1-4 Comparison of the Performance of the Two Types of Ionization Chambers (IC-1,2 : ionization volume 100 cm^3, with bird-cage type electrode, IC-3 : ionization volume 1500 cm^3, without bird-cage type electrode).

2. System Analysis

2.1 Development of simulation procedure for stage processes

2.1.1 Great improvement of computer simulation procedure for hydrogen isotope distillation columns

The previous simulation procedure treated all the basic equations simultaneously and utilized the Newton-Raphson method where a set of temperatures and liquid flow rates were chosen for the independent variables. However, for narrow boiling mixtures like hydrogen isotope solutions, there is no need to treat the overall material and heat balances simultaneously with the other equations. Hence, the main iterative loop has been divided into two loops : an inner loop for temperature corrections by the quasi-Newton method and an outer loop for flow rate corrections by the successive iteration approach without any matrix calculation. As a consequence, the total computation time has been shortened by almost one order of magnitude.

2.1.2 Development of new simulation procedure for water distillation columns

An efficient simulation procedure has been developed for water distillation columns. The atomic balance for two of the three elements (H, D and T) are linearized by using the approximation that the isotopic exchange reactions in the liquid phase are equilibrated. As a result, the Jacobian matrix has a block-tridiagonal form and the order of the arrays is just two even in cases of the six component system (H_2O, HDO, HTO, D_2O, DTO and T_2O). Thus, although the column has hundreds of stages and the number of unknown variables is extremely large, the procedure does not require any large computer storage and long computation time.

2.1.3 Development of new dynamic simulation model for equilibrium stage processes

It has first been pointed out that the contribution of the vapor holdups is great in cases where very volatile components are present within the column. Basic equations have been derived by accounting for vapor holdups so that the numerical integration techniques can directly be applied. The new dynamic simulation model thus developed has been used in the analysis on the helium effect on dynamic behavior of hydrogen isotope distillation columns.

2.2 Static and dynamic analysis of cryogenic distillation columns

2.2.1 Effects of helium on column behavior

Effects of helium on static and dynamic behavior of hydrogen isotope distillation columns have been analyzed on a digital computer by choosing the TSTA cascade (Fig. VIII.2-1) as an example. Column (2) is mainly affected by helium. The effect on dynamic column behavior is much larger than that on static column behavior. If the helium percentage in the feed to the cascade has a significant value (> 1 %), it will be impractical to perform all the three controls successfully : controls of the tritium level in the top gas, column pressure and liquid level in the reboiler. If it has only a small value, no special helium separator may be needed, but a larger condenser must be considered in the design stage.

2.2.2 Start-up analysis for cryogenic distillation column cascade

A start-up analysis has been performed for the TSTA cascade to write a scenario indicating how the full-normal composition profiles are achieved within all the four columns. As a result, two successful scenarios have been found out. In any case, the compositions of the gas mixtures first charged into the columns affect the start-up characteristics to a remarkable extent, so they must carefully be prepared.

2.3 System synthesis for cryogenic distillation column cascades

2.3.1 New column cascade in the main stream fuel circulation system for fusion reactor

A new cryogenic distillation column cascade (Fig. VIII.2-2) has been developed as a possible alternative to the TSTA cascade. Although the new one has a shortcoming of a larger amount of tritium inventory, it has great flexibility to the feed condition : even if the feed composition is rather greatly changed, the same performance can be assured just by adjusting the top, sidestream and bottom flow rates with the other parameters unchanged.

2.4 Pressure response analysis of glovebox system

In tritium handling the glovebox atmosphere is circulated through tritium removal system to reduce tritium concentration. The pressure balance is the important factor to lower tritium leakage from gloveboxes to working area and particularly the pressure of the gloveboxes must be

continuously maintained slightly negative than that of working area.

In order to maintain the pressure of the glovebox atmosphere in the range of 0 ∿ 40 mm Aq., pressure response analysis to the glove operation is carried out. Following the results of this analysis, a header device in the exhaust pipe of the gloveboxes is designed to moderate the pressure response caused by ordinary glove operation.

2.5 Design of fuel circulation and purification system of Fusion Experimental Reactor (FER) and INternational TOkamak Reactor (INTOR)

The design of tritium systems such as fuel circulation and purification system, tritium recovery system for blanket, the enclosures and tritium removal systems, tritiated waste disposal system, etc. for FER/INTOR has been successively conducted. A concept of chemical flow sheet for each system and images of each equipment are obtained, and preliminary safety analysis is carried out. The investigation of mass transfer in Li_2O blanket caused by LiOH formation has been performed.

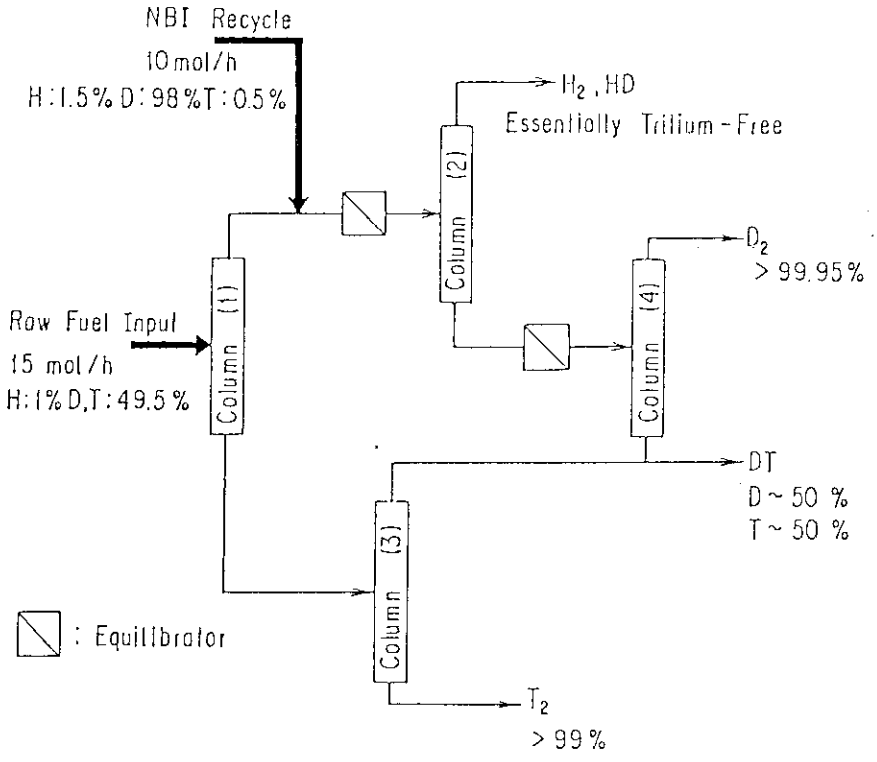

Fig. VIII.2-1 Flow schematic of the cryogenic distillation column cascade under development for the Tritium Systems Test Assembly(TSTA).

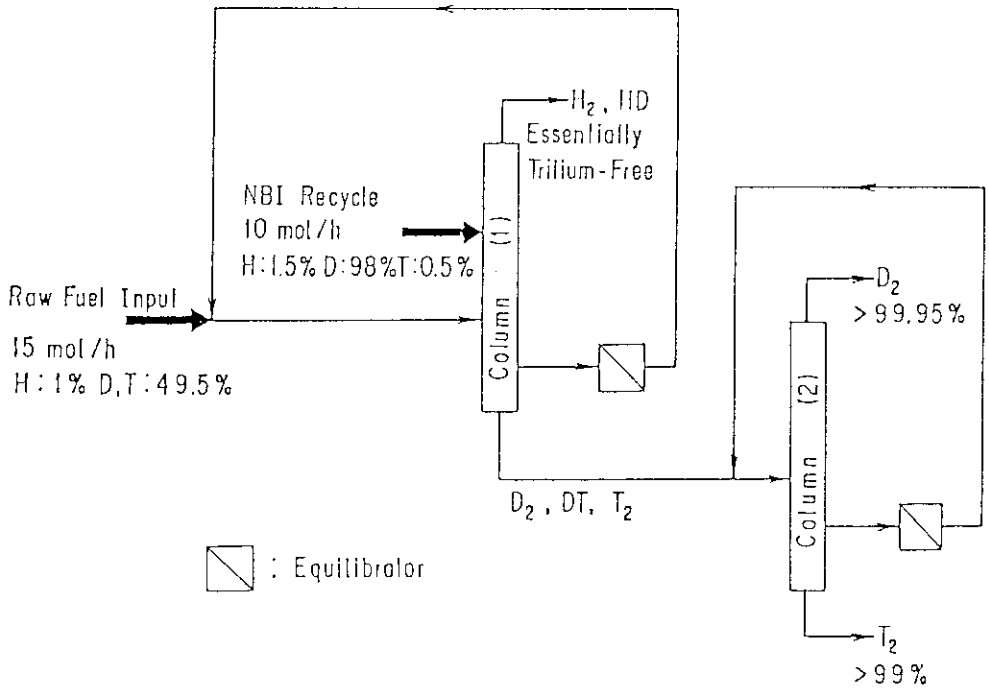

Fig. VIII.2-2 Flow schematic of the new cryogenic distillation column cascade (proposed at JAERI).

3. Present Status of Tritium Processing Laboratory

The construction of the building and its auxiliary systems such as the ventilation, the electricity, the cooling water, the liquid waste tanks, etc. has been completed in May 1984.

The major components for safe handling of tritium, that is the detritiation systems, the gloveboxes, tritium storage system and tritium monitoring and control system, are being fabricated.

Effects for the final design of the experimental apparatus and for obtaining of transport licence of tritium gas have been carried out.

IX. DESIGN STUDIES OF FUSION REACTOR SYSTEM

1. Design Study of Tokamak Power Reactor

Synthetic evaluation taking account of long-term strategy is necessary for planning effective research and development program of fusion reactor system.

The major design features of tokamak power reactor are : steady state operation, RF wave for plasma heating and current drive, and pumped limiter for ash exhaust. The key functions of fusion power reactor are tritium production for fuel self-sustaining and energy supply for electricity generation.

The feasibility of blanket structure for power reactor is clarified in this study. Major design parameters of fusion power reactor are shown in Table IX.1-1. The conceptual design of water-cooled solid-breeder blanket for simultaneous tritium breeding and electricity generation is shown in Fig. IX.1-1. The major conclusions and design features obtained in this study are as follows :

(1) Steam conditions for electricity generation at a level of a PWR for water-cooled blanket and a steam power station for helium-cooled blanket are achievable, and breeding materials (Li_2O) can be maintained within the allowable temperature range for in-situ tritium recovery.

(2) First wall structure exposed under intense heat flux is integrated to the blanket wall from the view point of obtaining high breeding performance and avoiding the complexity of its own support system.

(3) Net tritium breeding ratio of about 1.1 is obtained by adoption of Li_2O breeder and beryllium neutron multiplier.

(4) Breeding materials are formed into small spherical pebbles in order to avoid the serious problems of thermal cracking and mass transfer, and to make assembling of blanket structure easy.

(5) From the safety points of view, two independent cooling systems in blanket region and double-wall cooling tube structure are adopted.

Table IX.1-1 Major Design Parameters of Fusion Power Reactor.

Operation mode	Steady state
Fusion power (MW)	3200
Net electrical power (MW)	1000
Neutron wall load (MW/m^2)	3.3
Plasma major radius/minor radius (m)	6.9/2
Plasma current (MA)	16
Toroidal field on axis (T)	5.2
Maximum toroidal field (T)	12
Net tritium breeding ratio	$\geq$ 1.05
Tritium breeding material	Li_2O
Structural material/coolant	PCA/H_2O Mo alloy/He

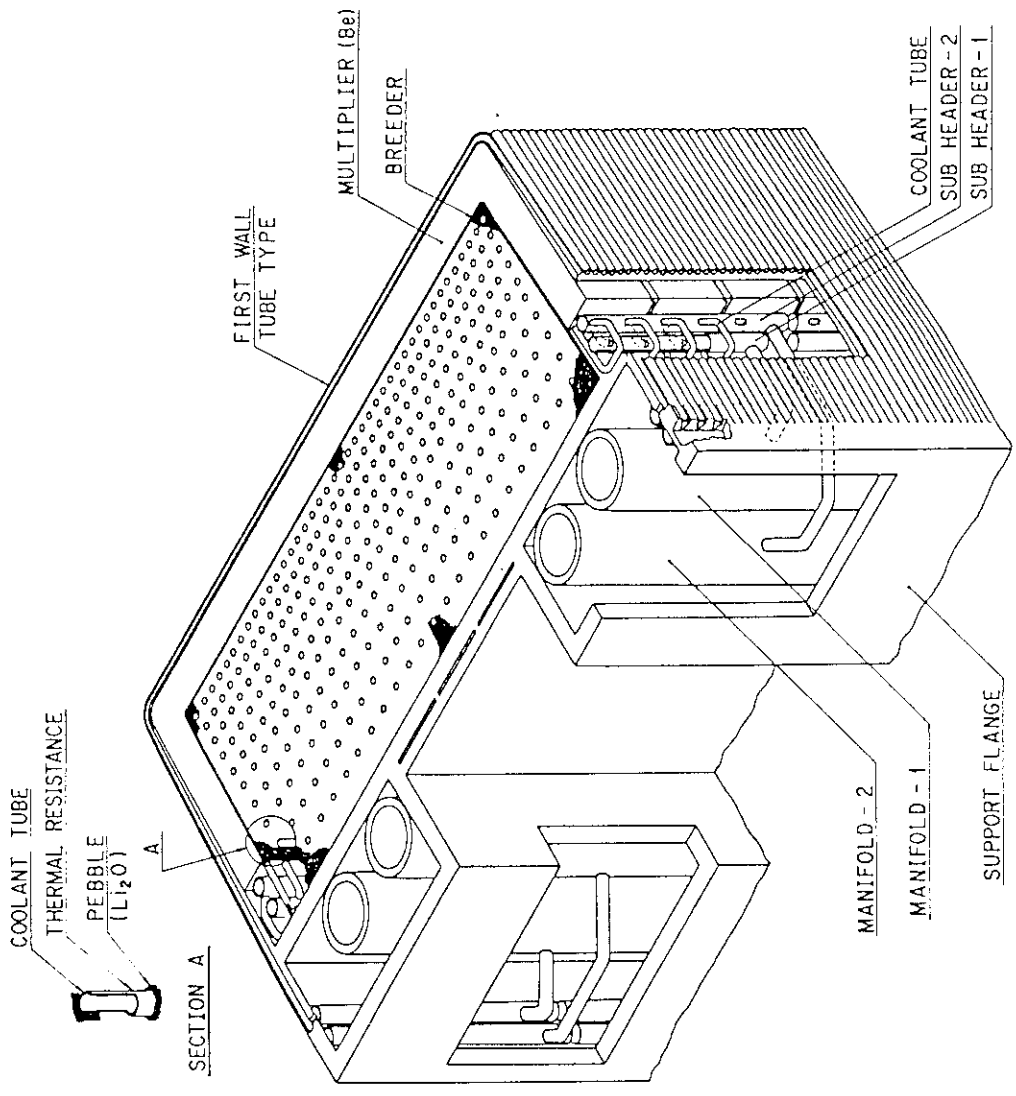

Fig. IX.1-1 Water-cooled Solid-breeder Blanket for Simultaneous Tritium Breeding and Electricity Generation.

X. DEVELOPMENT OF A LARGE TOKAMAK JT-60

1. Introduction

Efforts made by the JT-60 Project was rewarded by the progress achieved in this year. Assembling and installation work of its major components - tokamak machine, power supplies, and central control system - were advanced at the Naka site. Construction of JT-60 buildings and other facilities advanced as planned. The completion of JT-60 is expected in April 1985.

Efforts are also focussed on detailing experimental and operation programs to raise productivity of the JT-60 Project.

2. Outline of the Progress of JT-60

Remarkable progress of the construction of JT-60 was achieved in the fiscal year 1983: Assembling and installation of the JT-60 tokamak machine started in February 1983 made good progress during the year to complete the assembling of most of its major components such as the toroidal and poloidal field coils, the vacuum vessel and the vacuum pumping system. Preoperational testing of the power supplies and the central control system has been well advanced. The auxiliary facilities (secondary cooling system, power distribution system/emergency power supply) were completed and delivered to JAERI in November 1983 as scheduled. They have been in operation for testing of other JT-60 subsystems.

Construction of the experimental building was completed lastly among the major buildings for JT-60, and the 275 kV power substation was also completed in December 1983.

Fabrication of the JT-60 diagnostic system was well under way and several of its subsystems have been under testing at the Naka site. Construction of both the neutral beam injection heating system and the radio-frequency wave heating system was started in November 1983. The completion will be in the middle of 1986.

The experimental program of JT-60 was reviewed on the basis of the current progress in fusion plasma research, and a detailed program for the first OH plasma experiment was established with emphasis on the poloidal divertor experiment. The operation program was also examined in detail with respect to operational procedures, manpower needs, operation and maintenance costs and the organization for operation.

The time schedule of the JT-60 program is shown in Fig. X.2-1. The completion of JT-60 is expected in April 1985.

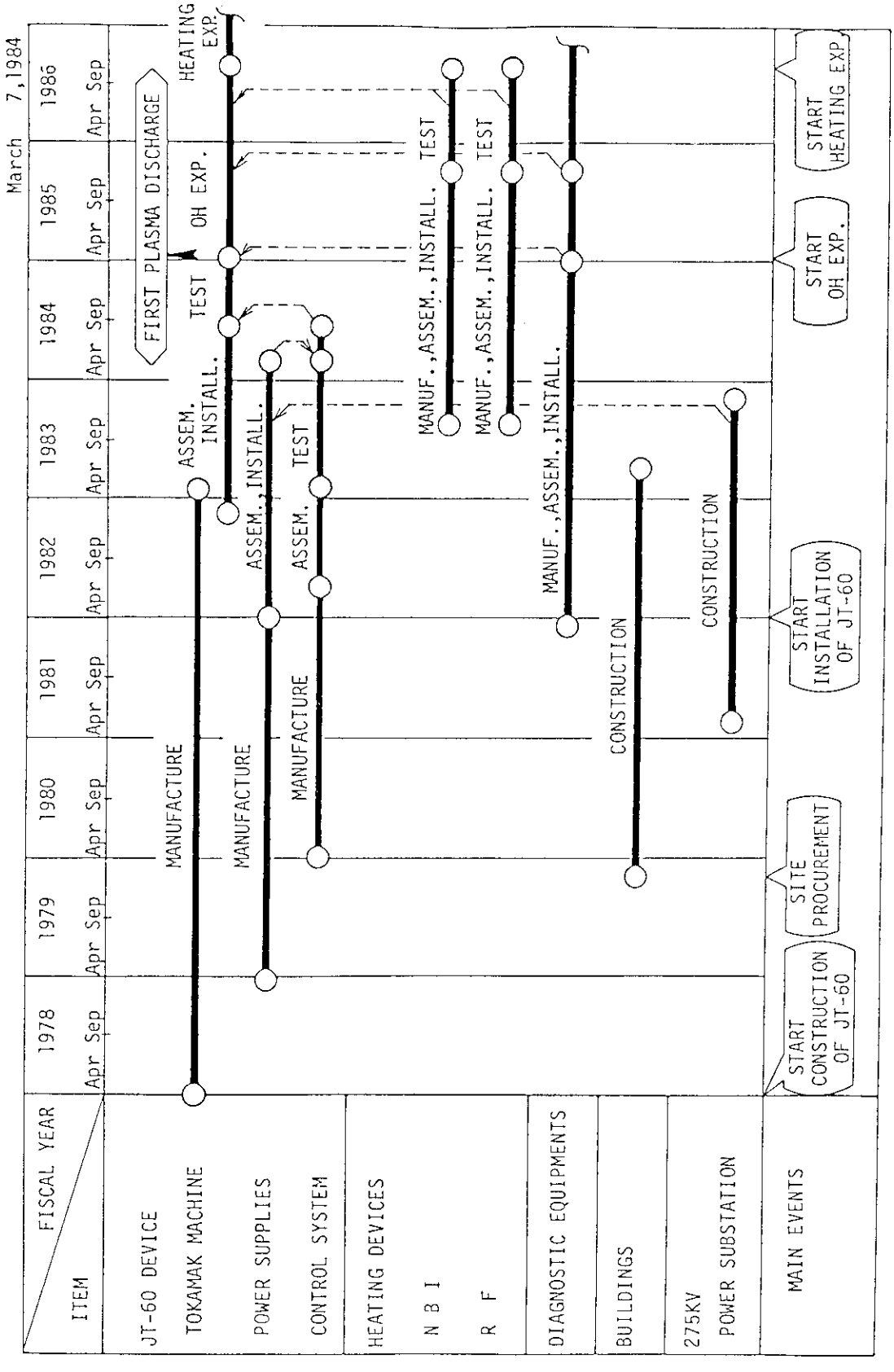

Fig. X.2-1 JT-60 Project schedule.

3. Status of Tokamak Machine

3.1 Major activities

The JT-60 tokamak machine is composed of vacuum vessel, toroidal field coils, poloidal field coils, support structures, a primary cooling system, a vacuum pumping system, fast movable limiters, a preionization system, a gas-feed system, adjustable limiters and a control system.

Fabrication of these components was finished including performance tests. The vacuum vessel in which the magnetic limiter coil was attached passed many kinds of tests including heating, cooling and helium leak tests. The poloidal field coils, grouped into five blocks, was assembled with support structure. Fabrication of the gas-feed and preionization system was almost finished. The toroidal field coils, the vacuum pumping system, fast movable limiters, adjustable limiters, support structure, and control system were finished in the factories.

Installation of the machine components at Naka site started in February 1983. The poloidal field coils and the vacuum vessel were installed on the lower support structure and were connected by welding, except for the gap which was left for installation of the toroidal field coils. Each toroidal field coil was inserted through the final connection part of the vacuum vessel and the poloidal field coils, and moved in the toroidal direction through the narrow space. After installation of all the toroidal field coils, the final segments of the poloidal field coils were welded and the final segment of the vacuum vessel was installed. The tests of the machine control system have continued with the central control system.

3.2 Status of machine component

3.2.1 Torus

(1) Structure of machine

The main components of JT-60 are shown in Fig. X.3-1. The support structure is composed of a base support structure, lower and upper structures, a center column, support columns of the vacuum vessel, and star-shaped trusses. These structures support the machine weight of 4500 tons, several types of magnetic forces and earthquake loads, etc.

The vacuum vessel, inside which three magnetic limiter coils are located, has an egg-shaped cross-section with a major radius of 3 m and a bore of 2 m × 2.8 m. It is composed of eight rigid rings and eight bellows made of Inconel 625. It has 182 ports, about 9000 first wall tiles, electrical heaters and cooling channels and magnetic sensors etc. It is supported by horizontal support arms fixed to the support columns of the vacuum vessel and to the poloidal field coil supports.

The poloidal field coils contain 176 turns installed outside the vacuum vessel and 16 torus installed inside the vacuum vessel. The outside coils are inside the toroidal field coils and are held by the 18 circular support structures which are supported by the lower support structure. The outside coils are able to be divided into four blocks.

The toroidal field coil system consists of 18 coil blocks with a circular shape which is shaved at the innermost side of the torus. The coil bore is about 4 m and its outside diameter is about 6 m. The weight of one coil block is about 90 tons. The coil blocks are supported by spacers fixed to the upper and lower support structures and by the center column.

(2) Assembly

Fabrication of the vacuum vessel and the poloidal field coils in a factory were completed. After the magnetic limiter coil was attached inside the two 180° sectors of the vacuum vessel, heating, cooling and leak tests of the vacuum vessel

were carried out. The results of the tests show good performance. Work on the titanium carbide coating of the first wall tiles continued. Poloidal field coils were assembled in five blocks – the inside one, the lower outside one of two 180° blocks in the toroidal direction, the upper outside one of two 180° blocks. Each block successfully passed the withstand voltage test etc.

The assembling of the torus started in February 1983 and will continue until September 1984. The outline is as follows. First, a base and lower support structures were installed on the floor. The poloidal field coil blocks – the inside coil block and the lower outside pair of coil blocks – were installed on the lower support structure and one of the two connection part at the site was welded and electrically insulated. Withstand voltage tests etc. were done for the connection part. The two 180° sectors of the vacuum vessel were installed and supported by support columns standing on the floor. One of the two connection part was welded and covered with thermal insulator.

The upper outside poloidal field coil blocks were assembled in the same way as the lower outside ones.

The installation of the toroidal field coil was started in October 1983 and continued for about five months. Each toroidal field coil was inserted through the final connection part of the vacuum vessel and the poloidal field coils, then moved in the toroidal direction. (See Fig. X.3-2)

Ports for diagnostics and heating etc. were welded to the vacuum vessel in the eighteen gaps between the toroidal field coils.

The connection of the final connection part of the vacuum vessel and the poloidal field coils started in February 1984 and will continue to the next fiscal year. The upper support structure was installed and connected to the wall of the torus hall by the star shape trusses. (See Fig. X.3-3). The vacuum pumping system, fast movable limiters, adjustable limiters and machine control system were installed. For the assembly of each component, many kinds of test and examination were carried out. The assembling schedule of each component is shown in Table X.3-1.

Investigations of a electrode for the electron beam gun of the preionization system was carried out and useful results were obtained.

(3) Test

In order to confirm the justification for the assembling of each component, many kinds of tests and examinations, for which the procedures had been investigated carefully by experts, were carried out.

The main results of the tests and examinations are as follows.

a) Visual test

All components were visually inspected in order to check whether there was any technical fault on the surface of the components such as defect, crack, dirt, dust, stain and so on. No faults were found.

b) Size examination

It is important to assemble the Tokamak machine with correct dimensions. For example, the largest cause of magnetic field error is the measurement error in the structure of the coils. The dimensions of each component were measured after assembling. The measurement results indicate good agreement with the design drawings.

c) Tests after connection of the poloidal coils

The welded parts of the poloidal field coils were checked by both ultrasonic test and liquid penetrant test to determine whether there was any technical defect in the conductor or on the surface.

Only a few conductors were re-welded because the defects larger than 10 mm diameter had been detected in the conductor by ultrasonic test.

The electric insulation integrity of the connection parts was also certified by a high voltage test.

Test voltages were 42.4 kV(DC) for the F coil, 35.4 kV(DC) for the V coil, 8.5 kV(DC) for the H coil, 16.8 kV(DC)

for the Q coil and 8.5 kV(DC) for the M coil, respectively.

d) Helium leak test

Welded parts inside of the vacuum vessel, magnetic limiter coil cans and ports were leak checked using helium gas. A helium leak rate higher than 5×10^{-10} Torr·ℓ/s, which is the leak detection sensitivity, was not found at any welded parts.

3.2.2 Primary cooling system

Installation of cables and pipes was completed. Sequence check and adjusting of the meters, the transducers and the sensors were carried out continuously. Pressure proof test was completed in March 1984. Cooling pipes without the clean up machine elements (heat exchangers, filter tanks and sensors) are now being flushed out by circulating demineralized water.

3.2.3 Fast movable limiters and adjustable limiters

After the final inspection test was completed in September 1982 in the factory, the fast movable limiter system, which was being stored in the factory, was installed in Naka site. The following installations and inspections have been carried out.

1) Shafts and bearing worked smoothly with the pre-operation testing system in the preparation building.
2) Oil pressure equipment to put the monable limiters in motion has been set up in the machine auxiliary equipment room.
3) The movable limiter system and the pre-operational testing system comply with the high pressure gas control safety regulations.
4) The lower movable limiter unit was installed into the vacuum vessel in the JT-60 machine room.

The upper unit is waiting for installition into the Vacuum Vessel in April 1984. The adjustable limiter system has also been installed in the site. Its performance alone was

tested before the installation into vacuum vessel at the installation room. The lower unit was installed into the vacuum vessel in October 1983. The upper unit is waiting for installation into the vacuum vessel in April 1984.

3.2.4 Gas feed and preionization system

The major components of the gas feed and preionization system have been fabricated and are being assembled without the manifold which is located near the Tokamak machine. Performance test at the factory had been carried out after assembly of the Piezoelectric valves (PEV) and Preionization devices (Electron Beam gun and J×B gun) using the power control panels in Aug. 1981.

Test results of the preionization device satisfy the design specification, such as 1.0 A emission current of EB guns, and 80 A discharge current of J×B gun. About 15 % rates decrease of PEV throughput had been observed for a long time. Efforts to improve the performance of the throughput have been carried out in this fiscal year. In order to get a good throughput performance, improved PEVs have been developed which have the following improvements: (1) the plastic deformation for the seal material has been reduced. (2) The nozzle was coated to avoid adhesion between the nozzle and the seal materials.

3.2.5 Tokamak machine control system

Interface test of the machine control system and Zenkei have been completed at Feb. 1982. Tests of the sequence, interlock, and safety action have been continuing in this fiscal year and the performance tests concerning the vacuum, baking and cooling characteristics using the machine control system were started in Aug. 1984.

3.2.6 Vacuum pumping system

The installation at Naka site of the vacuum pumping system (VPS) started in February 1983. The assembling and installation of periphral subsystems were completed and inspection of those subsystems finished in July 1983. Assembling of the manifold and manifold structures started in Nobember 1983, and installation of main pumping systems were completed in March 1984. A leak test was made and a leak was found at ϕ1000 flange. It was repaired perfectly because the position of it was expected. After the installation at Naka site of VPS completed, the inspections were finished in July 1984.

3.3 Related studies

3.3.1 Development of the electrode for the Electron Beam Gun preionization

Preionization systems of JT-60 are composed of the types such as electron beam gun type and J×B plasma gun type. The cathode filament of electron gun which is made of Tungsten may fail due to the electromagnetic force produced by the filament current and the toroidal field. A new type of electrode which adopted LM materials (Lanthanum oxide doped molybdenum) has been developed in this fiscal year. The performance of the new electrode is as follows.

(1) Emission current obtained much greater than 1.0 A.
(2) Reproducibility of the emission current is satisfactory.
(3) Failure of the electrode has not occured under the 1.7 times actual electromagnetic force.
(4) The new type of electrode is interchangeable with the fabricated EB gun using the Tungsten electrode.

Table X.3-1 Assembling Schedule of Main Component.

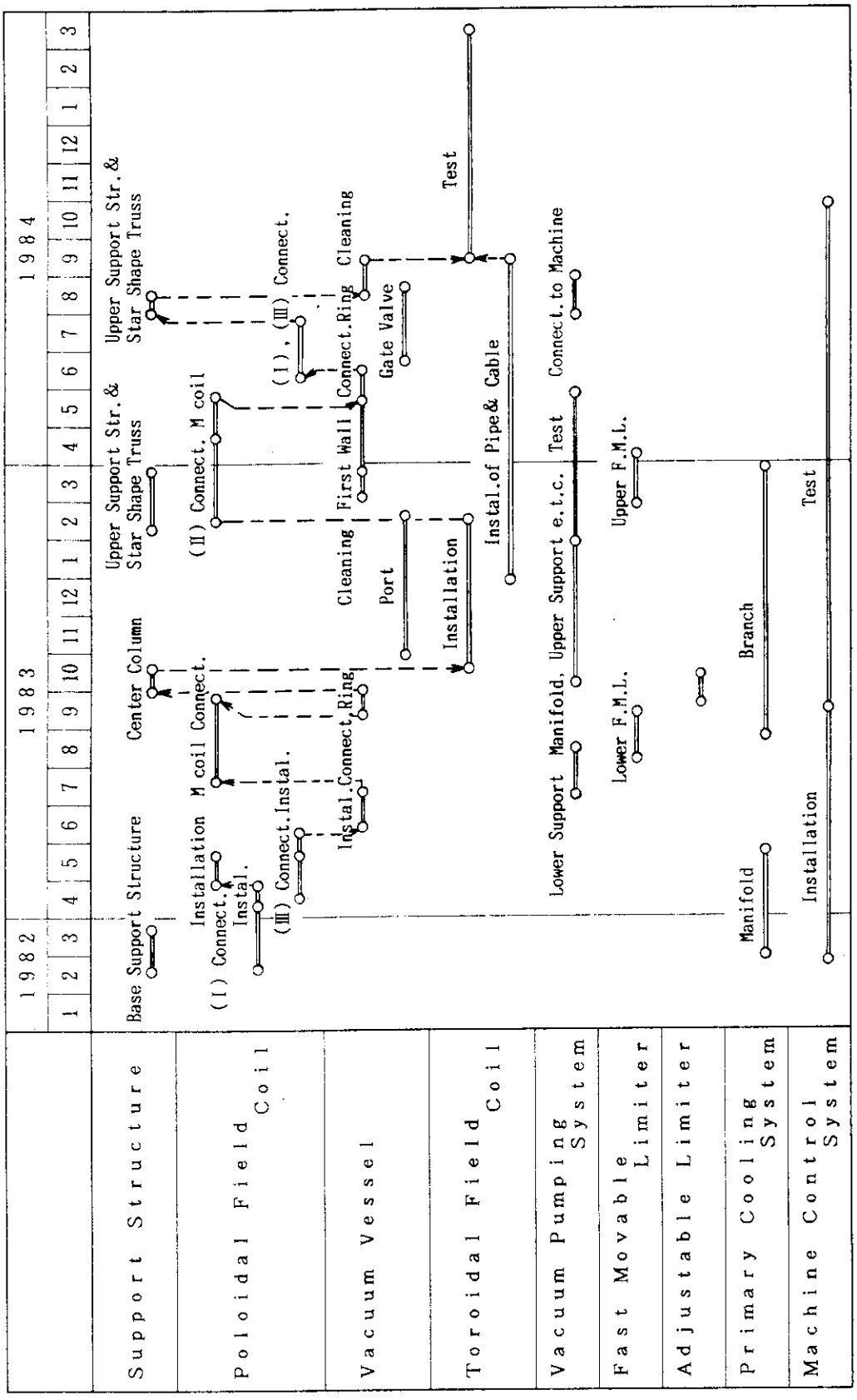

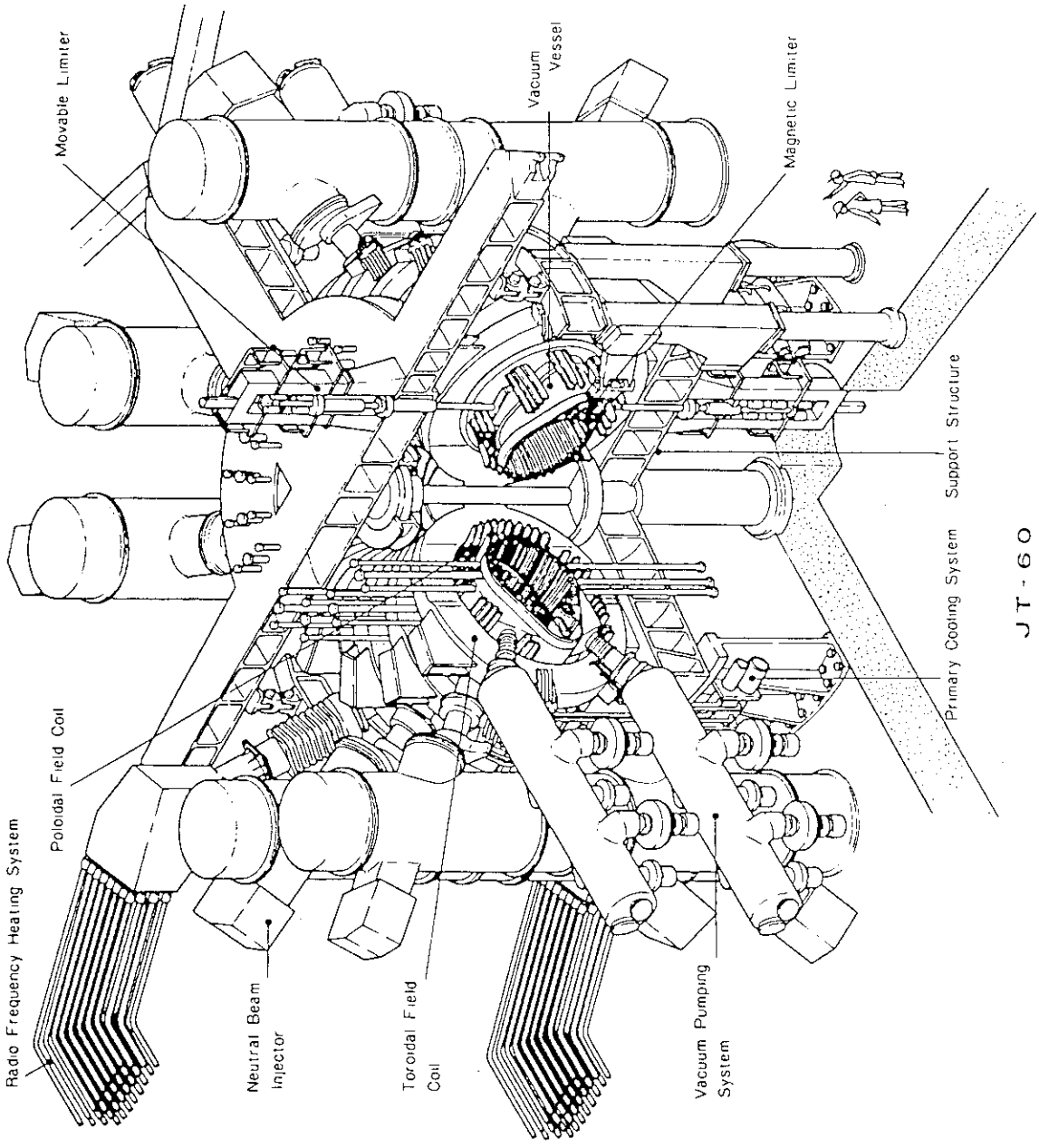

Fig. X.3-1 Bird's eye View of JT-60.

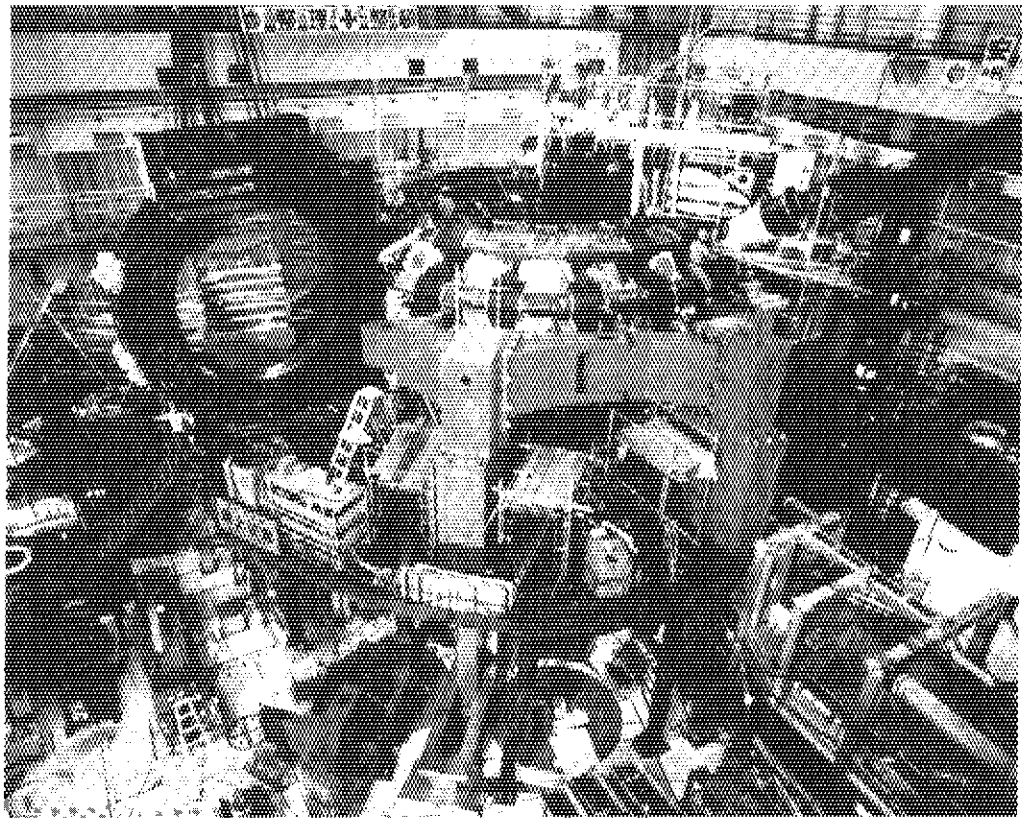

Fig. X.3-2 Assembling (12.1, 1983).

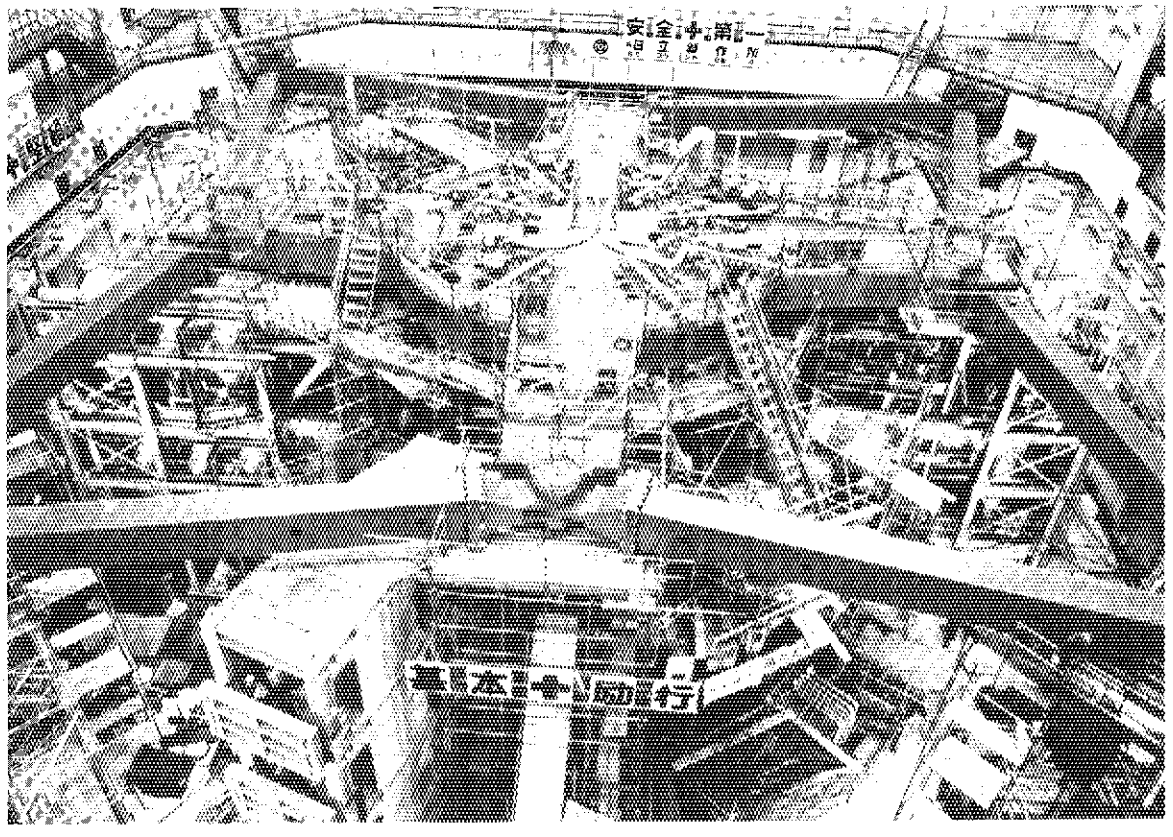

Fig. X.3-3 Assembling (3.24, 1984).

4. Status of Power Supply

4.1 General status

The assembling and installation of the poloidal field power supply (PFPS) were completed in March 1983. Preoperational testing on site was started from the beginning of April 1983.

The circuit of PFPS is highly complicated, and it may be changed according to the operational modes. Prior to the connection to the tokamak machine, various tests should be performed on the power supply system to understand the system behavior and to demonstrate required performance of the system. These tests should be a complete test which can evaluate all the operational characteristics of the system.

In order to achieve high reliability of the control system and avoid any trouble to load coils and tokamak machine, an electro-magnetic simulator which simulates almost a complete function of PFPS and JT-60 machine with reduced voltage and current ratings has been used to check the computer hardware/software in real time operation. The simulator test was carried out from July to September 1983.

A test using a dummy coil was carried out from November 1983 to March 1984. The dummy coil was used to check the DC circuit breaker operation in the ohmic heating circuit, and also used as a poloidal field coil to examine the controllability of the output current of thyristor convertors. The dummy coil test is essentially a full load test of PFPS, and the results will be mentioned briefly in the following section.

The installation of the generator with large flywheel of the toroidal field power supply (TFPS) was started in the generator building in April 1983. The flywheel is connected under the lower shaft of generator and is composed of six 100 ton-6.6 m diam. disks. All 24 units of diode rectifiers of TFPS with a total capacity of 53 kA-7 kV were installed, and successively the assembling and installation work on DC buses, AC cables, trays and the control system have also been completed. The short-circuit current test of the system will start in April 1984.

The inspection test of the third generator of 400 MVA-2600 MJ to be used for the neutral beam injection heating system and the radio-frequency wave heating system was finished in December 1983. The assembling and installation in the generator building was started in January

1984.

The JT-60 power supply is now deeply into the installation and test phase. It shows generally excellent schedule performance.

4.2 Poloidal field power supply

The assembling and installation of PFPS has been completed and the preoperational testing was successively started: component tests were continued till July 1983. A dynamic characteristic test of 500 MVA MG set was begun in early September 1983. As a result of the test and adjustment, we verified that the rotation loss was comparatively small and the vibration of the MG shaft was small enough for operation in 70-100 % revolution speed. Operational mode test for direct digital control (DDC) CAMAC system and protection interlock test for thyristor phase controller (PHC) were performed throughout the summer of 1983 using PFPS simulator having characteristics of 1/25 voltage and 1/4000 current. This was made to check almost all functions of the control system before the load test of PFPS. At the end of October 1983, all the PFPS components were brought to be ready for successive dummy coil test.

The purpose of the dummy coil test is two-fold: (1) To demonstrate the operation with maximum voltage and current ratings. (2) To verify the total controllability of DDC and timing system. Several topical test data are reported below.

Photograph 1 shows a commutation current through DC circuit breakers by the commutation capacitor C1. Since the peak current reaches to 98 kA with C1 charged at 25 kV, the rated current of 92 kA of the ohmic heating coil could be interrupted easily. Photograph 2 shows an interrupted current shape of 92 kA. The purpose of this experiment was to verify that the current decreasing rate at the zero crossing point did not exceed the limiting value. The result of 120 A/μsec is well below the maximum design value of the current decreasing rate of the DC circuit breaker. Photograph 3 shows a typical operation of the ohmic heating power supply (OHPS). The discharge conditions are : the premagnetization of the ohmic heating coil is 92 kA and the restriking voltage is 25 kV. It shows about 25 VSec of flux swing performance of the ohmic heating coil. Photograph 4 shows a typical operation of Taylor discharge cleaning power supply which is included in OHPS. The current peak reaches to the rated current of 8 kA. Photographs 5 and

6 demonstrate the controllability of the vertical field power supply with the minimum time control method. It shows a current response of about 5 kA/10 ms without overshoot and undershoot. Photographs 7 and 8 also demonstrate the current controllability with the non-interactive control method. It is clear that the circulating current has no interaction with the coil current. On the other hand, the circulating current has some spikes in spite of constant reference, but this brings no problem in the actual operation.

All the self-closed tests of PFPS as a single subsystem were completed in March 1984. Through those tests, both the reliability and the controllability of PFPS were fully demonstrated and found to be more fantastic than designers' expectation.

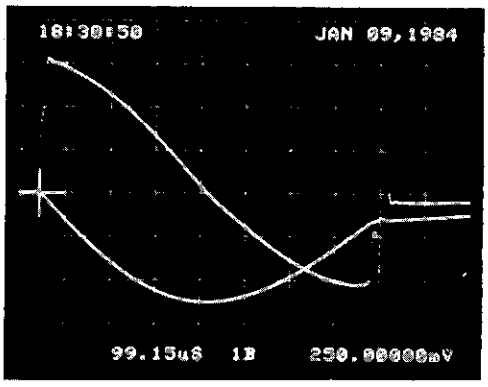

Photo 1. commutation condenser bank C1 discharge test

Rogowski coil output of VCB1 total current

commutation current [40KA/div]

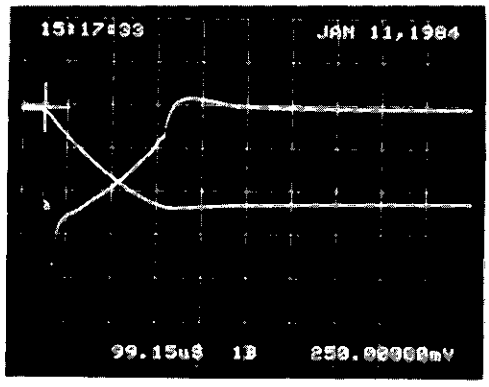

Photo 2. 92KA current interruption test

Rogowski coil output of VCB1 total current

interrupter current [40KA/div]

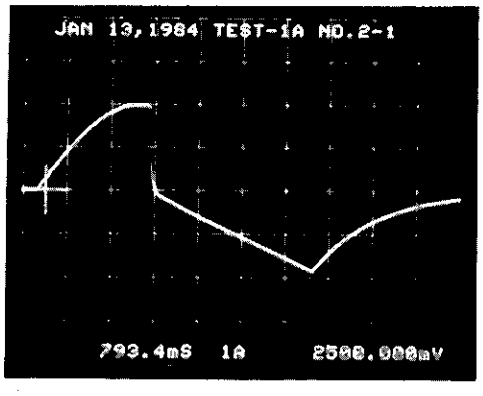

Photo 3. Typical operation of Ohmic Heating PS

OH-coil current (dummy coil)

premagnetization current :92KA

R1 :0.259 Ohm

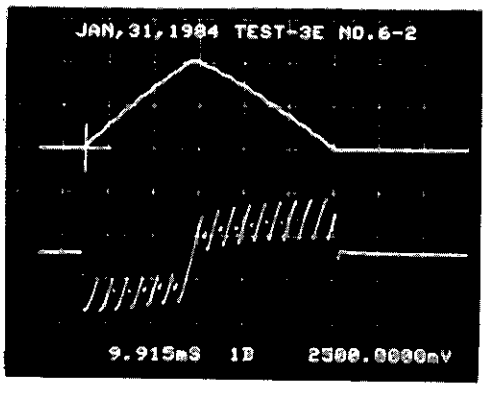

Photo 4. Typical operation of Taylor discharge cleaning PS

OH-coil current [4.0KA/div]

OH-coil voltage [2.0KV/div]

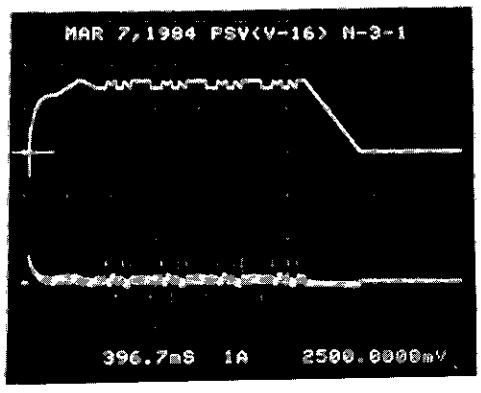

Photo 5. demonstration of current controllability of vertical field P/S

VF-coil current [30KA/div]

VF-coil voltage [5.0KV/div]

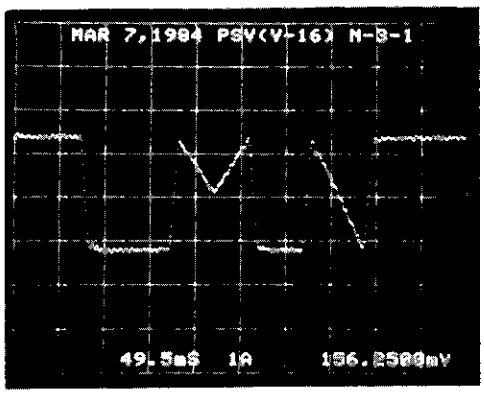

Photo 6. magnified shape of Photo 5.

50KA level

45KA level

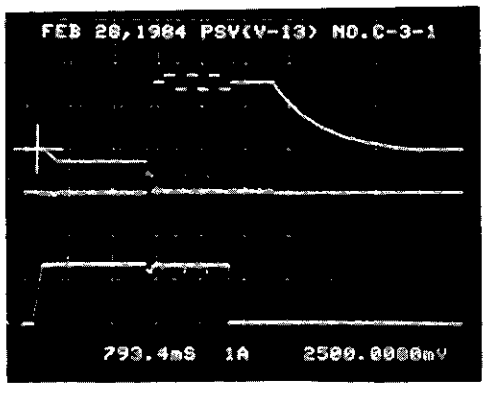

Photo 7. demonstration of current controllability of vertical field P/S

VF-coil current [30KA/div]

VF-coil voltage [5KV/div]

circulating current [3.48KA/div]

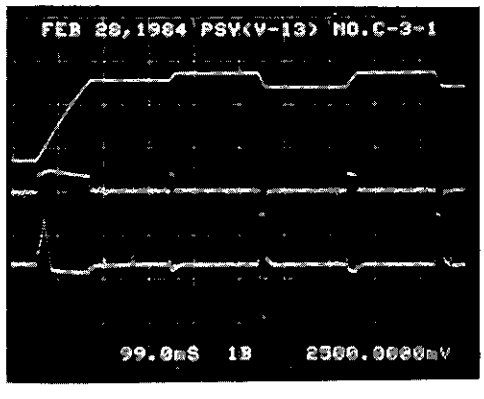

Photo 8. magnified shape of Photo7.

------ 53KA level

---- 43KA level

4.3 Toroidal field power supply

Main components of the toroidal field power supply (TFPS) have been manufactured in the works and tested under inspection of JAERI. The assembling and installation work of TFPS was carried out throughout this fiscal year.

The motor generator with flywheel (MGF) was constructed in the generator pit by the end of 1983. (Fig. X.4-1) It has been under the rotation test since January 1984 to check the dynamic balance.

The thyristor static starter of MGF accelerates MGF up to 600 rpm within 20 minutes. This includes thyristor convertor and invertor, AC and DC reactors, CR surge absorbers and a control panel. After the installation of them, the thyristor static starter has been tested in combination with MGF.

The exciter of MGF changes MGF's terminal voltage to control the toroidal field (TF) coil current. To increase controllability for the generator and DC current of TF coil, we choose some DDC programs for AVR of the exciter. Final checks of these programs will be done in next fiscal year.

The rectifier of TFPS consists of 24 units of water-cooled 6-pulse diode convertors, the output of which is carried to TF coil by the coaxial-type DC bus. (Fig. X.4-2)

TFPS's control systems consist of several CAMAC crates and hard-wired sequential and protective circuits. The former includes micro-computers controller which is watching over the TFPS's main devices. Therefore these are divided into discharge control crates and plant support crates. These were accomplished at works in December 1983. The latter is made of many sequential and protective relay devices. The devices are distributed into central control panel, local control panels, and protection interlock panels. The manufacturing of these panels was finished at works in September 1983.

These control systems were tested as a control subsystem from February 1984 and were put into linkage test with the JT-60 central controller, ZENKEI, in March 1984.

In March 1984, no load test of TFPS was started. Short circuit test of TFPS and combination tests with other systems will start soon.

4.4 Motor generator for plasma heating system

After the contract in March 1982, the final design examination of

the motor generator with flywheel (MGF) has been continued and several components of MGF have been already fabricated and installed at the Naka site.

The flywheel of MGF consists of three large disks having 6.1 m in diameter and 106 tons in weight each. In August 1983, its inspection tests of measuring the GD^2 value and checking the dynamic balance of the flywheel were carried out successfully.

The manufacturing of the 400 MVA generator of MGF was finished in November 1983. (Fig. X.4-3) Its test under inspection of JAERI was carried out in December 1983 to examine its electrical and mechanical characteristics specified.

The assembly and installation of MGF in the generator building were started in December 1983. (Fig. X.4-4)

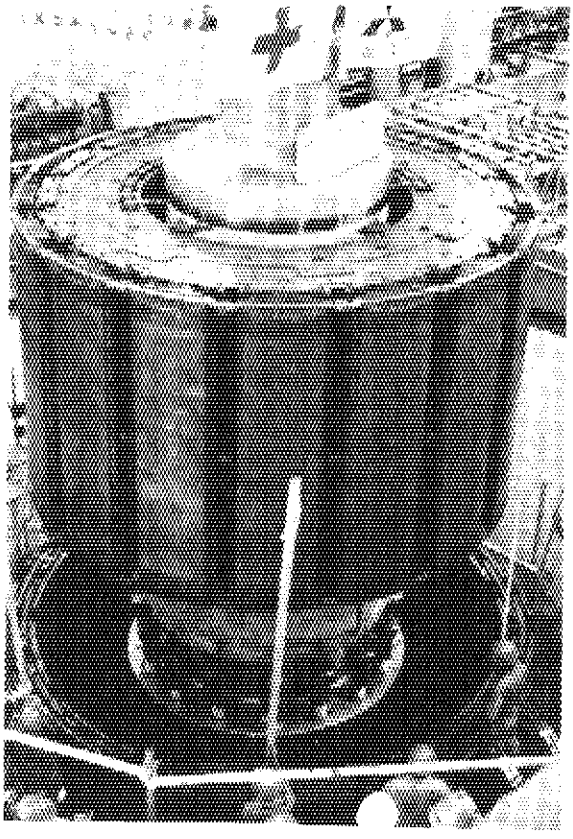

Fig. X.4-1 Installation of MGF's rotor of TFPS.

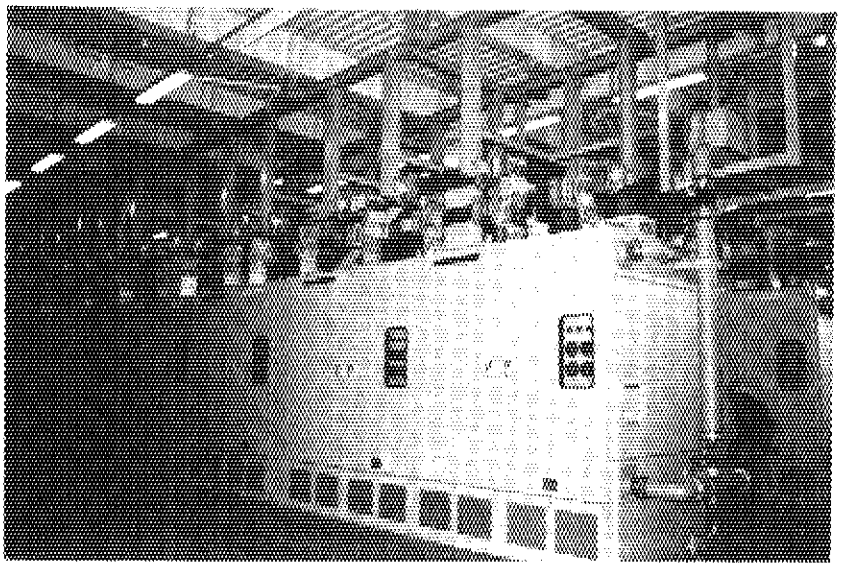

Fig. X.4-2 Water-cooled diode convertors of TFPS.

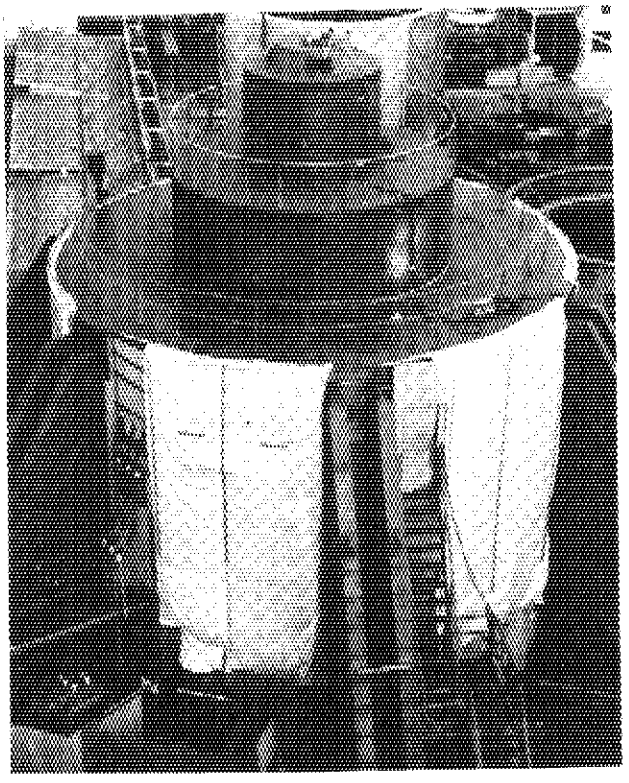

Fig. X.4-3 The generator of motor generator for plasma heating system.

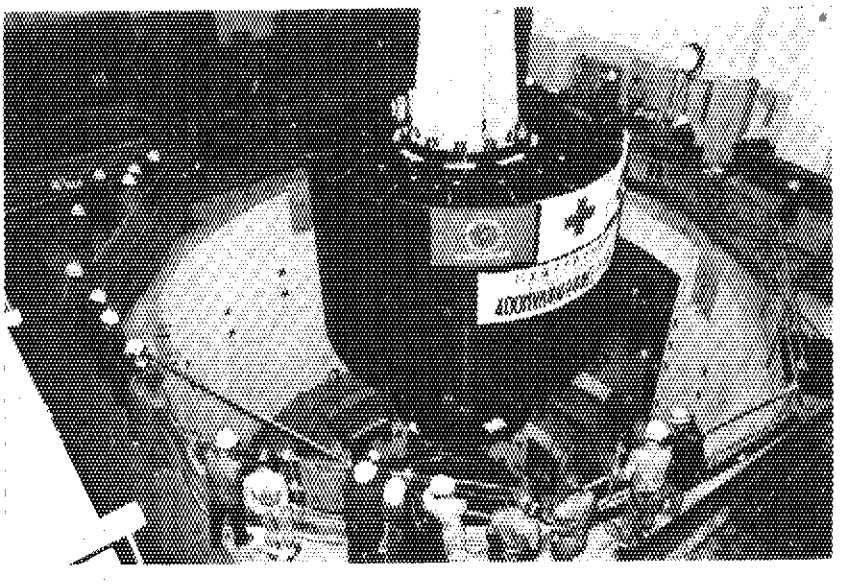

Fig. X.4-4 The rotor of 400MVA generator being lowered into the pit.

5. Status of Control System

5.1 Introduction

In JT-60, each subsystem such as the poloidal field power supply, the toroidal field power supply and the tokamak machine has its own control system with proper intelligence (control subsystem), and the control of JT-60 is to be performed in combination with these several control subsystems.

The installation and testing of Zenkei, the central control system of JT-60 were started first among other control subsystems at the Naka site. This was followed by the installation and testing of individual control subsystems, and then the linkage tests between Zenkei and each one of the subsystems were performed by and by according to its progress. A linkage test is a step of the physical integration process of the entire JT-60 control system.

The performance of the control system is confirmed in four stages such as the single device tests of Zenkei and the subsystems, the linkage tests, the total performance test with no load and that with load. During this term, the first and almost the second stages have been completed. JT-60 is controlled through several routes which are driven by corresponding computer system of Zenkei, such as the plant support computer system, the discharge control computer system, the real-time control computer and the feedback control computer system. A subsystem is linked with Zenkei through one to three of the control routes. Then, the tests have been performed according to the control routes in either case of Zenkei or subsystems. However, the dynamic actions of the real-time control route or the feedback control route are observed only when Zenkei and the corresponding subsystem are tightly linked with each other, then the performance is confirmed.

5.2 Start-up of Zenkei

Zenkei has been almost completed as a single device. After the start of the linkage tests many trouble points have been found out, and the most of them have been improved. On the other hand, through those tests, the corresponding performances of Zenkei itself have been confirmed. Figure X.5-1 represents the configuration of the computer and CAMAC system that is the main part of Zenkei. As observed in the figure, seven computers share the four roles, and each computer system

links with corresponding performance of subsystem. Among them, one that is driven by the plant support computer system groups and controls the over all status being based on the constant informations collection, performs necessary recordings, controls the operation mode, etc.

These performances is already running on the man-machine of the central console, the auxiliary graphic display, the linkage with the safety interlock system, etc. The linkage through this route is performed by serial highways. The communication protocols at the ACD module, which links the subsystems to the serial highway of Zenkei, have been tested at the factory of each subsystem with the use of a test module which is drived by a personal computer as if the communication were performed with Zenkei. Consequently it minimized the troubles at the stage of linkage test.

Among the performances supported by the plant support computer system, non-standard status diagnosis function, which is tightly linked when the safety interlock system, is to be used for the cause identification when an interlock item functions. To utilize this function, trip sequences are necessary to be collected from the subsystems and edited in proper format, but at this moment, it is not clear in which way the trip sequence takes place at a practical event, or if the buffer memory is roomy enough for saving trip sequence in each subsystem, etc. Such unknown points are to be revealed in the total performance test.

The discharge control computer system gives function parameters to the feedback control computer system through the optical data free way, to the timing system through a branch highway, to the actuators through serial highways or byte serial highways, to real-time control computer through the global memory, to NBI, RF and the data processing system through computer-computer communications with respective interfaces. On the contrary, it takes data from the devices about events and status of them. The computer system, as off-line functions, receives discharge parameters (as many as 3000 items), and manages the files of the parameters. On the other hand, it drives the discharge sequence as observed in Fig.X.5-2 and corresponding functions such as pre-shot and post-shot inspections, parameter settings, collection of shot result data, etc. The configuration of the functions of the computer system is represented in Fig.X.5-3, and the configuration for testing the functions is represented in Fig.X.5-4. In this testing configuration, debug support functions as represented in double square in the figure are used.

Figure X.5-5 represents the progress of the discharge sequence which gives the present moment in the sequence with blue flickering. When the sequence has stopped on the way, the line color changes to red, and the cause is found as a changed colored representation in the list of the checked points, given below the sequence lines. The sequence control has been used for linkage tests with the subsystems of the TFC and PFC power supplies and the gas injection system.

The amount of the shot result data is estimated as 1.5 M words, and whether the handling of these data (collection, edition, display and transfer to the data processing system) finishes in 4-5 minutes or influences to the shot to shot interval is one of the points that are to be revealed later.

About real-time control and feedback control, I/O simulations have been utilized for testing the function which is particular to the computers, however, the tests of dynamic characteristics which are particular to plasma control, must be performed in the linkage test with the subsystems of PFC and gas injection system, and at the stage of total performance test.

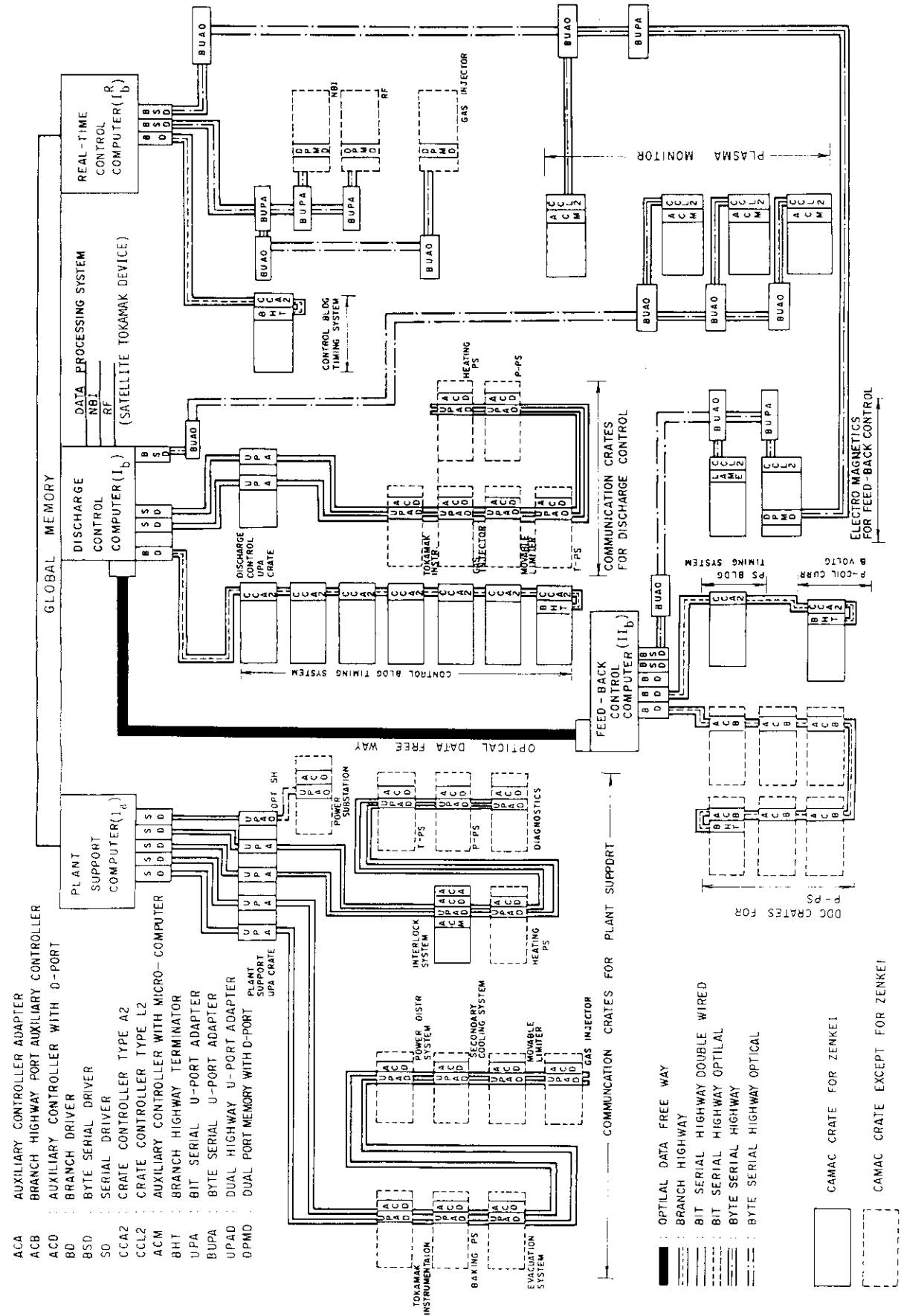

Fig. X.5-1 Computer and CAMAC configuration of Zenkei.

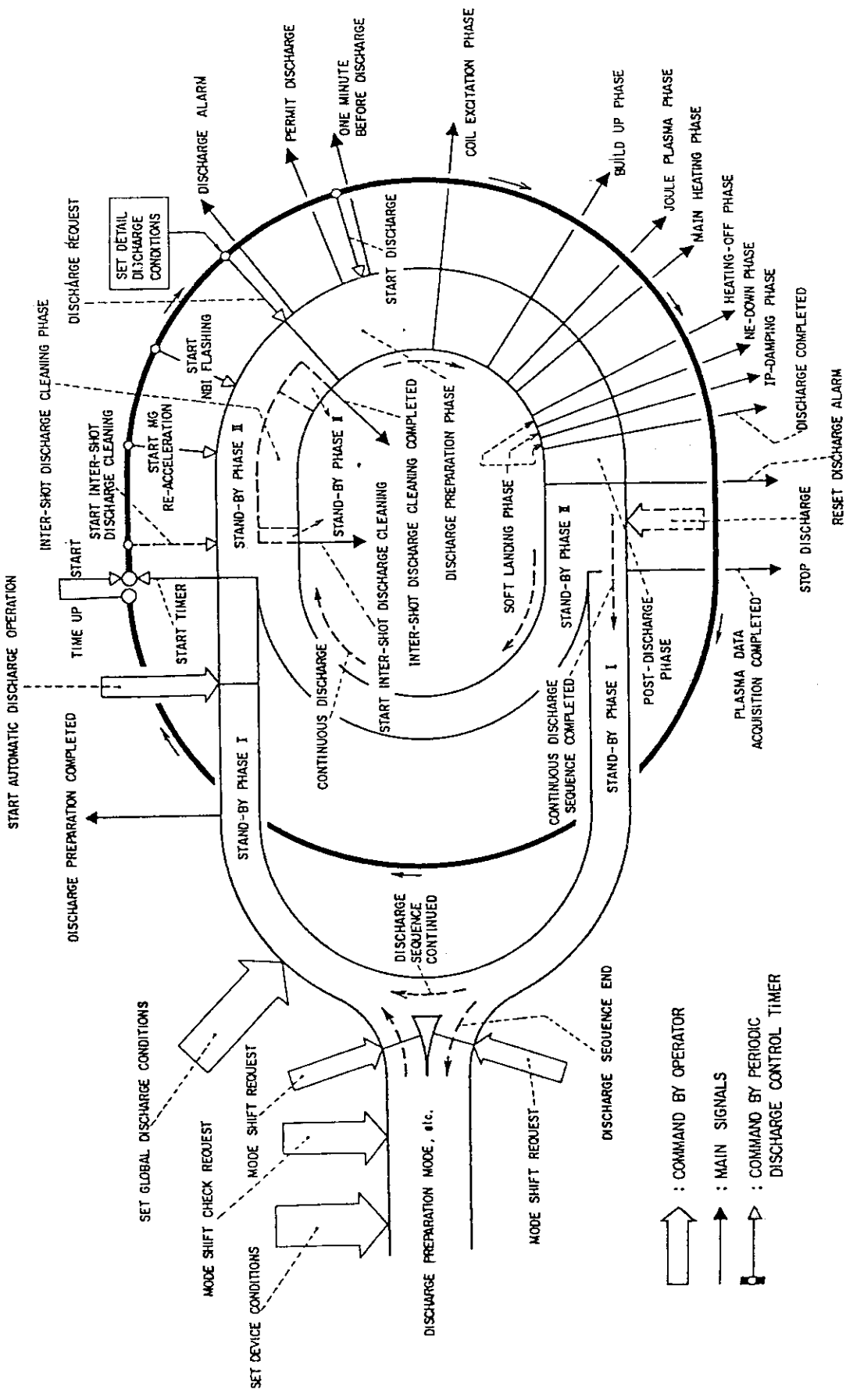

Fig. X.5-2 Time sequence of discharge control.

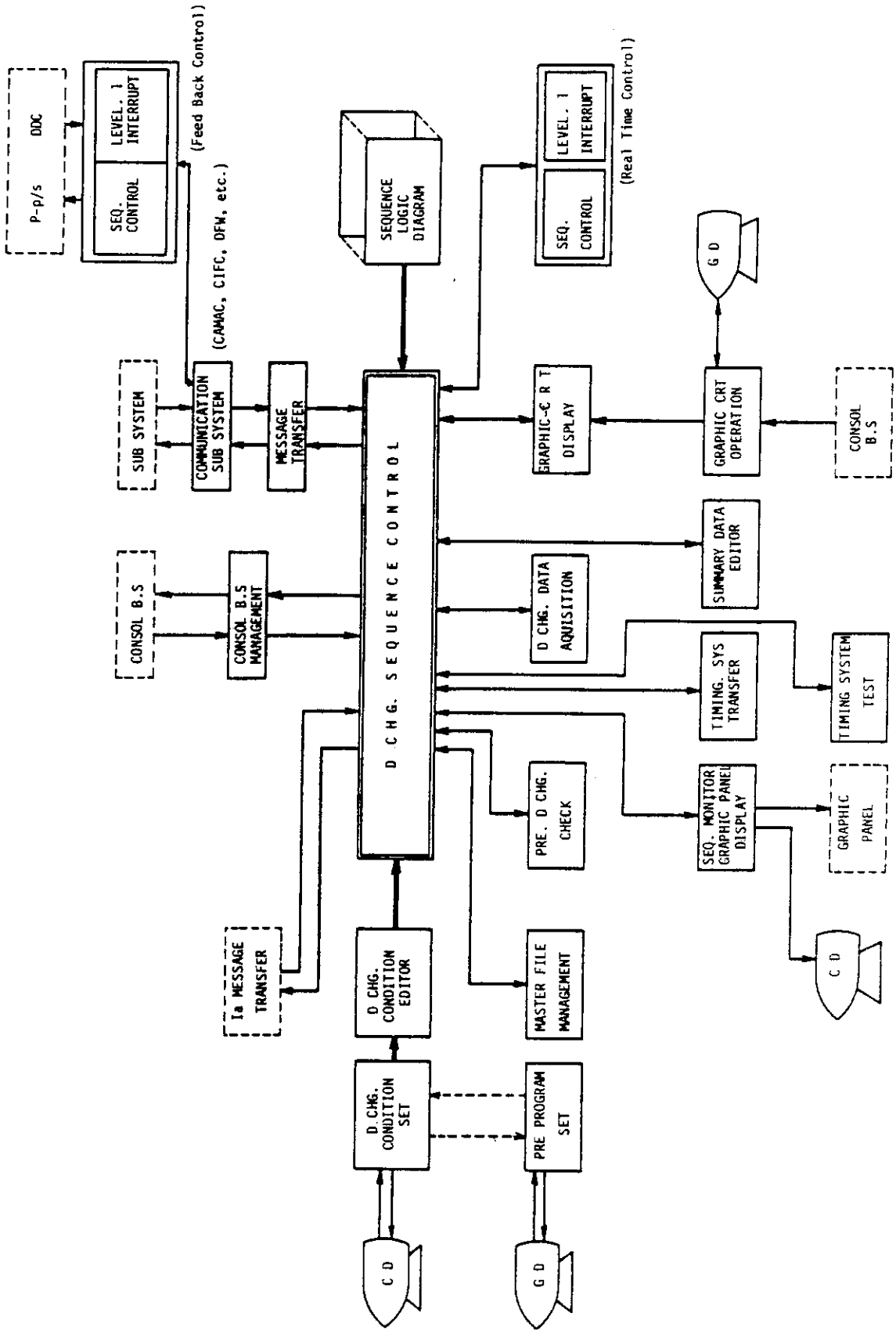

Soft Ware Structure of Discharge Control System "ZENKEI"

Fig. X.5-3 Software structure of discharge control system.

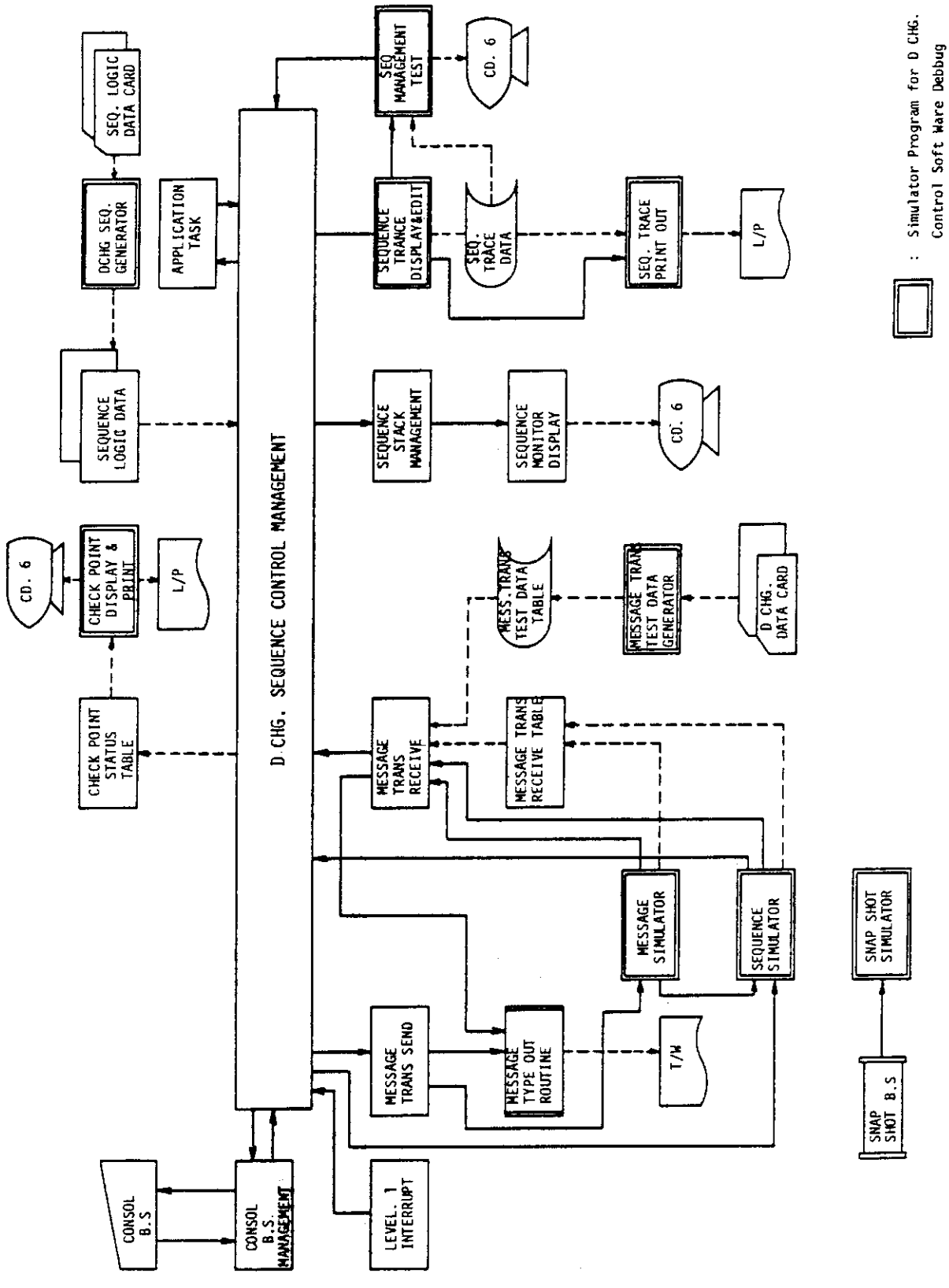

System Lay Out for D CHG. Sequence Control Test

Fig. X.5-4 System layout for discharge sequence control test.

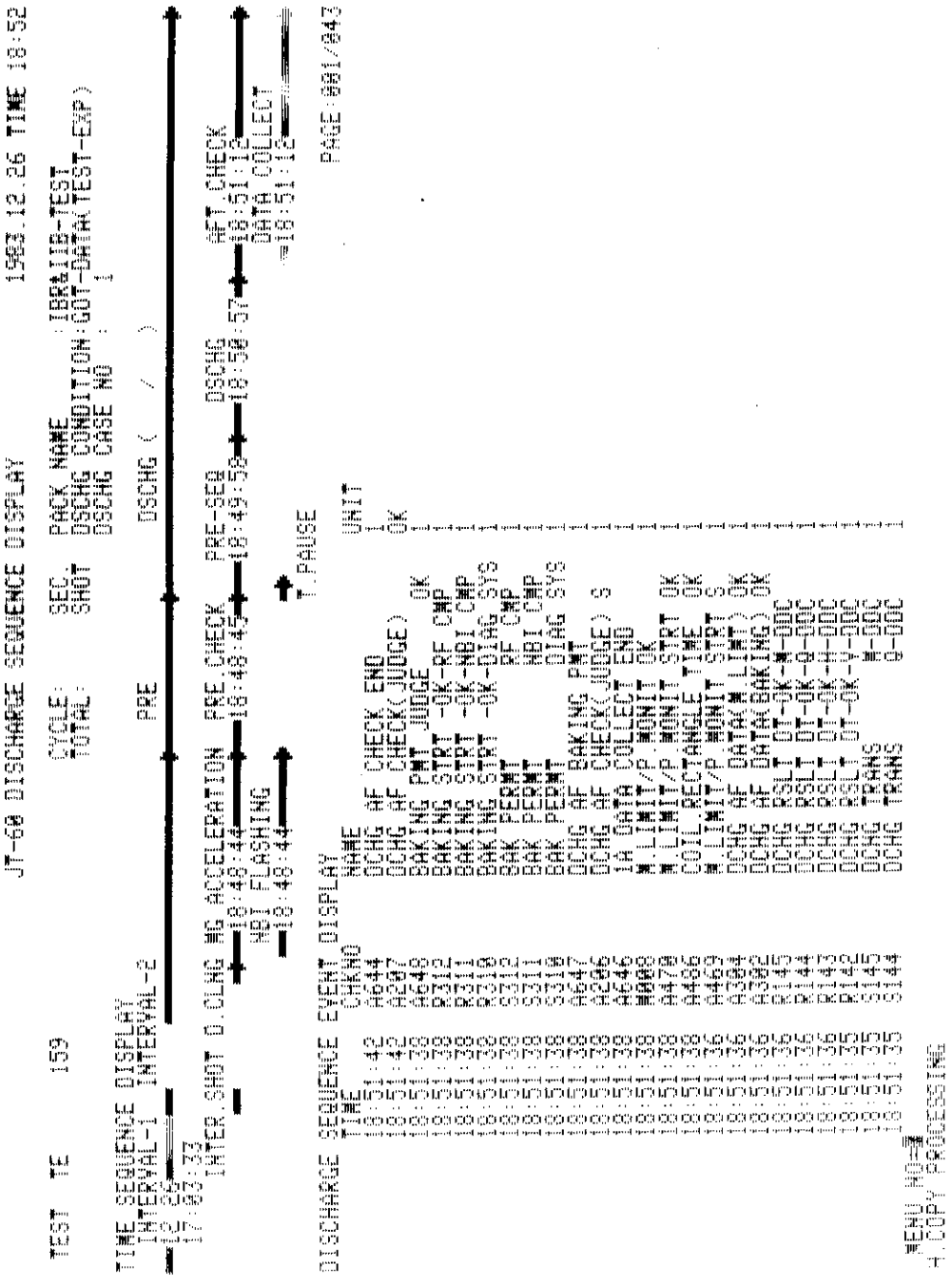

Fig. X.5-5 JT-60 discharge sequence display.

6. Status of Diagnostic System

Design and fabrication of Group A (Table X.6-1) diagnostic instruments have been continued for the last fiscal year.

6.1 Electron density and temperature measuring systems (A-1 and A-2)

Construction of A-1 system has been continued and fabrication in the firm has been completed. The test of the sub-mm wave (119 m) laser subsystems (A-1-a) has been successfully carried out with the results of 240 hrs. continuous operation with the frequency stability of $\Delta\lambda_{Beat}/\lambda \leq 10^{-9}$. A-2-a subsystem was completed in March 1984. It will be tested for calibration and installed within the next fiscal year. Construction of A-2-c multipulse laser subsystem has been started and it will be completed within the fiscal year of 1985.

6.2 Ion temperature and impurity measuring systems

Construction of A-3 system except A-3-c system has been continued and it will be completed within the fiscal year of 1985. A-3-c subsystem was completed in October 1983 and test and development of A-3-c subsystem have started in JAERI to achieve beam parameters of 200 keV and 3.5 A.

Construction of A-4 system has been continued and it will be completed within the fiscal year of 1985.

6.3 Rediation flux and peripheral plasma measuring systems (A-5 and A-6)

Design and fabrication of A-5 and A-6 system have been continued. A-5-a, A-6-b and A-6-c subsystems were completed in March 1984. All these subsystems will be re-tested in JAERI and installed within the fiscal year of 1984. A-6-d subsystem will be completed in March 1985.

6.4 Data processing system and diagnostic support system (A-7 and A-8)

Construction of A-7 data processing system has been continued and it will be completed in the fiscal year of 1984.

Construction of A-8 diagnostic support system has been continued and it will be completed in the fiscal year of 1985.

Table X.6-1(a) JT-60 diagnostics (A group) (part 1).

System	Symbol	Diagnostics	Specification	Feature
A-1 Electron Density Measuring System	A-1-a	Sub-mm Wave Interferometer	Main Plasma $\Delta n_e \geq 10^{12}cm^{-3}$, $\Delta t \sim \mu S$, X_1: 5 points, ΔX = 12 cm Divertor Chamber $\Delta n_e \geq 4 \times 10^{12}cm^{-3}$, $\Delta t \sim \mu S$	CH_3OH (200 mW) λ=118.8 μm Mechanical vibration free (with HeNe laser interferometer)
	A-1-b	MW Wave Interferometer	Main Plasma $\Delta n_e \geq 4 \times 10^{11}cm^{-3}$, $\Delta t \sim \mu S$ X_1: 2 points, ΔX = 6 cm	2 mm Wave (1W)
A-2 Electron Temperature Measuring System	A-2-a	FIR Spectrometer	$\Delta t \sim 10$ mS, X_1: 40 points ΔX= 15 ∿ 30 cm	Fourier Spectrometer real time FFT
	A-2-b	MM Wave Radiometer	$\Delta t \sim \mu S$, X_1: 10 points, ΔX= 15 ∿ 30 cm	126∿280 GHz
	A-2-c	Multipulse Laser Scattering Apparatus	$\Delta t \sim 20$/shot, X_1: 12 points ΔX= 12 cm	SHG(λ=0.526 μm) of Glass Laser(λ=1.053 μm)
A-3 Ion Temperature Measuring System	A-3-a	Neutral Particle Analyzer (E.S.)	E=0.1∿30 keV, $\Delta E/E$=0.05∿0.1 Δt=50∿500 mS, Z_1: 3 points	Electro-Static Analyzer
	A-3-b	Neutral Particle Analyzer (E.S. & M.A.)	E=0.1∿30 keV, $\Delta E/E$=0.1 Δt=50 mS, X_1: 1 point	Electro-Static with mass Analyzer E//B type (H & D)
	A-3-c	Active Beam Probing Apparatus	$\Delta T_i/T_i$=0.1, Δt=10∿100 mS Z_1: 1 point, ΔX=5cm, ΔZ=20cm	Beam: 3.5 A, 200 keV, He^+ Analyzer: E//B type, MCP
	A-3-d	Neutron Counter	E_n-E_{th}∿2.45 MeV, Δt=1∿100 mS X_1: 1 point	NE-213, PHA

Table X.6-1(b) JT-60 diagnostics (A group) (part 2).

System	Symbol	Diagnostics	Specification	Future
A-4 Impurity Measuring System	A-4-a	Light Impurity Spectrometer (Special Resolution)	λ=5∿500 A, Δt∿10 mS, Z_i: 15 points, ΔZ= 7 cm	Toroidal holographic grating, Flat field, Array detector
	A-4-b	Light Impurity Spectrometer (Doppler)	λ=1000∿2350 A (λ_i: 5 points) Δt∿1 mS, X_i: 1 point	Concave grating
	A-4-c	Heavy Impurity Spectrometer (Doppler)	λ=0.1∿10 A (λ_i: 3 points) Δt∿10 mS, X_i: 1 point	Crystal grating, Array detector
	A-4-d	Spectrometer for Divertor	λ=20∿1200 A, Δt∿10 mS, X_i: 1 point near x point	Same as "A-4-a".
	A-4-e	Visible Spectrometer for Absolute Calibration	λ=2000∿7000 A, X_i: 1 point	Photomul & Photograph
	A-4-f	Grazing Incidence Spectrometer for Absolute Calibration	λ=10∿1300 A, X_i: 1 point	Same as above
	A-4-g	A-4 System Calibration Devices		Light Source etc.
A-5 Radiation Flux Measuring System	A-5-a	High Speed Counting PHA	E=1∿200 keV, Δt∿10 mS X_i: 3 points	Si(Li) or Ge(I)
	A-5-b	High Speed Counting PHA Array (Spatial Resolution)	E=1∿200 keV, Δt∿1∿10 mS Z_i: 15 points	Same as above
	A-5-c	PIN Diode Arrays	Δt∿25 μS, Z_i: 15 points	PIN Diode or SSD, Computer Tomography
	A-5-d	Bolometer Arrays	Δt∿10 mS, Z_i: 15 points	Thermistor
	A-5-e	Runaway Monitor	Δt∿1 mS, X_i: 1 point	Hard X-ray Detector Array

Table X.6-1(c) JT-60 diagnostics (A group) (part 3).

System	Symbol	Diagnostics	Specification	Future
A-6 Peripheral Plasma and Wall Surface Measuring System	A-6-a	Infrared TV	t = 10 mS/Frame	Picture Elements; 100 × 100/frame
	A-6-b	Visible TV	t < 50 mS	Fields of view; overall > ±90°
	A-6-c	Electro-Magnetic Probe	Magnetic Probes Rogowski Coils One Turn Coils Saddle Coils Thermo-Couples	
	A-6-d	Spectrometer for periphery	λ=1000∿7000 A, Δt∿10 mS Z_j: 10 points at periphery	Real Time
	A-6-e	Hall detectors		
A-7 Data Processing System		(1) Inter Shot Data Processor (2) Real Time Data Processor (3) CAMAC Systems		General Purpose Computer
A-8 Diagnostic Support System		(1) Diagnostic Stages (2) Carriers (3) Cabling & Piping (4) Vacuum Connecting Instruments (5) Shielding Cases (Magnetic & Radiation Shield)		

7. Status of Auxiliary Systems

The construction of the secondary cooling system and the power distribution system/emergency power supply was finished in October 1983 as scheduled. These auxiliary systems are now in operation for various tests of other JT-60 subsystems.

7.1 Secondary cooling system

The outline of this system is as follows.

(i) Total circulation of water; 10,070 m^3/hr

(ii) Outlet temperature of cooling water; 31 °C

(iii) Inlet temperature of cooling water; 37 °C

(iv) Constitution of cooling system; four separate cooling lines (tokamak secondary cooling line, power supplies secondary cooling line, heating system secondary cooling line and auxiliary equipment cooling line)

(v) Water treatment; the quality of water is maintained through scale prevention, slime prevention and corrosion prevention treatments.

The flow diagram of this system is shown in Fig. X.7-1.

7.2 Power distribution system/emergency power supply

The specifications for the capability of the system are summarized below.

(i) the power distribution system 13 MVA

(ii) the emergency power supply 8.3 MVA

(iii) the AC no break power supply

static type invertor (CVCF) 500 kVA, 4 sets

battery (HS-2500) 2500 AH, 2 sets

(iv) the DC no break power supply

rectifier device 250 kVA, 2 sets

battery (HS-500) 500 AH, 2 sets

The wiring diagram of this power supply system is shown in Fig. X.7-2.

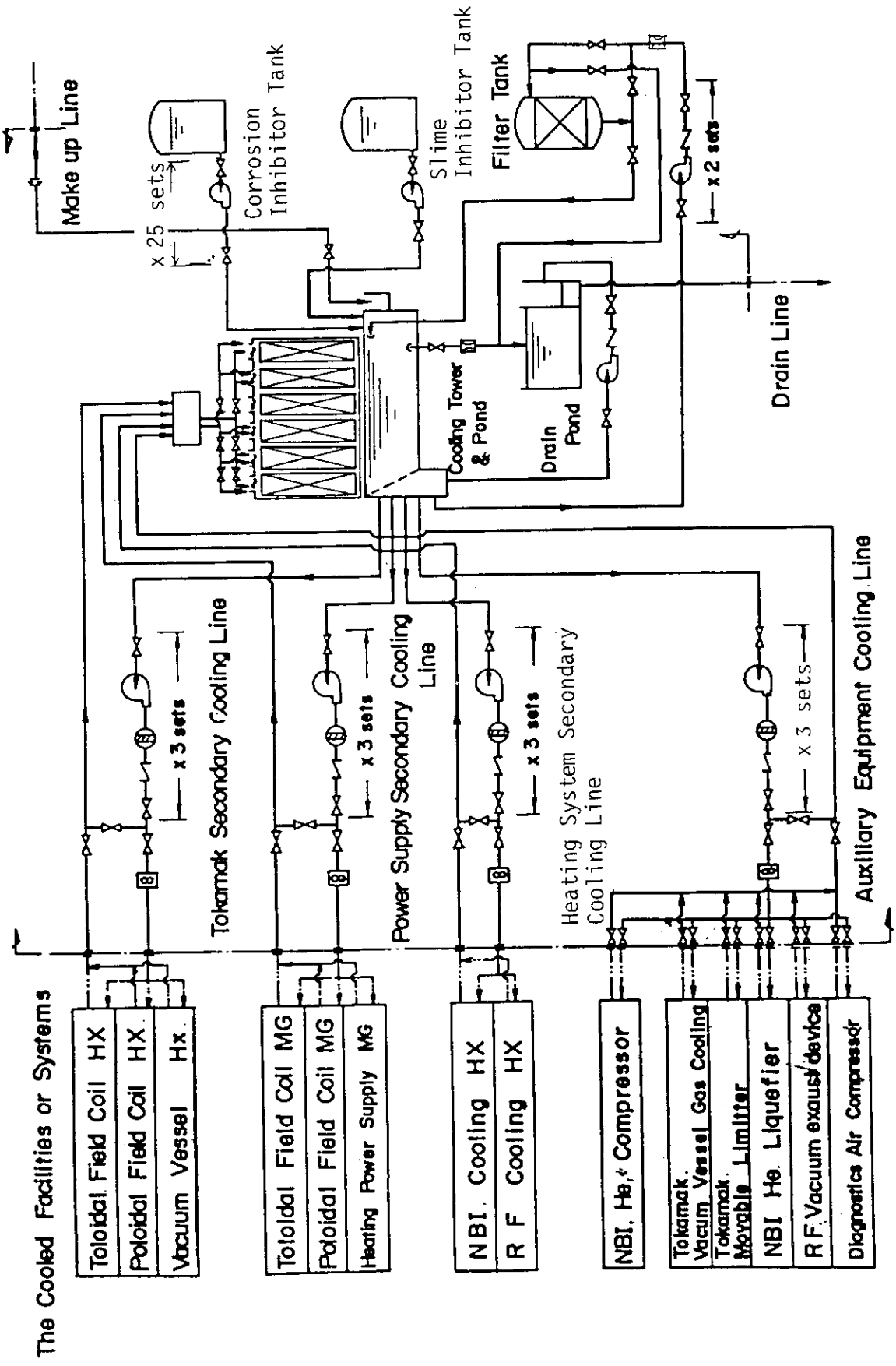

Fig. X.7-1 Secondary Cooling Flow Diagram.

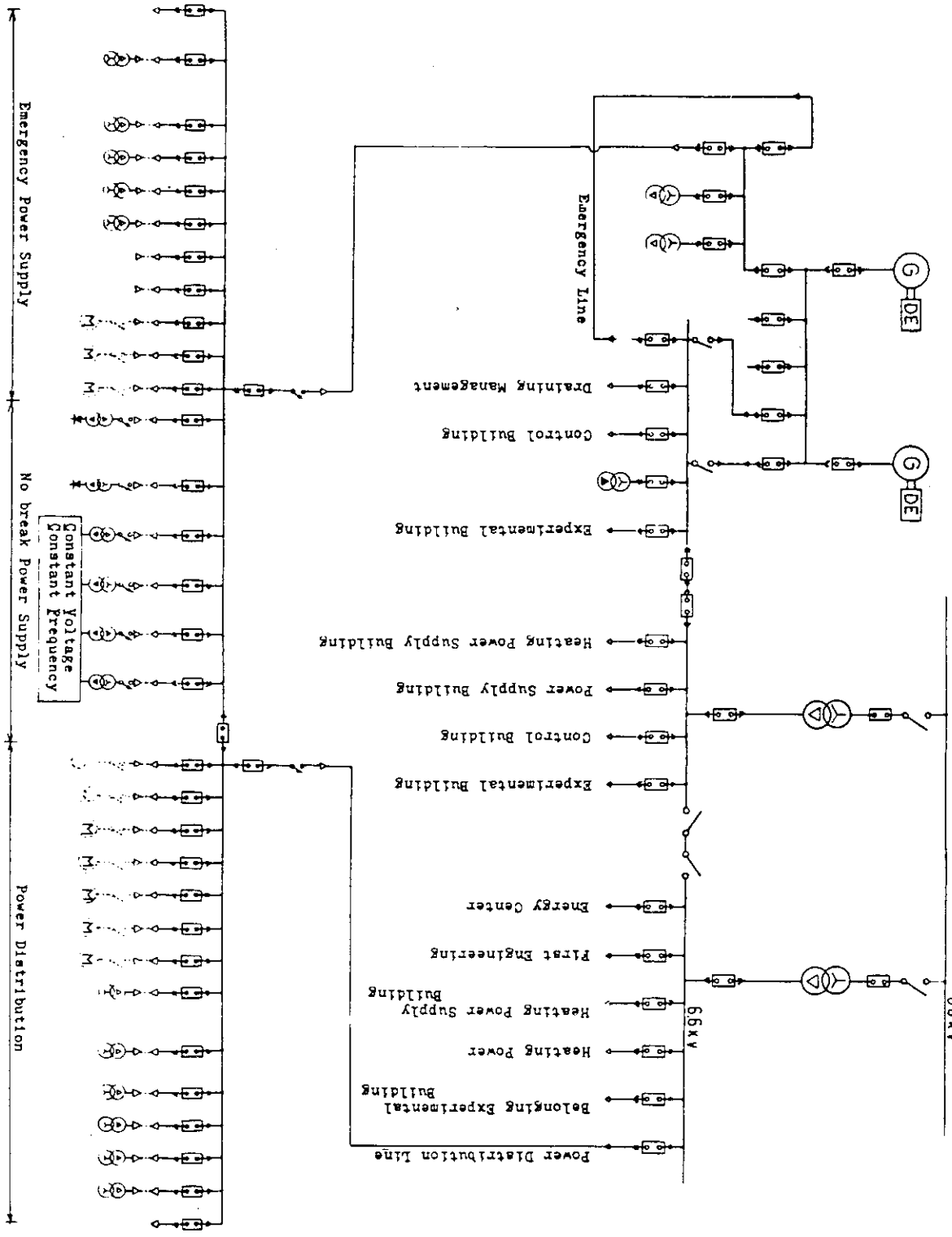

Fig. X.7-2 Schematic diagram of power distribution system/emergency power supply.

8. Status of Heating System

8.1 Construction of Neutral Beam Injector (NBI) for JT-60[1,2)]

In JT-60, 20 MW hydrogen neutral beam will be injected to achieve reactor-grade plasma using 14 injector units. Each unit is designed to deliver 1.43 MW neutral beam at energy of 75-100 keV for 10 sec using two ion sources rated at the 75-100 keV, 35A ion beam extraction.

The JT-60 NBI system consists of 14 beam lines, 14 power supply units, a cryogenic system, a cooling water system, an auxiliary vacuum pumping system, a control system and a diagnostic system. The cryogenic system consists of a helium refrigerator and a liquid nitrogen supply for the cryopumps installed in the beam line chamber. The cooling water system removes the heat load from beam dumps, calorimeters, etc. in the beam line. The auxiliary pumping system is used as a roughing pump before the cryopumps operation. The control system supervises all system of NBI and manages beam injection under the JT-60 central control system called ZENKEI.

A cross-sectional view of lower and upper units of beam line is shown in Fig. X.8-1. The basic performance characteristics of the JT-60 NBI are tabulated in Table X.8-1.

The significant features of JT-60 NBI are following.

+ Long pulse beam up to 10 sec is possible. This is the longest beam pulse in the injectors for large tokamak devices now under construction.
+ Beam energy can be changed within a pulse. This drastically alters the neutral beam injector concept and considerably increases availability of the injector system, since the beam energy can be matched at any instance to the plasma density.
+ High proton ratio (more than 90 %) and low impurities beam can be extracted.

Construction of NBI system was started in autumn of 1983. The test, which includes the beam extraction, of each beam line unit was started from April 1984 using a beam line test stand which was altered a part of prototype injector facility. All beam lines, after testing, will be installed on JT-60 device starting in July 1985, with completion of the whole system scheduled for the middle of 1986.

References

1) T. Shibata, et al., 10th Symp. on Engineering Problems of Fusion

Research, Philadelphia, 1983.

2) S. Matsuda, et al., 4th Int. Symp. on Heating in Toroidal Plasmas, Rome, 1984.

8.2 JT-60 radio frequency heating system

JT-60 radio frequency (RF) heating system consists of three heating units of lower hybrid range of frequencies (LHRF) at ∿2 GHz and one heating unit of ion cyclotron range of frequencies (ICRF) at ∿120 MHz. Specifications of the RF heating system are listed in Table X.8-2. The RF heating system, as shown in Fig. X.8-2, is composed of high voltage power supplies, high power amplifiers, transmission lines, coupling system, primary water cooling system, vacuum pumping system and control system[1,2]. In particular, the high power amplifier and the coupling system are the key components of the RF heating system. A klystron in an LHRF heating unit is a 1 MW class amplifier which has been developed especially for fusion application in JAERI. A tetrode in an ICRF heating unit is also a 1 MW class amplifier which is one of the most powerful tetrodes at present. As a launcher which is a main component of coupling system to radiate RF power into a plasma, a phased array of waveguides (4 rows × 8 columns) for an LHRF heating unit and a phased array of loop antennas (2 rows × 2 columns) described in the section V.2 for an ICRF heating unit are to be adopted. By feedback control of the phase difference between waveguides or loop antennas according to plasma parameters, more efficient plasma heating and current drive are expected in both LHRF and ICRF heating.

Contract of the whole RF heating system was made and its construction was started in November, 1983. A part of the primary water cooling system was already made so as to keep step with other equipments of JT-60. Moreover, main support structures and working stages of coupling system and transmission lines in the JT-60 torus hall are being made and will be installed in summer of 1984. The final design for production of main RF components is intensively continued.

References

1) Annual Report of April 1, 1982 to March 31, 1983, JAERI-M 83-182 (1983).

2) T. Nagashima, et al., in the proceeding of 10th Symposium on Fusion Engineering, Philadelphia, U.S.A., Dec. 5-9, 1983.

Table X.8-1 Basic performance of the JT-60 NBI

Beam Energy; 75-100 keV
Ion Beam Current; 70 A x 14
Beam Duration Time; 10 sec
Cold Gas Flow to the Torus ; 0.84 Pa m3/s

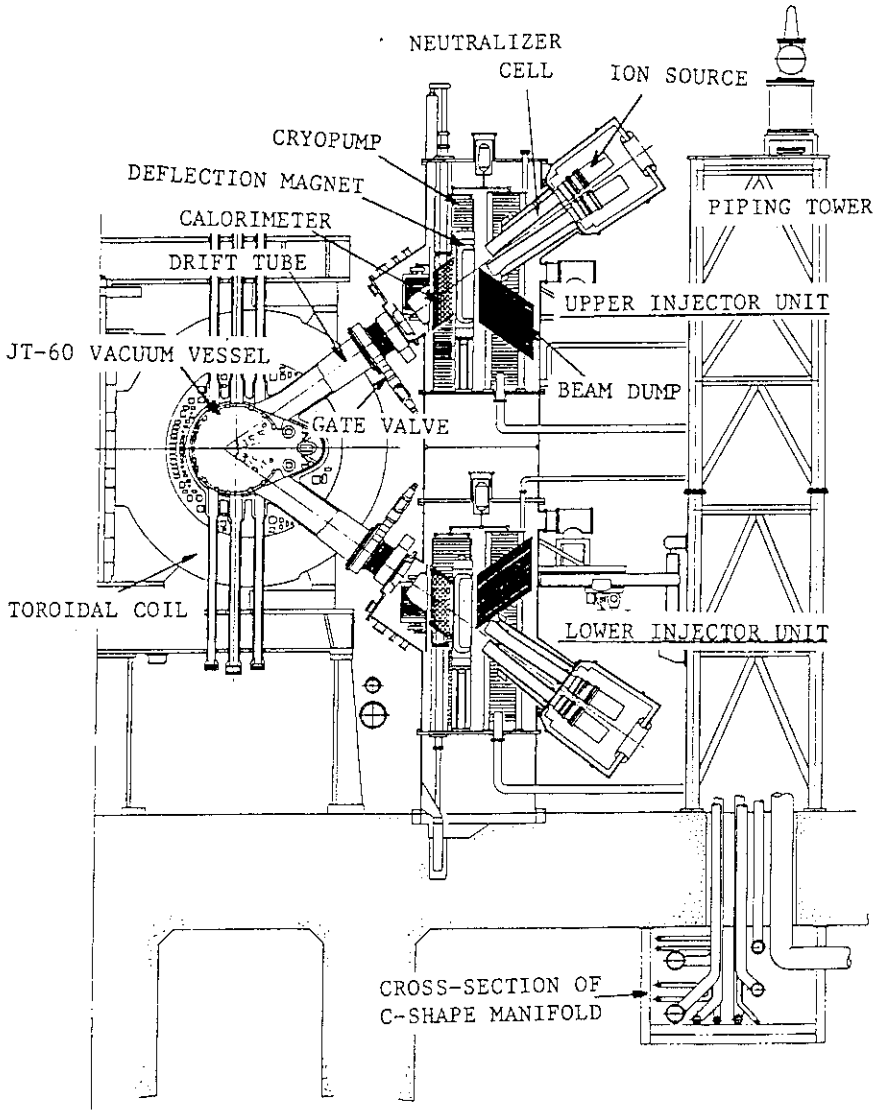

Fig. X.8-1 Cross sectional view of the JT-60 NBI.

Table X.8-2 Specifications of the JT-60 RF heating system.

	LHRF	ICRF
Number of unit	3	1
Frequency	1.7 - 2.3 GHz	110 - 130 MHz
Injection power	10 MW	
RF pulse length	10 sec	
Duty	1/60	
High power amplifier	klystron (8 tubes/unit)	tetrode (8 tubes/unit)
Launcher	Phased array of waveguides (4 rows × 8 columns)	Phased array of loop antennas (2 rows × 2 columns)

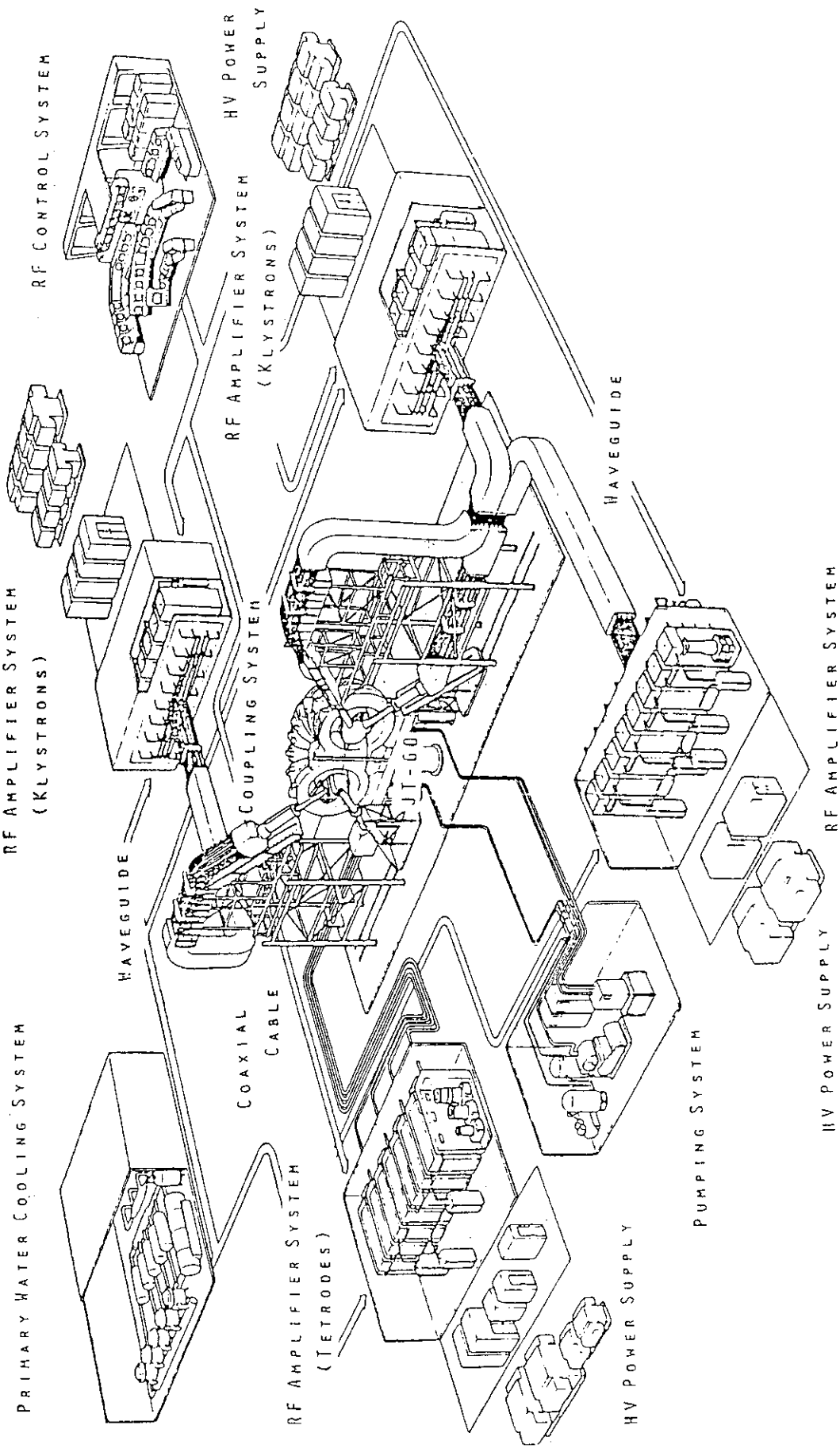

Fig. X.8-2 Overview of JT-60 RF heating system.

9. JT-60 Experimental Planning and Plasma Consideration

9.1 Experimental program and schedule

The experimental schedule was modified as shown in Fig. X.9-1, keeping original experimental programs. The objective of JT-60 is the study of a reactor grade plasma including plasma-machine interface phenomena. In other words, technology to generate and maintain a reactor grade plasma has to be investigated and it is necessary to show how we can build up and control a reactor core with realistic methods. The experimental programs are summarized in Fig. X.9-1 and are briefly summarized as follows:

1. Preliminary Experiment

   2.7 MA discharge with and without divertor
   NBI, ICRF and LHF heatings
   RF current drive

2. Reactor Like Plasma Experiment

   $\bar{n}\tau_E = (2-6)\times 10^{19}$ $m^{-3}s$
   $\bar{T} = 5 - 10$ keV
   $P_h = 30$ MW
   $t = 5 - 10$ s
   $V_p = 60$ m^3

3. R & D for Reactor Core Plasma Experiment

   a) Impurity Control with a High Power & Long Pulse Heating
      Simple Poloidal Divertor
      Boundary Plasma Control
      First Wall Material

   b) Long Pulse & High Power Heating
      NBI (20 MW/75 - 100 keV/10 s)
      LHRF (7.5 MW/1.7 - 2.3 GHz/10 s) → Modification
      ICRF (2.5 MW/Phase Array Antenna)

   c) Tokamak Plasma Improvement

      RF Current Drive

Hith β (with B_t = 4.5 T, profile control)
Disruption Control

4. Advanced Experiment

9.2 Plasma control

In a large tokamak, careful plasma control is essential not only for production of a high quality plasma but also for safety and machine protection. From this point of view, as well as for the position and shape control of a plasma, the real time control system is employed for other important features, e.g. controls of separatrix configuration, heating power, gas influx and disruption. All diagnostic instruments can be used as sensors for the real time control system to supply feedback informations to the major actuators; the poloidal coil system, divertor coils, hydrogen and impurity gas supply systems, 14 NBI injectors and 4 units of RF systems. Disruption control and soft plasma quenching will be intensively investigated as well as control of conventional plasma parameters. The compact poloidal divertor is one of the most essential characteristics of JT-60. The divertor is the promissing method for controlling plasma-wall interactions and for optimizing main plasma parameters. Divertor plasma parameters, neutral pressure in the divertor and heat flux on the divertor plate as well as the divertor configuration will be controlled.

A typical magnetic configuration with the divertor is shown Fig. X.9-2. In this configuration, the separatrix magnetic surface does not intersect any material except the divertor plate, and the following geometrical factors have to be controlled.

R_p^* : plasma center position,

δ_{30}: the minimum clearance between the separatrix magnetic surface and toroidal limiter,

δ_t : clearance between the separatrix magnetic surface and the main divertor coil,

x_p : position of the separatrix magnetic surface on the divertor plate.

Control of these geometrical factors has been numerically studied in detail and the results are summarized as follows: The plasma center position R_p^* can be controlled by conventional Fourier analysis methods

such as the feedback control of vertical magnetic field B_v. The clearance δ_{30} is rather complex but can be essentially controlled by changing the index n [$n = -(R/B_v)\partial B_v/\partial R$] which is a strong function of quadrupole coil current. Since the throat clearance δ_t has a dependence on the magnetic field pattern in the divertor chamber, the poloidal field direction at a suitable position (B_ρ/B_ω in Fig. X.9-2) gives a rather accurate value for δ_t under a wide range of discharge conditions. The position of the separatrix on the divertor plate x_p is a linear function of δ_t, i.e. $x_p = 4.2(\delta_t - 4)\pm 1$ cm. The separatrix magnetic surface, therefore, can be controlled by using B_ρ/B_ω in the divertor chamber.

In order to reduce the time-averaged heat flux density on the divertor plate or to change the neutral particle conductance between the divertor and the main chamber (Fig. X.9-3), the separatrix magnetic surface can be moved from $\delta_t = 2$ cm to $\delta_t = 6$ cm or from $x_p = -9$ cm to $x_p = +8$ cm in 70 ms. In this swinging, the separatrix magnetic configuration in the divertor region can be controlled without changing the main plasma configuration. Therefore average heat flux or divertor plasma parameters can be controlled without changing the main plasma. If we take into account a finite width of the scrape-off layer, this scanning range has to be limited. For this reason, a direct measurement of heat flux profile onto the divertor plate will be done by using infrared cameras in the initial phase of experiment and the heat profile will be directly controlled in the heating experiment. Control of the divertor plasma, especially reducing electron temperature and remote cooling, is also very important to reduce plasma wall interactions and to pump out particles. From this point of view, divertor plasmas are analyzed by using a fluid model as shown in the following subsection. And cold and dense plasma is shown to be realized with reasonable conditions. By combining the remote cooling technique and the swing of the separatrix magnetic surface, a serious high heat flux can be reduced down to a reasonable flux as shown in Fig. X.9-3.

9.3 Plasma consideration

Divertor plasma in JT-60 is mainly investigated this year. A possibility to obtain an ideal divertor plasma in the compact divertor, i.e. cold and dense plasma in front of the divertor plate, is studied by a fluid model. In this analysis, fluid equations consisting of the

particle, momentum and energy conservation equations along magnetic field lines are coupled with neutral particle transport which is simulated by Monte Carlo method. Their interaction through ionization, charge exchange, and excitation process are solved self-consistently by using an iterative procedure. Impurity ionization and radiation loss is also taken into account assuming 1% oxygen impurity.

The maximum total heat flux into both divertor throats, P_{th} = 20 MW. The total particle flux corresponds to a main plasma with mean density of 10^{14} cm^{-3} and average particle confinement time of 0.1 s. Net input power into the plasma is 20 - 30 MW in order to obtain a reactor like plasma. Then the total heat flux into the divertor of 20 MW is reasonable assuming some radiation loss in the main chamber. The results indicate a rather cold and dense plasma in front of the divertor plate with a relatively small heating power as shown in Fig. X.9-4, e.g. $T_{ed} \leq 20$ eV, $n_{ed} = (2 - 3) \times 10^{13}$ cm^{-3} and $P_{th} \leq 10$ MW, where T_{ed}, n_{ed} and P_{th} are electron temperature, density and the total heat flux into the both divertor throats, respectively. Increasing P_{th} up to 20 MW, increases T_{ed} dramatically and n_{ed} decreases (Fig. X.9-4), because amplification of the plasma flux in the divertor is not enough for the high heating power. Wall erosion and heat flux on the divertor plates become serious in this situation. If the total particle flux into the divertor or the main plasma density increases, the plasma density n_{ed} in the divertor increases non-linearly and the electron temperature T_{ed} decreases. In this case, however, a very high particle flux F_{th} is required, e.g. $F_{th} > 10^{23}$ s^{-1}. Therefore it is very important to control the divertor plasma without changing F_{th}. In JT-60, two possible methods to increase particle recycling or density only in the divertor are considered as follows: Neutral particle back flow through the divertor throat reduces as the vacuum region between the scrape-off layer and the sub divertor coil is decreased (Fig. X.9-2). Then the plasma density as well as neutral particle density increases only in the divertor. The other method is gas puffing directly into the divertor. Combining these methods, plasma parameters near the divertor plate change strongly as shown by solid line in Fig. X.9-5. In this high compression case, T_{ed}=9 eV and $n_{ed} = 1.45 \times 10^{14}$ cm^{-3} with the standard total particle flux of 6×10^{22} s^{-1}. By using this method, T_{ed} can be controlled at a low value, e.g., T_{ed} is kept at 7 - 9 eV when P_{th} increases from 2 MW to

20 MW (Fig. X.9-5). In this operational scenario, radiation loss in the divertor increases linearly as increasing heating power, because the plasma density in the divertor increases linearly with a constant value of the electron temperature. Then a strong remote cooling reduces the heat flux onto the divertor plate by a factor of 2 - 3.

The analysis suggests that the ideal divertor operation can also be realized in JT-60 by optimizing operation conditions.

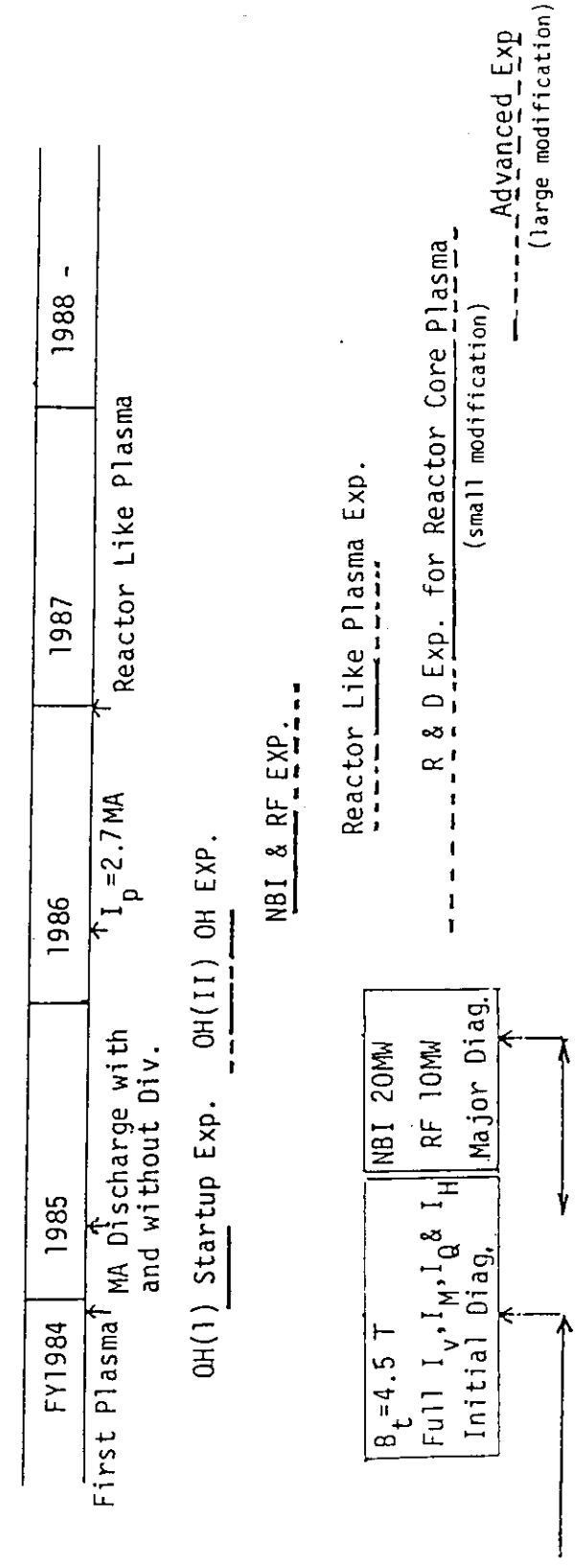

Fig. X.9-1 Experimental program and schedule of JT-60.

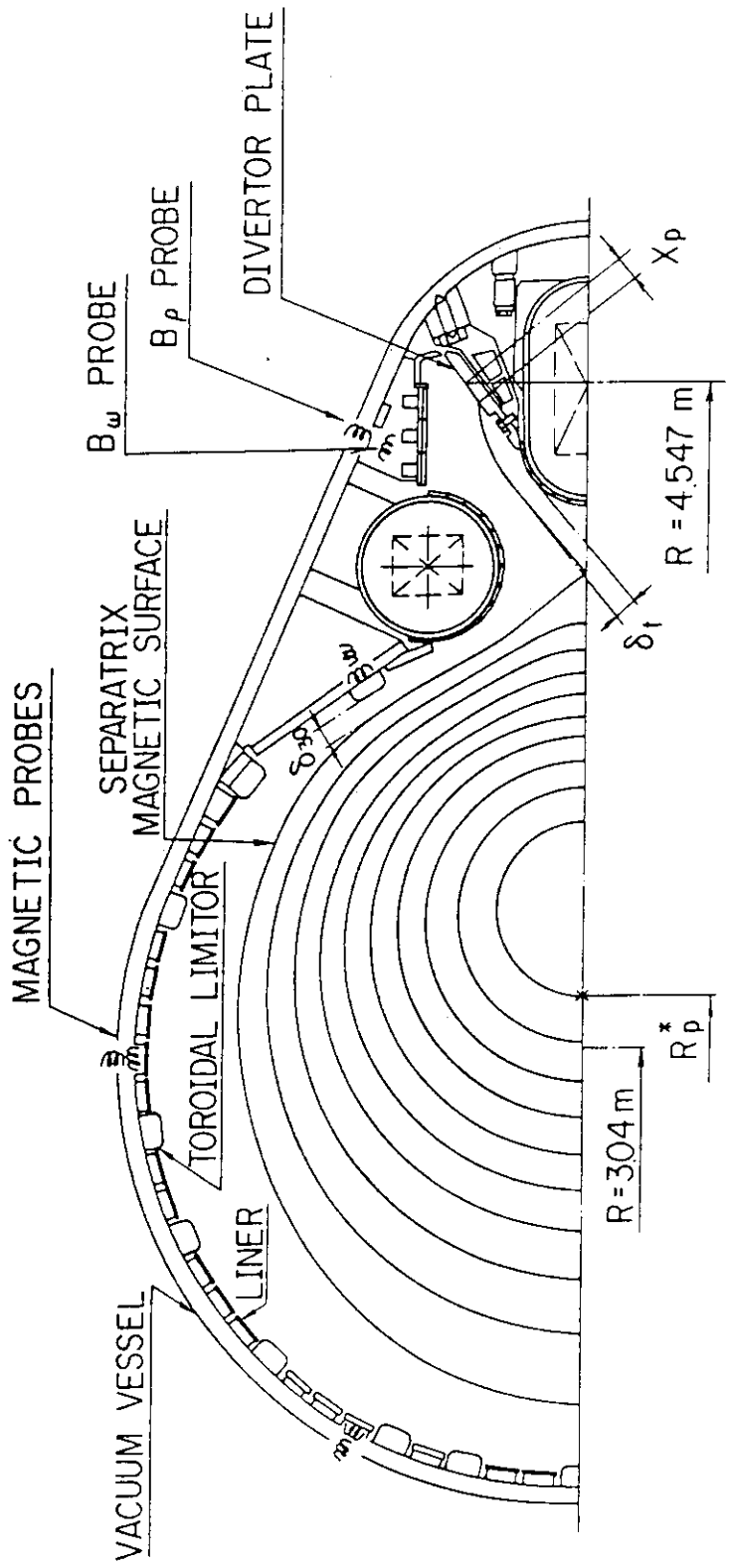

Fig. X.9-2 Cross sectional view of JT-60 vacuum vessel.
R_p^* : plasma center position
δ_{30}: the minimum clearance between separatrix magnetic surface and toroidal limiters
δ_t : clearance between separatrix magnetic surface and main divertor coil
x_p : position of separatrix magnetic surface on divertor plate.

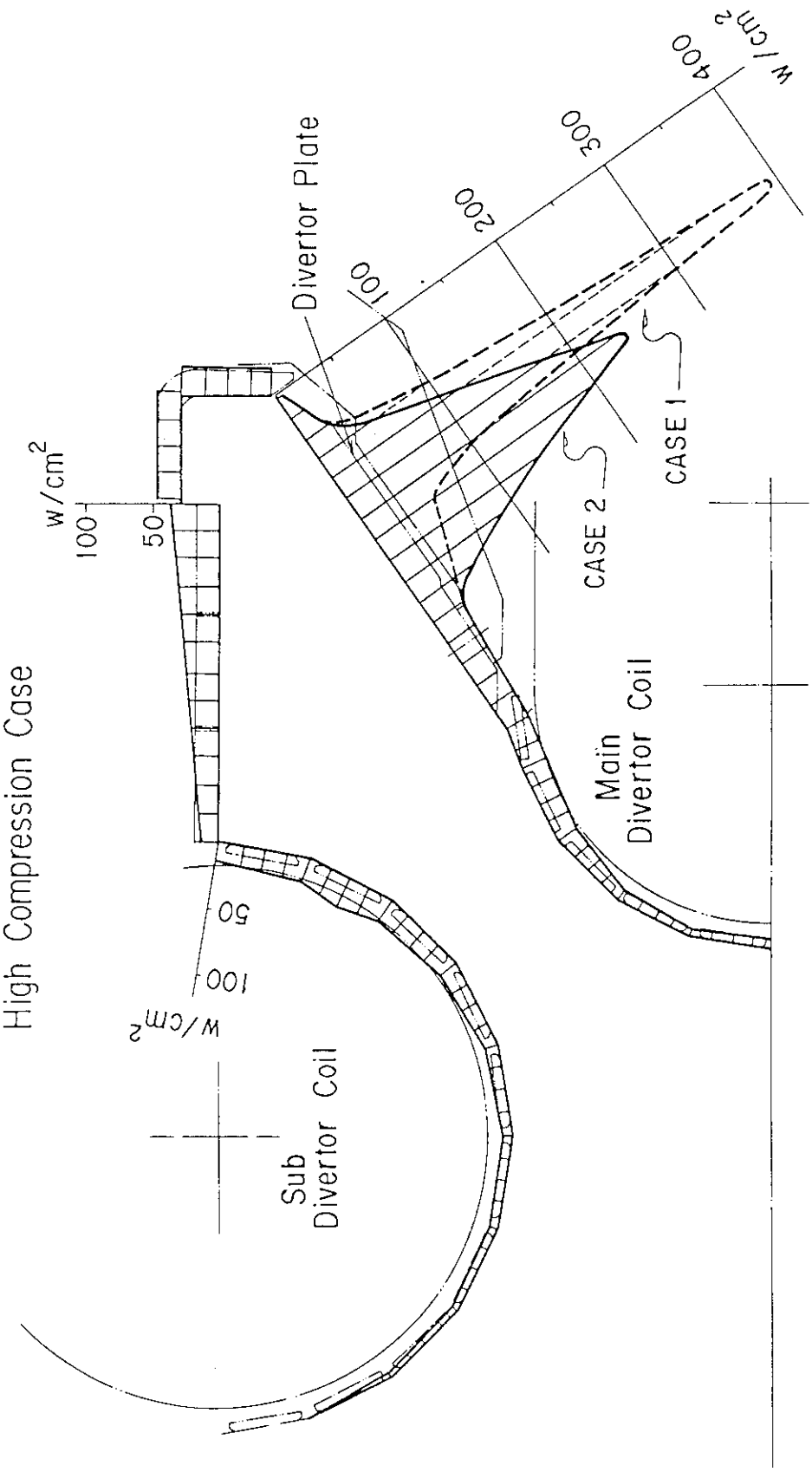

Fig. X.9-3 A typical heat flux density profile of the first wall in the divertor with a remote cooling and the total heat flux of 20 MW. Case 1: without swing, Case 2: with ±1.5 cm swing. The maximum heat flux density is about 1 kw/cm^2 without the remote cooling and the swing.

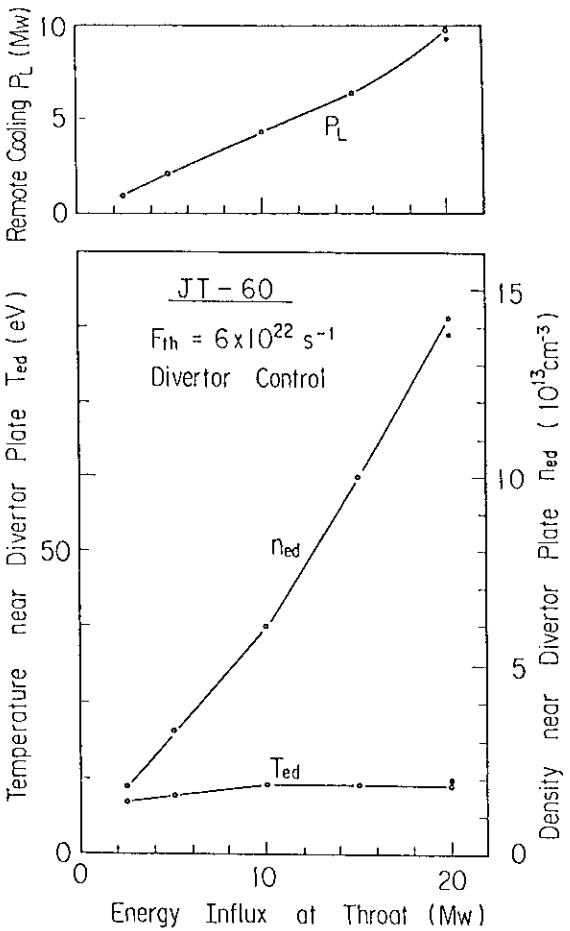

Fig. X.9-4 Electron temperature T_{ed} and density n_{ed} near divertor plate vs. the total energy influx into both divertor throats with δ_t of 2.5 cm and F_{th} of 6×10^{22} cm^{-3}, where δ_t, F_{th} and P_L are clearance between separatrix magnetic surface and main divertor coil, the total particle influx into both divertor throats and remote cooling power in divertor.

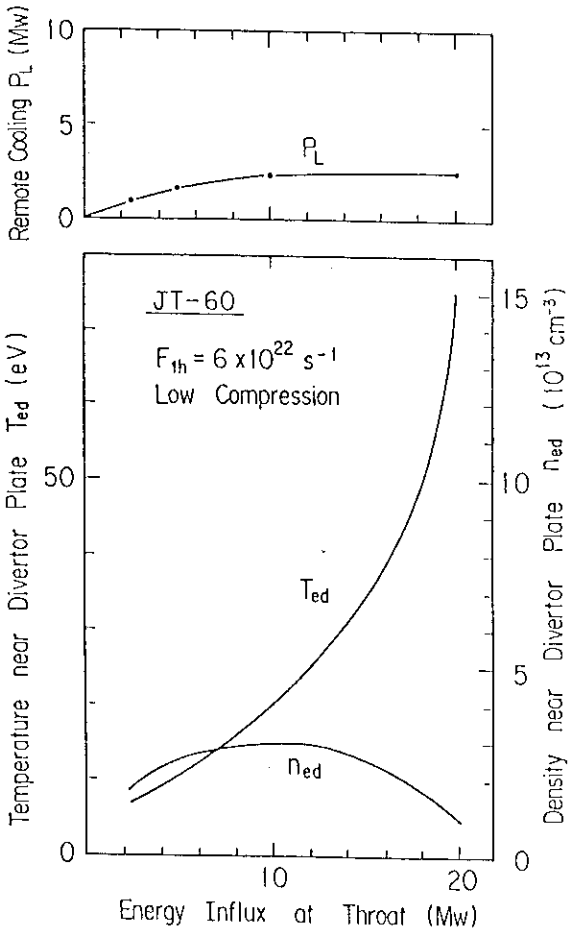

Fig. X.9-5 Electron temperature control by increasing multiplication of plasma flow in divertor when the total heat flux increase from 2 MW to 20 MW.

10. JT-60 Operation Program

Basic data to plan and evaluate operation procedures, manpower needs and project costs in various operation phases were developed and refined in detail.

During the initial OH plasma experiment, JT-60 operation will be performed by two week standard cycle (Fig. X.10-1) without midnight shift operation to save cost and manpower. In the JT-60 operation, large part of operation and maintenance of conventional facilities such as AC power supply systems and water cooling systems will be done by non JAERI peoples dispatched from industries by contract.

System design of computerized maintenance management system which is essential to achieve effective operation was initiated and overall system skeleton was developed. Detailed design work was focused on management program for drawings and technical materials.

Draft of JT-60 Safety Policy and related safety manuals were prepared for internal discussion. Preparation and integration of JT-60 operation and maintenance manuals are now proceeding aiming at completion in April 1985.

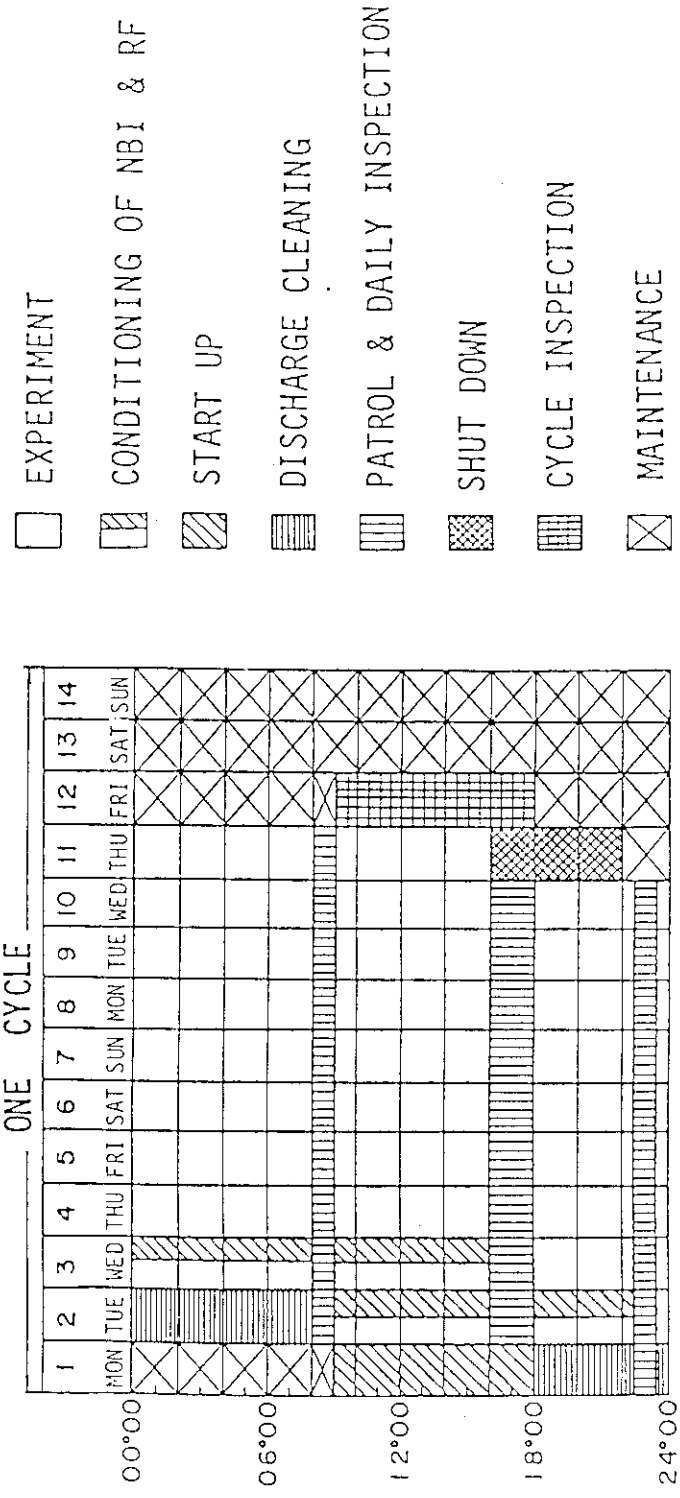

Fig. X.10-1 Standard cycle operation of JT-60.

XI. DESIGN STUDY OF THE NEXT GENERATION DEVICE

1. Fusion Experimental Reactor (FER)

1.1 Introduction

Continued from FY82 an in-depth design study of the pulsed operation FER which was selected as a reference option has been conducted. In parallel with the reference concept a conceptual design based on an advanced scenario of non-inductive plasma current drive has been developed[1]. Its overview is described below.

1.2 Reactor concept

Two versions of plasma operation scenarios based on RF current drive have been developed. One is a quasi-steady state operation scenario with the same device parameters as those for the previous design of a pulsed-operation FER[2] which employed a conventional inductive current drive. This operating scenario consists of alternating cycles of high density plasma burn during which time plasma current is maintained by magnetic flux supplied from ohmic heating (OH) coils followed by a period of low density RF current drive during which time the OH coils are recharged for the next high density plasma burn cycle. A design study based on this scenario is conducted as a reference option for PER. Device and plasma parameters were optimized while meeting the requirements from the FER objectives under plausible physics data base and the engineering restrictions such as confinement scaling, beta limit, divertor configuration and maximum magnetic fields on superconducting coils. All the superconducting coils system is enclosed in a common cryostat vacuum chamber (belljar type) and the PF coils are placed external to the toroidal field (TF) coils. A poloidal divertor configuration (double-null) with a cold and dense divertor plasma is employed. The tritium breeding blanket is installed all around the plasma and at the back side of divertor chambers to enhance breeding ratio. The reactor structure design concept is the same as that of the pulsed operation FER, because magnetic flux supplied from OH coils and plasma parameters for burn phase are the same.

The other is a steady state operation scenario on which an optimization of device parameters and the structure design have been newly conducted. The purpose is to demonstrate attractive features of a steady state operation FER, though its experimental data base is

insufficient. Major parameters for the above three operation scenarios are shown in Table XI.1-1.

1.3 Plasma startup and current drive

1.3.1 Quasi-steady state operation scenario

Based on the experimental data base for current ramp-up[3] and sustainment with oposing dc electric field[4] by lower hybrid wave (LHW) current drive, quasi-steady operation is considered to be promising. In this operation scenario, the key issue is to shorten the current ramp-up time and the recharging time of OH coils during power-dwell to increase the duty factor and to reduce the total required RF energy for ramp-up and recharging. Since these times essentially depend on the L/R time of the plasma, the plasma temperature must be carefully evaluated by the power balance equation consistent with the deposited RF power for current drive. An analytic model based on a quasi-linear theory of current drive coupled with the point model power balance and equivalent circuit equations is developed to optimize both items[5]. The minimization of both times can be attained by appropriately adjusting the parallel refractive index. The essential point is to drive large current without increasing plasma temperature so much to keep the one-turn resistance small. The plasma and RF parameters thus optimized are summarized in Table XI.1-2. Impurity contamination and/or temperature decrease resulting from deterioration of energy confinement can greatly reduce these times due to an increase of the one-turn resistance.

Major expected benefits for engineering design are (i) longer burn time, (ii) reduction of thermal and mechanical stress fatigue, (iii) reduction of magnetic energy loss during transfer between PF coils and the energy storage system. All of the benefits can be maximized by ramping-up the plasma current by LHW up to about 4 MA and then driving the current up to 5.3 MA by OH coils and sustaining it throughout the burning phase, and by sustaining the current at about 4 MA by LHW again during recharging of OH coils. Burn time can be prolonged to about 2000 s by this operation scenario from 100 s for the pulsed-operation FER based on an inductive current drive. The reduction of the number of burn pulses mitigates thermal and mechanical stress fatigue. In particular, the time variation of the over-turning force on TF coils can be reduced by magnitude of order by appropriate changes of the plasma current and poloidal beta from burning phase to recharging phase

or vice versa. Magnetic energy consumption normalized by the burn time of 2000 s can also be greatly reduced by this scenario (12 GJ → 3 GJ). Although the reduction of total energy consumption is lessened by the RF energy consumption, total reduction of energy consumption of about 10 GJ (70 % reduction) for 2000 s burn can be expected as compared with the pulsed-operation FER.

1.3.2 Steady state operation scenario

Applicability of three candidate driver waves to a steady state operation FER has been examined. The waves envisaged are compressional Alfvén wave (CAW), LHW and high speed magnetosonic wave (HSMW). CAW is chosen as a primary candidate wave for current driver due to its potential advantages in a commercial reactor - theoretically highest driving efficiency and good accessibility to the plasma center even in high density plasma. Major radius is decreased down to 4 m from 5.5 m of the pulsed-operation FER by removing the innermost PF coils. Although the magnetic field on axis is reduced down to 4.5 T from 5.7 T by the reduction of plasma major radius with a fixed maximum field on the TF conductor, almost same plasma performance as the pulsed-operation FER can be recovered without increasing the minor radius by taking account of an additional heating input power from current drive and heightened beta value due to the reduced aspect ratio. Major benefits on the reactor design by the steady state operation are (i) smaller reactor size (R = 4 m), (ii) vacuum vessel with no bellows for common use of the shell for vertical position control, (iii) reduction of power supply capacity of poloidal coil system (2 GVA (pulsed FER) → 0.2 GVA).

References

1) TONE, T., et al., "Japanese Contributions to the Japan-US Workshop on FER/ETR Design", JAERI-M 84-107 (1984).

2) TONE, T., et al., "Conceptual Design of Fusion Experimental Reactor (FER)", Nuclear Technology/Fusion (Proc. 5th Topical Meeting on the Technology of Fusion Energy, Knoxville, 1983), Vol. 4, No. 2, Part 2 (1983) 573. More detailed descriptions (in Japanese) are given in JAERI-M 83-213 ∿ 83-216 (1984).

3) YAMAMOTO, T., et al., Phys. Rev. Lett. 45 (1980) 716.
KUBO, S., et al., Phys. Rev. Lett. 50 (1983) 1994.

4) STEVENS, J., et al., PPPL-2018 (1983).

5) SUGIHARA, M., et al., Nucl. Eng. Design/Fusion 1 (1984) 265.

Table XI.1-1 Major plasma and device parameters for pulsed, quasi-steady and steady operation scenarios.

Operation mode	Pulsed (Ref.[2])	Quasi-steady	Steady
Burn time (s)	100	2000	∞
Number of pulses	~ 10^6	~ 5×10^4	-
Current drive	magnetic flux	LHW [startup, recharging]	CAW
		magnetic flux (burn)	
RF power of current drive (MW)	-	15	18
Ion temperature (keV)	10		13
Ion density (m^{-3})	1.36×10^{20}		9×10^{19}
Fusion power (MW)	440		250
Major radius (m)	5.5		4.0
Minor radius (m)	1.1		1.1
Toroidal field (T)	5.7		4.5
Plasma current (MA)	5.3		6.4

Table XI.1-2 Plasma and RF paramenters to minimize ramp-up and recharging times by lower hybrid wave current drive.

	Ramp-up	Recharging
Time (s)	~ 100	200 - 100
Power (MW)	5 - 10	10 - 15
Spectrum	1.0 - (4.0 ~ 6.0)	1.0 - (3.0 ~ 4.0)
Density ($\times 10^{18}$ m^{-3})	3 - 5	3 - 5
Temperature (keV)	1 - 2	3 - 5

2. INTOR

The INTOR workshop of Phase 2A, Part 1 was completed in July 1983, and the workshop was then extended into Phase Two A, Part 2.

The objective of the Phase 2A, Part 1 is that the major critical issues identified in the conceptual design during Phase I were concentratively assessed aiming size-minimization and high efficiency of the reactor. The work in the Phase Two A, Part 1 INTOR workshop is documented in the report. The major parameters of INTOR are shown in Table XI.2-1 and its cross section is illustrated in Fig. XI.2-1. The major results are as follows.

(1) The RF (Ion Cyclotron Range of Frequency) heating is adopted as a reference instead of the NBI heating, which was chosen for the conceptual design of Phase 1. This choice needs the strong promotion for the RF heating research and development, and also expects a steady improvement on the NBI heating as a back-up option.

(2) The divertor concept is decided to be continued as a reference for impurity control, from concentrative comparative studies between the divertor and pump limiter. High density and low temperature divertor plasmas, which were demonstrated in the recent divertor experiments and are intensively analyzed theoretically, could ease engineering difficulties on the divertor plates. On the other hand, the limiter, which is a strong candidate in future tokamak reactors, has some difficulties in temperatures of scrape-pff plasmas and limiter materials. The research and development on the limiter should be continued in parallel with the divertor.

(3) The breeding blankets employing lithium oxide were designed as a reference.

(4) The bore of the toroidal coils is reduced by 15% in their area compared with the conceptual design of Phase 1. This induces the reduction of the power supply for the poloidal coil system. Those reductions result in major factors cutting down the capital cost. The reduction in size of the toroidal coils is realized by increasing toroidal field ripple up to 1.2%, which enhances the loss of alpha-particle up to around 10%.

(5) A universal design concept, which can accomodate the divertor or the limiter as shown in Fig. XI.2-1, is adopted for future critical issues studies in the INTOR workshop.

(6) The cost sensitivity analysis is performed changing major parameters such as toroidal field ripple, heating method (NBI → RF), impurity control (divertor → limiter), and so forth, from a reference of the conceptual design. It is found that the capital cost is reduced by 20 % by employing the reduced toroidal coils and the RF heating.

Major objectives of the Part 2 are to study critical technical issues, and to assess scientific and technical data bases, and to finally upgrade the INTOR design concept, which will be completed in July 1985.

To study critical technical issues that affect the feasibility or practicability of the INTOR design concept, the following five groups are organized.

A : Impurity control and first wall

B : RF heating and current drive

C : Transient electromagnetics

D : Maintainability

E : Technical benefit

In addition to those groups, the three disciplinary groups are organized to assess the worldwide scientific and technical data bases

that exist now and will exist 4-5 years to support the detailed design and construction of an INTOR-like machine, and to identify additional R & D that is required.

F : Physics

G : Engineering

H : Nuclear

Table XI.2-1 Major deisgn parameters of INTOR.

Plasma major radius (m)	5.3
Plasma minor radius (m)	1.2
Plasma elongation	1.6
Plasma volume (m^3)	240
Axial toroidal field (T)	5.5
Plasma current (MA)	6.4
Average ion temperature (keV)	10
Average ion density ($10^{20}/m^3$)	1.4
Energy confinement time (sec)	1.4
Average beta (%)	5.6
Q value	ignition
Peak fusion power (MW)	620
RF heating power (MW)	
ICRF (85 MHz)	60
ECRF (140 GHz)	10
Burn time (sec)	200
Duty cycle (%)/Availability (%)	80/50
Neutron wall load (MW/m^2)	1.3
Toroidal magnetic field coil	superconducting
Poloidal magnetic field coil	superconducting
Divertor	yes
Tritium consumption (kg/year)	7
Initial tritium inventory (kg)	4
Tritium breeding ratio	0.65

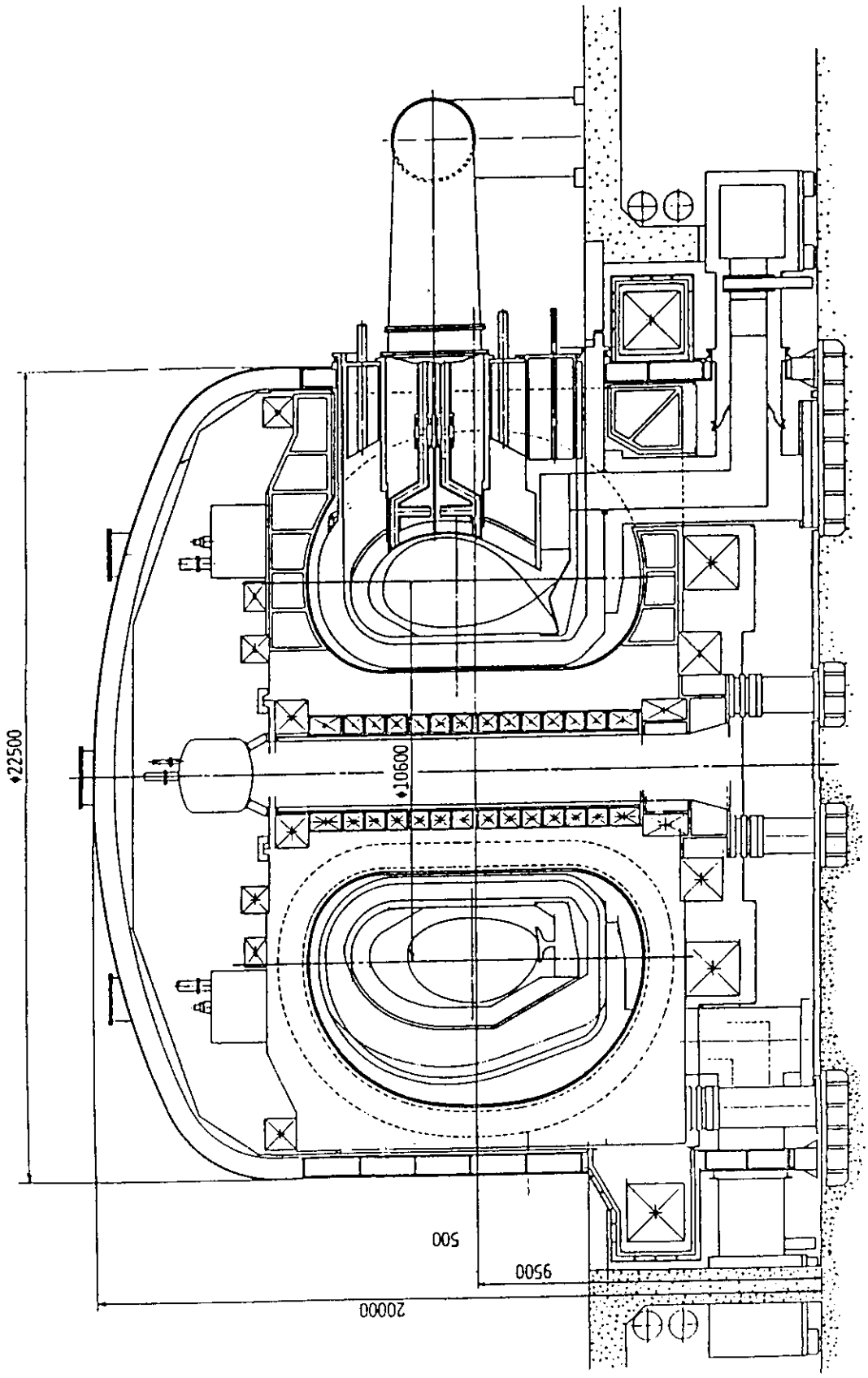

Fig. XI.2-1 INTOR universal configuration.

APPENDIX

A.1 Publication List

A.1.1 List of JAERI-M reports

1) Kumagai M.[*2], Tsunematsu T., Tokuda S., Takeda T. : "Positional Instability Analysis of Tokamak Plasma by ERATO", JAERI-M 83-085 (June 1983) (in Japanese).

2) Harafuji K.[**4], Tsunematsu T., Azumi M., Takeda T. : "MHD Equilibria in a Straight System with a Non-Planar Magnetic Axis", JAERI-M 84-035 (Mar. 1984) (in Japanese).

3) Tokuda S. : "Stability Analysis of Tokamak Plasmas by Computer Simulation", JAERI-M 84-040 (Mar. 1984) (in Japanese).

4) Kawashima H., Yamauchi T., Matoba T. : "Evaluation of the Error for Electron Temperature and Density Measurement on JFT-2 Plasma", JAERI-M 83-130 (Aug. 1983) (in Japanese).

5) Hoshino K., Kawashima H., Hata K.[*33], Yamamoto T. : "A Design of a Mode Convertor for Electron Cyclotron Heating by the Method of Normal Mode Expansion", JAERI-M 83-148 (Sep. 1983).

6) Matoba T., Ogawa T., Kawashima H., Kimura T. : "Development of a High Counting Rate Pulse Height Analyzing System of Plasma Diagnostic", JAERI-M 83-162 (Sep. 1983) (in Japanese).

7) Odajima K., Matsumoto H., Kimura H., Yamamoto T., Hoshino K., Kasai S., Kawakami T., Kawashima H., Maeno M., Matoba T., Matsuda T., Miura Y., Mori M., Ogawa H., Ogawa T., Ohta K.[*11], Ohtsuka H., Sengoku S., Shoji T., Suzuki N., Tamai H.[**29], Uesugi Y., Yamamoto S., Yamauchi T., Yanagisawa I.[*3], Nakamura H., Katagiri M. : "Second Harmonic ICRF Heating in the JFT-2M Tokamak", JAERI-M 83-190 (Oct. 1983).

8) Shoji T., Odajima K., Mori M., Suzuki N., Matsuzaki Y., Tani T., Yokokura K., Kikuchi K., Hasegawa K., Okano F., Ishibori I., Kashimura T., Kashiwa Y., Kazawa M., Matoba T., Funahashi A., Tanaka Y., Suzuki K., Kunieda S., Ohta K.[*11], Yanagisawa I.[*3], Kimura H., Matsumoto H., Matsuda T., Ogawa T., Kawashima H., Kasai S., Miura Y., Uesugi Y., Ogawa H., Kawakami T., Yamauchi T., Hoshino K., Yamamoto T., Yamamoto S., Maeno M., Sengoku S., Ohtsuka H. : "An Outline of the JFT-2M Device --Design, Construction, Tset--", JAERI-M 83-194 (Oct. 1983) (in Japanese).

9) Matsuoka M., Horiike H., Itoh T., Kuriyama M., Matsuda S., Morita

H.[*2], Ohara Y., Tanaka S. : "Structual Design of the Neutralizer for JT-60 NBI", JAERI-M 83-069 (May 1983) (in Japanese)

10) Akiba M., Horiike H., Kuriyama M., Ohara Y., Okumura Y., Shibata T., Tanaka S. : "Evaluation of Heat Loadings to the Arc Chamber", JAERI-M 83-099 (June 1983) (in Japanese).

11) Tanaka S. : "Study on the Cathode of Ion Source for Neutral Beam Injector", JAERI-M 83-131 (July 1983) (in Japanese).

12) Mukaida H.[*2], Kuriyama M., Araki M. : "The Dynamic Property of Fast Shutter for JT-60 NBI", JAERI-M 83-154 (Aug. 1983) (in Japanese).

13) Wells R.[**28], Horiike H., Kuriyama M., Ohara Y. : "Evaluation of Thermal Stress in the Anode Chamber Wall of a Large Volume Magnetic Bucket Ion Source", JAERI-M 84-011 (Feb. 1984).

14) Tominaga G.[**30], Nakamura K., Murakami Y. : "Materials and Methods for Attaining to Low Outgassing Rates without High Temperature Bakeout (A Survey Report)", JAERI-M 83-112 (July 1983) (in Japanese).

15) Abe T., Obara K., Yokokura K., Hasegawa K., Okano F. : "Experimental Studies on Scattered Particle Phenomena during In-situ Coating Process", JAERI-M 83-087 (June 1983) (in Japanese).

16) Hiroki S., Abe T., Inagawa K.[*21], Obara K., Murakami Y. : "Fabrication and Testing of a Quartz Oscillator Microbalance", JAERI-M 84-012 (Feb. 1984) (in Japanese).

17) Sone K. : "Report of Workshop on Computer Simulation of Atomic Collision Process in Solids - Research Committee on A & M Data - (3. Hydrogen Isotope Recycling Problems in Relation to Radiation Damage at Wall Surface in Tokamaks)", JAERI-M 83-226 (Jan. 1984) p.14 (in Japanese).

18) Murakami Y. : "Report of the 2nd Workshop on Particle Material Interactions for Fusion Research - The Research Committee on A & M Data of JAERI - (I.2 Some Problems of Plasma-Wall Interactions in Development of Tokamak Fusion Device)", JAERI-M 83-235 (Feb. 1984) p.4 (in Japanese).

19) Yamada R. : "Report of the 2nd Workshop on Particle Material Interactions for Fusion Research - The Research Committee on A & M Data of JAERI - (III.7 Chemical Sputtering)", JAERI-M 83-235 (Feb. 1984) p.130 (in Japanese).

20) Yoshida H., Matsui T., Kurasawa T., Miyauchi T., Takeshita H.,

Kajimoto Y., Goto T., Watanabe K., Naruse Y., Watanabe H. : "In-Pile Experiment for Tritium Release from Li_2O under High Neutron Fluence ---Detritiation and Tritium Monitoring ---", JAERI-M 83-204 (Nov. 1983) (in Japanese).

21) Kurasawa T., Yoshida H., Watanabe H., Miyauchi T., Takeshita H., Miura K., Kaneda Y., Aizawa M., Sasajima F., Umei H. : "In-pile Test of Tritium Release from Lithium Oxide - An Evaluation Study on Neutronics and Thermohydraurics of Sweep Gas Capsule Packed with Li_2O Pellets -", JAERI-M 84-013 (Feb. 1984) (in Japanese).

22) Kinoshita M., Bartlit J.R.[**31], Sherman R.H.[**31] : "Revision of the Design Model for a Cryogenic Falling Liquid Film Helium Separator", JAERI-M 83-073 (May 1983).

23) Ozeki T., Nakamura Y. : "Model Analysis of Eddy Current in JT-60 Multi-Torus System", JAERI-M 83-159 (October 1983).

24) Ninomiya H., Ozeki T., Yoshida H., Seki S. : "Selecting Method of the Dominant Eigenmodes of Eddy Current for Plasma Control Study", JAERI-M 84-028 (February, 1984) (in Japanese).

25) Sengoku S., Shimada M., Miya N., Kasai M.[*3], Burrell K.[*5], Kahn C.[*5] : "Observation of Very Dense and Cold Divertor Plasma in Beam Heated Doublet III Tokamak with Single-Null Poloidal Divertor", JAERI-M 58-008 (February, 1983).

26) Seki S., Ninomiya H., Yoshida H. : "Stabilizing Effect of Passive Conductors with Arbitrary Shape for Positional Instabilities", JAERI-M 58-165 (September, 1983) (in Japanese).

27) Konoshima S., Aikawa H., Azumi M., Hoshino K., Kameari A.[*3], Kasai M.[*3], Kitsunezaki A., Kobayashi T.[*4], Matsuda T., Miya N., Nagami M., Ninomiya H., Sengoku S., Shimada M., JAERI team, Angel T.[*5], Armentrout C.[*5], Blau F.[*5], Bramson G.[*5], Brooks N.[*5], Fairbanks E.[*5], Hsieh C.[*5], Jahns G.[*5], Seraydarian R.[*5], Snider R.[*5], Stambaugh R.[*5], Strait T.[*5], GA Technologies : "Fluctuations observed in NBI Heated Doublet III Divertor Discharges", JAERI-M

28) Takatsu H., Yamamoto M., Shimizu M., Kimishima T.[*4], Kajiura S.[*4], Owada K.[*4] : "Mechanical Strength Evaluation of the Formed Bellows for the Ports of the JT-60 Vacuum Vessel", JAERI-M 83-077 (May, 1983).

29) Takatsu H., Simizu M. : "Design of the Foundation Components for the JT-60 Tokamak Machine", JAERI-M 83-102 (June, 1983).

30) Ando T., Nakamura H. : "Thermal Capability of JT-60 Magnetic

Limiter Plate", JAERI-M 83-220.

31) Takatsu H., Yamamoto M., Shimizu M., Suzuki K.[*4], Sonobe T.[*4], Mizuno G.[*27] : "Type Tests of the Welded Bellows for the Ports of the JT-60 Vacuum Vessel", JAERI-M 84-034.

32) Nakamura H., Shimizu M., Masuda M., Shimizu T., Miyauchi Y.[*28], Ohta M. : "Design of JT-60 First Wall", JAERI-M 84-062.

33) Nagashima A. : "Phase Distortion by Concave Lens Effect for FIR Interferometry", JAERI-M 83-109.

34) Takeuchi H., Matsuda T., Nishitani T., Shino M., Konagai C., Kimura H. and Maeda H. : "Active Beam Scattering Apparatus and its Application to JFT-2 Tokamak", JAERI-M 83-146.

35) Takeuchi H., Matsuda T., Miura Y., Shino M., Maeda H., Hashimoto K. and Hayashi K. : "Mass Separated Neutral Particle Energy Analyser", JAERI-M 83-146.

36) Nishitani T., Sugie T., Tanaka R., Nakamura Y., Hirao T., Kaneko S., Mori H., Yamashita T., Kinpara M., Nagata H., Matsumoto A., Nakazawa M. and Maeda H. : "Irradiation Effects on Components of Spectroscopic Measurement Device for JT-60 Diagnostics", JAERI-M 84-047 (in Japanese).

37) Ikeda Y., Seki Y., Maekawa H., Oyama Y. and Nakamura T. : "An Experimental Study of Induced Activity in Type 316 Stainless Steel by Irradiation in D-T Neutron Fields", JAERI-M 83-177 (1983).

38) Maekawa H., Tsuda K., Iguchi T., Ikeda Y., Oyama Y., Fukumoto T., Seki Y. and Nakamura T. : "Measurement of Tritium Production-Rate Distribution in Simulated Blanket Assemblies at the FNS", JAERI-M 83-196 (1983) also as NEACRP-L-268.

39) Seki Y., Kawasaki H., Maekawa H., Oyama Y., Ikeda Y. and Nakamura T. : "Calculation of Absolute Fission-Rate Distribution Measured in Graphite Reflected Lithium Oxide Blanket Assembly", JAERI-M 83-061 (1983).

40) Sugihara M., Saito S.[*4], Fujisawa N. and Miki N.[*2] : "Optimum Configuration and Operation Regime of Pumped Limiter in INTOR", JAERI-M 83-059 (April 1983).

41) Sugihara M. and Nishio S. : "Preliminary Study on the Concept of Steady Fusion Experimental Reactor (FER) by RF-Current Drive", JAERI-M 83-139 (September 1983) (in Japanese).

42) Sugihara S., Fujisawa N., Yamamoto T., Yoshizu T., Nakajima A., Ueda K.[*11], Nishio S. and Iida H. : "Physics Design Considerations

of Steady and Quasi-State Fusion Experimental Reactor by Lower Hybrid Wave Current Drive", JAERI-M 83-174 (October 1983).

43) Fusion Reactor System Laboratory : "Conceptual Design of Fusion Experimental Reactor (FER) (Option A)", JAERI-M 83-213 (1984).

44) idem., "(Option B)", JAERI-M 83-214 (1984).

45) idem., "(Option C)", JAERI-M 83-215 (1984).

46) idem., "Conceptual Design of Blanket Structures for Fusion Experimental Reactor (FER)", JAERI-M 83-216 (1984).

A.1.2 List of GA-A Reports

1) Nagami M., Aikawa H., Kasai M.[*3], Kitsunezaki A., Kobayashi T.[*4], Konoshima S., Matsuda T., Miya N., Ninomiya H., Shimada M. and Yokomizo H. : "Energy Confinement of Beam Heated Divertor and Limiter Discharges in Doublet III", GA-A 17056.

2) Yokomizo H., Kasai M., Aikawa H., Kitsunezaki A., Konoshima S., Matsuda T., Nagami M., Shimada M., JAERI team, Taylor T.[*5], Callis R.[*5], Doll D.[*5], GA Technologies : "Major Disruption Correlated with High Heat Deposition onto Limiter Surface", GA-A17269.

3) Yamamoto T., Abe M.[*4], Hirayama T., kameari A.[*3], Kitsunezaki A., Kodama K., Konoshima S., Nagami M., Sengoku S., Shimada M., Takizuka T., Washizu M[*2], JAERI team : "Electron Temperature and Density Measurements by Harmonic Electron Cyclotron Emissions from the Doublet-III Tokamak Plasma", GA-A 17635.

4) Hirayama T., Takizuka T., Shimada M., Nagami M., Konoshima S., Abe M[*4], Kameari A., Kitsunezaki A., Kodama K., Sengoku S., Washizu M.[*2], Yamamoto T., JAERI team and Burrell K.H.[*5], Brooks N.[*5], Groebner R.[*5], GA Technologies Inc. : "Numerical Transport Studies of Injected Titanium into Doublet III Beam Heated Discharges", GA-A17406.

A.1.3 Papers published in Journals

1) Tani K., Takizuka T., Azumi M., Kishimoto H. : "Ripple Loss of Superthermal Alpha Particles during Slowing Down in a Tokamak Reactor", Nucl. Fusion 23 (1983) 657.

2) Itoh K., Itoh S-I.[**1] : "Energy Deposition Profile of Shear Alfvén Wave Heating", Plasma Phys. 25 (1983) 1037.

3) Kurita G., Azumi M., Tsunematsu T., Takeda T. : "Numerical Studies of Toroidal Coupling on Low-m Resistive Modes", Plasma Phys. 25 (1983) 1097.

4) Fukuyama A.[**3], Nishiyama A.[**3], Itoh K., Itoh S-I.[**1] : "Kinetic Description of Propagation and Absorption Structures of ICRF Waves", Nucl. Fusion 23 (1983) 1005.

5) Shigeta M.[**1], Fukuyama A.[**3], Takizuka T. : "Electron Diffusion in a Tokamak due to High-n Ballooning Mode", J. Phys. Soc. Japan 53 (1984) 1058.

6) Itoh K., Itoh S-I.[**1], Fukuyama A.[**3] : "Three-Dimensional Structures of ICRF Waves in Tokamak Plasmas", Nucl. Fusion 24 (1984) 13.

7) Itoh S-I.[**1], Fukuyama A.[**3], Itoh K. : "Simultaneous Heating by ICRF Wave and Neutral-Beam Injection", Nucl. Fusion 24 (1984) 224.

8) Maeno M., Yamamoto S., Ohtsuka H. : "Possibility of Arcing Phenomena in Future Large Tokamas", Jpn. J. Appl. Phys. 22 (1983) 764.

9) Isler R.C.[**14], Murray L.E.[**14], Crume E.C.[**14], Bush C.E.[**14], Dunlop J.L.[**14], Edomonds P.H.[**14], Kasai S., Lazarus E.A.[**14], Murakami M.[**14], Neilson G.H.[**14], Pare U.K.[**14], Scott S.D.[**14], Thomas C.E.[**14], Wooton A.J.[**14] : "Impurity Transport and Plasma Rotation in the ISX-B Tokamak", Nucl. Fusion 23 (1983) 1017.

10) Okamoto M.[**2], Yamamoto S., Shimizu K., Maeno M., Sengoku S., Yamauchi T., Miura Y., Matsumoto H., Ohtsuka H., Tani K. : "Electron Thermal Diffusivity in JFT-2 Tokamak with NBI Heating", Jpn. J. Appl. Phys. 22 (1983) 1686.

11) Miura Y., Matsumoto H., Kimura H., Odajima K., Mori M., Matsuda T., Takeuchi T., Hoshino K., Kasai S., Kawashima T., Konoshima S., Maeno M., Matoba T., Ohasa K., Ohtsuka H., Ogawa T., Sengoku S., Shoji T., Sugie T., Suzuki N., Uesugi Y., Yamauchi T., Yamamoto S., Yamamoto T. : "Analysis of Charge Exchanged Spectra during ICRF Heating in the JFT-2 Tokamak", Nucl. Fusion 24 (1984) 211.

12) Matsumoto H., Kimura H., Odajima K., Hoshino K., Kasai S., Kawakami T., Kawashima H., Konoshima S., Maeno M., Matoba T., Matsuda T., Miura Y., Nakamura H., Mori M., Ohasa K., Ohtsuka H., Ogawa H., Ogawa T., Sengoku S., Shoji T., Sugie T., Suzuki N., Takeuchi H., Uesugi Y., Yamauchi T., Yamamoto S., Yamamoto T. : "Power Balance Analysis of ICRF Heating Experiments in JFT-2 Tokamak", Nucl. Fusion 24 (1984) 283.

13) Ohara Y., Akiba M., Araki M., Horiike H., Kuriyama M., Matsuda S., Matsuoka M., Okamura Y., Tanaka S. : "Geometrical Efficiency of the Prototype Neutral Beam Injector Unit for JT-60", Rev. Sci. Instrum. 54 (1983) 921.

14) Tanaka S., Akiba M., Horiike H., Okumura Y., Ohara Y. : "Effect on Magnetic Field on the Characteristics of a Hollow Cathode Ion Source", Rev. Sci. Instrum. 54 (1983) 1104.

15) Okumura Y., Horiike H., Mizuhashi K. : "High Magnetic Field, Large-Volume Magnetic Multiple Ion Source Producing Hydrogen Ion Beams with High Proton Ratio", Rev. Sci. Instrum. 55 (1984) 1.

16) Nagashima T., Matsuda S. : "Plasma Heating Systems for Nuclear Fusion", J. IEEE Japan 103 (1983) 321 (in Japanese).

17) Ohtsuka H. : "A Cause of the Motion of Arcs in the Presence of a Magnetic Field", Vacuum 33 (1983) 155.

18) Yamada R., Sone K. : "On the Influence of Incident Energy of Protons on Chemical Erosion of Graphite", J. Nucl. Mater. 116 (1983) 200.

19) Yamada R., Sone K. : "Chemical Erosion Yield of Graphite Simultaneously Bombarded with Energetic Protons and Thermal Atomic Hydrogens", J. Nucl. Mater. 120 (1984) 119.

20) Saidoh M., Sone K. : "Low Energy Selfsputtering Yields of Molybdenum and Tungsten", Jap. J. Appl. Phys. 22 (1983) 1361.

21) Nakamura K., Murakami Y. : "Present Status of R & D on Cryosorption Panels for Helium Pumping", Cryogenic Engineering 18 (1983) 49 (in Japanese).

22) Sone K., Yamada R. : "Chemical Sputtering", Oyo Butsuri 53 (1984) 217 (in Japanese).

23) Tada E., Takahashi Y., Ando T., Shimamoto S. : "Experiences on High Current Leads for Superconducting Magnet; Seven Types from 1 kA to 30 kA", Cryogenic Engineering 18 (1984) 324 (in Japanese).

24) Katsuta H., Konishi S., Yoshida H. : "Solubility and Diffusivity of Hydrogen in Li_2O", J. Nucl. Mater. 116 (1983) 244.

25) Ohno H., Konishi S., Yoshida H., Watanabe H. : "Conductivities of a Sintered Pellet and a Crystal of Li_2O", J. Nucl. Mater. 118 (1983) 242.

26) Matsuo T.[**5], Ohno H., Noda K., Konishi S., Yoshida H., Watanabe H. : "Nuclear Magnetic Resonance Investigations of Lithium Diffusion in Li_2O, Li_2SiO_3 and $LiAlO_2$", J. Chem. Soc., Faradey

Trans. 2, 79 (1983) 1205.

27) Yoshida H., Konishi S., Naruse Y. : "Preliminary Design of a Fusion Reactor Fuel Cleanup System by the Palladium-Alloy Membrane Method", Nucl. Technol. Fusion 3 (1983) 471.

28) Yoshida H., Takeshita H., Konishi S., Ohno H., Kurasawa T., Watanabe H., Naruse Y. : "A Feasibility Study of the Catalytic Reduction Method for Tritium Recovery from Tritiated Water", Nucl. Technol. Fusion 5 (1984) 178.

29) Yamanishi T., Konoshita M. : "Preliminary Experimental Study for Cryogenic Distillation Column with Small Inner Diameter, (I)", J. Nucl. Sci. Technol. 21 (1984) 61.

30) Okuno K., Kudo H. : "Thermal Release of Tritium Produced in Sintered Li_2O Pellets", J. Nucl. Mater. 116 (1983) 82.

31) Kudo H., Okuno K. : "Chemical Behavior of Tritium in Neutron-irradiated Li_3N", J. Nucl. Mater. 116 (1983) 78.

32) Naruse Y. : "Tritium Systems in Fusion Reactor", Nucl. Engineering, 29 No.5, p.46.

33) Kinoshita M., Hashimoto I.[**9], Takamatsu T.[**9] : "A New Simulation Procedure for Multicomponent Distillation Column Processing Non-ideal Solutions or Reactive Solutions", J. Chem. Eng. Japan 16 (1983) 370.

34) Kinoshita M., Hashimoto I.[**9], Takamatsu T.[**9] : "A Simulation Procedure for Multicomponent Distillation Column within which Three Phase of Vapor and Partially Immiscible Liquid are Present", J. Chem. Eng. Japan 16 (1983) 513.

35) Kinoshita M., Bartlit J.R.[**31], Sherman R.H.[**31] : "Proportional-Integral Control Modes for a Hydrogen Isotope Distillation Column", Nucl. Technol. Fusion 5 (1984) 30.

36) Kinoshita M. : "Computer-Aided Simulation Procedure for Water Distillation Columns", J. Nucl. Sci. Technol. 21 (1984) 299.

37) Tanaka M. : "Tokamak Research at Japan Atomic Energy Research Institute", Plasma Phys. and Controlled Fusion 26 (1984) 117.

38) Nagami M., Aikawa H., Kasai M.[*3], Kitsunezaki A., Kobayashi T.[*4], Konoshima S., Matsuda T., Miya N., Ninomiya H., Shimada M., Yokomizo JAERI team, Angel T.[*5], Armentrout C.[*5], Blau F.[*5], Bramson G.[*5], Brooks N.[*5], Chase R.[*5], Colleraine A.[*5], Fairbanks E.[*5], Fasolo J.[*5], Fisher R.[*5], Hino T.[*5], Hong R.[*5], Jahns G.[*5], Kamperschroer J.[*5], Kim J.[*5], Lieber A.[*5], Lohr J.[*5], McColl D.[*5], Rottler L.[*5],

Seraydarian R.[*5], Silagi R.[*5], Smith J.[*5], Snider R.[*5], Taylor T.[*5], Tooker J.[*5], Vaslow D.[*5], Wojtowicz[*5], GA Technologies : "Energy Confinement of Beam Heated Divertor and Limiter Discharges in Doublet III", Nucl. Fusion 24 (1984) 183.

39) Yokomizo H., Konoshima S., Aikawa H., Kasai M[*3], Ninomiya H., Kobayashi T.[*3], Matsuda T., Miya N., Nagami M., Shimada M., Kitsunezaki A. : "Plasma Shapes for Achieving High Heating Efficiency During Neutron Beam Injection in Doublect III", Japan Journal of Applied Physics 23 (1984) L316.

40) Sengoku S., Shimada M., Miya N., Kasai M.[*3], Aikawa H., Azumi M., Hoshino K., Kitsunezaki A., Kobayashi T.[*4], Konoshima S., Matsuda T., Nagami M., Ninomiya H., Nishikawa M.[*3], Tokutake T., Yamauchi T., Yokomizo H., JAERI team : "Observation of Very Dense and Cold Divertor Plasma in the Beam-Heated Doublet III Tokamak with Single-Null Poloidal Divertor", Nucl. Fus. 24 (1984) 415.

41) Otsuka M.[*4], Nagami M. Matsuda T., JAERI team : "BIRTH: A Neutral Beam Deposition Code for Non-Circular Tokamak Plasmas", J. of Computational Phys. 52 (1983) 219.

42) Yoshikawa M. and Tomabechi K. : "JT-60 Project and Its Present Status", Nucl. Technol./Fusion 4 (1983) 299.

43) Ioki K.[*3], Nagami M., Yoshida H., Yokomizo H., Shimada M., Izumi S.[*4], Shinya K.[*3], Brooks N.[*5], McMahon T.[*5] and Kitsunezaki A. : "Heat Flux on Limiters in low q Discharges", Nucl. Eng. Design 74 (1983) 393.

44) Shimomura Y., Keilhacker M.[**27], Lackner K.[**27] and Murmann H.[**27] : "Characteristics of the Divertor Plasma in Neutral Beam-Heated ASDEX Discharges", Nucl. Fusion 23 (1983) 869.

45) Takatsu H., Shimizu M., Ohta M., Nakamura Y.[*28], Sakai K.[*28], Uchino K.[*28] : "Fatigue Evaluation of the JT-60 Vacuum Vessel under the Dynamic Electromagnetic Forces", Nuclear Engineering and Design 74 (1982) 325-337.

46) Miyauchi Y., Masuda M., Shimizu M. : "A Transient Finite Element Analysis of Natural Convection Around A Horizontal Hot Cylinder", International Journal for Numerical Methods in Fluids Vol. 3 (1983) 249-443.

47) Yokomizo H., McClain F.W. and Jensen T.H. : "Quantitative Comparison of Experimental and Theoretical Growth Rates of the Positional Instability in Doublet III", Nuclear Fusion 23 (1983) 1593.

48) Takeuchi H., Matsuda T., Miura Y., Shiho M., Maeda H., Hashimoto K. and Hayashi K. : "Multi-Channel Mass Separated Neutral Particle Energy Analyses for Simultaneous Measurements of Hydrogen and Deuterium Atoms Emitted from Tokamak Plasma", Jpn. J. Appl. Phys. 22 (1983) 1709.

49) Takeuchi H., Matsuda T., Nishitani T., Shiho M., Konagai C., Kimura H. and Maeda H. : "Active Beam Scattering Method for Measurement of Ion Temperature in JFT-2 Tokamak Plasma", Jpn. J. Appl. Phys. 22 (1983) 1717.

50) Saito S.*4, Sugihara M., Fujisawa N., Ueda K.*4 and Abe T. : "Analysis of Pumping Requirement for Exhausting Duct in Close Vicinity of Divertor in Tokamak Reactor", Nuclear Technology/Fusion 4 (1983) 498.

51) Tone T., Fujisawa N., Seki Y., Iida H., Tachikawa K., Sugihara M., Minato A., Nishio S., Yamamoto T., Kitamura K.*2, Ueda K.*11, Saito S.*4, Shimada R., Matsuda Y., Naruse Y., Shimamoto S., Tamura S., Yoshikawa M., Tomabechi K. : "Conceptual Design of Fusion Experimental Reactor (FER)", Nuclear Technology/Fusion, Vol. 4, No.2, Part 2 (1983) 573.

52) Seki Y., Oyama Y., Ikeda Y., Tanaka S., Maekawa H., Nakamura T. and Kawasaki H. : "Monte Carlo Calculations of Source Characteristics of FNS Water Cooled Type Tritium Target", J. Nucl. Sci. Technol., 25 (8), (1983) 686.

A.1.4 Papers published in Conference Proceedings

1) Itoh K., Itoh S-I.**1 : "Integral of Wave Kinetic Equation of Drift Waves", US-Japan Workshop on Statistical Plasma Physics (Nagoya, Japan, Feb. 1984).

2) Takizuka T., Tani K., Azumi M. : "Particle Simulation of Divertor Plasma", US-Japan Workshop on Theoretical Modeling of Impurity and Particle Control of Fusion Plasmas (Nagoya, Japan, Mar. 1984).

3) Tsunematsu T., Kurita G., Azumi M., Takizuka T., Takeda T. : "Nonlinear Evolution of External Kink Mode in Tokamaks and Comment on Resistive Internal Kink Mode", US-Japan Workshop on 3D MHD Studies (Oak Ridge, USA, Mar. 1984) CONF-840370 p.158.

4) Itoh S-I.**1, Fukuyama A.**3, Itoh K. : "Kinetic Analysis of ICRF Wave Propagation and Absorption", 4th International Symposium on

Heating in Toroidal Plasma (Rome, Italy, Mar. 1984).

5) Itoh S-I.[**1], Fukuyama S.[**3], Goto A.[**7], Itoh K. : "Three Dimensional Study of Coupling Efficiency of ICRF Wave Heating", ibid.

6) Yamamoto T. and JFT-2 group : "Study of the Current Drive by the Lower Hybrid Wave in a Tokamak", IAEA Technical Committee Meeting on RF Heating and Current Drive (London, England, 1983).

7) Kasai S. : "Atomic Process in Diagnostics of Tokamak Plasma", Symposium on Atomic Collision Data for Diagnostics and Modelling of Fusion Plasma (Nagoya, Japan, Aug. 1983).

8) Shoji T., Funahashi A., Hoshino K., Kasai S., Kawakami T., Kawashima H., Kimura H., Maeno M., Matoba T., Matsuda T., Matsumoto H., Miura Y., Mori M., Odajima K., Ogawa H., Ogawa T., Ohta K.[*4], Ohtsuka H., Sengoku S., Suzuki N., Nakamura H., Tamai H.[**29], Tanaka Y., Uesugi Y., Yamamoto S., Yamamoto T., Yamauchi T., Yanagisawa I.[*3], Hasegawa K., Honda A., Ishibori I., Kashimura T., Kashiwa Y., Kazawa M., Kikuchi K., Kunieda S., Matsuzaki Y., Ohuchi K., Okano F., Shibata T., Shibuya T., Shiina T., Suzuki K., Tani T., Tajima Y., Yokokura K., Yokoyama K. : "Results from the JFT-2M Experiments", 11th European Conference on Controlled Fusion and Plasma Physics A-8 (Aachen, West Germany, Sep. 1983).

9) Shimada M., Sengoku S., Kobayashi T.[*4], Miya N., Kasai S. and JAERI team, Kahn C.L.[*5], Burrell K.H.[*5] and GA Doublet III group[*5] : "Experimental Observation of a Dense and Cold Divertor Plasma in D-III Beam-Heated Divertor Discharge and its Numerical Simulation", ibid. C-25.

10) Matoba T., Yamauchi T., Uesugi Y., Nagashima A. : "Laser-Aided Plasma Diagnostics on JFT-2M and JT-60", The Kyushu International Symposium on Laser-Aided Plasma Diagnostics (Fukuoka, Japan, 1983).

11) Nagashima T., Fujii T., Hara M.[*16], Honda M., Iida K.[*9], Ikeda Y., Imai T., Kimura H., Nakamura T.[*2], Saigusa M., Sakamoto K., Sawahata M., Shirakata H., Suzuki N., Uehara K. : "JT-60 Radio Frequency Heating System and Testing of 1 MW-10 sec Klystron", 10th Symposium of Fusion Engineering (Philadelphia, USA, 1983).

12) Odajima K., Matsumoto H., Kimura H., Yamamoto T., Hoshino K., Kasai S., Kawakami T., Kawashima H., Ogawa H., Ohta K.[*11], Ohtsuka H., Sengoku S., Shoji T., Suzuki N., Tamai H.[**29], Uesugi Y., Yamamoto S., Yamauchi T., Yanagisawa I.[*3], Nakamura H., Katagiri M. : "Second Harmonic ICRF Heating Experiment in the JFT-2M Tokamak",

4th International Symposium on Heating in Toroidal Plasma (Rome, Italy, Mar. 1984).

13) Ohara Y. : "Development of the Neutral Beam Injector for JT-60", Proc. International Ion Engineering Congress (Kyoto, Japan. Sep. 1983) p.447.

14) Itoh T., Horiike H., Matsuda S., Matsuoka M., Ohara Y., Okumura Y., Shitomi M., Takeuchi H., Watanabe K. : "Development of 20 keV 3.5 A Helium Beam Injector for Active Beam Diagnostic", ibid. p.483.

15) Akiba M., Araki M., Dairaku M., Horiike H., Itoh T., Kawai M., Kuriyama M., Kitamura S., Matsuda S., Matsuoka M., Mizuhashi K., Ohara Y., Ohga T., Ohuchi Y., Okumura Y., Komata M., Shibanuma K., Shibata T., Shirakata H., Tanaka S., Watanabe K., Wells R.[**28] : "Beam Extraction at the Prototype Injector Unit for JT-60", 10th Symposium on Engineering Problems of Fusion Research (Philadelphia, USA, Dec. 1983).

16) Shibata T., Akiba M., Araki M., Dairaku M., Horiike H., Itoh T., Kawai M., Kuriyama M., Kitamura S., Matsuda S., Matsuoka M., Mizuhashi K., Ohara Y., Ohga T., Okumura Y., Shibanuma K., Shigematsu H.[*8], Shirakata H., Sugawara T.[*4], Tanaka S., Watanabe K. : "JT-60 Neutral Beam Injection System", ibid.

17) Matsuda S., Nagashima T., Shimomura Y. : "Plasma Heating System for JT-60", 4th International Symposium on Heating in Toroidal Plasmas (Rome, Italy, Mar. 1984).

18) Okumura Y., Akiba M., Araki M., Dairaku M., Horiike H., Itoh T., Kawai M., Komata M., Kuriyama M., Kitamura S., Matsuda S., Matsuoka M., Nagamura H.[*2], Ohara Y., Ohuchi Y., Shibanuma K., Shibata T., Tanaka S., Watanabe K., Wells R.[**28] : "Experimental Results on JT-60 Neutral Beam Injection Prototype Unit", ibid.

19) Itoh T., Matsuda S., Matsuoka M., Ohara Y., Shitomi M., Watanabe K. : "Development of 200 keV Helium Beam Injector", ibid.

20) Horiike H. : "High Power Test of Prototype Injector Unit for JT-60", Neutral Beam Workshop (GA, USA, Mar. 1984).

21) Shirakata H. : "JT-60 Neutral Beam Injection System and Related R & D Works", IAEA Technical Committee Meeting on Operating Plans for Large Tokamak Experiments (Princeton, USA, Jan. 1984).

22) Shirakata H. : "JT-60 RF Heating System and Related R & D Works), ibid.

23) Fujii T., Imai T., Sakamoto K., Saigusa M., Ikeda Y., Honda M., Yokokura K., Hara M.[*16], Uehara K., Nagashima T. : "R & D Works of Waveguide Launchers for JT-60 RF Heating System", 10th Symposium of Fusion Engineering (Philadesphia, USA, 1983).

24) Kimura H., Fujii T., Ikeda Y., Saigusa M., Imai T., Sakamoto K., Nakanishi M., Odajima K., Uehara K., Nagashima T. : "Design Study of an ICRF Coupler for JT-60P, 4th International Symposium on Heating in Toroidal Plasmas (Rome, Italy, Mar. 1984).

25) Murakami Y. : "The Vacuum and Surface Technological Aspects of the JT-60 Tokamak", Proc. 9th International Vacuum Congress & 5th International Conference on Solid Surfaces (Madrid, Spain, 1983) p.532.

26) Sone K., Murakami Y. : "The Effect of Wall Materials on Hydrogen Recycling in JT-60", Symposium on Energy Removal and Particle Control in Toroidal Fusion Devices (Princeton, USA, July 1983).

27) Yamada R., Wienhold P.[**32], Waelbroeck F.[**32], Winter J.[**32], Rota E.[**32], Banno T.[**32] : "In-situ Measurement of the Hydrogen Recycling Constant of the TEXTOR Liner", 3rd Topical Meeting on Fusion Reactor Materials (Albuquerque, USA, Oct. 1983).

28) Sone K. : "Hydrogen Recycling at Wall Surfaces", Japan-US Workshop on Impurity and Particle Control, Theory and Modelling (Nagoya, Japan, Mar. 1984).

29) Shimamoto S., Ando T., Hiyama T., Tsuji H., Takahashi Y., Tada E., Nishi M., Yoshida K., Okuno K., Koizumi K., Nakajima H., Kato T., Takahashi O.[*15], Oshikiri M., Iida F.[*4], Yasukochi K.[**6] : "Japanese Progress in the Large Coil Task and the High Field Cluster Test Program", ANS 5th Topical Meeting on Technology of Fusion Energy (Knoxville, USA, Apr. 1983).

30) Shimamoto S., Ando T., Hiyama T., Tsuji H., Takahashi Y., Tada E., Nishi M., Yoshida K., Okuno K., Koizumi K., Nakajima H., Kato T., Takahashi O.[*15], Oshikiri M., Ogasawara T.[**6], Kuroda K.[*4], Hattori Y.[*11], Osaki O.[*2], Yasukochi K.[**6] : "Progress in Large Superconducting Pulsed Conductors and Coils for the Fusion Experimental Reactor", ibid.

31) Nakajima H., Yoshida K., Takahashi Y., Tada E., Oshikiri M., Koizumi K., Shimamoto S., Miura R.[*12], Shimada M[*14], Masumoto H.[*34], Sakamoto T.[*34] : Development of the New Cryogenic Structural

Material for Fusion Experimental Reactor", Cryogenic Engineering Conference/The International Cryogenic Materials Conference (Colorado, USA, Aug. 1983).

32) Tsuji H., Takahashi Y., Okuno K., Tada E., Yoshida K., Nishi M., Koizumi K., Nakajima H., Kato T., Oshikiri M., Takahashi O.*15, Hiyama T., Ando T., Shimamoto S. : "Development of a 500-m-ID Pulsed Magnet for Testing of High-Current Pulsed Conductors", ibid.

33) Tada E., Shimamoto S. : "Pressure Rise Analysis in Superconducting Coils during Dumping", ibid.

34) Sakamoto T.*34, Nagasawa Y.*34, Yamauchi I.*34, Zaizen T.*34, Nakajima H., Shimamoto S. : "Nitrogen Containing 25Cr-13Ni Stainless Steel as a Cryogenic Material", ibid.

35) Tone S.*14, Shimada M.*14, Horiuchi T.*14, Kasamatsu Y.*14, Nakajima H., Shimamoto S. : "The Development of a Nitrogen-Strengthened High-Manganese Austenitic Stainless Steel for Large Superconducting Magnet", ibid.

36) Masumoto H.*34, Suemune K.*34, Nakajima H., Shimamoto S. : "Development of a High-Strength High Manganess Stainless Steel for Cryogenic Use", ibid.

37) Miura R.*12, Nakajima H., Takahashi Y., Yoshida K. : "32Mn-7Cr Austenitic Steel for Cryogenic Application", ibid.

38) Ando T., Shimamoto S., Hiyama T., Tsuji H., Takahashi Y., Nishi M., Tada E., Yoshida K., Okuno K., Koizumi K., Kato T., Nakajima H., Takahashi O.*15, Oshikiri M., Yasukochi K.**6 : "Test Results of 60-cm Bore Nb_3Sn Test Module Coil (TMC-I) in the Cluster Test Facility", 8th International Conference on Magnet Technology (Grenoble, France, Sept. 1983).

39) Nishi M., Ando T., Hiyama T., Tsuji H., Takahashi Y., Okuno K., Yoshida K., Tada E., Koizumi K., Kato T., Nakajima H., Takahashi O.*15, Oshikiri M., Shimamoto S., Yasukochi K.**6 : "Stability Test Result of the Japanese Test Coil for the Large Coil Task at the Domestic Test", ibid.

40) Shimamoto S., Koizumi K., Ando T., Hiyama T., Tsuji H., Takahashi Y., Tada E., Nishi M., Yoshida K., Okuno K., Nakajima H., Kato T., Takahashi O.*15, Oshikiri M., Kawano K., Takahashi R.*4, Hattori Y.*11, Yasukochi K.**6 : "Coil System Design of Medium Sized Superconducting Tokamaks", 10th Symposium on Engineering Problem

of Fusion Research (Philadelphia, USA, Dec. 1983).

41) Shimamoto S., Tsuji H., Takahashi Y., Tada E., Okuno K., Hattori Y.[*11], Takahashi R.[*4], Ando T., Hiyama T., Nishi M., Yoshida K., Koizumi K., Nakajima H., Kato T., Takahashi O.[*15], Oshikiri M., Kawano K., Yasukochi K.[**6] : "Design and Verification Tests for a 20-MJ Pulsed Poloidal Coil", ibid.

42) Ando T., Takahashi Y., Nishi M., Tada E., Koizumi K., Okuno K., Tsuji H., Nakajima H., Hiyama T., Yoshida K., Kato T., Shimamoto S., Yasukochi K.[**6] : "12 T Test Module Coil (TMC-II) in the Cluster Test Program", ibid.

43) Seki Y., Tone T., Naruse Y., Shimamoto S., Yoshida Y., Tomabechi K. : "Overview of Fusion Safety Studies in JAERI", IAEA Technical Committee on Environmental and Safety Aspects of Fusion (Ispra, Italy, Oct. 1983).

44) Yoshida Y., Naruse Y., Katagiri H., Hirata S.[*18], Tanaka K., Kokubu M. : "Environmental Safety on Releases of Tritium from a Fusion Facility", ibid.

45) Yoshida H., Konishi S., Takeshita H., Kurasawa T., Watanabe H., Naruse Y. : "Water Adsorption on Lithium Oxide Pellets in Helium Sweep Gas Stream", ANS 3rd Topical Meeting on Fusion Reactor Materials (Albuquerque, USA, Sept. 1983).

46) Kurasawa T., Takeshita H., Watanabe H., Yoshida H., Umei H., Miyauchi T., Miura K. : "In-situ Tritium Recovery Experiment from Lithium Oxide under High Neutron Fluence", ibid.

47) Shimada M., JAERI team : "A Fast Numerical Simulation of Dense and Cold Divertor Plasmas in Doublet III", 10th Conference on Numerical Simulation of Plasmas (San Diego, January 1983).

48) Shimada M., Sengoku S., Miya N., Kasai M.[*3], JAERI team : "Recent D-III Single-Null Poloidal Divertor Experiments and Modelling", Fourth Topical Conference on Atomic Processes in High Temperature Plasmas (Princeton, April 1983).

49) Nagami M. : "Energy Confinement of High Density, High Temperature Dee Shaped Plasmas in Doublet III", Gordon Research Conference (New London, June 1983).

50) Konoshima S. : "Fluctuations in Dee Shaped and/or Diverted Plasmas in Doublet III", Gordon Research Conference (New London, June 1983).

51) Shimada M. : "Experimental Observations of a Dense and Cold

Divertor Plasma in D-III Beam-Heated Divertor Discharges and its Numerical Simulation", Gordon Research Conference (New London, June 1983).

52) Miya N. : "Heat Load on the Divertor Plate in D-III", Symposium on Energy Removal and Particle Control in Toroidal Fusion Devices (Princeton, July 1983).

53) Shimada M. "Modelling of Dense and Cold Divertor Plasma in D-III", Symposium on Energy Removal and Particle Control in Toroidal Fusion Devices (Princeton, July 1983).

54) Kobayashi T.[*4], Shimada M., Sengoku S., Konoshima S., JAERI team, Kahn C.L.[*5], Burrell K.H.[*5], GA Technologies : "Langmuir Probe Measurements in Beam-Heated D-III Divertor Discharges", Symposium on Energy Removal and Particle Control, PPPL, July 26-29, 1983.

55) Nagami M., Kasai M.[*3], Aikawa H., Kitsunezaki A., Kobayashi T.[*4], Konoshima S., Matsuda T., Miya N., Ninomiya H., Shimada M., JAERI team, Angel T.[*5], Armentrout C.[*5], Blau F.[*5], Barmson G.[*5], Brooks N.[*5], Chase R.[*5], Colleraine A.[*5], Fairbanks E[*5], Fasolo J.[*5], Fisher R.[*5], Hino T.[*5], Hong R.[*5], Jahns G.[*5], Kamperschroer J.[*5], Kim J.[*5], Lieber A.[*5], Lohr J.[*5], McColl D.[*5], Rottler L.[*5], Seraydarian R.[*5], Silagi R.[*5], Smith J.[*5], Snider R.[*5], Taylor T.[*5], Tooker J.[*5], Vaslow D.[*5], Wojtowicz S.[*5], GA Technologies : "Production of High Density and High Temperature Plasmas by Controlling Edge Particle Recycling in Doublet III Divertor Equilibria", Symposium on Energy Removal and Particle Control, PPPL, July 26-29, 1983.

56) Nagami M., Aikawa H., Hoshino K., Kasai M.[*3], Kitsunezaki A., Kobayashi T.[*4], Konoshima S., Matsuda T., Miya N., Ninomiya H., Sengoku S., Shimada M., Yamauchi T., Yokomizo H., JAERI team, Angel T.[*5], Armentrout C.[*5], Blau F.[*5], Bramson G.[*5], Brooks N.[*5], Chase R.[*5], Colleraine A.[*5], Fairbanks E.[*5], Fasolo J.[*5], Fisher R.[*5], Groebner R.[*5], Hong R.[*5], Hsieh C.[*5], Jahns G.[*5], Kamperschroer J.[*5], Kim J.[*5], Lieber A.[*5], Lohr J.[*5], McColl D.[*5], McMahon T.[*5], Overskei D.[*5], Peterson P.[*5], Seraydarian R.[*5], Silagi R.[*5], Smith J.[*5], Snider R.[*5], Taylor T.[*5], Tooker J.[*5], Treglio J.[*5], Vaslow D.[*5], Wojtowicz S.[*5], GA Technologies : "High Temperature and High Density Plasmas in Beam Heated Divertor Discharges in Doublet III", 11th European Conf. on Controlled Fusion and Plasma Physics, Aachen,

Sept. 5-9, 1983.

57) Shimada M., Sengoku S., Kobayashi T.[*4], Miya N., Kasai M.[*3], JAERI team, Kahn C.L.[*5], Burrell K.H.[*5], GA Technologies : "Experimental Observation of a Dense and Cold Divertor Plasma in D-III Beam-Heated Divertor Discharges and its Numerical Simulation", 11th European Conf. on Controlled Fusion and Plasma Physics, Aachen, Sept. 5-9, 1983.

58) Shimada M., Hirayama T., Sengoku S., Washizu M.[*2], Miya.N., Kobayashi T.[*4], Kasai M.[*3], Nagami M., Konoshima S., Kameari A.[*3], Abe M.[*4], Kodama K., Yamamoto T., Kitsunezaki A., JAERI team and Kahn C.L.[*5], Fairbanks E.S.[*5], Hsieh C.L.[*5], Burrell K.H.[*5] and the Doublet III groups GA Technologies Inc. : "Summary of Experimental Results of Single-Null Poloidal Divertor in D-III", INTOR Mtg, Vienna, Jan. 1984.

59) Nagami M., Kasai M.[*3], Aikawa H., Kitsunezaki A., Kobayashi T.[*4], Konoshima S., Matsuda T., Miya N., Ninomiya H., Shimada M., Yokomizo H. : "High Temperature and High Density Plasmas in Beam Heated Divertor Discharge", 11th European Conference on Controlled Fusion and Plasma Physics (Aachen, FRG, September, 1983).

60) Nagayama Y.[**5], Tsuji S., Miyamoto K.[**5], Kawahata K.[**2], Noda N.[**2], Tanahashi S.[**2] and Fujita J.[**2] : "A Study of Tokamak Disruption in JIPPT-II Using Soft X-Ray Imaging", ibid.

61) Hosogane N., Aikawa H., Ogiwara N., Yamamoto M., Matoba T. and Suzuki Y. : "Development of Magnetic Probe and Rogowski Coil in JT-60", 10th Symposium on Fusion Engineering (Philadelphia, USA, December 1983).

62) Miya N., Shimada M. and Kasai M.[*3] : "Heat Load on the Divertor Plate in D-III", Symposium on Energy Removal and Particle Control in Toroidal Fusion Devices, (Princeton, USA, July 1983).

63) Seki S., Takizuka T., Saito S.[*4], Ninomiya H., Yoshida H., Tani K., Azumi M., Ando T., Sugihara M. and Shimomura Y. : "Experimental Program of JT-60 and Its Relevance with the Research of Divertor", ibid.

64) Shimada R., Aoyagi T., Matsukawa M., Ikeda H.[*2], Yamagishi K.[*2], Ujiie K.[*2] and Nakagawa S.[*2] : "Control and Protection of Thyristor Convertors for JT-60 Poloidal Field Coils", 10th Symposium on Fusion Engineering (Philadelphia, USA, December 1983).

65) Kurihara K., Yonekawa I., Kimura T., Hosogane N., Yoshino R., Anno M., Takahashi M. and Kondo I. : "System Design for JT-60 Failure Mode Analysis and Prediction", ibid.

66) Kondo I., Kimura T., Hosogane N., Yoshino R., Kurihara K. and Yonekawa I. : "Reliability Aspects in the JT-60 Central Control System Design", ibid.

67) Kimura T., Kurihara K., Kumahara T., Yoshino R., Hosogane N., Yonekawa I. and Kondo I. : "Communication System in JT-60 Control", ibid.

68) Yamamoto M., Takatsu H., Shimizu M., Okubo M., Ogiwara N., Itoh Y.[*4], Takizawa .[*4], Kajiura S.[*4], Kunii T.[*4] : "Quality Control and Leak Test on JT-60 Vacuum Components", IX International Vacuum Congress-V International Conference on Solid Surface, Madrid, Sep. 1983.

69) Nakamura H., Ando T., Masuda M., Shimizu M., Shimizu T., Horie T. : "Evaluation of Operation Region of JT-60 First Wall Related High Heat Flux", 10th Symposium on Fusion Engineering (Philadelphia, Dec. 1983).

70) Shimizu T., Shimizu M., Nakamura H., Kajiura S.[*4], Sato K.[*4], Koda T.[*4] : "Heating and Cooling System for JT-60 Vacuum Vessel", ibid.

71) Takatsu H., Yamamoto M., Shimizu M., Suzuki K.[*4], Sonobe T.[*4], Hayashi Y.[*27], Mizuno G.[*27] : "Mechanical Strength Evaluation of the Welded Bellows for the Ports of the JT-60 Vacuum Vessel", ibid.

72) Ogiwara N., Arai T., Shimizu M., Takizawa T.[*4], Kimishima F.[*21] : "Reliability Test of 40 cm ID all Metal Gate Valve and 54 cm ID Ceramic Break for JT-60", ibid.

73) Ohkubo M., Ando T., Masuda M., Watanabe T.[*4], Kamiya H.[*4] : "Fabrication of JT-60 Poloidal Field Coil", ibid.

74) Sato H.[*4], Kajiura S.[*4], Owada K.[*4], Kanamori N.[*4], Karatsu Y.[*4], Sasajima T.[*4], Shimizu I., Yamamoto M., Takatsu H. : "Fabrication of JT-60 Vacuum Vessel", ibid.

75) Hayashi K., Hashimoto K., Takeuchi H., Miura Y., Nishitami T., Shiho M. and Maeda H. : "Charge Exchange Neutral Particles Mass and Energy Analyser for JT-60", IEEE 10th Symposium on Fusion Engineering (Philadelphia 1983).

76) Ohasa K., Toyokawa R., Mochizuki O., Yanai Y. and Kambe T. :

"Inter-Shot Processor System for JT-60", ibid.

77) Ohasa K., Mochizuki O. and Kurimoto K. : "Data Management Facility for JT-60", ibid.

78) Ohasa K. : "System Configuration of Data Processing System for JT-60", Japan-US Workshop on Computer Control and Data Acquisition (Naka, Japan, 1984).

79) Ohasa K. : "CAMAC Hardware of Data Processing System for JT-60", ibid.

80) Tanaka M. : "Tokamak Research at JAERI", 11th European Conference on Controlled Fusion and Plasma Physics. (Jülich, Sept. 1983).

81) Seki Y., Tanaka S., Oyama Y., Sasamoto N., Kawasaki H., Ikeda Y., Maekawa H. and Nakamura T. : "Monte Carlo Analysis of a Streaming Experiment of D-T Neutron and Gamma Rays Through a Concrete Bent Duct", Proc. Conf. Radiation Shielding, May 16-20, (1983) Vol. II., 898.

82) Yamauchi M., Kawai M., Seki Y. and Ebisawa K. : "The Analysis of the Radiation Streaming Through RF Heating and Exhaust Duct of a Tokamak Fusion Reactor", ibid. 908.

83) Mori S., Mohri K., Seki Y. and Kawasaki H. : "Nuclear Analysis of Blanket and Shield Design for Tokamak Fusion Experimental Reactor", ibid. 704.

84) Seki T., Tone T., Naruse Y., Shimamoto S., Yoshida Y. and Tomabechi K. : "Overview of Fusion Safety Studies in JAERI", IAEA Technical Committee Meeting on Environmental and Safety Aspects of Fusion, Oct. 17-21, Ispra (1983).

85) Okazaki T.[*4], Maki K.[*4], Yoshioka K.[*4], Sugihara M. and Fujisawa N. : "Steady-State Tokamak Reactor Using Compressional Alfven Wave", APS 25th Annual Meeting (California, 1983).

86) Nishio S., Honda T., Sawada Y. : "Japanese Contribution to Structural Mechanical and Stress Analysis of INTOR", 7th International Conference on Structural Mechanics in Reactor Technology, August 22-26 Chicago, Illinois USA (1983).

87) F. Farfabetti-Casali, Brown T.G., Shannon T.E. Churakov G., Serebrennikv D., Nishio S., Reynolds P., Uchida T. : "INTOR Mechanical Configuration Concept", ibid.

88) Iida H., Ehst D.A., Peng Y-K.M. : "Parametric Study of LH Current Drive for FED-A 5th Topical Meeting of the Technology of Fusion Energy (Knoxville, US).

A.1.5 List of Other Reports

1) Tsuji S. : "Soft X-Ray Imaging Study on Disruptions in the JIPPT-II Tokamak", IPPJ-630 (April 1983).
2) Itoh S-I.**1, Fukuyama A.**3, Itoh K. : "Successive Heating by ICRF Wave and Neutral Beam Injection", HIFT-75 (Hiroshima Univ., Aug. 1983).
3) Itoh K., Itoh S-I.**1, Fukuyama A.**3 : "Three Dimensional Structure of ICRF Waves in Tokamak Plasmas", HIFT-76 (Hiroshima Univ., Aug. 1983).
4) Itoh S-I.**1, Itoh K. : "Fusion Engine Cycle in Reactor System by Adiabatic Compression", HIFT-77 (Hiroshima Univ., Aug. 1983).
5) Fukuyama A.**3, Itoh S-I.**1, Itoh K. : "Study of ICRF Waves in a Second Cyclotron Resonance and Two-Ion-Hybrid Resonance Heatings", HIFT-86 (Hiroshima Univ., Oct. 1983).
6) Yoshida H. : "Effects of Impurities on Hydrogen Permeability through Palladium Alloy Membranes at Comparatively High Pressures and Temperatures", New Silver Technology (The Silver Institute, Washington, USA, 1983) p.3.
7) Iida H., Ehst D.A., Peng Y-K.M. : "Parametric Study of Lower Hybrid Current Drive in the FED-A Design", ORNL/TM-8578 (1983).

A.2 Personnel of the Center

A.2.1 Number of the Staff of the Divisions

	FY1981	FY1982	FY1983
Regular staff	185	220	250*1
Staff on loan	32	30	31*2
Guest scientist	5	3	3*3
Scholarship fellow	1	1	2

*1 Including scientists, technicians and secretaries

*2 From industry

*3 From Nihon University, University of Tokyo and Kogakuin University

A.2.2 List of scientific staff and officers during FY 1983

Fusion Research Center

ISO Yasuhiko (Director General)

(A) Department of Thermonuclear Fusion Research

OBATA Yukio (Director)

TANAKA Masatoshi (Deputy Director)

NAKANO Akira (Administrative Manager)

Plasma Theory Laboratory

ADACHI Masao*1

AZUMI Masafumi (Senior Scientist)

HARAFUJI Kenji**4 (Scholarship Fellow)

ITOH Kimitaka

KUMAGAI Michikazu*2 (-- Apr. 1983)

KURITA Gen-Ichi

TAKEDA Tatsuoki (General Manager)

TAKIZUKA Tomonori

TANAKA Yukio*1

TOKUDA Shinji

TSUNEMATSU Toshihide

TUDA Takashi (Senior Scientist)

WATANABE Masami*32 (Sep. 1983 --)

Experimental Plasma Physics Laboratory

HOSHINO Katsumichi

KASAI Satoshi (Senior Scientist)

KAWAKAMI Tomohide

KAWASHIMA Hisato

KIMURA Haruyuki

MAENO Masaki (Senior Scientist)

MATOBA Tohru (Senior Scientist)

MATSUDA Toshiaki

MATSUMOTO Hiroshi

MIURA Yukitoshi

MORI Masahiro

ODAJIMA Kazuo

OGAWA Hiroshi

OGAWA Toshihide

OHTA Kanji*11

SHOJI Teruaki

SUZUKI Norio

TAMAI Hiroshi**29 (Scholarship Fellow)

TANAKA Yuji (General Manager)

UESUGI Yoshihiko

YANAGISAWA Ichiro*3

YAMAMOTO Shin (Senior Scientist)

YAMAMOTO Takumi

YAMAUCHI Toshihiko

Facility Operation and Engineering Division

HASEGAWA Kouichi

HONDA Atsushi

ISHIBORI Ikuo

KASHIMURA Takanori

KASHIWA Yoshitoshi

KAZAWA Minoru

KIKUCHI Kazuo

KUNIEDA Shunsuke (General Manager)

MATSUZAKI Yoshimi

OHUCHI Katsuji (Apr. 1983 --)

OKANO Fuminori

SHIBATA Takatoshi

SHIBUYA Toshihiro (Apr. 1983 --)

SHIINA Tomio

SUZUKI Kihachiro (Deputy General Manager)

TAJIMA Yoshihiro (-- Apr. 1983)

TANI Takashi

YOKOKURA Kenji (-- Apr. 1983)

YOKOYAMA Kenji

Plasma Heating Laboratory I

AKIBA Masato

DAIRAKU Masayuki

HORIIKE Hiroshi

ITOH Takao

KOMATA Masao

MATSUDA Shinzaburo (Senior Scientist)

MATSUOKA Mamoru
MIZUHASHI Kiyoshi
OHARA Yoshihiro
OKUMURA Yoshikazu
SHIBANUMA Kiyoshi
SHIBATA Takemasa
SUZUKI Yoshimi*9
TANAKA Masatoshi (General Manager)
TANAKA Shigeru
TERAKADO Takuya*9
WATANABE Kazuhiro
WELLS Russel**28

Plasma Heating Laboratory II

FUJII Tuneyuki
HARA Mitsuru*16
IIDA Kazuhiro*9
IMAI Tsuyoshi
NAGASHIMA Takashi (General Manager)
NAKAMURA Tetsurou*2
SAIGUSA Mikio
SAKAMOTO Keishi
SAWAHATA Masayuki

Plasma Engineering Laboratory

ABE Tetsuya (Senior Scientist)
HIROKI Seiji
INAGAWA Konosuke*21
MURAKAMI Yoshio (General Manager)
NAKAMURA Kazuyuki
OBARA Kenjiro
OHTSUKA Hidewo
SAIDOH Masahiro (Senior Scientist)
SONE Kazuho (Senior Scientist)
YAMADA Rayji

Superconducting Magnet Laboratory

ANDO Toshinari
HATTORI Yasuhide*11

HIYAMA Tadao
KATO Takashi
KAMIYA Shoji*18
KAWANO Katsumi
KOIZUMI Koichi
NAKAJIMA Hideo
NISHI Masataka
OKUNO Kiyoshi
OSHIKIRI Masayuki
SHIMAMOTO Susumu (General Manager)
TADA Eisuke
TAKAHASHI Osamu*15
TAKAHASHI Ryukichi*4
TAKAHASHI Yoshikazu
TSUJI Hiroshi
YOSHIDA Kiyoshi

Tritium Engineering Laboratory

AISAWA Takeshi*8
HIRATA Shingo*18
HONMA Takashi
KINOSHITA Masahiro
KONISHI Satoshi
MATSUDA Yuji
MUNEMOTO Iwao*10
NARUSE Yuji (General Manager)
OKUNO Kenji
TANAKA Kichizo (Senior Scientist)
YAMADA Masayuki
YAMANISHI Toshihiko
YOSHIDA Hiroshi (Senior Scientist)

(B) Division of Large Tokamak Develpment

TOMABECHI Ken (Director)
YOSHIKAWA Masaji (Deputy Director)

Large Tokamak Administration Section

NARUI Masao (Administrative Manager)

JT-60 Program Office

IIJIMA Tsutomu (General Manager)
KISHIMOTO Hiroshi (Deputy General Manager)

* Planning and Coordination Group
AIKAWA Hiroshi (Senior Scientist)
MIYA Naoyuki
OIKAWA Akira
OZEKI Takahisa
SUZUKI Kunihiro

* Experimental Planning Group
HIRAYAMA Toshio
HOSOGANE Nobuyuki
KIKUCHI Mitsuru
NAKANISHI Masahiro
NINOMIYA Hiromasa
SEKI Shogo
SHIMIZU Katsuhiro
SHIMOMURA Yasuo (Senior Scientist)
SHINTANI Kiyomori*31
TANI Keiji
TSUJI Shunji
YOSHIDA Hidetoshi
YOSHINO Ryuji

* Doublet-III Experiment Group
ABE Mitsushi*4
KAMEARI Akihisa*3
KITSUNEZAKI Akio (Senior Scientist)
KONOSHIMA Shigeru
NAGAMI Masayuki
SENGOKU Seio
SHIMADA Michiya
WASHIZU Masao*2

* Operation Planning Group
KODAMA Kozo
KOIKE Tsuneyuki
SEIMIYA Munetaka
TAKEDA Takashi
TOKUTAKE Toshikuni

JT-60 Project Office I

TAMURA Sanae (General Manager)

OHTA Mitsuru (Deputy General Manager)

* Machine Group

AKINO Noboru

ANDO Toshiro

ARAI Takashi

HARA Yasuhiro

HIRATSUKA Hajime

HORIE Tomoyoshi

INOUE Hiromi

ISAKA Masayoshi

KASUGA Takemitsu

KAWASAKI Kozo

KOYA Kisei (Oct. 1983 --)

MASUDA Michio

NAKAMURA Hiroo

NAKAO Keizo

NISHIYAMA Takeji*4

NOSHIROYA Syoji*21

OGIWARA Norio

OHKUBO Minoru

OTSU Kazuyoshi

SERIZAWA Yasunori

SHIMIZU Masatsugu (Senior Scientist)

SHIMIZU Tohru

SUNAOSHI Hidenori

TAKATSU Hideyuki

TANAKA Takejiro

TOYOSHIMA Noboru

URAKAWA Hiroshi

YAMAMOTO Masahiro

YANAI Munetoshi

YASUDA Masaharu (-- Sept. 1983)

JT-60 Project Office II

TAMURA Sanae (General Manager)

KONDO Ikuo (Deputy General Manager)

* Power Supplies Group

AOYAGI Tetsuo
ARAKAWA Kiyotsugu
ICHIGE Hisashi
MATSUKAWA Makoto
MATSUKAWA Tatsuya
MIZUNO Makoto
NAGAYA Susumu
SHIINA Minoru
SHIMADA Ryuichi
TAKAHASHI Shunji
TERAKADO Tsunehisa
TSUNEOKA Masaki

* Control Group

ANNO Katsuto
ITOH Yasuhiro
KIMURA Toyoaki
MIYACHI Kengo
TAKAHASHI Minoru
TOTSUKA Toshiyuki
YONEKAWA Izuru

JT-60 Project Office III

SUZUKI Yasuo (General Manager)

* Diagnostics Group

FUKUDA Takeshi
HARUE Morihito*1
KITAHARA Katsumi
KURIHARA Kenichi
MAEDA Hikosuke (Senior Scientist)
NAGASHIMA Akira
NAKAMURA Yukiharu
NEYATANI Yuzuru
NISHITANI Takeo
NOMATA Hideyuki
OHASA Kazumi
OHSATO Yukio*24

OHSHIMA Takayuki
SATO Masayasu
SHIHO Makoto (Senior Scientist)
SHITOMI Morimasa
SUGIE Tatsuo
TAHIRA Shigeo
TAKAHASHI Toranosuke
TAKAYASU Toshio
TAKEUCHI Hiroshi
URAMOTO Yasuyuki
YAMASHITA Osamu
YOKOMIZO Hideaki
YOKOUCHI Shigeru*23

JT-60 Project Office IV

SHIRAKATA Hirofumi (General Manager)

* NBI Group

ARAKI Masanori
KAWAI Mikito
KITAMURA Shigeru
KURIYAMA Masaaki (Senior Scientist)
MIZUTANI Yasuhiko*19
NAGAMURA Hidehiro*2
OHGA Tokumichi
OHUCHI Yutaka
SHIGEMATSU Hirotsugu*8
SUGAWARA Tadayoshi*4

* RF Group

HONDA Masao
IKEDA Yoshitaka
KIHARA Yoshihiko*10
SUGANUMA Kazuaki
SUZUKI Norio
UEHARA Kazuya
YOKOKURA Kenji

JT-60 Operation Division

AKAO Yohichiro

IMAHASHI Koichi

ISHIHARA Masaru

KUNIEDA Shunsuke (General Manager)

NAOE Teruo*6

HIRUTA Kazuharu

HOSODA Ryujiro

OHMORI Ken-ichiro

OHMORI Shunzo

SEKIGUCHI Shuichi

TOMIYAMA Yoshimi

Fusion Reactor System Laboratory

YOSHIKAWA MASAJI (General Manager)

FUJISAWA Noboru (Principal Scientist)

HITOKI Shigehisa*11

IIDA Hiromasa (Senior Scientist)

MINATO Akio*18

NISHIO Satoshi

OKAZAKI Takashi*4

SEKI Yasushi (Senior Scientist)

SUGIHARA Masayoshi

TONE Tatsuzo (Principal Scientist)

TACHIKAWA Katsuhiro

TACHIKAWA Nobuo*2

TSUJIMURA Seiichi*8

YAMAMOTO Takashi*6

Guest Scientist

MIYAMOTO Goro**5

YAMAMURA Sakae**5

YASUKOCHI Ko**6

*1 Fujitsu Ltd.
*2 Toshiba Corp.
*3 Mitsubishi Atomic Power Industry Inc.
*4 Hitachi Ltd.
*5 GA Technologies Inc.
*6 Fuji Electric Co., Ltd.
*7 Kaihatsu Denki Co., Ltd.
*8 Mitsubishi Heavy Indu., Ltd.
*9 Nuclear Engineering Co., Ltd.
*10 Sumitomo Heavy Ind., Ltd.
*11 Mitsubishi Electric Co., Ltd.
*12 Japan Steel Works Ltd.
*13 Nippon Atomic Industry Group
*14 Kobe Steel Ltd.
*15 Saginomiya Johnson Controls Co., Ltd.
*16 Nippon Electric Co., Ltd.
*17 Hitachi Cable Co.
*18 Kawasaki Heavy Ind., Ltd.
*19 Nissin Electric Co., Ltd.
*20 Touyo Information System Co., Ltd.
*21 ULVAC Co.
*22 Nippon Kogaku Co., Ltd.
*23 Osaka Vacuum Ltd.
*24 Nissei Sangyo Co., Ltd.
*25 Century Research Center Co.
*26 Yokokawa Electric Works Ltd.
*27 Irie Koken Co., Ltd.
*28 Ishikawajima-Harima Heavy Ind. Co., Ltd.
*29 Kishikawa Special Valve Co., Ltd.
*30 Mitsui Engineering & Shipbuilding Co.
*31 Japan Information Service Ltd.
*32 Nuclear Data Corporation
*33 Nuclear Energy Data Center
*34 Nippon Steel Co.

**1 Hiroshima University
**2 Nagoya University
**3 Okayama University
**4 Tohoku University
**5 The University of Tokyo
**6 Nihon University
**7 Osaka University
**8 Tokyo Institute of Technology
**9 Kyoto University
**10 National Research Institute for Metals
**11 National Laboratory for High Energy Physics
**12 Power Reactor and Nuclear Fuel Development
**13 Confédération Suisse, Ecole Polytechnique Fédérale de Lausanne
**14 Oak Ridge National Laboratory
**15 Culham Laboratory
**16 FB-National Magnetic Laboratory
**17 Argonne National Laboratory
**18 University of Wisconsin
**19 Princeton Plasma Physics Laboratory
**20 Max-Planck Institute für Plasmaphysik
**21 Centre d'Etude Nucléaires, Fontenay-aux-Rose
**22 Bell Laboratories
**23 JET Joint Undertaking
**24 Institute für Angewandte Physik II, Universitäte Heidelberg
**25 Academia Sinica, Peking, The Peoples Republic of China
**26 The Institute of Fundamental Technological Research, Warsaw/Poland
**27 Institut für Plasmaphysik (Garching)
**28 Lawrence Berkeley Laboratory, Univ. of California
**29 Tsukuba University
**30 Toho University
**31 Los Alamas National Laboratory
**32 KFA-IPP, Jülich

A.3 Budget of the Center

(unit : Million ¥)

	FY 1981*1	FY 1982*1	FY 1983*1
JT-60 Construction*2	23,943	28,936	26,020
Research & Development*3	3,619	3,117	3,348
Japan-US Cooperation	3,875	3,042	1,436
Site Construction	4,100	5,633	7,771

*1 From April to March

*2 Including cashing of the financial obligation in each FY

*3 Excluding fusion-related R&D in other divisions than the Center